Theoretical and Experimental Investigation of Hydrocyclone Performance and the Influence of Underflow Pumping Effect

by
Reza Sabbagh

A thesis submitted in partial fulfillment of the requirements for the degree of

Doctor of Philosophy

Department of Mechanical Engineering
University of Alberta

Abstract

Centrifugal separators have many applications in industry. Comprehensive information based on performance and energy consumption for a detailed comparison between different types of centrifugal separators is essential to allow design optimization and is the focus of this work.

Equivalent settling area factor is typically used to compare and scale up centrifuge separators. A performance chart based on this factor is available in the literature that compares the performance of different centrifuge separators including hydrocyclones. However, the available performance chart for centrifuge separators is problematic in terms of over-predicting the hydrocyclone performance and not being updated for the progresses in the centrifuges technologies.

Predicting the equivalent settling area of the hydrocyclones is important for selection and design of the device. It also allows comparison of hydrocyclones to other separators that work using a similar concept. A mathematical model based on the physics of the separation phenomenon in the reverse flow hydrocyclones is developed to predict the equivalent area factor of the hydrocyclone. A framework for comparing performance with an updated performance chart for four types of centrifugal separators and a comparison with a continuous gravity settling tank is described. A model and chart for performance and energy consumption, which

makes it possible to compare different separators, is a key result of this work which extends current available handbooks and guidelines.

Studying the effect of using a pump in the underflow on the operating conditions is another focus of this study. This effect can be used for controlling the device as the underflow of the hydrocyclone is usually adjusted to overcome the variable conditions of the feed flow to achieve a desired performance. It is observed that a pump in the underflow through either back pressure or by pump suction allows simulating the function of underflow variable pipe size or valves to control the flow rate. An empirical correlation is developed in this research for the effect of underflow pumping that can be used to predict the pumping influence on the hydrocyclone operating variables and for controlling the hydrocyclone performance.

Keywords: hydrocyclone, separation, performance, energy consumption, equivalent settling area, underflow pumping, design chart, centrifugal separator

In memory of my father

To my mother and my wife
With love and eternal appreciation

Preface

This thesis is original work by Reza Sabbagh. Some parts of this research chapter 1 and 2 and 3 of this thesis have been published or presented as:

- R. Sabbagh, M. G. Lipsett, C. R. Koch, D. S. Nobes, Hydrocyclone Performance and Energy Consumption Prediction: A Comparison with Other Centrifugal Separators, *Separation Science and Technology* 50 (6) (2015) pp. 788-801.,

- R. Sabbagh, M. G. Lipsett, C. R. Koch, D. S. Nobes, Theoretical and experimental study of hydrocyclone performance and equivalent settling area, *ASME 2014 International Congress and Exposition IMECE2014*, ASME, Montreal, Quebec, Canada. doi:10.1115/IMECE2014-37482.,

- R. Sabbagh, M. G. Lipsett, C. R. Koch, D. S. Nobes, A mathematical model of equivalent settling area for predicting hydrocyclone separation performance, *European Conference on Fluid Particle Separation-FPS 2014*, October 15-17, 2014, Lyon, France, Societe Francaise des Separations Fluides-Particles.

Chapter 4 has been used for submission for publication as:

- R. Sabbagh, M. G. Lipsett, C. R. Koch, D. S. Nobes, Predicting Equivalent Settling Area Factor in Hydrocyclones; A Method for Determining Tangential Velocity Profile, Submitted to *Separation and Purification Technology* Journal, SEPPUR-D-15-01191.

Acknowledgements

I am eternally grateful and thankful to Allah, the Almighty Who continues to bless my life.

It has been an unforgettable experience and I like to thank a number of people for making four years of my life such an amazing time.

Foremost, I would like to express my sincere gratitude to my supervisor Dr. David Nobes for his continuous support, patience and guidance and for providing me with a rich and rewarding academic experience. I have also been lucky to work with Dr. Michael Lipsett and I would also like to thank him for his wisdom, and knowledge. David and Mike have participated in this project with much interest and enthusiasm and have inspired and motivated me.

I specially would like thank Dr. Robert Koch for his support during my PhD program, preparing the publications and his grateful thought who shared with me.

I thank Dr. Suzanne Kresta for being in my supervisory committee and for her insightful comments during my candidacy exam, which helped me to develop a more profound understanding of the nature of this research.

Thanks to the members of my examining committee, Dr. Timothy Eisele and Dr. Alexandra Komrakova for reviewing my thesis and Dr. Prashant Waghmare for chairing the exam seminar.

Thanks to my friends and lab mates for their support, friendship and help. I thank Alireza Setayeshgar and Mahdi Vaezi for the brainstorming discussions on different aspects of my research. I acknowledge the help from my friends Aleksey Baldygin, Sina Rafati, Mojtaba Izadi, Pooria Joulani, Yogesh Agrawal, Mehdi Rezaei, Alireza Setayeshgar, Hirad Soltani and Arun Majumdar during the experiments and code development.

A greatest thank you to my mother and my late father for their love and sacrifice. My father's memory will be with me always. No words can fully express my gratitude to my mother and my brothers Ali and Mahdi and my sister Fatemeh. They have supported me in any and every possible way throughout my education. Many thanks to my grand parents and parents-in-law whom I am grateful for their assistance. Your prayer for me is what sustains me thus far.

I would like to sincerely thank my beloved wife, Narges Shaabani for her love, understanding and support, and for being with me through ups and downs. Also special thanks goes to my little daughters Sara and Saba. I feel lucky to have such lovely companions to spend the rest of my life with.

Lastly, I offer my regards and blessings to all of those who supported me in any respect during the completion of the thesis.

Contents

List of Tables

List of Figures

Nomenclature

A	Tank surface area
A_c	Settling area in a centrifuge
AIC	Akaike information criterion
B	Bias (systematic) uncertainty
C	Constant in tangential velocity relation
c	Volume fraction of solid particles in the mixture
c_u	Underflow solid volume concentration
D	Hydrocyclone diameter
d	Particle diameter
d'_{50}	Reduced 50% cut size
D_i	Inlet pipe hydraulic diameter
D_o	Hydrocyclone overflow pipe diameter
D_u	Hydrocyclone underflow pipe diameter

D_1 Diameter of the LZVV relative to the hydrocyclone centerline

D_2 Diameter of the hydrocyclone wall relative to the hydrocyclone centerline

D_{50} Median size of a distribution

d_{50} 50% separation cut size

dr Distance element in radial direction

dt Time element

dz Distance element in vertical direction

Eu Euler number

F Centrifugal force on the particle

$f(c)$ Function of solid volume concentration

F_b Buoyancy force

F_D Drag force on a spherical particle

F_w Weight force

g Gravity acceleration

$G'(x)$ Reduced grade efficiency

$G(x)$ Grade efficiency

g_r Body forces

$G\ factor$ Ratio of centrifugal acceleration to the gravitational acceleration

H	Inlet pipe height
h	Settling tank height
K	Number of model parameters of regression
k	Coefficient in hindered settling velocity
L	Hydrocyclone total length
l	Length of vortex finder in hydrocyclone
L_1	Length of cylindrical portion in hydrocyclone
m	Mass difference between particle and fluid it displaces
m_l	Liquid particle mass
m_s	Solid particle mass
N	Number of observations of regression
n	Empirical exponent in tangential velocity relation
n_d	Number of discs in a disc stack centrifuge
n_p	Optimized exponent in tangential velocity relation
n_{FPS}	Feed pump speed
n_{UPS}	Underflow pump speed
P	Pressure
P^*	Pressure ratio of underflow to overflow

P_i Inlet pressure

P_o Overflow pressure

P_R Power

P_u Underflow pressure

P_x Precision (random) uncertainty

Q Inlet (feed) volume flow rate

Q_n Normalized inlet flow rate

Q_{avg} Mean value of the inlet flow rates

R^2 Coefficient of determination in regression

r_1 Distance between the inlet pipe inner wall and the center line of hydrocyclone; or a radial distance in a centrifuge

r_2 Distance between the inlet pipe outer walls and the center line of hydrocyclone; or a radial distance in a centrifuge

R_f Underflow to inlet volumetric flow rate ratio (Flow ratio)

r_e Effective distance

R_w Water flow ratio (the proportion of feed water entering underflow)

Re Reynolds number

Re_p Particle Reynolds number

RSS Residual sums of squares of regression

t Time

t_r Residence time

t_s Settling time

U Flow velocity

U_x Total uncertainty

V Particle volume

v Hydrocyclone characteristic velocity

v_c Settling velocity in a centrifuge field

v_g Gravitational settling velocity

v_h Hindered settling velocity

v_p Particle settling velocity

v_r Radial velocity

v_s Characteristic settling velocity

v_z Vertical velocity

v_θ Tangential velocity component

W Work

w Inlet pipe width

$\bar{w}$ Work per unit mass

x Particle size

x Indication of horizontal axis

y Indication of vertical axis

Greek Letters

α_i Coefficient of regression, i = 1,2,...

β Variable in equivalent area factor

β_i Coefficient of regression, i = 1,2,...

χ^2 Goodness of fit test

$\Delta\rho$ Density difference between phases

ΔP Pressure drop in hydrocyclone

ΔP_u Underflow pressure drop

δ Uncertainty

μ Dynamic viscosity of the fluid

μ_m Mixture viscosity

μ_o Viscosity at zero concentration

ω Angular velocity

ρ Liquid density

ρ_s Solid particle density

Σ Equivalent area factor

Σ_c Modified equivalent area factor for concentration effect

θ Disc angle in disc stack centrifuge, cone angle in hydrocyclone

Subscript

i Inlet

o Overflow

u Underflow

Abbreviations

LPC Lavanchy et al. performance chart

LZVV Locus of zero vertical velocity

PS Particle size

ESAM Equivalent settling area model

PSD Particle size distribution

RMS Root mean squared

SE Standard error of the coefficients in regression

STD Standard deviation

VFD Variable frequency drive

Chapter 1

Introduction[1]

1.1 Introduction to separation technologies

Separation of particles from a fluid, is an important part of many industries such as in the production of medical products, food, chemical plants and oil industries. This is either to improve the quality of products or to make easier process for other apparatus or to protect environment from undesired waste materials. There are many separation techniques which are used in industry and laboratories, particularly for liquids. These can be categorizing based on the forces employed for separation or phases which are involve or chemicals that are used. Force due to gravity or centrifugal field, acoustic force and electrical forces are some of the forces that are used in separation [16]. For the phase based separation, solid, liquid and gas are

[1]Parts of this chapter are based on R. Sabbagh, M. G. Lipsett, C. R. Koch, D. S. Nobes, "Hydrocyclone Performance and Energy Consumption Prediction: A Comparison with Other centrifugal Separators", Separation Science and Technology 50(6)(2015) pp 788-801 [15]

the three main phases for classification of the separation techniques. Typically, the major component in the mixture is important to determine the separation method. A list of separation techniques is presented in Appendix A-1 which lists different techniques depend on the phases in the mixtures. Solid-liquid separation techniques and ranges of application are listed in Appendix A-2. Particle size is another important parameter in categorizing the separation techniques. Fine, coarse, micro [8] are some terms that are typically used in this field. However, there is no unique definition to categorize particle sizes or particle size based separation techniques. A sample terminology for particle size is provided in Appendix A-3.

Physical separation processes such as centrifugal separators have many applications in industry [17, 18]. Industrial devices have process flows comprising at least two different phases, such as solid particles in a fluid or gas bubbles in a liquid. Separation of phases is often necessary and so separation devices are employed. Some separation processes must be done at very large scale, especially for large industrial users of water. To both minimize clean water use and to improve process efficiency, water re-use or recycling [6] is becoming more prevalent, requiring separation of solid particulate from water.

Several types of solid/liquid separators based on different operating principles are commercially available, including but not limited to: vacuum and pressure filtration, gravity settlers and filtration, centrifugal separators, and force field separators [12, 16]. Focusing on centrifugal-based separation technology, the literature highlights that centrifuges can be used over a broad range of particles, from fine particles (< 5 μm) to coarse particles (> 50 μm) making them an important tool for industry [18]. It is important to a have a suitable methodology for design and

comparison for process efficiency and operating cost.

1.2 Background theory

1.2.1 Equivalent area factor

A physical solid-liquid separator is studied by comparing the settling velocity and flow rate to a simple separation device analogy such as a continuous gravity settling tank [19, 20]. A schematic of the continuous gravity settling tank is shown in Fig. 1.1. For a settling tank with height h, the time needed for a particle to reach the bottom of the tank, the settling time t_s, is obtained from the particle characteristic settling velocity v_s as:

$$t_s = \frac{h}{v_s} \tag{1.1}$$

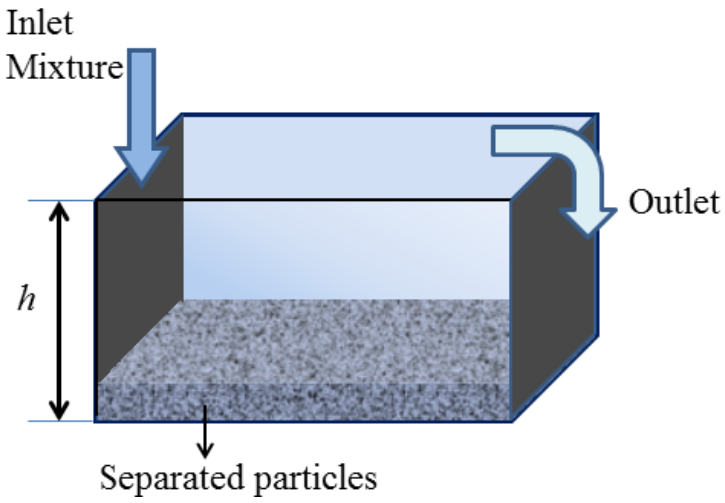

Figure 1.1: Schematic of a continuous gravity settling tank

Particle settling time in the tank should be at least equal to the tank residence time for separation to occur. The particle residence time in a continuous gravity

settling tank is dependent on the flow rate and volume of the tank. Particle residence time t_r is represented as:

$$t_r = \frac{Ah}{Q} \tag{1.2}$$

where A is tank surface area and Q is volume flow rate. Eqs. (1.1) and (1.2) can then be equated, simplified and rearranged to give:

$$Q = v_s A \tag{1.3}$$

which relates volume flow rate to characteristic settling velocity through the surface area of the settling tank. This relation shows that for a tank with unit surface area, the value of characteristic settling velocity is equal to the amount of flow rate.

Using this analogy, an equivalent area factor [21] is defined for centrifuge separators. For a distribution of particles in operation, volume flow rate and gravity settling velocity are correlated [22] and a relation is derived for equivalent area factor (Σ), also called theoretical capacity factor [23] such that:

$$Q = 2v_g\Sigma \tag{1.4}$$

Here, a 50% cut size, where 50% of particles (by mass) which are larger (smaller) than this size pass through each of the outlets of the separator, is used. This size represent separation efficiency of 50%. This size is defined in Fig. 1.2 on a sample separation efficiency curve. The particle size associated with the efficiency equal to 0.5 (50%) is the 50% cut size [24]. The particle 50% cut size is represented by d_{50} and called separation cut size or simply cut size.

The settling velocity v_g under gravitational acceleration (not under centrifugal acceleration) is calculated using Stokes' law [25] such that:

$$F_D = 3\mu\pi U d \tag{1.5}$$

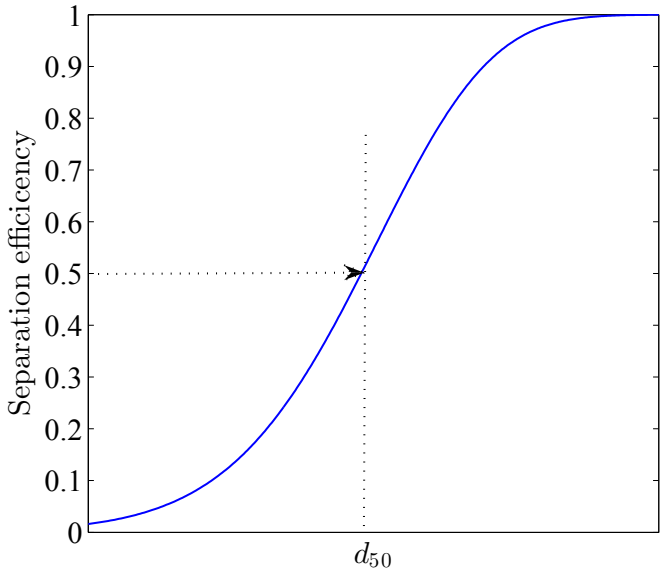

Figure 1.2: Definition of cut size on separation efficiency curve

where F_D is drag force on a sphere particle with diameter d suspended in a flow with velocity U and μ is dynamic viscosity of the fluid. For a particle that settles with settling velocity v_g, balancing the drag force with buoyancy F_b and weight force F_w gives [22]:

$$F_D = F_w - F_b = m_s g - m_l g = mg \tag{1.6}$$

where g is gravitational acceleration, m_l is mass of the liquid particle transported due to movement of the solid particle with mass m_s and m is the mass difference between solid and liquid particles. Replacing these masses with density and volume of the liquid and solid particles and replacing U with v_g results in:

$$3\mu\pi v_g d = (\rho_s - \rho)Vg = \Delta\rho\frac{\pi d^3}{6}g \tag{1.7}$$

$$v_g = \frac{\Delta\rho d^2 g}{18\mu} \tag{1.8}$$

where V is volume of the particle (that is equal for solid volume and volume of liquid particle transported due to movement of the solid particle), $\Delta\rho$ is density difference between phases equals $(\rho_s - \rho)$ and d is particle diameter that is typically 50% cut size particle. Deviation from the assumptions used in developing Stokes' law results in deviation of Eq. (1.8) from theory. Non spherical particles, hindered settling [26], non Newtonian liquid and non uniform flow invalidate the Stokes' law assumptions. It implies from Eq. (1.8) that increasing the particle size, density difference and gravitational force and reducing the liquid viscosity can improve sedimentation of the particle. Among these parameters, increasing the gravitational force is a key element in developing centrifuge separators.

In a centrifuge separator, the gravity acceleration is replaced with a high acceleration field due to centrifugation. This results in increasing the force on particle which in turns increases the settling velocity. Therefore, for a similar settling area, a centrifuge separator can process more flow compared to a gravity settling tank. Replacing the gravity with centrifugal acceleration, the settling velocity in a centrifuge v_c with angular velocity ω can be written as [27, 28]:

$$v_c = \frac{\Delta\rho d^2}{18\mu} r\omega^2 \tag{1.9}$$

This can be rearranged in the following form:

$$v_c = v_g \frac{r\omega^2}{g} \tag{1.10}$$

In an analogous with Eq. (1.4) for a centrifuge separator:

$$Q = 2v_g \frac{r\omega^2}{g} A_c \tag{1.11}$$

where A_c is the settling area of a centrifuge device. The term $\frac{r\omega^2}{g} A_c$ is known as the

equivalent settling area of a centrifuge device and is calculated for different types of centrifugal separators [22].

1.2.2 Hindered settling

Typically increasing the concentration bring the particles closer to each other, which in turn allows them to cluster. This should increase the settling velocity, however, in most situations such as the flow in a hydrocyclone (where the shear rate is high) the cluster does not survive and the settling rate reduces with increasing concentration [29]. This is known as hindered settling [26] and is mathematically combined with the settling velocity relation and a function of concentration such that:

$$v_h = v_g f(c) \tag{1.12}$$

where v_h represents the hindered settling velocity and c is solid volume concentration in the mixture [30].

One dimensional models are usually developed to predict the hindered settling velocity [31]. These models assume that there is no flow across the directions other than the settling direction. This assumption can represent many phenomena in the real world applications [31]. The one dimensional assumption brakes where the particles are considerably large compared to the settling distance as the ratio of the particle diameter to the settling distance is greater than 10^{-4} [31].

A well-known relation for the effect of concentration on Stokes (gravitational) settling velocity has been proposed by Richardson and Zaki [32]. It has been observed that the settling velocity changes with changes in the solid fraction c in the mixture such that the Stokes settling velocity v_g multiplies in $(1-c)^k$ and k is a coefficient that is experimentally determined to be 4.75 [32]. Several researches have

been dedicated to this subject such as [31, 33–36]. A method for determining k is presented in [36] and it is shown that the value of k is dependent on the material and may vary significantly from what is suggested by Richardson and Zaki [32]. For sand particles, a review of the settling models can be found in [30].

1.3 Literature review

Centrifuges or centrifugal separators are types of separators that are used either to separate or classify particles. These devices are categorized as fixed wall or moving wall separators. Comparisons of performance and energy consumption in such equipment are important for device selection and design. Particularly, a comparison between the fixed wall and moving wall centrifuge separators can be important considering the advantages and disadvantages of the two types of centrifugal separators.

1.3.1 Centrifugal separators

Centrifuges, also called centrifugal separators, are relatively simple devices that separate particles from a fluid based on the particle/fluid density difference. In a gravity separator, particles are separated with a settling velocity under the influence of gravity, which is calculated using Stokes' law [25]. Centrifuges increase the sedimentation efficiency through increasing particle settling velocity. This can be achieved by accelerating the particle/fluid mix in a high curvature rotating field, often aligned normal to the gravitational field. A much larger force than weight due to gravity can be realized on the denser phase, causing the dense material to move toward the outer wall of the device. The dense phase leaves the field (and the device) typically at the outside radial location. Conversely, the less dense phase is forced toward the center and leaves the separator on the centerline of the rotating field. The rate that separation occurs is governed by the *G-factor*, the ratio of acceleration in the centrifugal field to the acceleration in a gravity field. The *G-factor* may vary from 70 to 65,000 for different centrifuge devices depending on their size

and design specifications [16]. With the potential to apply such a strong force on suspended particles, centrifuges are commonly used in industry for separation as they have simple construction, handle a variety of flow rate throughput, and operate in either a batch or a continuous process [18].

Solid-liquid centrifugal separators can be sub-divided into either moving wall or fixed wall (hydrocyclone) categories as shown in Fig. 1.3. Tubular bowl [37], scroll decanter [38] and disc stack machine [39] are different types of rotary/moving wall centrifuges that can be employed for both solid-liquid sedimentation separation or for liquid-liquid separation [37]. Tubular bowl centrifuges can handle small throughputs with low concentration and can be used in semi-continuous processes [16]. Decanters can handle a variety of sludge in large amounts even with high concentration systems but they may have poor quality in outlet liquid and are more affected by fluctuations in the inlet feed [40]. Higher maintenance costs and a high wear rate are disadvantages for this type of separator. Similarly, disc stack centrifuges can be employed for large throughputs of sludge with finer particles and produce supernatant of good quality [40]. However, disc centrifuges have high maintenance requirements as they are complex and expensive devices and larger particles may cause them to clog [16].

The equivalent area factor Σ, (with SI units of m^2) of a gravity settling tank with the same separation capability as a centrifuge that has the same equivalent area factor can be calculated. Here, it is assumed that an individual particles settle without any interaction with other particles, as opposed to hindered settling [32]. Equivalent area factor (capacity factor) for a tubular bowl, disc stack and scroll decanter centrifuge separators have been derived by Ambler [22] and are defined

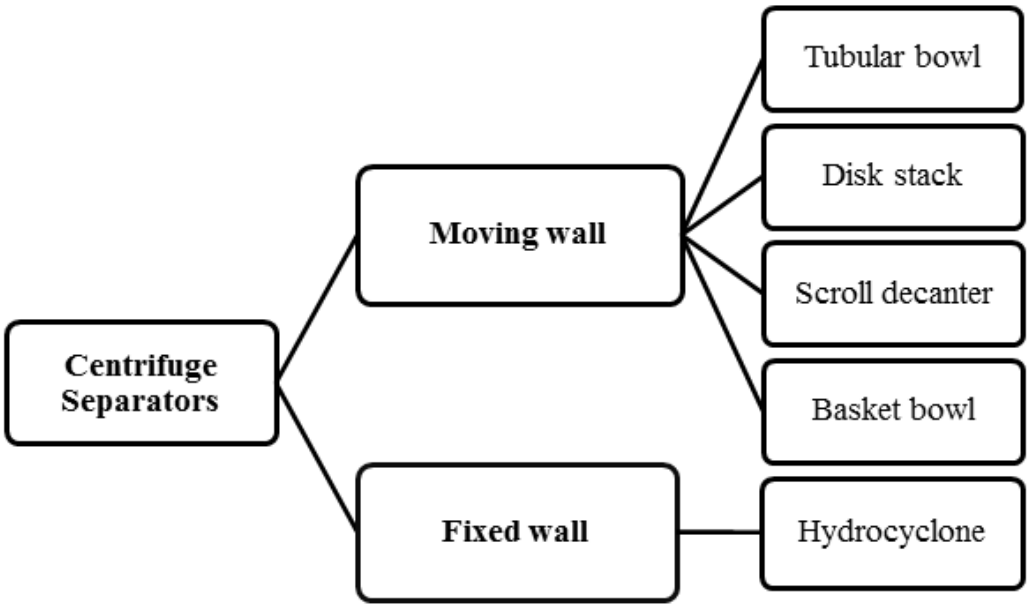

Figure 1.3: Types of centrifugal separators

as:

$$\Sigma_{tubular} = \frac{2\pi l\omega^2}{g}(\frac{3}{4}r_2^2 + \frac{1}{4}r_1^2) \tag{1.13}$$

$$\Sigma_{disc\ stack} = \frac{2\pi n_d\omega^2(r_2^3 - r_1^3)}{3g\tan\theta} \tag{1.14}$$

$$\Sigma_{decanter} = \frac{2\pi\omega^2}{g}[l_1(\frac{3r_2^2 + r_1^2}{4}) + l_2(\frac{r_2^2 + 3r_1r_2 + 4r_1^2}{8})] \tag{1.15}$$

where ω is angular velocity of centrifuge device, and n_d is the number of discs in a disc stack centrifuge. A number of specific geometric parameters are also needed for each specific design type. The definition of each of these is illustrated in Fig. 1.4 to Fig. 1.6 for the corresponding device. Each figure shows the location of a single particle in relation to geometric features of the different separators.

Considering Eq. (1.4), the ratio of volume flow rate to equivalent area factor Q/Σ is the characteristic velocity of the system. That is, twice the settling velocity

of particles at the particle cut size under gravitational settling. Knowing properties of the particle and fluid, it is possible to find the diameter of a particle that is settling in a separator by utilizing Stokes' settling velocity. Higher values for Q/Σ indicate larger particle separated in a centrifuge as a result of either higher flow rate or smaller capacity factor. The equivalent area factor can be applied for evaluating the performance of different centrifugal separation devices [22].

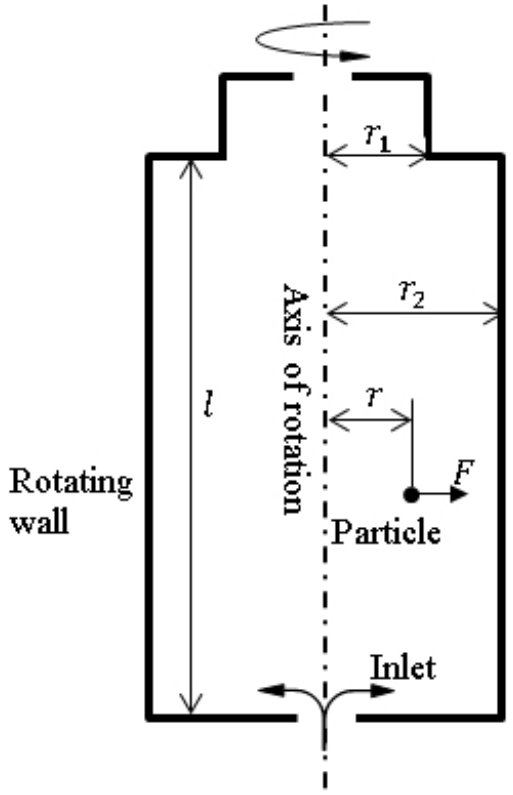

Figure 1.4: Schematic of tubular bowl centrifuge with a settling particle

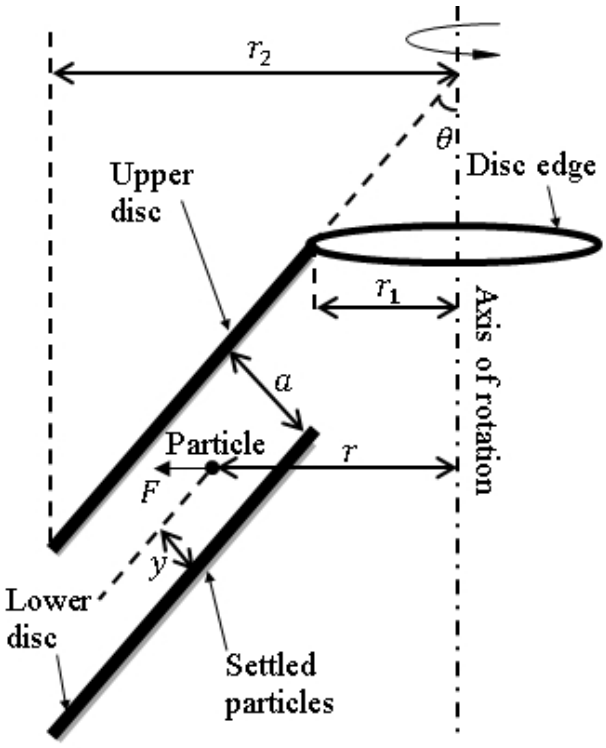

Figure 1.5: Schematic of two discs in disc stack centrifuge with a settling particle

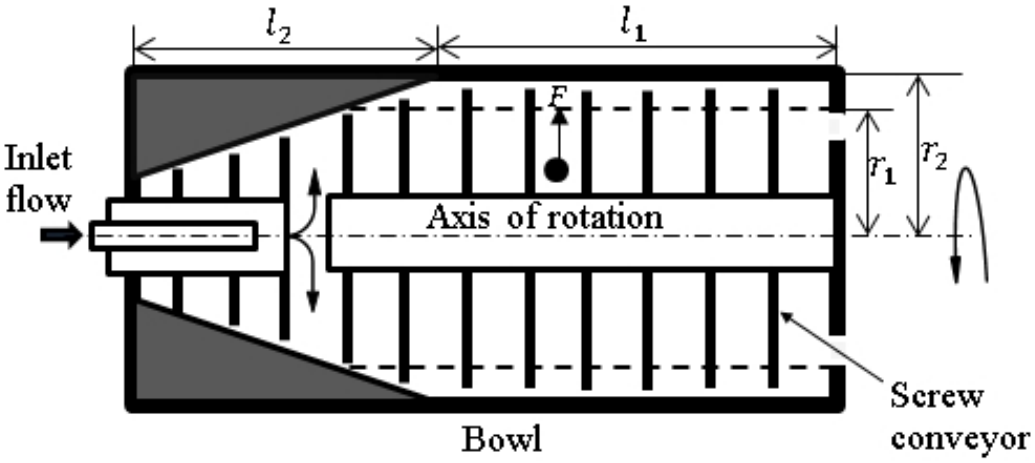

Figure 1.6: Schematic of decanter centrifuge

1.3.2 The Lavanchy chart

Centrifuge separators are usually designed through a scaling procedure using scaling factors. Since these factors are calculated based on simplifying assumptions such as Stokes' law and evenly distributed particle sizes, they are usually augmented by empirical correlations. The equivalent settling area factor, Σ is a scaling parameter proposed by assuming plug flow in a centrifuge device [22]. Equivalent area factor is an indication of separation device performance compared to a continuous gravity settling tank. This factor is combined with flow rate to design geometrically similar centrifuges. To overcome the simplifications used in deriving the equivalent area factor, this factor is multiplied by an efficiency factor to obtain the scaled-up overflow. Efficiency factors are documented in the literature and are 0.45-0.73 for disc stack centrifuges, 0.54-0.67 for scroll decanters, and 0.90-0.98 for tubular bowl centrifuges, respectively [41].

Selecting a centrifuge for a specific application is also dependent on many other parameters that are installation or application specific. These include: desired particle size in the outlet, cost of installation and operation, space availability, working environment, and properties of the feed flow. For instance, tubular bowl centrifuges can treat solid volume concentration of 0-4% whereas this range is 1%-30% and 5%-80% for continuous nozzle disc and decanter centrifuges respectively [42]. During the development of centrifuge technology several guidelines for selecting centrifugal separators have been developed that provide recommendations based on the type of application, concentration of mixtures, and particle size in the phases [43–45]. Terminology used to define particles and particle size are described in Appendix A-3 Most of these guidelines, as in [9], are based on particle size and

inflow concentration.

Utilizing an empirical correlation and theoretical model, [23] generated a limited performance and energy chart for comparing hydrocyclones and disc centrifuges. Later, following Keith's study [23], Lavanchy et al. [10] proposed a performance chart for comparing centrifugal separators along with hydrocyclones. This chart is regenerated in Fig. 1.7 and has been used as a guideline chart for sedimentation centrifuge separators selection and design [9, 12]. The Lavanchy et al.'s performance chart (LPC) [10] represents centrifugal devices performance utilizing twice gravitational settling velocity of particles $2v_g$ and volumetric flow rate Q on logarithmic scales. For a known density difference between phases, fluid properties and particle size the gravitational settling velocity is calculated and knowing the process flow one or more appropriate devices can be determined from the chart. It also shows the limits of each device for the amount of flow that can process or the range of settling velocity of the particles that can be separated by a separator. Since settling velocity is a function of particle size, this leads to a range for particle size in separation for each device. It also shows how effective a centrifuge separator is comparing the performance of a continuous gravity settling tank with unit settling area of 1 m^2.

This chart allows the selection of a centrifugal device for a specific separation application based on the flow properties such as the flow rate in the process, density difference between the solid and liquid phases and the required separated particle size. Knowing the densities, fluid properties and the particle size the gravity settling velocity is obtained from Eq. (1.8). The amount of the flow rate together with this settling velocity can refer to a point on the chart within the region of a separator device. This separator device can be a desired separator for such flow properties.

When there is an overlap between the devices, there is more options than a single device to process the flow. The LPC is introduced in the literature as a guideline chart for selection and design of centrifugal separators [9, 12, 38, 46].

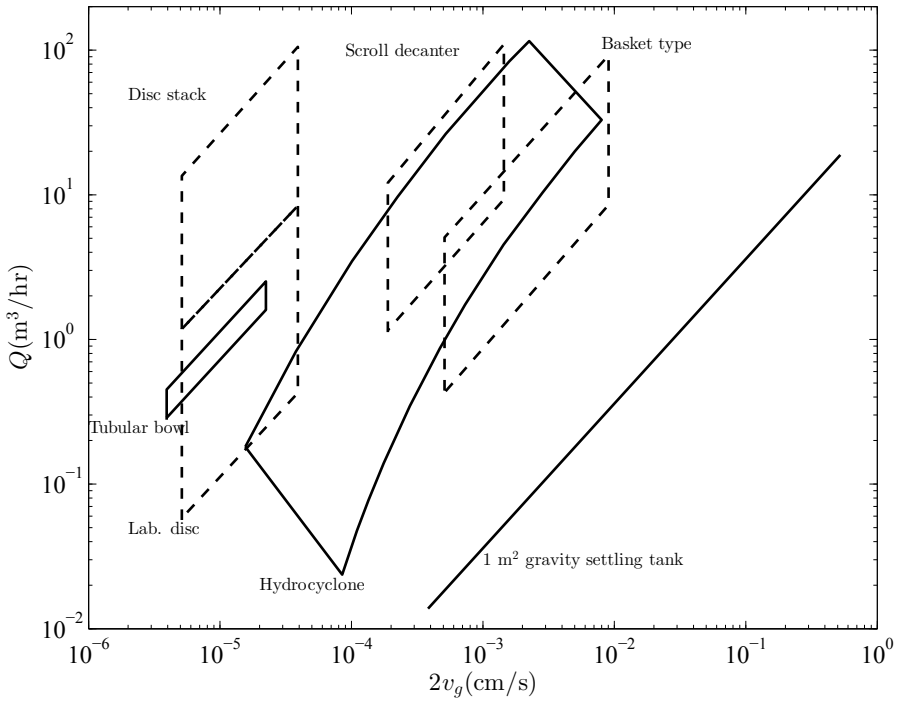

Figure 1.7: Performance of sedimentation equipment; regenerated from [9]

Although the chart provides a good tool for selecting the device, it cannot show which device is better when there is an overlap on their performance region on the chart. This needs more information to help selecting a device such as the concentration of the particles in the process. The energy consumption analysis can also help in solving such issue. The LPC [10] initially published in 1964 and was republished by [46] in 2005 with no changes. Hence, it is expected that the chart does not take into account ant progress in the centrifuge technologies. Using the hydrocyclone performance chart and the particle size associated with it from [46], it is also found that the chart cannot predict the common types of hydrocyclone performance.

The determination process behind this chart has not been released in details. Clearly, some minimum and maximum values for equivalent area factor of different centrifuge separators have been used to derive a performance range for each device. It is not clear, however, how those values are obtained. The derivation method of the equivalent area factor for hydrocyclone is not clear, too. Therefore, there is a need to evaluate the LPC to examine how well it predicts the performance of the centrifugal separators of the current technology in order to update it into a more effective chart.

While centrifuge separators are still operating according to designs that date back to original concepts, recent information [47] shows that current separators are designed with larger equivalent area factor values. Although the LPC [10] has been applied as a guideline performance chart for centrifugal separator for many years, a design method based on information related to the latest progress in centrifugation technology would improve predictions. It should also have the capability to be used as a part of a model for comparative evaluation of energy and performance for a wider set of devices.

Energy consumption is another important factor that should be considered along with separation performance in the selection and design of centrifugal separators. While there has been some research related to the cost of centrifugation, those studies have restricted the cost to parameters such as materials, manufacturing, and installation [48, 49]. Empirical correlations and studies investigating disc centrifuges and hydrocyclones to predict the operating specific energy consumption are considered in [23]. Other than that, operational or settling-related energy efficiencies of different centrifuge separator devices have not been compared in the literature. Al-

though different centrifuges are used in a variety of applications, it is important to have a good understanding about their energy consumption in a specific application and there is still a need for further investigation into energy consumption of other different sedimentation centrifuge separators.

1.3.3 Hydrocyclones

Hydrocyclones are used in industrial processes to separate liquid or solid particles from a liquid phase of a different density [6, 50–55]. Hydrocyclones have a fixed wall for the separation chamber and are based on implementing a centrifuge force that is generated by a tangential inlet of a high velocity stream into the cyclone chamber. Interaction with the wall turns the flow, creating centrifugal acceleration force which drives the separation of the particles from the liquid. The mixture is usually pumped to the inlet pipe where it is directed tangentially to the hydrocyclone chamber. The flow starts to rotate and the centrifugal force due to rotation pushes the denser phase toward the hydrocyclone wall where it is separated. The separated particles leave the chamber through the outlet pipe. However, since separation is not perfect, a portion of each phase leaves the hydrocyclone at both the overflow and underflow.

Compared to other types of centrifuge separators, hydrocyclones have no moving parts and therefore have low maintenance costs [13]. Hydrocyclones are considered to be relatively low capital cost devices that are easy to install [13]. They are inexpensive to construct and they need little space for installation and operation. High capacity and simplicity are of the other advantages of this separation apparatus [54]. Hydrocyclones are sensitive to flow rate and they produce wall shear

forces that result in wear [29]. In addition, the flow has a limited residence time under the high *G-factor* loading for achieving separation of the particle/fluid stream. This specific feature of hydrocyclones makes them different from other centrifugal separators in both design and application. Although both centrifuges and hydrocyclones are possibilities as compact separators, when the available space is a limit for selecting a separator device, the chosen separator is usually a hydrocyclone due to economic reasons [56].

To understand the swirling flow in the hydrocyclone, the flow pattern has been investigated through experimental measurement of velocity components [7, 57–61]. In addition, models have been developed to predict the hydrocyclone behavior [5, 62–70]. These include empirical models [1, 5, 66, 71], analytically developed models on the basis of physics of flow in the hydrocyclone [62–64, 67, 69, 72] and more often, numerical models [73–75]. Review of such studies can be found in [73, 76–78]. Although models have been developed to predict the performance of the hydrocyclones, these models are not in a form that allows direct comparison with other types of centrifugal separators.

The equivalent settling area is a concept used to compare the performance and scaling up of different centrifugal separators [12, 20]. For hydrocyclones, despite the importance of the performance in terms of the equivalent area there is limited available information for developing the equivalent area [15, 79]. A mathematical model to obtain the equivalent settling area of the device is lacking in the literature. As the equivalent settling area in centrifuges is derived for a cut size particle in the device, such a model should be based on the same concept to make it possible to be compared with other centrifuge separators. This concept is known as residence

time theory. A model has been proposed by [23] for determining equivalent area in hydrocyclones, but the derivation technique has not been fully explained. It is also observed that the proposed model uses the relations in [62, 80] for tangential velocity that are based on equilibrium orbit theory [13] which is inherently different from residence time theory [13].

Geometry

A schematics of a hydrocyclone and its components are shown in Fig. 1.8. Hydrocyclones typically have a cylindrical section at the top attached to a cone shape portion in the bottom. The length of the cylindrical and conical portions vary from manufacturer to manufacturer. In some cases the cylindrical section in extended to the bottom and the conical section is removed. Two well-known geometrically similar hydrocyclones are Rietema [12] and Bradley hydrocyclones [12]. These hydrocyclones are similar in shape but different in size and cone angle. The cylindrical portion diameter is used to define the size of other components of the hydrocyclone including the inlet, overflow and underflow diameters, vortex finder, cylindrical portion and total length in a hydrocyclone as they are proportional to the diameter of the cylindrical portion shown in Fig. 1.8. The hydrocyclone diameter varies between 10 mm and 2.5 m [81].

Inlet pipe

The inlet pipe in a hydrocyclone has either a circular or a rectangular cross-section. This pipe is attached to the cylindrical portion of the hydrocyclone in a way that conducts the flow to follow the geometry of hydrocyclone wall to provide a smooth flow pattern. Tangential and involuted entry are two common types of inlet geometries. Some hydrocyclones are designed with more than one inlet pipe

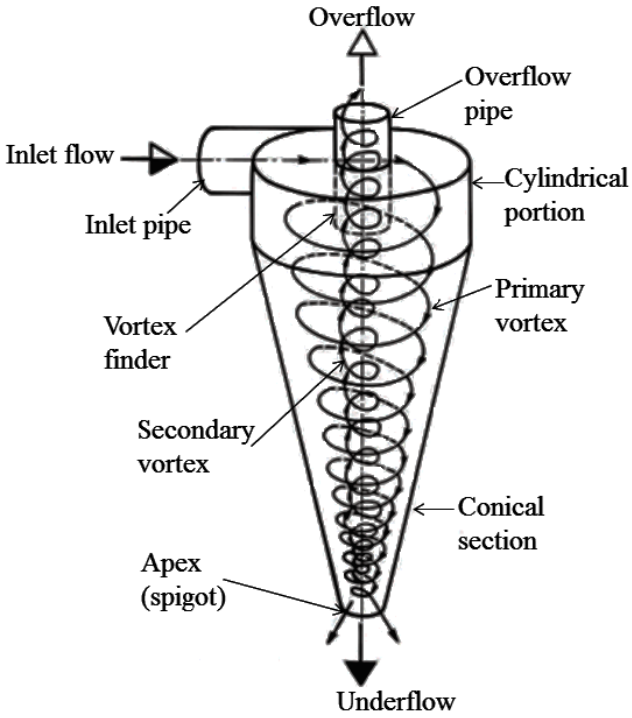

Figure 1.8: Trajectory of particles in a hydrocyclone and the definition of the hydrocyclone portions

to achieve a better symmetry in the flow [82]. Increasing the inlet pipe size results in reducing the inlet kinetic energy and hence increases the separated particle size.

Overflow pipe

This pipe is attached to the cylindrical portion on the top and extended into the hydrocyclone. The extended portion of this pipe is called the vortex finder. Finer particles separated from the mixture leave the hydrocyclone through the overflow pipe. This is usually known as the clean part of the separation in hydrocyclones with solid-liquid mixtures. Increasing the overflow pipe size increases the amount of coarse particles in the underflow [13].

Underflow pipe

The pipe that the coarse part of the separation pass through it is known as the underflow pipe and the section is some times called the apex or spigot. This pipe

has an important role in hydrocyclones as it is used to control the separation performance. The shape of the underflow may vary from a spray (or umbrella) shape [83] to a rope shape [83] and is an indication of the effectiveness of the separation. Changing the underflow pipe size affects the shape of the underflow slurry. Reducing the apex size results in increasing the coarser particles in the underflow and reduces the portion of the flow that leaves the hydrocyclone through the underflow pipe [13].

Flow rate and pressure drop

Pressure drop and flow rate are interdependent variables for a hydrocyclone. The pressure drop is typically considered the difference between inlet pressure and the overflow pressure. This is approximately equal to the square of the flow rate [13] ($\Delta P \sim Q^2$). Typically, pressure drop increases with flow rate to the power of greater than two. Experimental correlations show that the pressure drop and flow rate are connected to each other through other variables such as design parameters and feed solid concentration. Some of the empirical correlations are investigated in [1]. The pressure drop in hydrocyclones varies between 34 kPa to 586 kPa and the feed flow rate varies between 0.1 m^3/hr to 7,200 m^3/hr depending on the hydrocyclone diameter [81].

Particles

As the separation in hydrocyclones are based on density difference, there should be a finite difference between density of solid particle and liquid phase. Increasing the density difference increases the separation performance. The shape and size of the particles affect the separation. Particle shape directly influences the settling velocity as the drag force changes with the shape [82]. Large particles usually

sediment to the hydrocyclone wall and are separated. The fine particles however may entrain with the liquid phase and leave the hydrocyclone through the overflow pipe or they may attached to the coarse particles or trapped in the wakes around the larger particles and particles and go to the underflow portion. This results in a change in the fine section of the particle size distribution known as the fish hook effect [70, 84, 85].

Feed concentration

It has been observed that the performance of a hydrocyclone is affected by feed solid concentration. High concentration of solids in the hydrocyclone leads to lower settling velocity comparing to the Stokes settling velocity. Influence of inlet solid concentration on the hydrocyclone performance has been studied theoretically and experimentally [26, 86]. Increasing the feed concentration and keeping all other parameters constant results in more particles in the overflow and coarser particles in the underflow [26]. This has been interpreted as the effect of hindering in radial direction where particles move toward the wall [26]. Limited capacity of the underflow diameter and changes in the flow field are named as other reasons for entrainment of the particles in the hydrocyclone which eventually lead to less efficiency of separation. A reduction in pressure drop at higher flow rates has also been related to the effect of hindered settling [26].

Attempts have been undertaken to model the effect of solid concentration in hydrocyclones by applying a function of solid volume fraction in the mixture c into a hydrocyclone performance model [5, 70, 87–89]. Some researches have adopted the Richardson and Zaki [32] hindered settling correlation into their hydrocyclone models [87, 90] and some have formed a different nonlinear relation from gravity

settling relation [70, 91].

As the theoretical solution for the effect of hindered settling is complex, most of the models are based on experimental correlations. Performing the experiments and developing experimental correlations for sets of different designs of hydrocyclones, [5] shows that concentration affects the hydrocyclone parameters (such as pressure drop, flow rate and cut size).

Flow control

The separation performance of a hydrocyclone is affected by the inlet flow conditions. This is a major disadvantage of hydrocyclones [92] when the upstream flow conditions fluctuate. In a solid-liquid hydrocyclone, changes in the inlet flow rate, particle size distribution, particle shape and concentration affect the outlets flow properties. Changes in the separation efficiency as a function of the separation cut size (the particle size that has 50% chance of being separated in the device) and the flow ratio (the ratio of the volumetric underflow flow rate to the feed flow rate) are observed. For some operating conditions, this may lead to impracticability of using a hydrocyclone at some conditions. Controlling the hydrocyclone performance is desired to avoid such conditions [13].

There are several methods available for monitoring and controlling the hydrocyclone performance. These methods are either based on the shape of the air core [93–96], the internal particle distribution [97] or the shape (spray/rope) or other properties of the underflow [83, 98]. The control typically actuates a flow stream at either of the inlet [99] or the outlets [100, 101]. For instance, a set of hydrocyclones that are used in a group have been controlled by regulating the overflow [92]. Other methods include injecting water through the hydrocyclone wall [102], water injec-

tion to the underflow discharge pipe [103] or using an electrical hydrocyclone [90] which can be used to control the device separation performance.

The flow stream in a hydrocyclone is usually controlled by changing the geometry and particularly by changing the apex size (shown in Fig. 1.8). Changing the apex size changes the underflow capacity and therefore the solid concentration and the separation cut size [104, 105]. Commercial hydrocyclones are often supplied with several replaceable orifice sizes to allow the appropriate size to be used based on typical operating conditions. In addition, several designs for the underflow orifice are available [6, 13]. Different types of discharge orifices that are used for manipulating the underflow are discussed in [13].

Since changing the underflow diameter is not always feasible, a valve at the underflow is also used to control the flow [6]. This valve is adjusted either manually or automatically by a control valve. However, this method has the risk of blocking the apex and should be used with caution. Although solutions to avoid apex blockage have been developed, both changing the apex pipe size or using a throttling valve at the underflow have the disadvantage of increased chance of clogging in the underflow pipe.

1.3.4 Summary

The literature review shows there is a need to compare the performance and energy consumption of the centrifuge separators with hydrocyclones. The equivalent area factor can be used as a useful criterion for performance comparison. A guideline performance chart published in 1964 (LPC) was discussed. The determination procedure for the charts has not been fully explained in the literature. In addition, no evidence has been found in the literature showing that the chart areas have been validated for centrifuge separators or hydrocyclones. It was highlighted that a model that can predict the equivalent area of hydrocyclones is lacking in the literature. Therefore, LPC needs to be evaluated for the performance of the centrifugal device to verify the functionality of the chart and to update it for the progresses in centrifuge technology since 1964. Also, a model to predict the performance of a hydrocyclone device in terms of equivalent area factor needs to be developed.

1.4 Scope and objectives

The main objectives of this thesis that define the scope of the work are:

- development of a method to compare the performance and energy consumption of hydrocyclones with other centrifugal devices,
- theoretical and experimental study of the developed model that describes the equivalent area factor for hydrocyclones,
- investigation of the effect of solid concentration on the equivalent area factor,
- investigation of the effect of hydrocyclone underflow pumping in order to be used as a control technique.

To achieve the objectives, the equivalent settling area factor is used as an important criterion for comparing the performance of the centrifugal separator equipment. This factor is calculated for centrifuge separator according to the most recent available information in the literature for the current technologies of centrifuges and hydrocyclones and the LPC performance chart is evaluated.

A mathematical model is also developed to predict the hydrocyclone performance and the results are compared with the performance of the centrifuge separators. The specific energy consumption in the centrifugal separators is calculated by developing a mathematical model. This model considers the forces applied on a particle that is suspended in a centrifugal field and obtains the amount of energy that is consumed to sediment the particle in a centrifugal separator.

The developed model for hydrocyclone performance is validated by performing a set of experiments at different operating conditions. This model is further

investigated and modified for the effect of concentration and is validated using the experimental data.

To investigate the underflow pumping effect, a test rig is designed and built for this study using a commercial hydrocyclone. The setup is equipped with an underflow pumping device to experimentally study this effect on a hydrocyclone performance. An empirical correlation is also developed to predict the underflow pumping effect on hydrocyclone operating variables.

1.5 Thesis organization

In Chapter 1 the research is introduced and the background theory of this research project is explained. A detailed literature review for centrifuges and hydrocyclone performance and energy consumption modeling is provided with a focus on identifying and developing a criterion and its application for comparing the performance of the hydrocyclone and other centrifuges. Following the literature review, the research objectives and the scope of the work and the organization of the thesis are described.

In Chapter 2, a semi-empirical model is developed to predict hydrocyclone performance. This model and available information from the literature are used to develop a performance chart that allows comparing the performance of different centrifugal separators including hydrocyclones. This performance chart is compared with an available chart in the literature and the differences between the charts are detailed by highlighting the need for developing a mathematical model for hydrocyclones. A theoretical model is also developed in this chapter to predict the energy consumption required to sediment a single particle in a centrifuge or hydrocyclone separator. This model is a basis for developing an energy chart to compare the energy consumption of the devices that is undertaken in this chapter.

In Chapter 3, the experimental setup and procedure are detailed. The test rig and its features are explained, the details of performing the experiments and particle sizing are described and a sample data from particles is discussed to help understanding the repeatability and reproducibility in sampling. The uncertainty in the measurements and the accuracy of the measuring device are also detailed and the

novelty of the experimental setup for pumping the underflow is discussed.

In Chapter 4, the modeling approach for developing a theoretical model for hydrocyclone equivalent settling area factor is detailed. A model is developed from the basic concepts that allows predicting the equivalent area factor for hydrocyclones under low concentration inlet flow. The model is validated with experimental data of the current study and literature. The developed model is then used to predict the tangential velocity profile in hydrocyclones and the result is validated with data from literature.

In Chapter 5, the equivalent area factor model is modified for the effect of solid concentration in the inlet flow and details of modification technique is described. This modified model allows prediction the equivalent area factor under low to high inlet solid concentration. Guideline charts are developed based on this model that are helpful in selecting and design of hydrocyclones and comparing the hydrocyclone performance with centrifuge separators. An updated performance chart is provided for the hydrocyclones.

In Chapter 6, the effect of using a pump in the hydrocyclone underflow to control the system is investigated. The investigation is based on an experimental study using the novel experimental setup. The experimental data is used to study the effect of underflow pumping on the bulk flow characteristics. Following the evaluation of the pump effect, an experimental model is developed that allows predicting the pumping influence on hydrocyclone operating variables.

Finally, in Chapter 7, the main concluding remarks of the analytical and experimental studies of this thesis are explained and the main contributions of this work are highlighted. Following that, an overview of possible future steps and directions

of this work and and the research contributions are listed.

In the appendices, a summary of separation techniques (Appendix A-1), solid-liquid separation methods and range of applications (Appendix A-2), a simple particle terminology (Appendix A-3) and the uncertainty in calculation of the equivalent area factor in the experiments (Appendix A-4) are provided. The Stokes' law assumption for the hydrocyclone and particles used in this research is justified in Appendix A-5.

Chapter 2

Modeling performance and energy consumption[1]

2.1 Introduction

The importance of separation performance and energy consumption in centrifugal separators, the significance of the equivalent area factor and the application of the energy and performance charts were discussed in Chapter 1. It was shown that there is a lack of a model in the literature to predict the equivalent area for hydrocyclones from the basic principles of the equivalent area factor. To address this, a predictive model to compare the performance and energy consumption of the different centrifugal devices to each other and to a simple separation device such as a gravity settling tank is the focus of this chapter. Using the concept of equivalent area factor the performance of centrifugal separators are calculated based on the available information in the literature. For hydrocyclones, an equivalent area factor is modeled based on a semi-empirical equation from the literature. The performance results are then compared with Lavanchy et al.'s performance chart (LPC) and discussed.

[1]Parts of this chapter is based on R. Sabbagh, M. G. Lipsett, C. R. Koch, D. S. Nobes, "Hydrocyclone Performance and Energy Consumption Prediction: A Comparison with Other centrifugal Separators", Separation Science and Technology 50(6)(2015) pp 788-801 [15]

Applying the forces on a single particle sedimenting in a centrifuge separator and a hydrocyclone the specific energy consumption is modeled. The obtained energy consumption relations are then used to develop charts that allow comparing the centrifugal separator devices. The results for performance and energy consumption in hydrocyclones are also compared with experimental data from literature and discussed in detail.

2.2 Performance chart development for centrifugal separators

2.2.1 Centrifuge separation performance

Utilizing the equivalent area factors defined in Eqs. (1.13) to (1.15) with Eqs. (1.4) and (1.8), it is possible to generate a performance chart to compare different centrifugal separators. There are several parameters needed for creating a performance chart, including flow parameters and system characteristics. Among those parameters the equivalent area factor is independent of flow characteristics in centrifuge separators and is a function of the geometric characteristics of the centrifuge (as detailed in the previous section). Applying suitable dimensions and angular velocity of a separator, the equivalent area factor value is calculated from Eqs. (1.13) to (1.15) for tubular bowl, disc stack and scroll decanter centrifuges. From the settling velocity, the volume flow rate can be obtained using Eq. (1.4) and an expected range of typical conditions can be used to develop a performance chart. This process, from calculating equivalent area factor to calculation of volume flow rate, should be repeated for several sizes and rotational speeds of each device over the range of

settling velocities of particles to generate Q and Σ for each device. Data generated for volume flow rate and settling velocity can be inserted into a chart and bounded to demonstrate a region of performance for a particular separator. Plotting different separators on the same chart then allows for direct comparison of operational ranges.

While it is vital to know the design parameters of centrifugal separators (such as physical dimensions, rotational speed, etc.) to obtain the equivalent area factor, these parameters are proprietary and are not usually readily available. Centrifuge dimensions and rotational speeds are instead obtained from the literature [47] and the calculated theoretical equivalent area factor is then multiplied by the efficiency factor of each device. Efficiency factors in this study were selected to be 0.95 for tubular bowl centrifuge, 0.70 for a disc stack centrifuge, and 0.62 for a decanter centrifuge, in agreement with suggested ranges [41].

2.2.2 Overview of hydrocyclones separation performance

For hydrocyclones, unlike other types of centrifugal separators, the speed of rotation of the flow is not a design parameter as it is a function of the inlet flow rate, which in turn is directly related to the pressure drop across the hydrocyclone. Hence, the theoretical equivalent area factor for a hydrocyclone is not simply a characteristic of the system as with other centrifugal separators. In this work, the performance of hydrocyclones has been first investigated through empirical correlations in order to find flow rate and settling velocity. The hydrocyclone used is designed according to aspect ratios suggested in [106]. With the aid of empirical correlations, the separation performance of hydrocyclones is predicted for a range of small to large

hydrocyclones with diameters from 10 mm to approximately 1000 mm. This is undertaken using the Plitt empirical model [71] which has a good accuracy compared with other empirical models [66, 107] given as:

$$\Delta P = \frac{1.316 \times 10^5 Q^{1.78} \exp(0.55c)}{D^{0.37} D_i^{0.94} (L-l)^{0.28} (D_u^2 + D_o^2)^{0.87}} \tag{2.1}$$

$$d = \frac{0.00269 D^{0.46} D_i^{0.6} D_o^{1.21} \exp(6.3c)}{D_u^{0.71} Q^{0.45} (L-l)^{0.38} (\rho_s - \rho)^{0.5}} \tag{2.2}$$

$$Q = 0.00133 \Delta P^{0.56} D^{0.21} D_i^{0.53} (L-l)^{0.16} (D_u^2 + D_o^2)^{0.49} \exp(-0.31c) \tag{2.3}$$

where Q is inlet volume flow rate, d is 50% cut size, ΔP is the pressure drop across the hydrocyclone (between the inlet pressure and overflow pipe pressure), μ is dynamic fluid viscosity, ρ and ρ_s are liquid and solid densities, c is solid volume concentration (fraction). SI units must be employed and all other parameters are hydrocyclone dimensions as defined in Fig. 2.1.

For two cases of small and large solid-liquid density differences of 50 kg/m^3 and 3000 kg/m^3, pressure drops and particle cut size in the hydrocyclone are obtained from the Plitt model [71]. This procedure is repeated for several inlet flow rates. Since pressure drop in hydrocyclones is a function of flow rate, iteration is required. An initial flow rate is chosen and then corrected according to the pressure drop to be in the range of 40 to 600 kPa [13] which refers to a minimum and a maximum flow rate. When calculating the flow rate, the fluid density is assumed to be 1000 kg/m^3 with the viscosity of 1 mPa.s (water). Different cases of solid volume concentration from 0.005 to 0.2 are substituted into Eq. (2.2) for calculating 50% cut size of

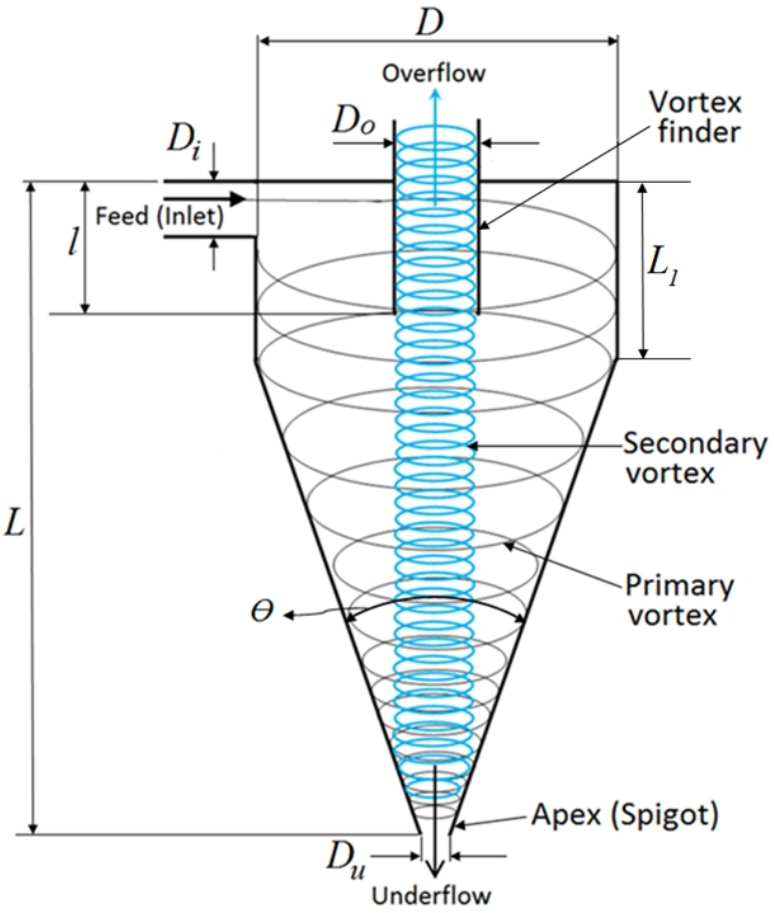

Figure 2.1: A schematic of a hydrocyclone showing basic components and operation principles

particles. The gravitational settling velocity is calculated from the particle cut size and Eq. (1.8). This value is utilized to evaluate the separation performance.

Derivation of a equivalent area factor for hydrocyclones is scarce in the literature. Utilizing an empirical correlation and a theoretical model, Keith [23] tried to use this concept for hydrocyclones and developed an equivalent area factor relation. Assuming a simplified settling area for the hydrocyclone Rovinsky [108] developed an equation supported with empirical coefficients for the equivalent area factor of a hydrocyclone. Neither of these two works validated their results with

experimental data. Although the equivalent area factor in hydrocyclone depends on operation characteristics, it is possible to define an equivalent area factor based on flow modeling, flow properties and experimental knowledge [106]. The following is a semi-empirical relation for flow properties in a hydrocyclones developed by Rietema [106] for a set of geometrically similar hydrocyclones:

$$d^2 \Delta\rho L \Delta P = 3.5 \mu\rho Q \tag{2.4}$$

Rearranging Eq. (2.4) to be analogous to Eq. (1.4) and using Eq. (1.8) gives Σ, the equivalent area factor of a hydrocyclone as:

$$Q = 2v_g(\frac{18L\Delta P}{7\rho g}) \rightarrow \Sigma_{hydrocyclone} = \frac{18L\Delta P}{7\rho g} \tag{2.5}$$

This semi-empirical equivalent area factor is used to calculate the performance and is a function of pressure drop between the hydrocyclone inlet and the overflow outlet. The value of the pressure drop found in the previous section is then used to calculate the equivalent area factor using Eq. (2.5). Having the value of equivalent area factor and 50% particle cut size (from Eq. (2.2)) the volume flow rate can be calculated from Eq. (1.8). Comparing this value with flow rate from Eq. (2.1) can be an indication of compatibility of performance based on equivalent area factor and what has been derived from experimental correlations. For an extended region of applications, the amount of overflow rate (See Fig. 2.1) is considered to be 0.6 to 0.95 of the inlet flow and then this value is used to plot a performance chart for hydrocyclones.

For the purpose of designing a hydrocyclone and describing the flow parameters in the hydrocyclones a number of correlations are available [1, 107]. Due to the complex behavior of the system, none of these correlations are sufficient to sat-

isfactorily describe the full range of hydrocyclones operation [1]. However, it is possible to provide a useful design procedure based on available correlations. A design flow chart outlining this procedure is provided in this chapter. A selected model [5] based on a group of dimensionless parameters for a hydrocyclone design is detailed following the flow chart. Other available correlations in the literature for predicting hydrocyclone variables can also be used through this proposed design procedure provided that the necessary design equations are available and the limiting assumptions are respected.

2.3 Modeling energy consumption

While a performance chart can be employed as a guideline for designing a separator, it does not indicate how much energy is consumed for a particular separation technique. An energy consumption chart would be useful to help designers to make the right decision for a specific application. In this research, energy consumption is obtained using a model of the centrifugal force exerted on a particle to push it toward the settling wall. To do this, the equivalent area factor of centrifugal separators, settling velocity, and volumetric flow rate are assumed to be known, as they can be calculated using the equations in the previous section. All of the assumptions applied to derive the separation performance charts still apply. The effect of cake formation within the centrifuge is ignored and all other work on the particle except for centrifugal force work is neglected in the energy calculation.

The method of energy calculation is described below, using a bottle centrifuge separator as a simple example. This procedure is then extended to the other devices.

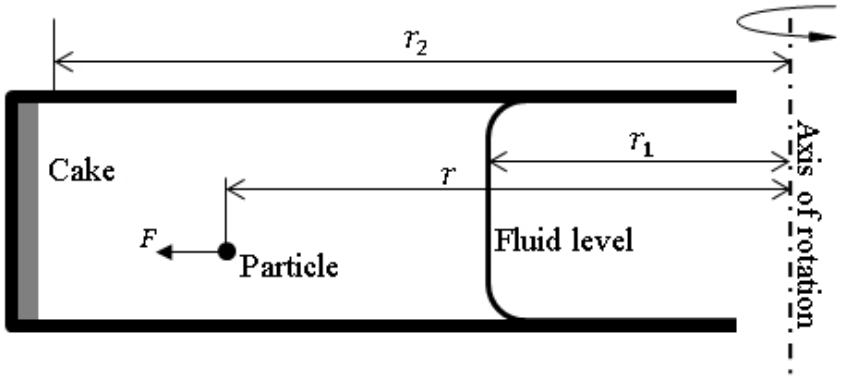

Figure 2.2: Schematic of bottle centrifuge along with a settling particle

For the bottle centrifuge separator shown in Fig. 2.2, the work required to settle a particle is calculated through the integration of centrifugal force through a distance. In this case, the force is:

$$F = mr\omega^2 = \frac{\Delta\rho\pi d^3 r\omega^2}{6} \tag{2.6}$$

where F is the centrifugal force on the particle, ω is angular velocity of centrifuge and r is particle distance from the axis of rotation. This force acts toward the centrifuge wall where the particle settles. The effective distance $r_e = \sqrt{(r_1^2 + r_2^2)/2}$ is obtained based on the assumption that the particle size is equivalent to the 50% cut size and can be found by writing a mass balance relation in each hypothetical volume at both sides of the particle [22]. The total work on the particle is then:

$$W = m\overline{w} = \int_{r_e}^{r_2} F dr = m\omega^2(\frac{3r_2^2 - r_1^2 + 2r_1 r_2}{8}) \tag{2.7}$$

where W is the amount of work and $\overline{w}$ is W/m , m is mass difference between particle and the fluid it displaces, dr is the element of distance, and r_1 and r_2 are the minimum and maximum radius in a centrifuge that a particle can displace as shown in Fig. 2.2. The particle residence time is used to calculate the amount of power needed for the settling of a particle by dividing the force by residence time.

This residence time is obtained using the volume of the centrifuge and the volume flow rate, which are known from the equivalent area factor and the settling velocity. Assuming that the particle settles on the wall through the longest possible path, the power (P_R) which is consumed for sedimenting a particle is calculated during the residence time of the particle in the separator such that:

$$P_R(\text{bottle}) = \frac{W}{t} = \frac{\Delta\rho d^2}{18\mu} m\omega^4 \left(\frac{3r_2^2 - r_1^2 + 2r_1 r_2}{8 \ln \frac{r_2}{r_1}}\right) \tag{2.8}$$

For a 50% cut size and following the same procedure as that of the bottle centrifuge power consumption can be found for tubular bowl, disc stack, and scroll decanter centrifuge for settling a particle as:

$$P_R(\text{tubular}) = \frac{\Delta\rho d^2}{36\mu} m\omega^4 \left(\frac{3r_2^2 + r_1^2}{2}\right) \tag{2.9}$$

$$P_R(\text{disc stack}) = \frac{\Delta\rho d^2}{27\mu} m\omega^2 \frac{2n_d(r_2^3 - r_1^3)}{a(r_2^2 - r_1^2)} \cos\theta \left[\frac{\omega^2}{2}\left(2r_1 \frac{a}{\cos\theta} + \frac{a^2}{(\cos\theta)^2}\right) + \frac{g(r_2 - r_1)}{\tan\theta}\right] \tag{2.10}$$

$$P_R(\text{decanter}) = \frac{\Delta\rho d^2}{12\mu} m\omega^2 \left[\omega^2 \left(\frac{3r_2^2}{4} - \frac{r_1^2}{2} + \frac{r_2 r_1}{2}\right) - \frac{3g}{2}(r_2 - r_1)\right] \times \frac{l_1(6r_2^2 + 2r_1^2) + l_2(4r_1^2 + r_2^2 + 3r_2 r_1)}{3l_1(r_2^2 - r_1^2) + l_2(r_2^2 + r_1^2 + r_2 r_1)} \tag{2.11}$$

The geometric parameters in Eq. (2.9) to (2.11) are shown in Fig. 1.4, Fig. 1.5 and Fig. 1.6. The amount of energy consumption can be obtained per unit volume of feed flow (kWh/m^3) by dividing power consumption by volume flow rate. A cut size particle in hydrocyclone has the same chance of being in the overflow or the underflow. Therefore, it is assumed that the vertical velocity of such a particle is zero. The locus of particles with zero vertical velocity (LZVV) is the the imaginary location where underflow and overflow particle are separated and the vertical

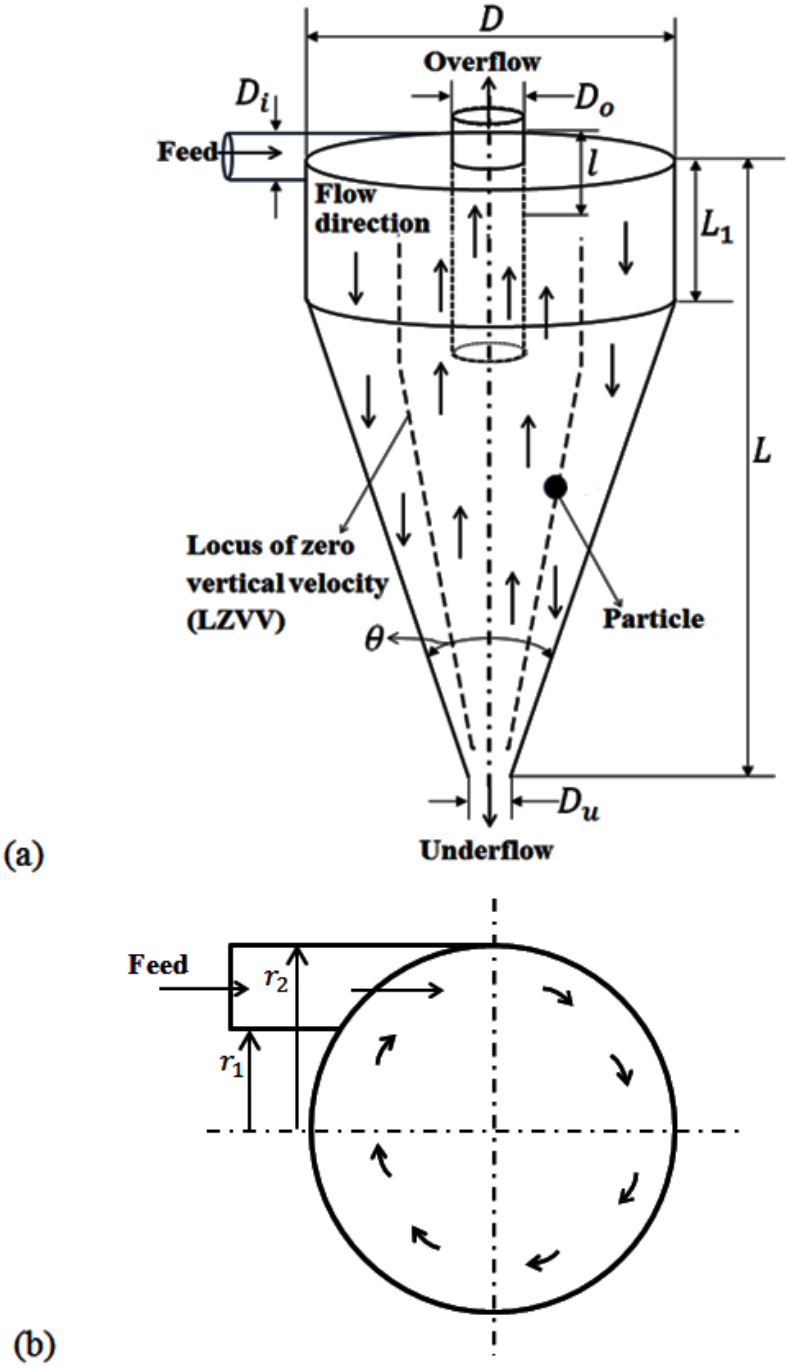

Figure 2.3: (a) Locus of zero vertical velocity and a single particle in a hydrocyclone, (b) cross section of inlet pipe and its wall distances from hydrocyclone centerline

component of the velocity vector is zero [13]. This locus is shown on Fig. 2.3(a) as dashed line.

Calculation of energy consumption in a hydrocyclone using an individual particle model is problematic as defining a precise relation for equivalent area factor and determining the variable angular velocity and LZVV is difficult. However, it is possible to calculate the amount of work needed for sedimenting a single particle under some simplifying assumptions. Assuming that a particle represents 50% cut size in the hydrocyclone, it starts its settling from LZVV and moves toward the hydrocyclone wall due to centrifugal force as shown in Fig. 2.3(a). Centrifugal force in a hydrocyclone is related to the tangential velocity component at each radius location and this component varies exponentially with radius in the outer vortex as described in [80]:

$$v_\theta = \frac{C}{r^n} \tag{2.12}$$

where v_θ is the tangential velocity component in the hydrocyclone inlet, r is particle orbit radius, and n is an empirical exponent, usually between 0.5 and 0.9 [13] in the outer vortex. The constant C can be obtained from a mass balance and is defined as:

$$C = \frac{Q(1-n)}{H(r_2^{1-n} - r_1^{1-n})} \tag{2.13}$$

where Q is the inlet volume flow rate, and r_1 and r_2 are distances between the inlet pipe walls and the center line of hydrocyclone as indicated in Fig. 2.3(b), and H is the inlet pipe height.

The tangential velocity v_θ is obtained by combining Eq. (2.12) and (2.13) to

give:

$$v_\theta = \frac{Q(1-n)}{H(r_2^{1-n} - r_1^{1-n})r^n} \tag{2.14}$$

Utilizing this velocity component, the amount of work W for settling a particle is found from integration of centrifugal force F from the following relations when the particle moves from LZVV to the hydrocyclone wall:

$$F = m\frac{v_\theta^2}{r} \tag{2.15}$$

$$W = \frac{mQ^2(1-n)^2}{2nH^2(r_2^{1-n} - r_1^{1-n})^2}[(\frac{D_1}{2})^{-2n} - (\frac{D_2}{2})^{-2n}] \tag{2.16}$$

where D_1 and D_2 are diameters of the LZVV and hydrocyclone wall relative to the hydrocyclone centerline, respectively. The centrifugal work and power can be calculated by considering the distance a particle of 50% cut size moves from its separation position, the LZVV to the hydrocyclone wall. The maximum distance between LZVV and the hydrocyclone wall occurs at $0.43D$ where D is hydrocyclone diameter [80], as shown in Fig. 2.1, and hence $D_1 = 0.43D$ and $D_2 = D$.

Knowing the volume flow rate and volume of the hydrocyclone it is possible to find the average residence time of a particle in the hydrocyclone [6]. The average residence time can be applied along with the amount of work for calculating the power that is consumed for a particle settling in a hydrocyclone. Since particle mass is related to its density and volume, Eq. (2.16) can be rearranged to give the power:

$$P_R(\text{hydrocyclone}) = \frac{2^{2n}d^3Q^3(0.43D^{-2n} - D^{-2n})\Delta\rho[\frac{1-n}{H(r_2^{1-n} - r_1^{1-n})}]^2}{3n[(\frac{L-L_1}{D-D_u})(\frac{D^3-D_u^3}{3}) + D^2L_1 - D_o^2l]} \tag{2.17}$$

Alternatively, similar to the separation performance calculation, it is also possible to directly use empirical relationships to find the amount of energy consumption

in a hydrocyclone. Since pressure drop in a hydrocyclone is an indication of energy consumption per volume flow rate, Eq. (2.1) can be used to find energy consumption for different flow rates. A similar procedure is followed as the one for deriving the separation performance to generate energy consumption curves. These curves indicate a region of energy consumption of the device and can be bounded to the operating region to generate a chart for a hydrocyclone.

2.4 Discussion

The relationships for separation performance and energy consumption of centrifugal separators have been obtained using the above described procedure. For calculations related to generating separation performance and energy of centrifuges, the same range of particle settling velocity of the centrifuge devices follows [46]. The data points for the performance and energy consumption are bounded to show the device operating region and are used to compare the different separators. The region of separation performance obtained from the result of calculating the equivalent area factor is compared with the separation performance resulting from equivalent area factor reported by Axelsson and Madsen [11]. For hydrocyclones, performance and energy consumption calculations are compared to data from experimental studies [1–3] to validate the proposed performance and energy chart. The FLSmidth Krebs Hydrocyclone company data sheet [4] has also been employed to examine the results. Raw data from the literature [1–3] and manufacturer data along with the reported flow rate and pressure drop resulting from their experiments is used to evaluate the performance and energy consumption and to calculate particle settling

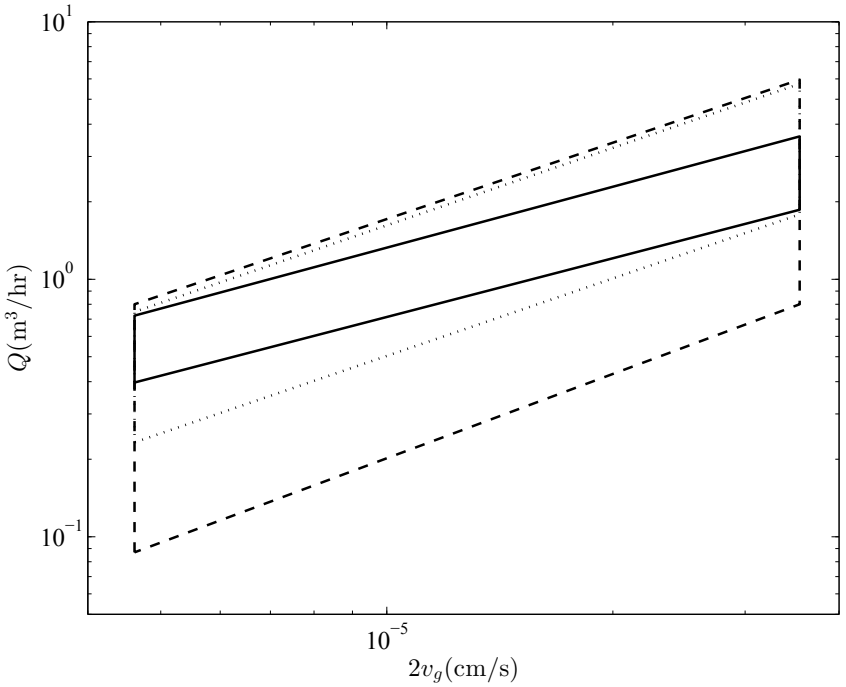

Figure 2.4: Performance chart for tubular bowl centrifuges. solid lines: LPC [10], dashed lines: current work, dotted lines: based on Σ from [11].

velocity. The detailed parameters used to obtain the required values for performance, energy and calculating settling velocity are given in Table 2.1.

2.4.1 Centrifugal separation performance

The performance calculations for tubular bowl, disc and decanter centrifuges are shown as dashed lines in Fig. 2.4, Fig. 2.5, and Fig. 2.6. These are compared to the LPC (solid line). In addition, the minimum and maximum values of equivalent area factor for centrifugal separators reported by [11], shown as a dotted line, depict an additional separation performance chart that is used for comparison. The values for the equivalent area factor are 1,400-4,500 m^2, 35,000-180,000 m^2 and 400-25,000 m^2 for tubular bowl, disc stack, and scroll decanter, respectively [11].

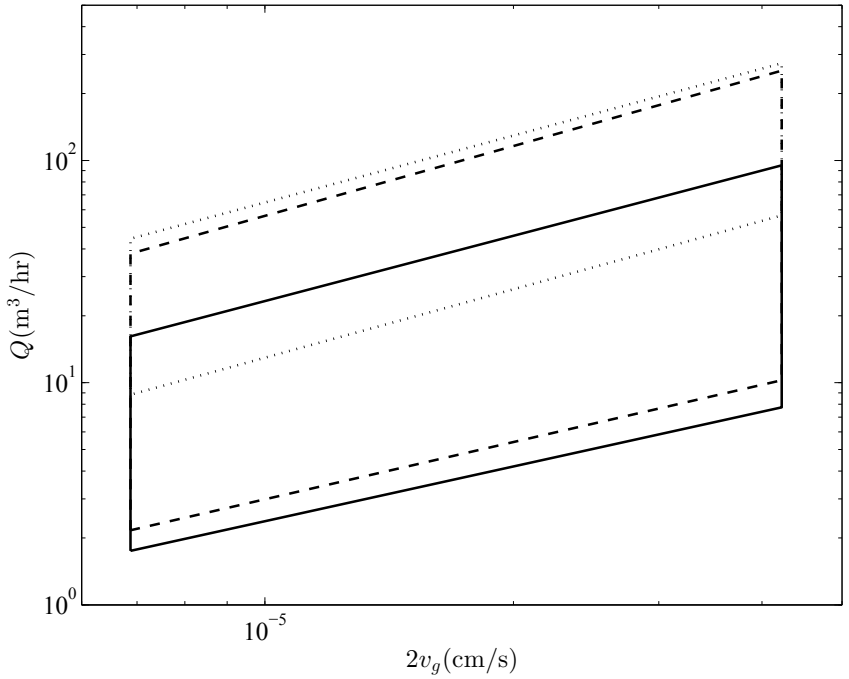

Figure 2.5: Performance chart for disc centrifuges. solid lines: LPC [10], dashed lines: current work, dotted lines: based on Σ from [11].

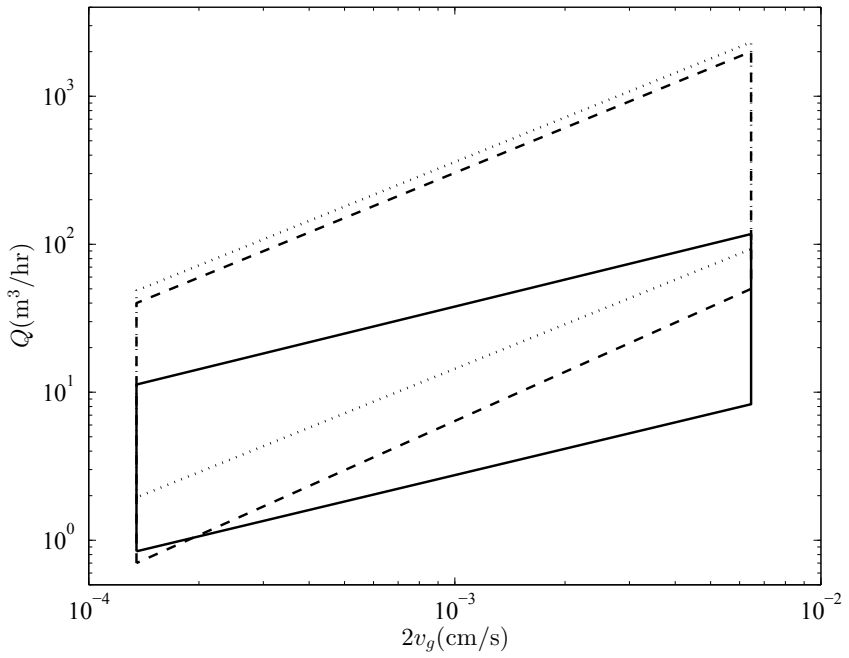

Figure 2.6: Performance chart for decanter centrifuges. solid lines: LPC [10], dashed lines: current work, dotted lines: based on Σ from [11].

In Fig. 2.4 to Fig. 2.6 the maximum performance of centrifuges is clearly higher than the LPC. In all cases, the maximum flow rate values are in good agreement with performance chart directly derived from equivalent area factor reported by Axelsson and Madsen [11]. However, the minimum performance calculated here represents a lower flow rate and this might be due to a discrepancy between the more recent data [11] and the data reported in [47] which comes directly from an earlier work [109]. However, Lavanchy et al. [10] and later Letki and Corner-Walker [46] have provided limited information on how they determined the settling velocity ranges and developed their performance chart. It is therefore difficult to fully critique their derivation method and hence the source of discrepancies between the charts.

Comparing the maximum separation performance shown in Fig. 2.4 to Fig. 2.6 from the current work with the LPC, the most significant difference is in Fig. 2.6 for the decanter centrifuge. Here, the flow rate has increased to more than 1000 m^3/hr showing higher performance for the device. Such a flow rate usually belongs to feeds with coarser particles, which leads to lower bowl speed and hence centrifugal acceleration and larger bowl diameter ($>$ 1m). For example, a decanter centrifuge with bowl diameter of 1.35 m (54 inches) can provide a *G-factor* about 370 and a maximum throughput of 3520 m^3/hr with [110] detailing the improvement in decenter technology.

Overall, comparing the LPC with the charts obtained in this study, it appears that while LPC predicted regions of separation performance for centrifuge separators, it is limited to regions of lower flow rates. One possible reason for this could be due to changing in technology in recent years. The updated performance chart obtained

in the current research covers this gap in performance charts to include the latest technology of centrifuge separators.

2.4.2 Hydrocyclone performance

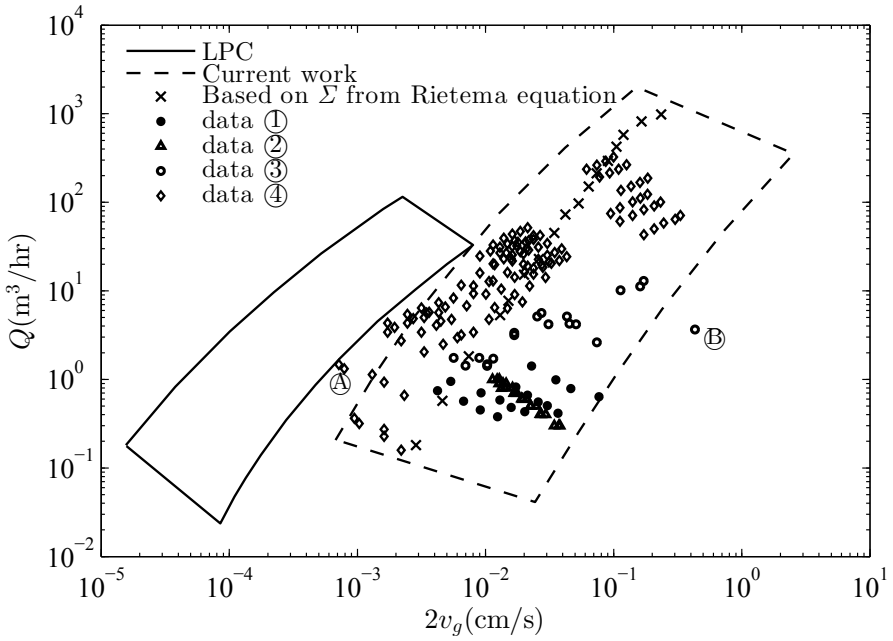

Figure 2.7: Comparison of performance charts with experimental data for hydrocyclones

The performance chart obtained for a hydrocyclone (dotted line) is combined with the LPC (dashed line) in Fig. 2.7. The large discrepancy between these two charts requires further investigation. To find the applicable region, several approaches have been considered. The first approach is to compare the charts to experimental data from the literature and to manufactures data sheets. Also, the performance obtained based on the equivalent area factor concept is compared. Evaluating the settling velocity and practical particle size range for the hydrocyclones is another approach. These approaches are described below.

The charts in Fig. 2.7 have been evaluated using 61 data points calculated/extracted

from data reported in experimental studies [1–3] and detailed in Table 2.1. The data points have been used for computing settling velocity along with values for flow rate to plot the performance chart in Fig. 2.7. It can be seen that except for a few data points almost all experimental data are inside the region of the performance chart obtained in this research. This comparison demonstrates that the LPC is over-predicting the separation performance of hydrocyclones and predicts a smaller settling velocity and hence that finer particles can be separated using hydrocyclones. It also shows a lower value for the maximum possible flow rate for hydrocyclones than what is predicted by the current study and observed in experimental data used. To further investigate, values of flow rate for a specified volume concentration (1%) have been calculated using the equivalent area factor of Eq. (2.5) that is based on the Rietema equation. These values are shown in Fig. 2.7 as '$\times$' points. This data also falls in the same region on the separation performance chart. Both experimental data points from literature and data based on equivalent area factor concept seems to confirm that the chart obtained for hydrocyclone performance from this work is more representative of real hydrocyclone performance compared to the LPC.

Data from a hydrocyclone manufacturer [4] has also been utilized to evaluate the charts in Fig. 2.7. Taking the liquid as water and 1-2% weight concentration of silica particles with a 1650 kg/m^3 density difference, the settling velocity has been calculated for a range of hydrocyclone diameter sizes from approximately 1 cm to 40 cm. These data points are shown in Fig. 2.7 as diamonds '$\diamond$'. Again, this data covers a part of plot that belongs to the proposed chart in this study rather than the one prepared in [10]. This further supports the results of this study in generating a separation performance region for hydrocyclones. Although some of the points

Table 2.1: Descriptions of tests and obtained values from literature [1–3] and FLSmidth Krebs Hydrocyclone data sheet [4] for validating performance and energy consumption of hydrocyclones

Case	Ref.	Description in the reference	d50 (μm)	Volume flow rate (m^3/hr)	Liquid density (kg/m^3)	Solid density (kg/m^3)	Dynamic viscosity (mPa.s)	Pressure drop (kPa)
data①	[2]	Series 1, Series 2, Series 3, Series 4	Extracted from Fig. 7 and Fig. 8	Extracted from Fig. 7 and Fig. 8	Assumed to be 1000 for water	1180	Assumed to be 1 for water	Extracted from Fig. 7 and Fig. 8
data②	[3]	20°C, 40°C, 50°C	Extracted from Fig. 13	Extracted from Fig. 13	Assumed to be 998, 992 and 988 based on temperatures	2300	Extracted from Fig. 14	-
data③	[1]	L3, L8, L14, L16, L18, TD1 to TD12, GB1, GB2	Values from Table A3	Values from Table A2	Values from Table A2	Values from Table A2	Values from Table A2	Values from Table A2
data④	[4]	Hydrocyclone diameter range from 0.5” to 15”	Values in hydrocyclone data sheet	Values in hydrocyclone data sheet	1000	2650	Assumed to be 1 for water	Values in hydrocyclone data sheet

are out of the dotted line region (for example the points labeled Ⓐ) these can be explained due to the high pressure design (50 psi) which violates the assumptions made in this study for calculating flow rate and 50% particle cut size. Point Ⓑ on the right hand side with Q of approximately 4 m^3/hr is another outlier that violates the efficient application region of hydrocyclones, as is shown later. Fig. 2.7 indicates that the chart of Lavanchy et al. [10] is over-predicting the hydrocyclone performance in terms of settling velocity and hence the particle size.

To further examine the results for a hydrocyclone, the settling velocity range of 50% cut size is studied. Assuming the liquid viscosity as 1 mPa.s (water), the settling velocity range was evaluated for two density differences of 1000 kg/m^3 and 10 kg/m^3. For a range of particle size from 2-250 μm (which is the applicable range for hydrocyclones [12]) the settling velocity range is $2.2\times10^{-6}-3.4\times10^{-2}$ m/s for 1000 kg/m^3 and $2.2\times10^{-8}-3.4\times10^{-4}$ m/s for 10 kg/m^3 density difference. This settling velocity range in the LPC is $1.8\times10^{-7}-7.5\times10^{-5}$ m/s for a hydrocyclone, which is even smaller than the range obtained for 10 kg/m^3 density difference. This is not a practical range for settling velocity in a real application of hydrocyclones, where density difference between the phases is the major driver of separation.

Converting the settling velocity from the LPC to particle size by assuming density difference equals 1000 kg/m^3, the particle sizes will vary from about 0.3 μm to about 7 μm for hydrocyclones operation, which is much lower than what is generally accepted for hydrocyclones (2 to 250 μm [12] or 5 to 500 μm [16]). This demonstrates that the charts in [10] and [46] are over predicting the 50% cut size for a hydrocyclone than what is observed in industry. One reason for this discrepancy could be that the calculations in Lavanchy et al. are based on theory and do

not take into account the practical performance of hydrocyclones.

2.4.3 Updated performance chart

By considering several criteria including performance, settling velocity range, and particle sizes, and by comparing experimental studies, it is now possible to propose an updated general chart for centrifugal separators that includes tubular bowl, disc stack, scroll decanter and hydrocyclone. As a result, when LPC is replaced by the updated dotted line for centrifuge separators shown in Fig. 2.4 to Fig. 2.6 an improved performance prediction of centrifuges is obtained compared to the dashed line in Fig. 2.4 to Fig. 2.6. The hydrocyclone performance chart on LPC can also be replaced with the updated hydrocyclone performance chart shown in Fig. 2.7 with the dashed line.

Fig. 2.8 shows the modified separation performance chart for centrifugal separators. This updated chart represents performance of current centrifugal separation technology based on the latest available information. It represents the range of settling velocity of the particles, which can be converted to particle size if fluid viscosity and density difference of phases involved in separation are known. This is a main result of this work and can be used to aid designers.

The performance of the centrifugal devices is also compared to the separation performance of a continuous gravity settling tank that has unit surface area of 1 m^2 in Fig. 2.8. This comparison indicates the increased effectiveness of the device compared to the gravity settling tank. In other words, it demonstrates the surface area of a gravity settling tank that can perform similarly to the centrifugal separator in terms of flow rate and separation efficiency. It is worth noting that not all ap-

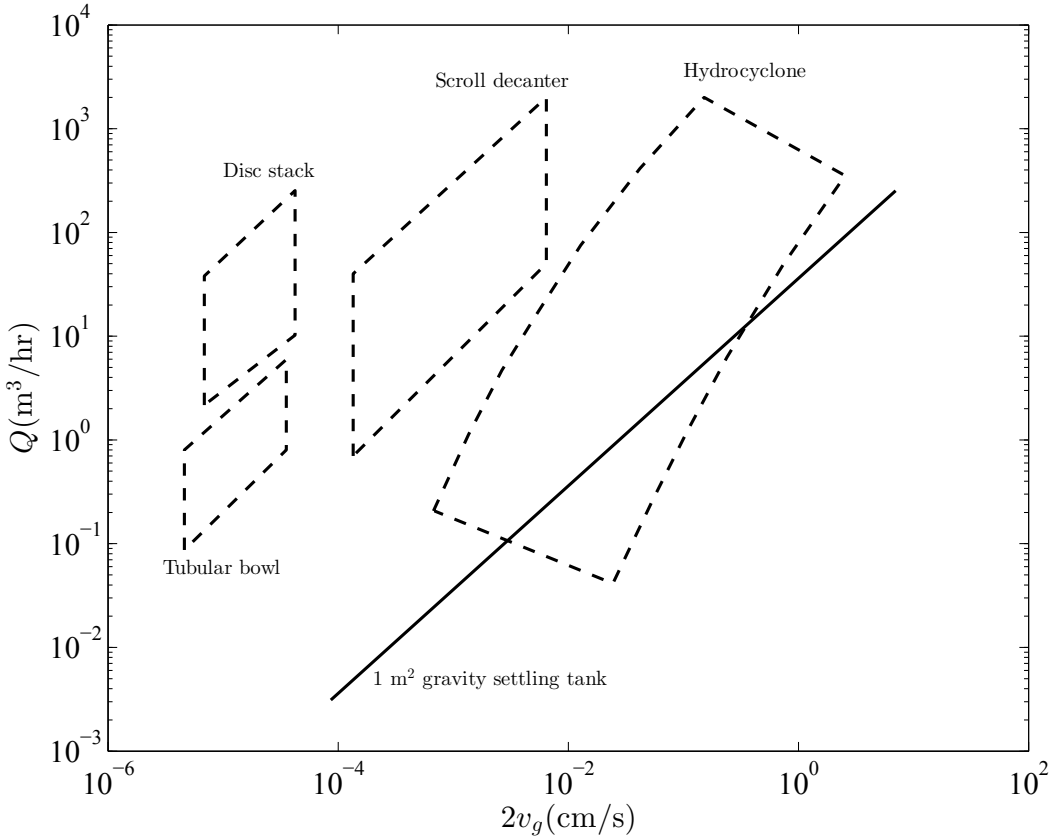

Figure 2.8: Performance chart for centrifugal separator devices along with 1 m^2 gravity settling tank considering overflow discharge rate

plications of hydrocyclone are more efficient than a gravity settling tank. Improper operation of a hydrocyclone may provide poorer separation efficiency than a gravity settling tank. Therefore, a minimum flow rate and pressure drop should be used to maintain an efficient device and to prevent the performance from falling into the low performance region.

2.4.4 Energy consumption

The results of the calculation of energy consumption for four types of centrifugal separators in kWh/(kg.m^3) based on the model developed in the previous section for a single particle are shown in Fig. 2.9. The specified energy consumptions of disc

stack and tubular bowl centrifuges are similar; and they have higher energy consumption than scroll decanters and hydrocyclones. However, disc centrifuges may need less energy than tubular bowl separators for sedimenting a certain amount of solids depending on their operating conditions but are sensitive to the inlet flow rate. Considering equal flow rates for the different devices, the results shown in Fig. 2.9 are expected since the hydrocyclone cannot separate fine particles compared to other centrifuge devices. Disc centrifuges and tubular bowls have higher separation efficiency and usually work with higher *G-factor*s than scroll decanters and hydrocyclones. Fig. 2.9 also demonstrates that, for the same separation efficiency, hydrocyclone specific energy consumption for single particle sedimentation is $\sim$10 to 1000 times less than that of scroll decanter centrifuge.

Fig. 2.9 combined with Fig. 2.8 show the capability of hydrocyclones of handling larger flow rates with lesser energy consumption for particle sedimentation. The energy consumption chart combined with the performance chart provides design insight for these separators. It can provide a guideline for selecting a separator for understanding how much energy is consumed in the device. Energy consumption calculated using pressure drop for hydrocyclones is shown in Fig. 2.10 and compared with a chart presented in [23]. The specific energy consumption between [23] and this study are comparable but for a different settling velocity range and hence separation efficiency. This indicates that Keith's chart [23] is over-predicting the settling velocity and hence the capability of hydrocyclones in 50% cut size separation efficiency.

Experimental data from studies [1–3] that detailed in Table 2.1 are also shown in Fig. 2.10. Experimental values of data ③ are in the region of energy consump-

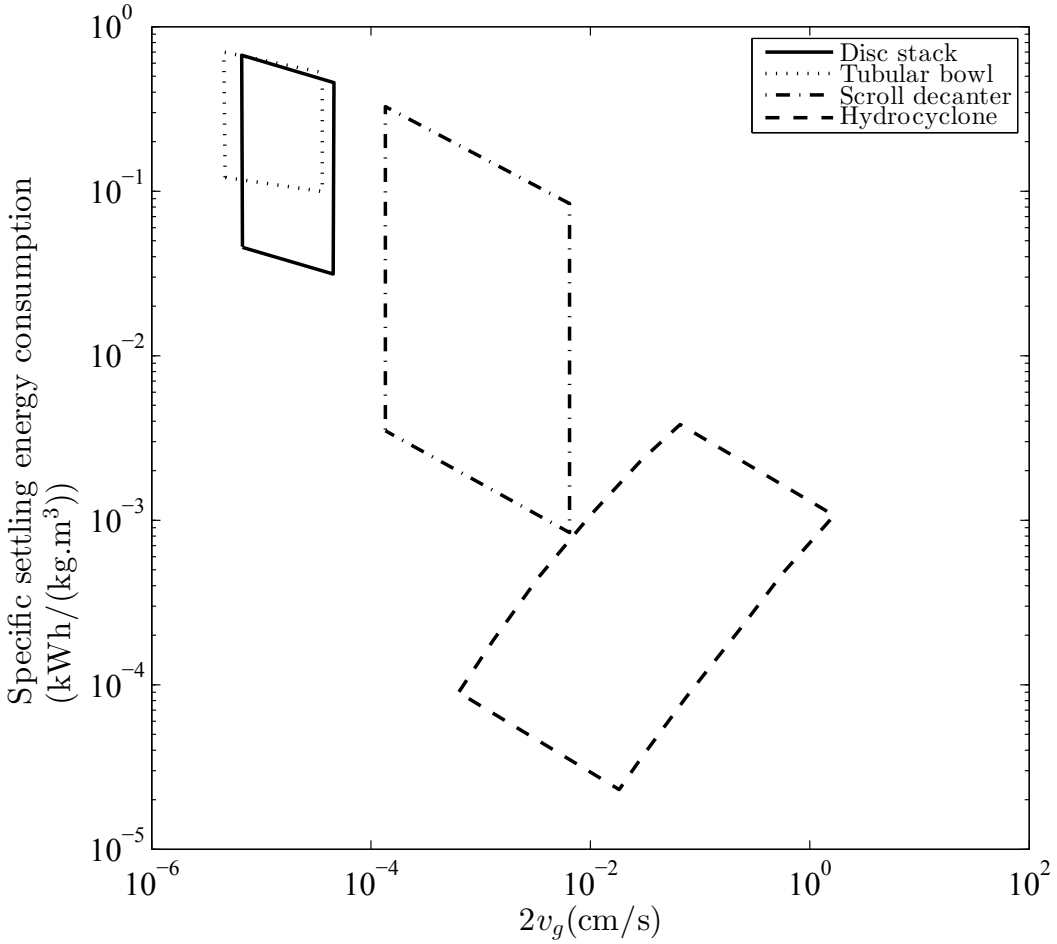

Figure 2.9: Centrifugal separators specific energy consumption for sedimentation of a single particle per unit volume of feed flow and particle mass (50% cut size settling velocity under gravitational acceleration)

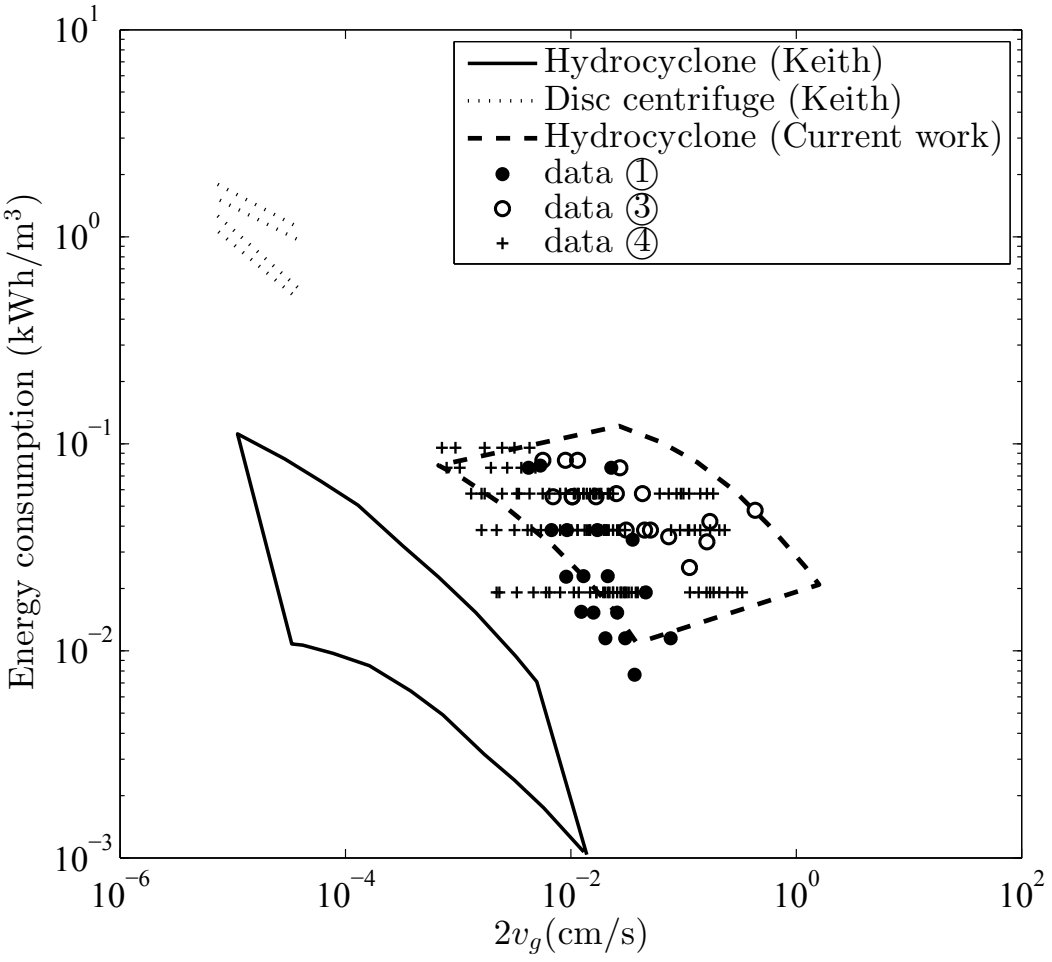

Figure 2.10: Comparison of useful specific energy consumption of hydrocyclone with experimental data

tion obtained in this study while some reported data of data ① shows lower energy consumption than what is predicted in the current study. This can be described by considering Fig. 2.7 and Fig. 2.8. Contrasting Fig. 2.7 and gravity settling tank performance line with unit surface area in Fig. 2.8, it can be seen that the hydrocyclone of data ① produces less efficiency than the settling tank showing less practical application of the device with low feed flow rate. This can be a reason for less pressure drop and hence the reason for consuming less energy than industrial hydrocyclones as shown in Fig. 2.10. Comparing the chart with the data ④, it is observed that most of their data confirm the proposed energy consumption chart but there are some data outside the predicted range of this study. This is attributed to the high pressure drop suggestion (345 kPa) for small hydrocyclones (13 mm-50 mm). Overall, data from the literature and manufacturer performance charts together support the proposed energy consumption chart, which can be used for future applications.

2.5 Design summary for hydrocyclones

A design flow chart shown in Fig. 2.11 is generated based on the proposed performance chart of the current work. This flow chart can be used to estimate the hydrocyclone dimensions for a required cut size at a certain available pressure. The following design flow chart can be used with different empirical models as long as it matches the requirements of the procedure. However, empirical models for hydrocyclone design have some limitations and should be used cautiously to avoid unreliable results. A possible set of equations for designing families of geometrically similar hydrocyclones [5] shown in Fig. 2.1 is provided here and is followed by the geometric proportions and limits of the equations. For other empirical models

the relevant equations should be used in the flow chart. For instance, for designing a hydrocyclone employing the Plitt model [71] Eq. (2.18) to Eq. (2.22) should be replaced with Eq. (2.1) to Eq. (2.2).

$$R_w = 1.18\left(\frac{D}{D_o}\right)^{5.97}\left(\frac{D_u}{D}\right)^{3.10} Eu^{-0.54} \tag{2.18}$$

$$Stk_{50}Eu = 0.12\left(\frac{D}{D_o}\right)^{0.95}\left(\frac{D}{L-l}\right)^{1.33}\left[\ln(\frac{1}{R_w})\right]^{0.79}\exp(12.0c) \tag{2.19}$$

$$Eu = 43.5D^{0.57}\left(\frac{D}{D_i}\right)^{2.61}\left(\frac{D}{D_o^2+D_u^2}\right)^{0.42}\left(\frac{D}{L-l}\right)^{0.98} Re^{0.12}\exp(-0.51c) \tag{2.20}$$

$$\Delta P = \frac{\rho v^2 Eu}{2} = 36.3D^{-3.55}Q^{2.12}\left(\frac{D}{D_i}\right)^{2.61}\left(\frac{D}{D_o^2+D_u^2}\right)^{0.42}\left(\frac{D}{L-l}\right)^{0.98}\rho^{1.12}\mu^{-0.12}\exp(-0.51c) \tag{2.21}$$

$$d = \left[\frac{18\mu D Stk_{50}}{(\rho_s-\rho)v}\right]^{0.5} = \frac{1.173D^{0.64}}{D_o^{0.475}(L-l)^{0.665}}\left[\frac{\mu\rho Q}{(\rho_s-\rho)\Delta P}\right]^{0.5}\left[\ln(\frac{1}{R_w})\right]^{0.395}\exp(6.0c) \tag{2.22}$$

where $Re = \rho v D/\mu$ is Reynolds number and $v = 4Q/(\pi D^2)$ is hydrocyclone characteristic velocity if Q represents inlet volume flow rate. Eu is the dimensionless Euler number, Stk_{50} is Stokes number related to 50% cut size of particles, R_w is the water flow ratio (the proportion of feed water entering underflow), ΔP is pressure drop and d is 50% reduced cut size. More details about these parameters can be found in [13]. Parameters μ and ρ represent liquid dynamic viscosity and density,

Table 2.2: Geometric properties for hydrocyclone design [5]

Parameter	Range
D_i/D	0.14-0.28
D_o/D	0.20-0.34
D_u/D	0.04-0.28
L/D	3.30-6.93
l/D	0.33-0.55
θ	9°-20°

ρ_s is solid particle density, and c is solid volume concentration. All other parameters are hydrocyclone dimensions as shown in Fig. 2.1. Eqs. (2.18), (2.19) and (2.22) can be used with any coherent system of units but Eqs. (2.20) and (2.21) are only valid for SI units. The set of equations are valid for the range of hydrocyclone geometric properties as in Table 5.2.

It should be noted that this is a general design flow chart which does not consider all the details of the flow conditions (such as chemical properties, abrasion, charge, etc.) which may affect some design equations. Those parameters may need extra work for considering their effects on the separation and hydrocyclone performance. Such a design flow chart may not completely remove the user from consulting a specialist. However, regardless of those details, this chart provides the users with hydrocyclone design parameters through a simplified design method which the only design parameters are hydrocyclone diameter and cone angle giving all other hydrocyclone design parameters.

2.6 Conclusions

While centrifuge separators have various applications in industry, from separation of liquid-liquid mixtures to concentration of slurries and wet classification a com-

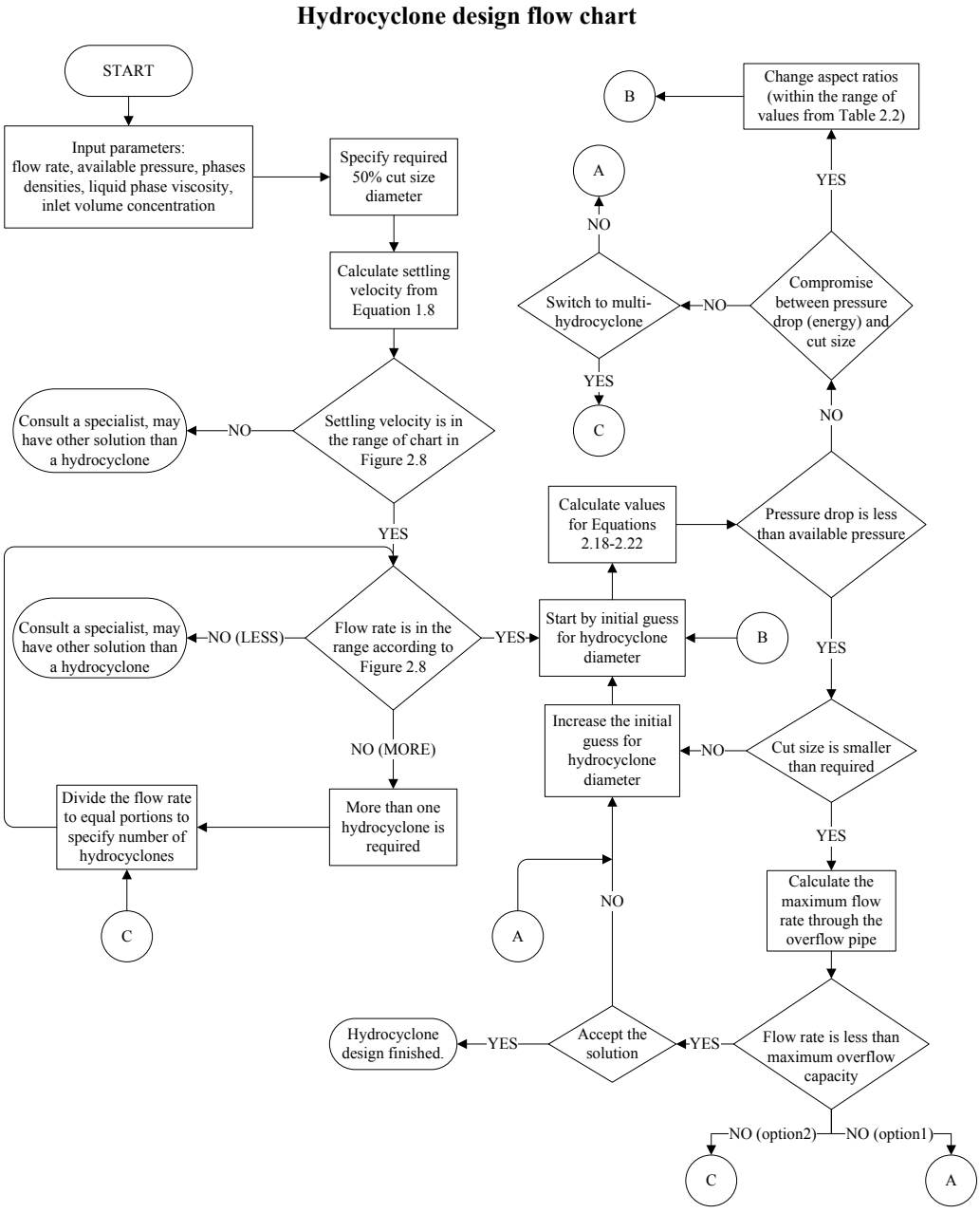

Figure 2.11: Hydrocyclone design flow chart

parison between different types of separators is rare in the literature. Using the latest available information, performance and energy consumption charts for four types of centrifugal separators are derived. The following conclusions can be drawn:

- A discrepancy between the hydrocyclone performance charts of this study and the one from the Lavanchy et al. [10] is found and it was shown that the LPC is over predicting the separation performance of the hydrocyclones. The reason for this is not clear as the theory behind developing the equivalent area and the hydrocyclone performance chart have not been released by the LPC developers. This is noticeable as the LPC is still being introduced in the literature as a guideline chart for selection and design of centrifugal separators. It is also found that the LPC has not been updated since 1964 to include changes in centrifuge separator technologies. Therefore, there is a need to introduce an update performance chart for centrifuge separators and hydrocyclones.

- The separation performance estimates of different centrifugal separation devices are updated in this chapter using more recent available information about centrifuging technology and a performance chart is proposed and compared with a gravity settling tank with unit surface area (Fig. 2.8).

- A semi-empirical model is developed to compute the work on an individual particle in centrifugal separators and a chart is developed for specific energy consumption in centrifugal separators (Fig. 2.9). This chart is helpful in providing better understanding of centrifugal separators in order to design and compare between different separation techniques.

- Hydrocyclone performance and energy charts are verified by employing ex-

perimental data from the literature and manufacturer data sheets. There is good agreement between the charts proposed in this study and empirical data. A mathematical modeling for generating such chart can help generating a chart according to basic physic principles of the separation phenomenon.

- To aid designers of this type of separation technology an updated design process is summarized in Fig. 2.11. The developed charts combined with the assumptions applies can be employed for predicting performance and energy consumption of the devices.

Chapter 3

Experimental setup

3.1 Introduction

Experiments are designed to study the hydrocyclone performance and validate the model developed for equivalent area factor. The experimental setup, flow loop design and procedures are explained in this chapter.

3.2 Experimental apparatus

An experimental flow circuit has been designed and built as shown in Fig. 3.1. Water with particles are pumped into the hydrocyclone using a centrifugal pump that provides different inlet flow rates and hence pressures. Pressure is monitored at the inlet and the outlets to obtain the pressure drop across the hydrocyclone.

A second pump (a progressive cavity pump) is connected to the underflow pipe to allow independent control of the underflow flow rate without clogging the underflow pipe. This method has an advantage compared to using a valve for manipulating the underflow flow rate since a valve in the underflow pipe can easily block [13]. Another important feature of using a pump for the underflow is it provides the opportunity to simulate underflow diameter variation. Each pump is controlled using

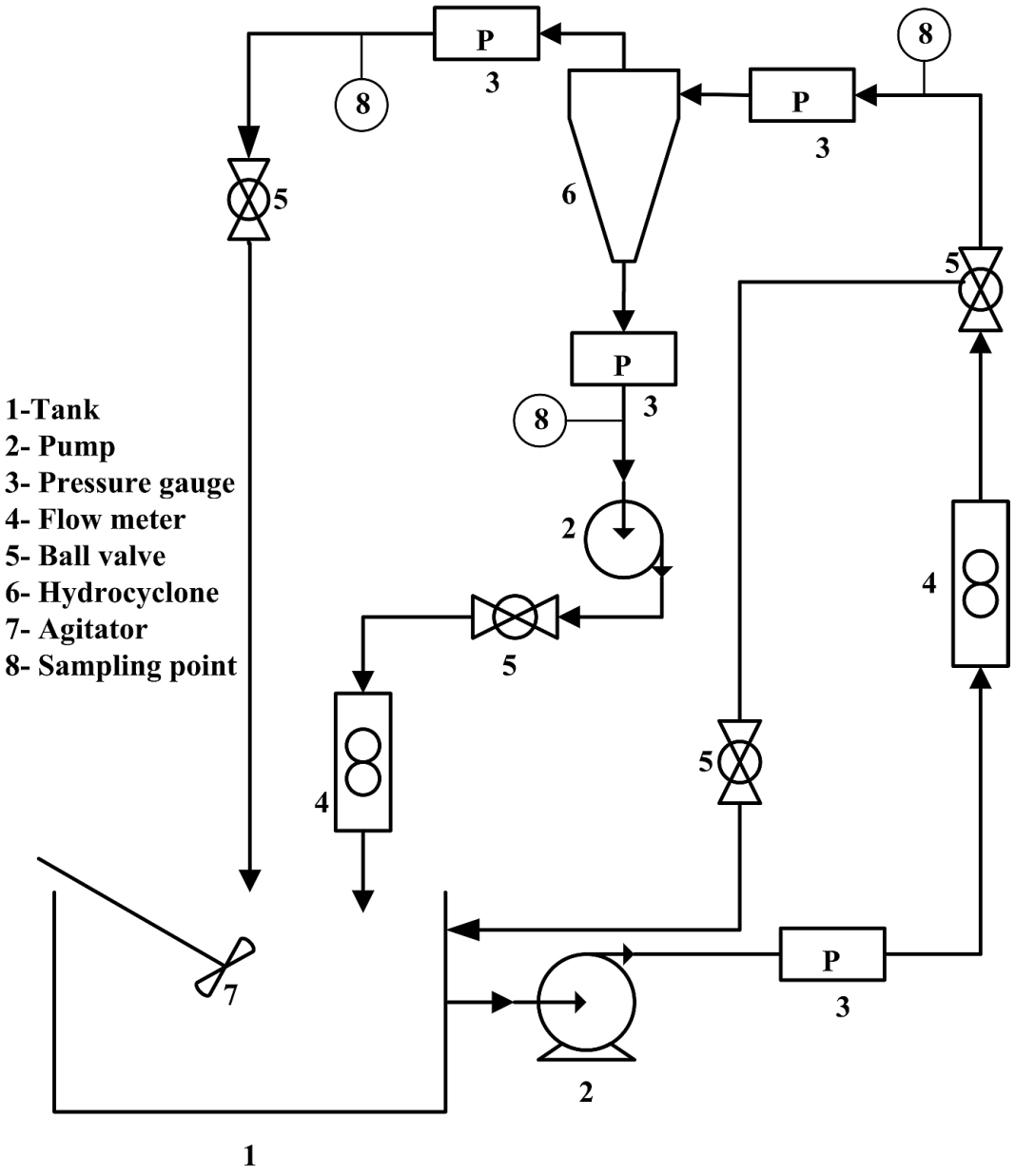

Figure 3.1: Process flow diagram for the experimental setup

a separate variable frequency drive (VFD). Both underflow and overflow are returned to the tank for recycling. The solid and liquid (water and soda lime glass beads particles) in the mixing tank are pumped to the hydrocyclone inlet as the feed stream. The clean part (fine particles) of the separation moves to the overflow of the hydrocyclone and is returned to the mixing tank. The coarser particles leave the hydrocyclone through the underflow pipe and a progressive cavity pump equipped with a VFD and controller are also returned this mixture to the mixing tank. To have a uniform distribution of the particles at the inlet, a mixer is used in the tank. The mixer is also equipped with a VFD to control the mixer speed.

Flow at the inlet and underflow are measured by a Coriolis flow meters (Promass 83I Endress+Hauser Ltd with maximum measurement error of $\pm 0.05\%$ for inlet flow; Optimass7300 KROHNE Messtechnik GmbH with maximum measurement error of $\pm 0.1\%$ of the actual measured flow ± 0.0018 m^3/hr for underflow). The Coriolis flow meters are located properly in the loop according to the manufacturers recommendations [111, 112]. Using the Coriolis meters, temperature, velocity, density and solid concentration are also measured.

Pressures in the system are measured near to the hydrocyclone inlet and both outlets. This is to minimize the pressure drop effects in the connected pipes on the measurements. Pressure transducers (AST4000) with 4-20 mA outputs are calibrated according to ASTM D5720-95 [113] and used for pressure monitoring. The accuracy is $\pm 0.4\%$ for the best fit straight line (BFSL) and the measurement range is from zero to 200 kPa. A sample calibration data sheet for one of the pressure sensors used in the experiments is presented in Table 3.1. Details of the calibration method and definition of the terms can be found in [113].

To examine the effect of solid concentration in the mixture on the mixture viscosity, the viscosity of mixtures with different solid concentration are measured using a rotational viscometer (Rheolab QC, Anton Paar USA Inc.) with a pre-installed double gap measuring system (DG42, Anton Paar USA Inc.).

A summary of the setup equipment is listed in Table 3.2 and the hydrocyclone dimensions are detailed in Table 3.4. A picture of the major parts of the test rig is shown in Fig. 3.2.

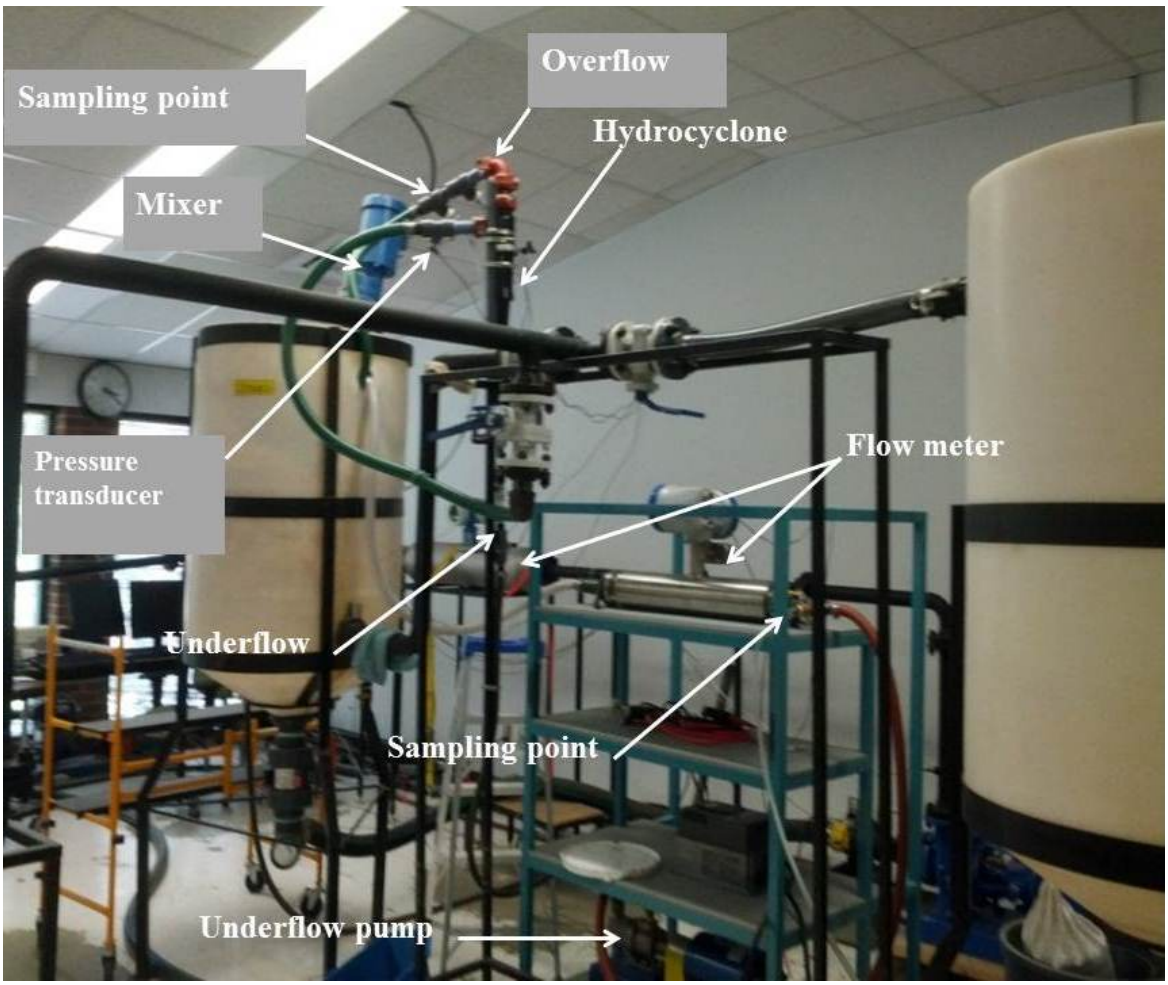

Figure 3.2: Test rig and the parts

Table 3.1: A sample calibration data for pressure sensor calibration

Calibration Data						Pressure Measurement System Calibration For system based on electronic pressure transducers **Calibration type:** gauge **Manufacture:** AST American sensor technologies **Model:** AST4000 **Performed by:** Reza Sabbagh **Date:** 11/07/2013	
		Output-trial1		Output-trial2			
Applied Pressure (kPa), (1)	**Theoretical output (kPa), (2)**	**Pressure increase(kPa), (3)**	**Pressure decrease(kPa), (4)**	**Pressure increase(kPa), (5)**	**Pressure decrease(kPa), (6)**		
0	0	-0.14	-0.14	-0.14	-0.14		
31.46	31.46	31.47	31.47	31.47	31.47		
61	61	60.96	61.09	61.09	61.09	**Lower limit**	0
92.65	92.65	92.57	92.94	92.69	92.82	**Upper limit**	200
122.83	122.83	122.81	123.06	122.93	123.06	**Full-scale output**	200
154.47	154.47	154.29	154.54	154.42	154.66	**Calibration pressure range**	200
187.92	187.92	187.64	187.77	187.77	187.89	**Number of observation**	**28**

Theoretical output (kPa), (2)	**Error computation**							
	(2),(3)	**(2),(4)**	**(2),(5)**	**(2),(6)**	**(3),(4)**	**(5),(6)**	**(3),(5)**	**(4),(6)**
0	0.1	0.1	0.1	0.1	0.0	0.0	0.0	0.0
31.46	0.0	0.0	0.0	0.0	0.0	0.0	0.0	0.0
61	0.0	0.1	0.1	0.1	0.1	0.0	0.1	0.0
92.65	0.1	0.3	0.0	0.2	0.4	0.1	0.1	0.1
122.83	0.0	0.2	0.1	0.2	0.2	0.1	0.1	0.0
154.47	0.2	0.1	0.1	0.2	0.2	0.2	0.1	0.1
187.92	0.3	0.2	0.2	0.0	0.1	0.1	0.1	0.1
Max error	0.3				0.4		0.1	
Accuracy	0.15				0.19		0.06	
Required accuracy	1				1		1	
Accept	✓				✓		✓	
Reject								

Table 3.2: Experiment equipment summary

Device	Model	Maker	Specifications
Centrifugal pump	XR-2(7)	Hayward Gordon Inc., Canada	1780 rpm, 40 ft head, 143 USgpm
VFD	ESV552N02TXB	Lenze, USA	4-20mA w/500 Ohm Total Impedance
Eectric motor		Weg	5.5 kW
Progressive cavity pump	33204 mechanical seal	Moyno, Inc., USA	0-100 psi discharge pressure
VFD	ID15H201-E	Baldor, USA	AC INVERTER,230V, Serial communication
Eectric motor		Baldor Electric, USA	0.37 kW, 1750 rpm, 6000 max. rpm
Pressure gauge	AST4000	American Sensor Technologies (AST), USA	4-20 mA, accuracy is 0.4% BFSL, 0 to 200 kPa
Coriolis flow meter	Promass 83I	Endress+Hauser Ltd, Canada	$\pm$0.05% maximum error, 4 to 20 mA
Coriolis flow meter	Optimass7300	Krohne Messtechnik GmbH, Germany	$\pm$0.1% of actual flow $\pm$0.0018 m3/hr maximum error, MFC300 transmitter, Modbus over RS485, 32 per line
Mixer	PHG Gear Drive	Promix	Hydrofoil impeller
VFD	174610.00	Leeson Electric, USA	1.5kW, 7A, 3ph
Eectric motor	C6T17FB65F	Leeson Electric, USA	1.49 kW
PSD analyser	HELOS/BR	Sympatec GmbH, Germany	_x0006_1% deviation with respect to the standard meter, measuring range from 0.1 m to 8750 m
Viscometer	Rheolab QC	Anton Paar Inc., USA	Measurements according to ASTM D562 using a special Krebs geometry at 200 rpm spindle speed, KU-Range: 40-150 KU
Hydrocyclone	U2-GMAX-3020	FLSmidth Krebs, USA	Krebs cyclone, 4-50 psi, G85LG-45-RU Apex, 4-50 psi, Dimensions are listed in Table 3.4

3.2.1 Hydrocyclone

A 50 mm diameter hydrocyclone (GMAX FLSmidth Krebs Hydrocyclones) is used in the experiment as the device under test. The main design parameters of the hydrocyclone are listed in Table 3.3 (Case 1) for geometrically similar hydrocyclones as shown in Fig. 2.3. This can be compared to other common hydrocyclone designs listed as Case 2 to Case 4 in Table 3.3. These hydrocyclones are also compared in Fig. 3.3. As it can be seen from the figure, the Bradley hydrocyclone and the hydrocyclone in the current research has a larger conical portion and total length comparing the Rietema and Demco 4H hydrocyclones. As the performance of the hydrocyclones are geometry dependent [13], the differences in the geometries will affect the separation performance and pressure drop. For instance, for a same hydrocyclone diameter a Bradley hydrocyclone provide lower reduced cut size while a Rietema hydrocyclone can perform with a higher flow rate but provides a larger reduced cut size [65]. The hydrocyclone of the current research has the largest length comparing the other types and it is expected to perform significantly different from other types of hydrocyclones. This will be discussed later by comparing the performance of the four types of hydrocyclones in terms of equivalent area factor in Chapter 4 .

Table 3.3: Hydrocyclone geometric parameters

Case	Parameter	D_i/D	D_o/D	L/D	L_1/D	l	θ
1	Current study	0.44	0.24	17.8	1.24	0.84	-
2	Rietema	0.28	0.34	5	-	0.4	20°
3	Demco 4H	0.26	0.33	3.3	0.55	0.55	18°
4	Bradley	1/7	1/5	-	1/2	1/3	9°

Table 3.4: Geometric parameters of the hydrocyclone in the current research

Geometric proportion	size (mm)
Hydrocyclone diameter, D	50
Inlet pipe hydraulic diameter, D_i	22
Overflow pipe diameter, D_o	12
Cylindrical section length, L_1	62
Vortex finder length, l	42
Hydrocyclone total length, L	890

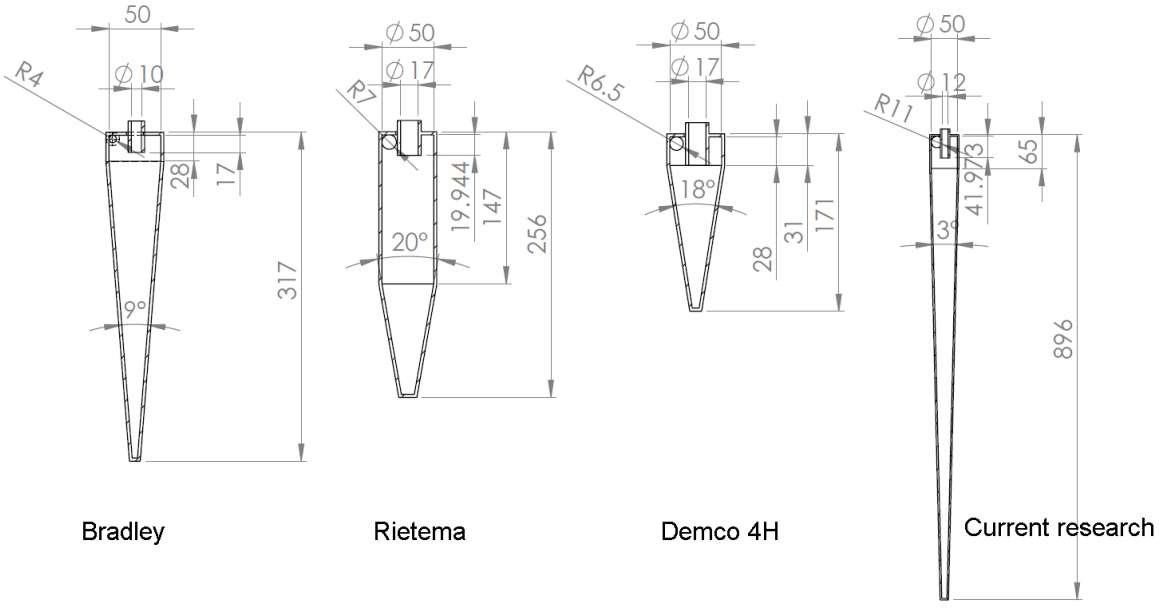

Figure 3.3: Comparison between geometry of different types of hydrocyclones (dimensions are in mm and scales are different)

3.3 Test conditions

Soda lime glass beads particles are mixed with water to obtain nominal solid volume at three concentrations equal to 0.1, 0.5 and 2%v/v. The average measured concentrations are 0.111%v/v, 0.480%v/v and 1.908%v/v, respectively. At each concentration three tests are done at different flow rates according to 1200, 1500 and 1800 rpm for feed pump (centrifugal pump) speed. For each flow rate the underflow pump speed is varied at 6 speeds from 300 to 1500 rpm. This results in 54 ($3\times3\times6$) test points each of which is repeated three times to check the repeatability of the experiments. Liquid properties are determined according to the temperature measured in the flow meter. The ratio of the volumetric underflow flow rate to the inlet flow rate (the flow ratio R_f as defined in Fig. 3.4) due to the underflow pumping varies from 0.2 to about 0.8. Total volume of the flow in the system is 260 liters. Each test is repeated three times and the average values of the data are used for the analysis. The experiments conditions are listed in Table 3.5.

Table 3.5: Experimental conditions

parameter	condition
Centrifugal pump speed (Hz)	40, 50, 60
Underflow progressive cavity pump speed (Hz)	10 to 50
Inlet pressure (kPa)	150 to 230
Inlet flow rate (m^3/hr)	1 to 2.4
Inlet solid volume concentration (%v/v)	0.1 to 2

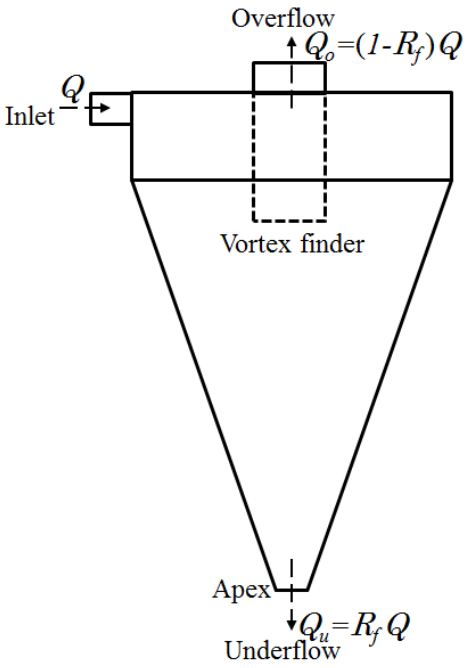

Figure 3.4: Schematics of the flow rates in a hydrocyclone

3.4 Experimental hardware control

3.4.1 Communication system

Control of the experimental hardware (including pumps and mixer VFDs), communication with Coriolis flow meters and recording the data from the devices and temperature and pressure sensors is performed using custom software developed in the laboratory. At steady state flow conditions information was recorded and filtered to remove noise and averaged. The mixture and flow properties of flow velocity, flow rate, solid concentration and temperature are measured in each flow meter and transmitted to the data acquisition system. A flow diagram including the communication lines of the experimental setup is shown in Fig. 3.5. Communication lines for flow meter transmitters, VFDs and pressure gauges that communicate to the data acquisition system are depicted with dashed lines in Fig. 3.5.

3.4.2 Software

A customized controlling and data logging software (LabWindows/CVI, National Instruments Corporation) has been developed to communicate with the devices and to record the data with the specifications are listed in Table 3.6. The codes are developed for different communication systems required for each apparatus and integrated as a single main software. The underflow Coriolis communicates through Modbus RTU over RS485, the underflow pump communicates in serial over RS232 and all other devices transmit voltage to the DAQ system. Some of the main pages of the software are shown in Fig. 3.6 to Fig. 3.8.

The pressure sensor data, temperatures and the inlet flow Coriolis flow meter data are logged in the main tab of the data logger software shown in Fig. 3.6. All

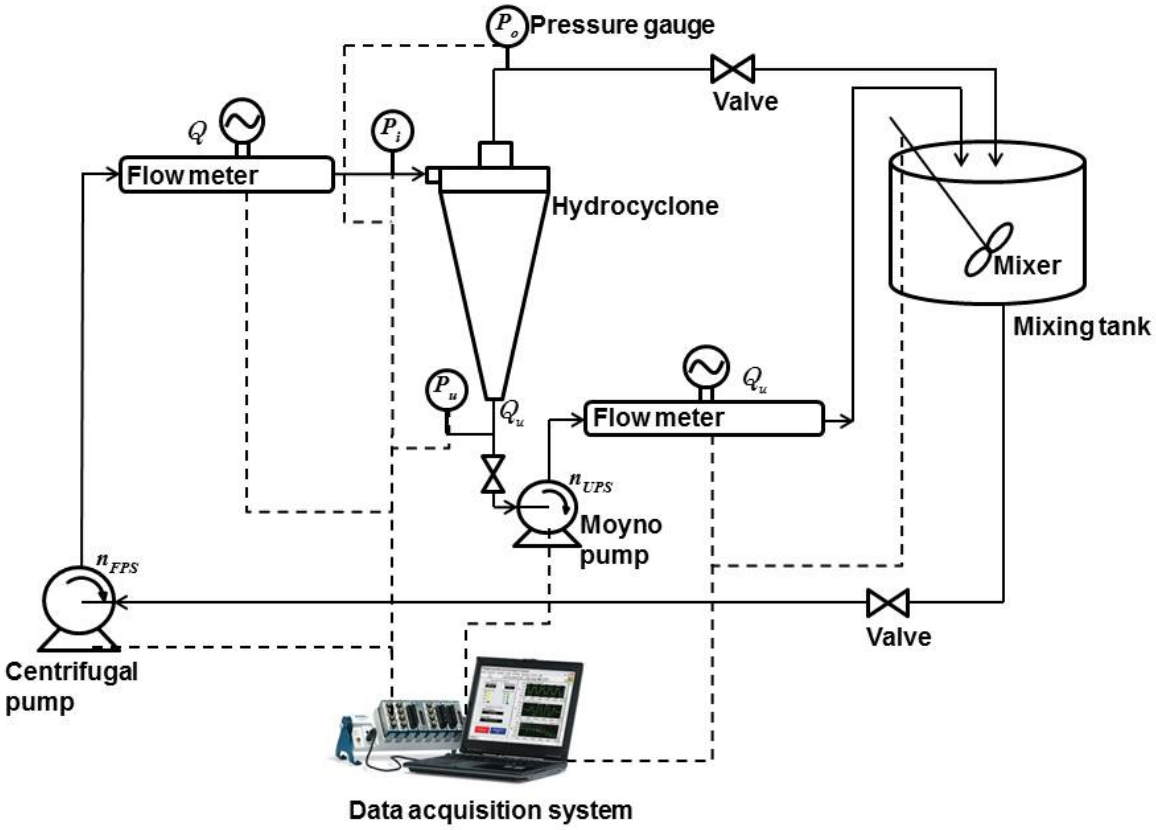

Figure 3.5: Schematic of the experimental setup

required data in the experiment is logged in a file defined by the user. The feed pump VFD and the mixer VFD are also controlled in this tab. There is an emergency button that shut down the feed pump and mixer and stops data logging system in case of emergency problem. The underflow Coriolis flow meter communicates with the software through a separate tab shown in Fig. 3.7. This tab also allows visual monitoring of the Coriolis flow meter variables such as the concentration, flow rate and flow velocity. This part of the software is programmed for communicating in Modbus according to [114] and [115]. As the underflow pump VFD comunication is different from the other equipment it is controlled in another tab shown in Fig. 3.8. All VFD settings for the underflow pump are performed in this tab. and the data from the pump VFD is collected and sent to the main page of the software for recording. The settings for the underflow pump VFD are programmed according to [116] and [117].

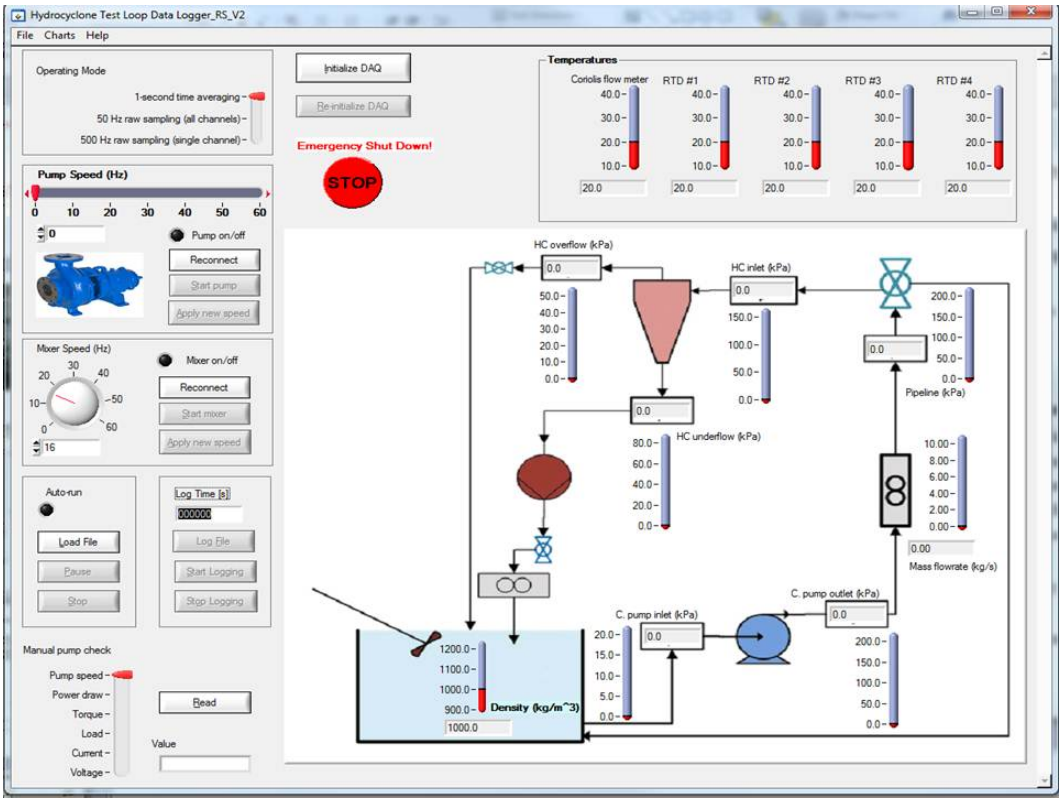

Figure 3.6: Data logger software for monitoring and controlling the devices and recording the data

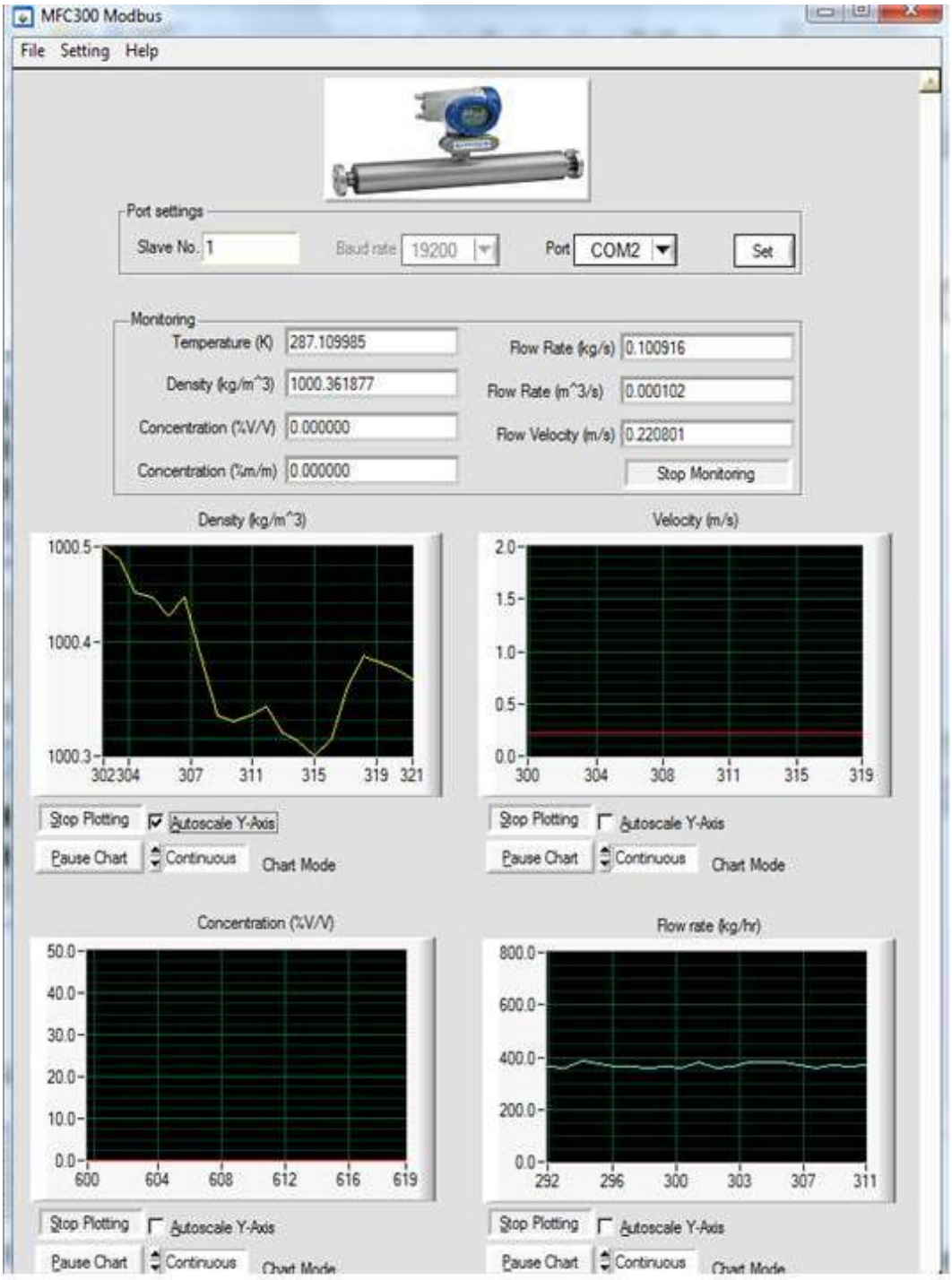

Figure 3.7: Example of data monitoring and recording in software for Coriolis flow meter

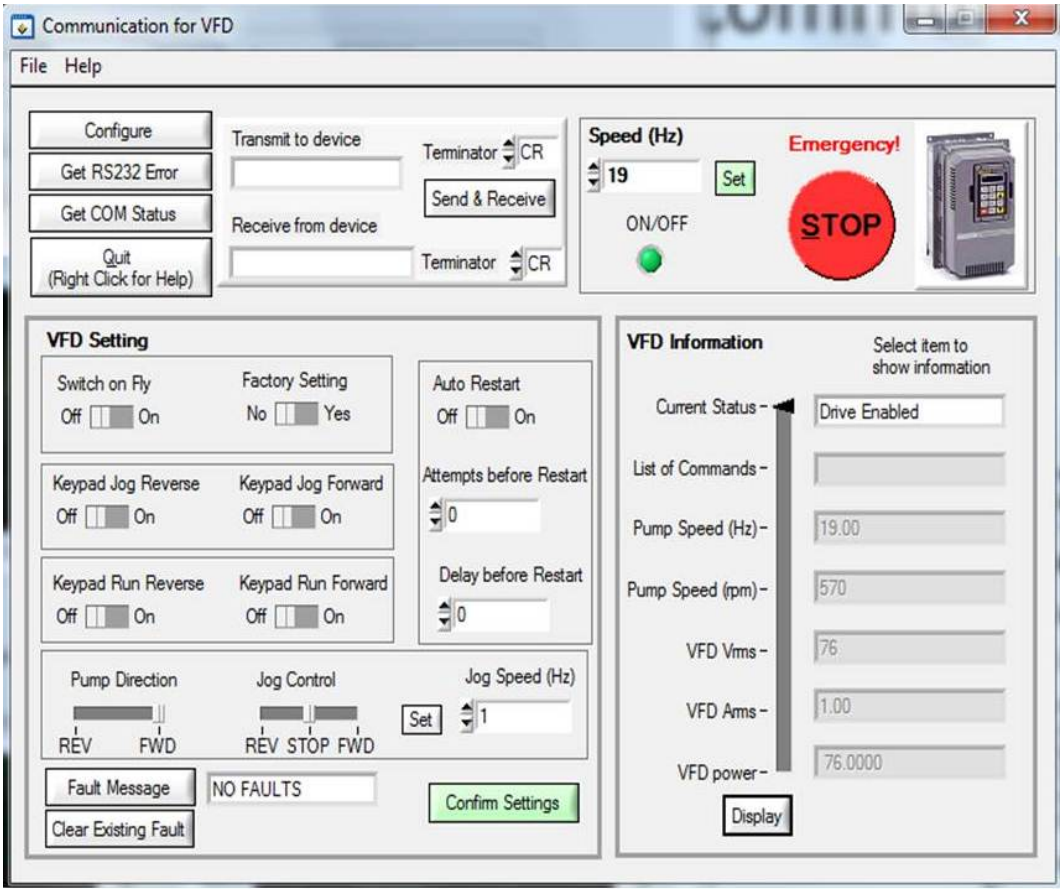

Figure 3.8: Software developed for monitoring and recording for VFD of the underflow pump

Table 3.6: Specifications of the data acquisition equipment

Device	Model	Maker	Specifications
DAQ module	NI 9208	National Instruments Corporation, Canada	16 channels, current inputs, 500 S/s, 21.5 mA
DAQ module	NI 9217	National Instruments Corporation, Canada	4 channels, 400 S/s (100 S/s per channel) PT100 RTD analog input
DAQ chasis	NI cDAQ-9178	National Instruments Corporation, Canada	8-Slot USB Chassi, up to eight NI C Series I/O modules

3.5 Flow sampling

Flow samples are taken using a sampling ball valves at three points in the loop shown on Fig. 3.1: the hydrocyclone inlet, the overflow pipe and the underflow pipes. To minimize the sampling errors and prevent the sampling at one point affects the other sampling points, the flow stream of the underflow is sampled first followed by sampling the overflow and then the inlet streams. The samples are used for determining particle size distribution (PSD) with a PSD analyzer and are described later. Each sample is diluted first to avoid image overlapping by the particle analyzer. Three samples from the flow are taken at each sampling point shown in Fig. 3.1 for particle size analysis. Each experiment and hence sampling is repeated three times and the average values of the data are used for the analysis.

3.6 Particles and particle size distribution (PSD)

3.6.1 Particles

Soda lime glass beads are added to the working fluid (water) to perform the experiments in the current study. The density of the particle is 2500 kg/m^3.

3.6.2 PSD for feed particles

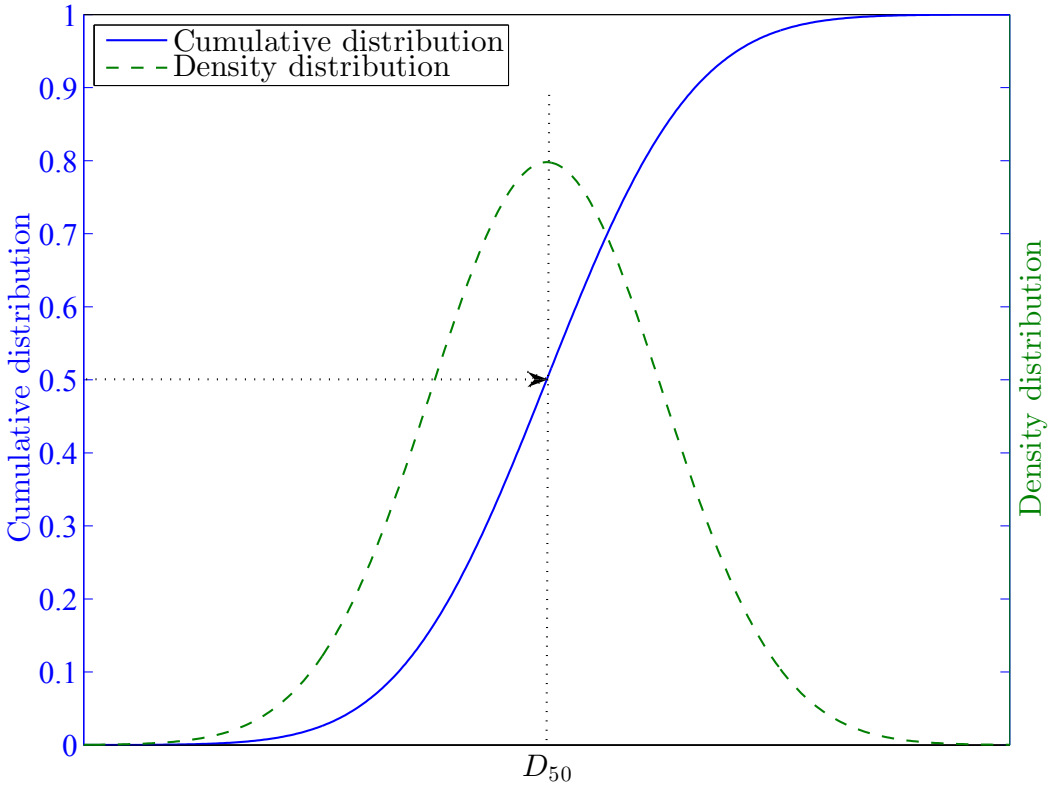

Figure 3.9: Definition of median value (D_{50}) on particle size distribution curves

A laser diffraction sensor (Sympatec GmbH, HELOS/BR) with $\pm 1\%$ deviation with respect to the standard meter is used for particle size distribution (PSD) analysis. The measuring zone for the insertion of wet disperses for particle size analysis varies from 0.1 μm to 875 μm.

Median values are defined as the value where half of the population resides

above this point, and half resides below this point [24]. The particle size (diameter) D_{50} is defined as median value of the distribution which is the size that splits the distribution with half above and half below this size [24]. This size is defined in Fig. 3.9 on a sample size distribution curve. The particle size associated with the cumulative distribution (dash line) equal to 0.5 (50%) is the median size. Typically value of the D_{50} is used to represent a particle size distribution. This value can be obtained for number, surface or volume distributions [12]. The D_{50} values in this research are associated with volume distributions obtained from the particle size analyzer.

A plot of a typical cumulative distribution of the particles for the inlet flow sample is shown in Fig. 3.10 on a semi-logarithmic chart. The data for the PSD is fitted using a log-normal [118] and Rosin-Rammler (also called Weibull distribution) [118] distributions as the uniformity of the distribution is tested with the chi-square (χ^2) goodness of fit test [119]. These results confirm that the data comes from a normal distribution at the 5% significance level. Both fitted curves appropriately predict the distribution ($R^2 > 0.99$) and indicate a uniform distribution of the particles in the hydrocyclone inlet pipe. Both the Rosin-Rammler distribution ($R^2 = 0.9984$) and the log-normal function ($R^2 = 0.9939$) are excellent fits to the data. The particle median size (D_{50}) is 4.53 μm from the experiment, and 4.05 μm and 4.38 μm from the log-normal and Rosin-Rammler distribution, respectively. The distribution functions for the log-normal (LN) and Rosin-Rammler (RR) distributions are [118] :

$$f(x)_{LN} = 0.5 + 0.5\frac{\text{erf}[(log(x) - log(x_g)]}{\sqrt{2}log(\sigma)} \tag{3.1}$$

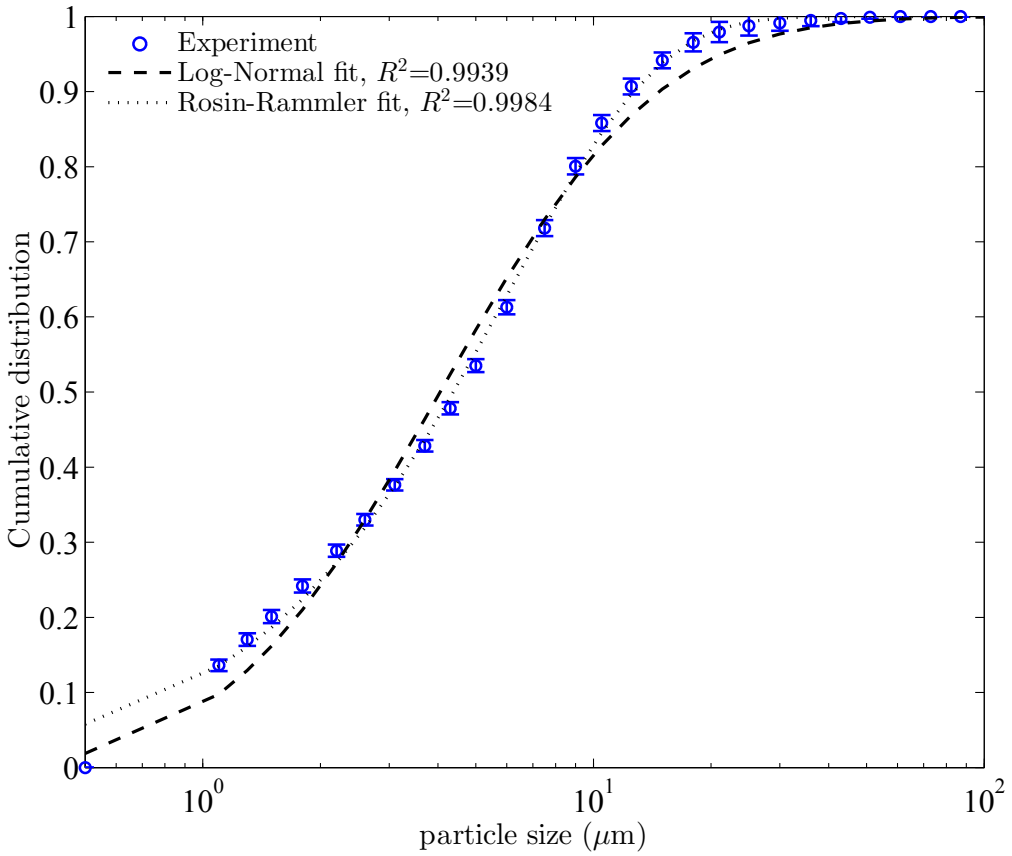

Figure 3.10: Particle size distribution for the particles in the current study with error bars ($D_{50} = 4.53$ μm) and the log-normal fit ($D_{50} = 4.05$ μm) and Rosin-Rammler fit ($D_{50} = 4.38$ μm)

$$f(x)_{RR} = 1 - \exp[-(\frac{x}{\lambda})^k] \tag{3.2}$$

where erf is the error function, x is particle size, and x_g, σ, λ and k are the fitting parameters. The parameters for the plots shown in Fig. 3.10 are $x_g = 4.051$ and $\sigma = 2.735$ for log-normal distribution and $\lambda = 6.054$ and $k = 1.131$ for Rosin-Rammler distribution.

3.6.3 Accuracy in PSD measurements

The particle size distribution for each stream sample is obtained using the particle size analyzer detailed in Table 3.2. Each sample is diluted first as required by the manufacturer and the accuracy of the size distribution measurements is tested with a known sample. The size distribution is performed for inlet and outlet streams.

The underflow sample size distribution results are discussed in detail for a specific case. The underflow PSD is shown in Fig. 3.11 as a cumulative distribution. Using a diluted sample from the underflow, the PSD measurement is repeated five times with the repeatability of the measurements also shown in Fig. 3.11. Confidence intervals in cumulative measurements at each particle size are shown on the figure as the error bars. For particle sizes the confidence interval is $\pm 1\%$ of the size [120] (not shown on the figure). It is observed that the PSD measurements are repeatable with maximum standard deviation of 0.01234 in the cumulative distribution. For each measurement, D_{50} the median size (the size that has cumulative distribution equal to 0.5 or 50%) is also obtained. The average D_{50} is 6.10 ± 0.1017 μm at 95% confidence level.

As the samples need to be diluted for the PSD measurements, the effect of diluting on the measurements is also tested by measuring PSD for five diluted samples reproduced from the same underflow stream sample source. This sample source is chosen to be the same sample as the repeatability test so the results can be compared to each other. The results of these reproducibility tests are shown in Fig. 3.12. The plots of distributions show a good agreement between diluted samples with maximum standard deviation of 0.01489 in cumulative measurements. The average D_{50} of 6.36 ± 0.1800 μm at 95% confidence level are obtained for the D_{50} measure-

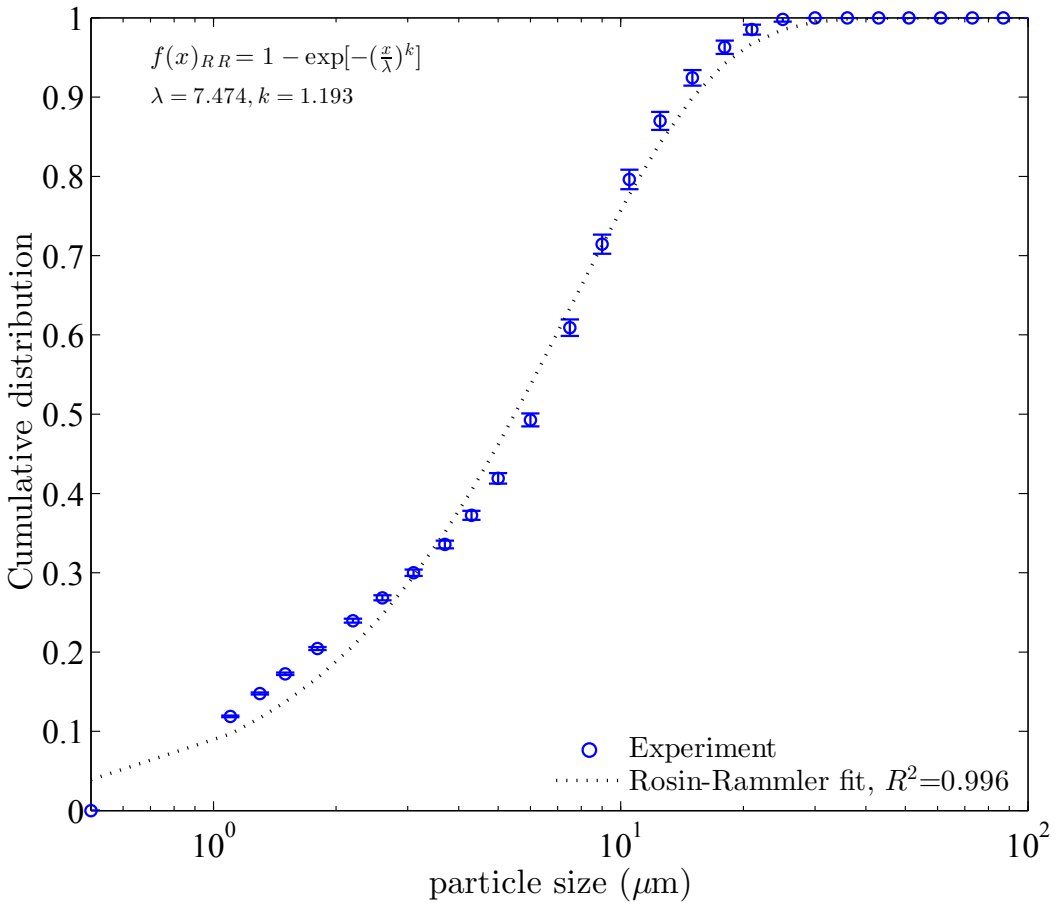

Figure 3.11: Repeatability of PSD measurements for an underflow steam sample; average $D_{50} = 6.10$ μm;

ments in this test. The discrepancy between the averaged D_{50} for repeatability of the measurements and the reproducibility of diluting the samples is 0.2 μm. These results confirm a good agreement in size analysis between the repeated tests and reproduced diluted measuring samples. It is also observed that the underflow size distribution can be fitted to a Rosin-Ramler (or Weibull) distribution that is a typical distribution for the solid particles used in the industry [118].

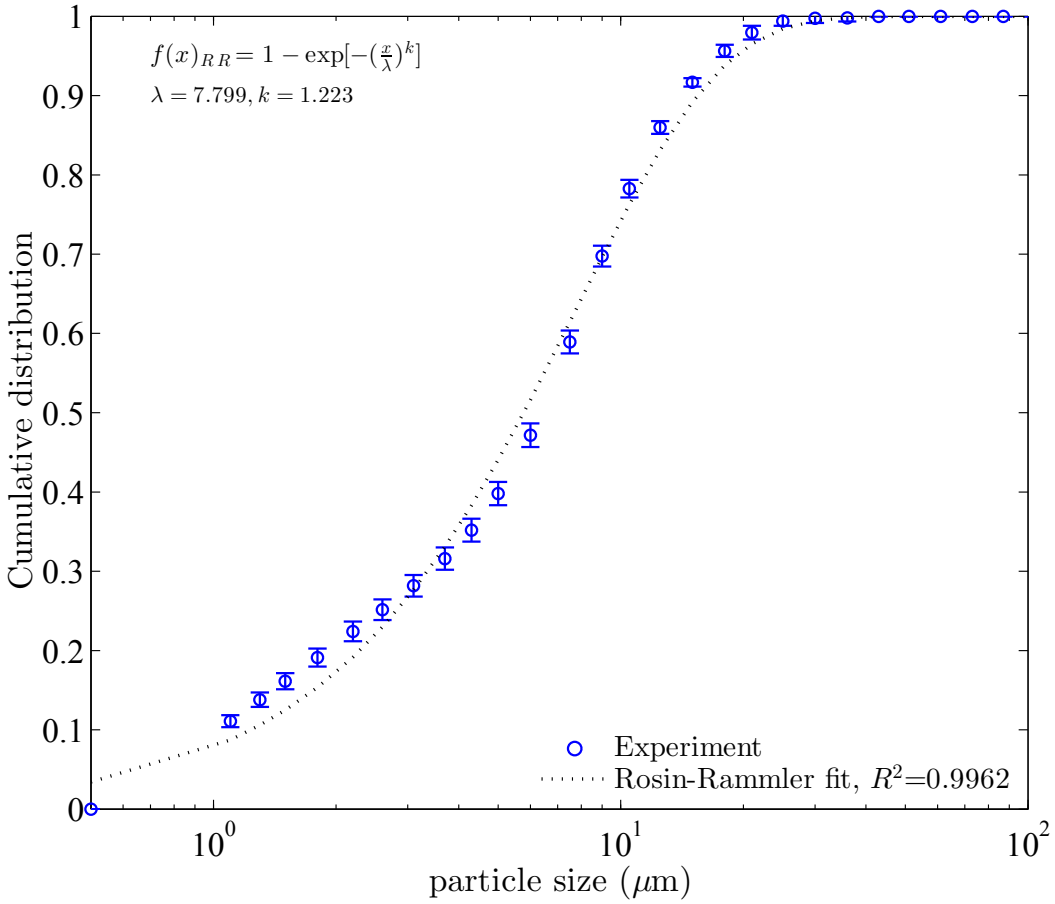

Figure 3.12: Cumulative distribution for reproducibility of the diluted samples from the same source as in Fig. 3.11; average $D_{50} = 6.36$ μm

3.7 Uncertainty analysis

Three sets of experiments for each feed flow conditions i.e feed pump speed (n_{FPS}), underflow pump speed (n_{UPS}) and feed concentration c are used to quantify uncertainty. Both precision (random) uncertainty (P_x) and bias (systematic) uncertainty (B) are determined from the experimental data [121]. Combining the two uncertainties using the root sum square formula [121] gives the total uncertainty (U_x). For a constant feed pump speed (1800 rpm) and underflow pump speed (1500 rpm) the uncertainty of the main variables and the standard deviation (STD) are listed in Table 3.7. The average value (mean) of each variable, the minimum uncertainty U_x(min.) and maximum uncertainty U_x(max.) for all 54 experiments are also listed in Table 3.7.

The effect of pump speed on the total experimental uncertainty (in terms of percent of the measured data) due to changing the inlet conditions are shown in Fig. 3.13 to Fig. 3.15. Increasing the n_{UPS} typically decreases the percent of total uncertainties of the density measurements as shown in Fig. 3.13 and Fig. 3.17. However, the uncertainty analysis for the inlet flow rate and pressure shown in Fig. 3.14 and Fig. 3.15 indicate neither an increasing or deceasing trend for the effect of pump speeds on uncertainties as in the density case. The uncertainties in measuring the underflow pressure and density are shown in Fig. 3.16 and Fig. 3.17. The underflow density uncertainties are decreasing with increasing the underflow flow rate which is due to increasing the inlet flow rate or the underflow rate by increasing the underflow or feed pump speeds.

These uncertainties will be used to determine the uncertainty of the measured

Table 3.7: Standard deviation and uncertainties for the experimental variables at n_{FPS} equal 1800 rpm and n_{UPS} equals 1500 rpm. (Mean, minimum and maximum values are for all 54 experiments)

Variable	STD	P_x	B	U_x	Mean	U_x(min.)	U_x(max.)
Inlet flow rate (m^3/hr)	0.014	0.023	0.005	0.023	1.620	0.006	0.044
Underflow flow rate (m^3/hr)	0.010	0.016	0.003	0.016	0.755	0.005	0.028
Inlet Pressure (kPa)	0.315	0.531	0.004	0.531	88.96	0.303	1.899
Underflow Pressure (kPa)	0.456	0.768	0.004	0.768	9.757	0.169	1.031
Overflow Pressure (kPa)	0.054	0.091	0.004	0.091	-8.301	0.048	0.261
Inlet stream density (kg/m^3)	0.161	0.272	0.5	0.569	996.3	0.569	2.776
Underflow stream density (kg/m^3)	0.171	0.289	0.5	0.578	998.7	0.289	2.178

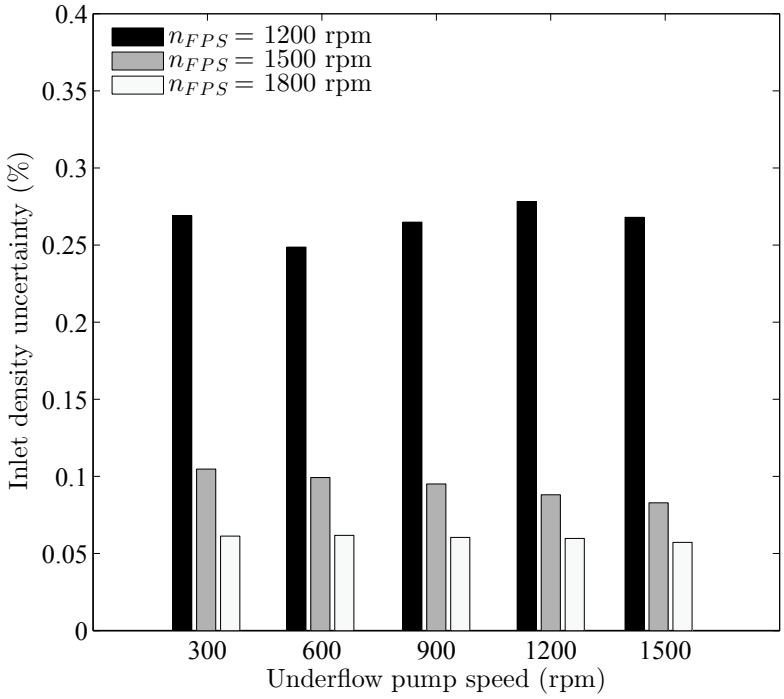

Figure 3.13: Effect of underflow pumping on the total uncertainty of the measured inlet mixture density; $c = 0.1\%$v/v.

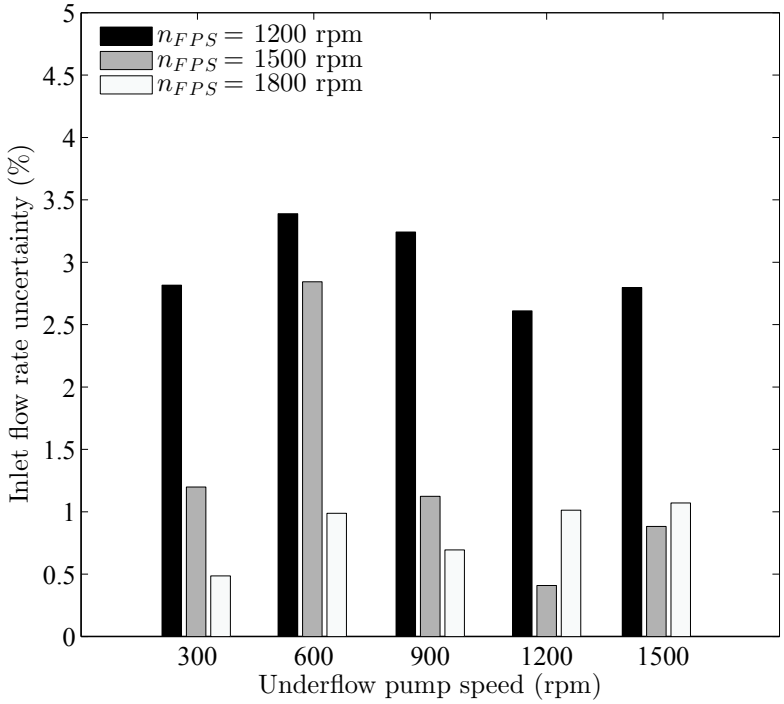

Figure 3.14: Effect of underflow pumping on the total uncertainty of the measured inlet flow rate; $c = 0.1\%$v/v.

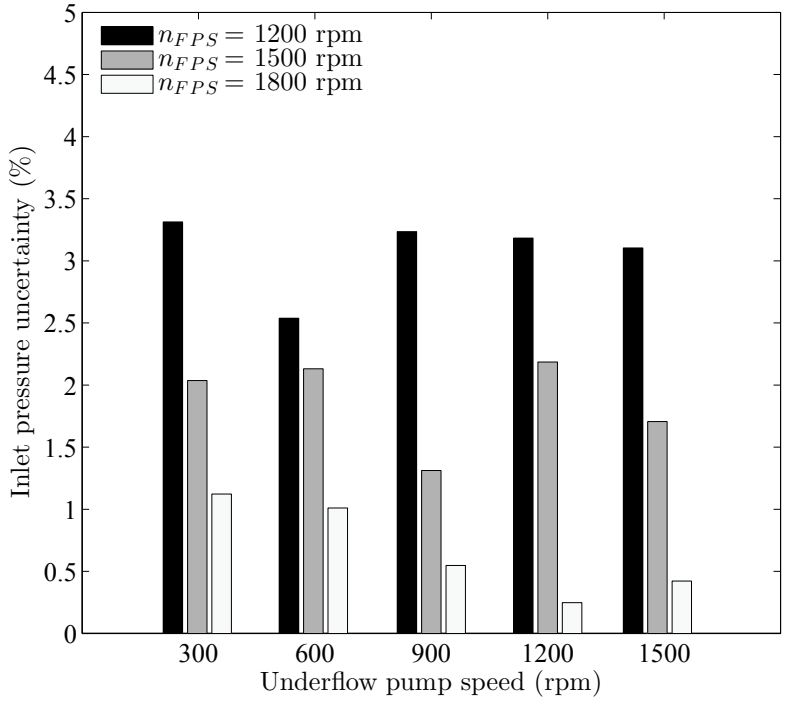

Figure 3.15: Effect of underflow pumping on the total uncertainty of the measured inlet pressure; $c = 0.1\%$v/v.

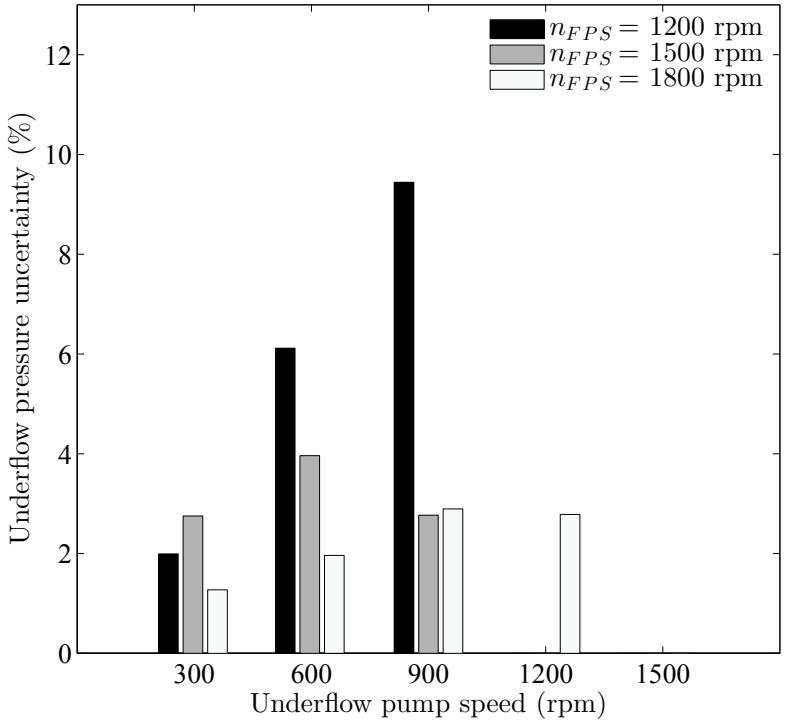

Figure 3.16: Effect of underflow pumping on the total uncertainty of the measured underflow pressure; $c = 0.1\%$v/v.

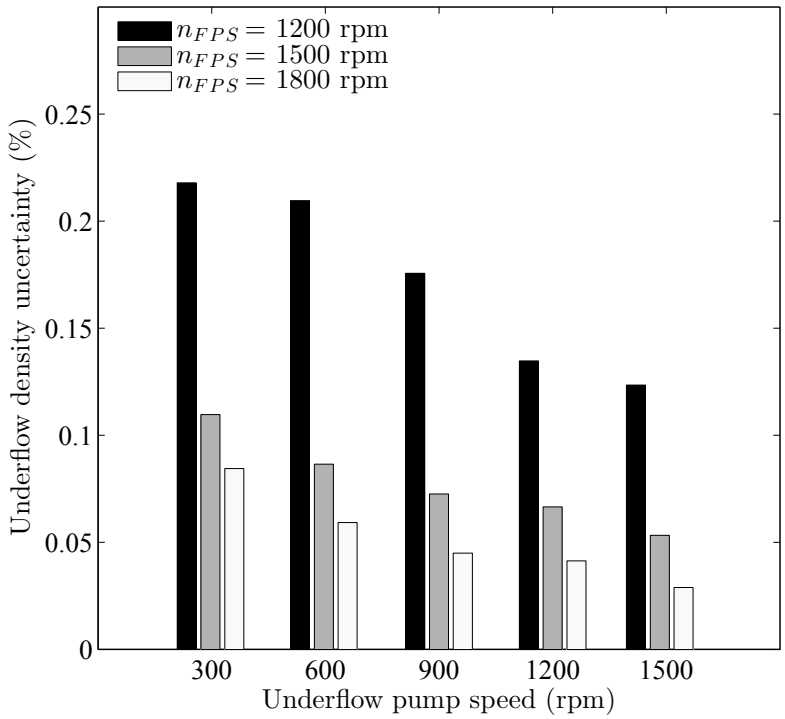

Figure 3.17: Effect of underflow pumping on the total uncertainty of the measured underflow density; $c = 0.1\%$v/v.

equivalent settling area factor obtained from the experimental data.

3.8 Conclusions

The experimental setup, procedures and details of the equipment are explained in this chapter. A test rig is designed and built that is used to undertake experiments to validate the theoretical models of equivalent area factor for the hydrocyclone. It also equipped with a pump in the underflow that allows investigating the effect of underflow pumping on the hydrocyclone performance. The sampling method is explained and a sample particle size analyzing from the inlet flow is detailed to show the distribution type and the repeatability of the particle size measurements. The sampling procedure is also shown to be reproducible. The experimental data is used in the consequent chapters to evaluate the theoretical results and to investigate

the underflow pumping effect. The uncertainties of the measured variables in the experiments are also obtained and discussed. The uncertainties will be used to determine the uncertainties of the models (to estimate the equivalent area factor in the hydrocyclone) that are developed in the next chapters.

Chapter 4

Modeling and experiement for equivalent settling area factor in hydrocyclones[1]

4.1 Introduction

In this chapter, a mathematical approach to develop an equivalent settling area model (ESAM) is presented to predict the performance of the hydrocyclone using a similar technique to other centrifugal separators. Such a model allows comparison of the device performance with other centrifuge separators. It also helps understanding the effect of design and operating variables on the performance of the device. The model can also be used to scale up a hydrocyclone for a desired performance. Basic concepts are discussed first and then the derivation of the ESAM is detailed. The results from the experiments are used to validate the ESAM. Four different types of hydrocyclone designs are studied for model validation. The effect of design parameters on the hydrocyclone performance is detailed and examined using the experimental results. The advantage of using the ESAM in flow predic-

[1] Parts of this chapter is based on R. Sabbagh, M. G. Lipsett, C. R. Koch, D. S. Nobes, "Theoretical and experiemntal study of hydrocyclone performance and equivalent settling area", ASME2014 International Congress and Exposition IMECE2014, ASME, Montreal. Quebec, Canada [122]

tion without performing a flow measurement is discussed. The ability of the ESAM in providing a quantifiable information for predicting the equivalent settling area factor is also investigated over broad ranges of design and operating conditions.

4.2 Analytical modeling

4.2.1 Basic concepts

In developing the equivalent settling area of a centrifuge (i.e the area of a continuous gravity settling tank that has the same performance as the centrifuge) a 50% cut size particle is assumed to be separated in the centrifugal separator during its stay in the device. This is a similar concept to residence time theory which assumes that a 50% cut size particle will be separated in a hydrocyclone during the residence time if it reaches the hydrocyclone wall when the particle is injected into the hydrocyclone exactly from the middle of the inlet section pipe [13]. The assumptions used for the residence time concept are the basis for developing an equivalent area for centrifugal devices [22]. Combining residence time theory with the assumptions of Stokes' law [25], the radial velocity due to the centrifugal acceleration is [13]:

$$v_r = \frac{\Delta\rho d^2}{18\mu}\frac{v_\theta^2}{r} \tag{4.1}$$

where d is the particle diameter, $\Delta\rho$ is density difference between phases, μ is dynamic viscosity of the fluid and the term v_θ^2/r is the centrifugal acceleration where v_θ is the tangential velocity component and r is the radius of the rotation. The radial velocity v_r can be related to the vertical velocity (v_z) using the chain rule. Assuming that the flow near the hydrocyclone wall follows the shape of the wall [13], v_r is approximated by:

$$v_r = \frac{dr}{dt} = \frac{dr}{dz}\frac{dz}{dt} = \frac{D}{2L}v_z \tag{4.2}$$

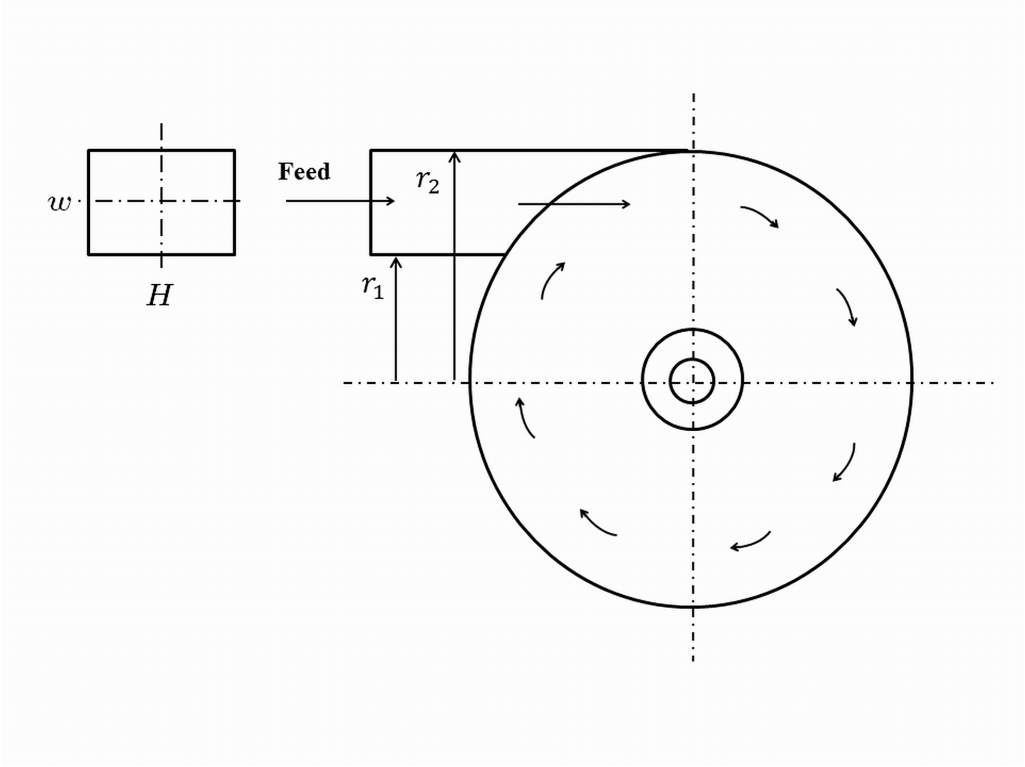

Figure 4.1: Plan view of the cylindrical portion of the hydrocyclone with a rectangular inlet for defining model variables.

where dr and dz are line elements in the radial and vertical directions, *dt* is the time element, D is the hydrocyclone diameter and L is the total length as defined in Fig. 2.3.

Assuming the vertical velocity of the particle equals that of the liquid [63], the average vertical velocity component can be estimated from the inlet flow rate Q in the hydrocyclone cylindrical section region as [123]:

$$v_z = \frac{4Q}{\pi(D^2 - D_o^2)} \tag{4.3}$$

where D_o is the overflow diameter. The flow rate can be obtained using Eq. (4.3)

combining with Eq. (4.1) and Eq. (4.2):

$$Q = \frac{\Delta\rho d^2}{9\mu}\frac{\pi(D^2 - D_o^2)L}{4D}\frac{v_\theta^2}{r} \tag{4.4}$$

which can be simplified to:

$$Q = 2v_g\frac{\pi(D^2 - D_o^2)L}{4gD}\frac{v_\theta^2}{r} \tag{4.5}$$

where v_g is settling velocity under gravitational acceleration (not under centrifugal acceleration) for 50% cut size particle where 50% of particles (by mass) which are larger (smaller) than this size pass through each of the outlets of the separator. The gravitational settling velocity v_g is defined as:

$$v_g = \frac{\Delta\rho d^2}{18\mu}g \tag{4.6}$$

where d is the particle 50% cut size diameter and v_g is calculated using Stokes' law assuming that particles are fine enough to satisfy Stokes' law assumptions and travel at terminal velocity.

For hydrocyclones it has been experimentally found that v_θ is a function of r such that $v_\theta = C/r^n$ where the constant C and exponent n are typically determined from experiments [13]. The constant C can be obtained from a mass balance by integrating the tangential velocity at the inlet section area from r_1 to r_2 (for a rectangular inlet pipe $r_1 = D/2$ and $r_2 = D/2 - w$ where w is the inlet pipe width as defined in Fig. 4.1) and then equating to the feed volume flow rate [122]. Therefore, v_θ is obtained such that:

$$v_\theta = \frac{Q(1-n)}{H(r_2^{1-n} - r_1^{1-n})r^n} \tag{4.7}$$

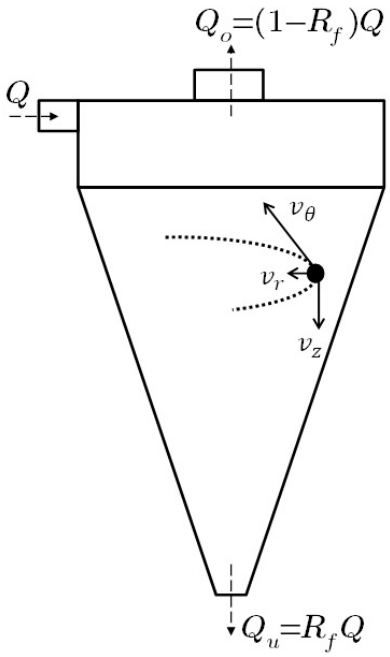

Figure 4.2: Schematics of velocity components and flow rates in a hydrocyclone

where H is the depth of the rectangular inlet pipe defined in Fig. 4.1. The tangential velocity component is also related to the pressure drop in the hydrocyclone. This is shown by considering the Navier-Stokes equation in cylindrical coordinates (r, θ, z) [25] for the radial direction as defined in Fig. 4.2 to be:

$$\frac{\partial v_r}{\partial t} + v_r\frac{\partial v_r}{\partial r} + \frac{v_\theta}{r}\frac{\partial v_r}{\partial \theta} + v_z\frac{\partial v_r}{\partial z} - \frac{v_\theta^2}{r} = \frac{-1}{\rho}\frac{\partial P}{\partial r} + \frac{\mu}{\rho}\left[\frac{\partial}{\partial r}\left(\frac{1}{r}\frac{\partial (r v_r)}{\partial r}\right) + \frac{1}{r^2}\frac{\partial^2 v_r}{\partial \theta^2} + \frac{\partial^2 v_r}{\partial z^2} - \frac{v_r}{r^2} - \frac{2}{r^2}\frac{\partial v_\theta}{\partial \theta}\right] + g_r \tag{4.8}$$

where t is time, P is pressure and g_r represents body forces. For a steady state flow and no gravity (body force) in the radial direction, the first and last terms of Eq. (4.8) are zero. Since the radial velocity in absolute terms is much smaller compared to the other velocity components [2, 124], the terms including v_r and its derivatives are neglected, resulting in:

$$v_r\frac{\partial v_r}{\partial r} - \frac{v_\theta^2}{r} = \frac{-1}{\rho}\frac{\partial P}{\partial r} + \frac{\mu}{\rho}\left(-\frac{2}{r^2}\frac{\partial v_\theta}{\partial \theta}\right) \tag{4.9}$$

The tangential velocity v_θ is also a function of the radial position in the hydrocyclone as in Eq. (4.7) and hence its θ and z derivatives are zero. The following relation is then an expression for pressure changes within the hydrocyclone:

$$\frac{1}{\rho}\frac{\partial P}{\partial r} = \frac{v_\theta^2}{r} \tag{4.10}$$

This expression balances the pressure force with centrifugal acceleration per unit volume and indicates that the pressure increases toward the hydrocyclone wall as the centrifugal force increases.

The pressure drop (ΔP) in a hydrocyclone is obtained by integrating Eq. (4.10). Replacing v_θ from Eq. (4.7) and integrating it in the radial direction between the overflow radius ($D_o/2$) and hydrocyclone radius ($D/2$) results in:

$$\Delta P = \frac{2^{2n-1}\rho}{n}\left(\frac{Q(1-n)}{D^n H(r_2^{1-n} - r_1^{1-n})}\right)^2 \left[\left(\frac{D}{D_o}\right)^{2n} - 1\right] \tag{4.11}$$

At a known flow rate this gives the pressure drop for a hydrocyclone if the exponent n is known. A good approximation for the value of n is 0.8 [125] which can be used for majority of the hydrocyclones.

4.2.2 Model

In a continuous gravity settling tank separator, flow rate is proportional to gravitational settling velocity of particles [15], where the proportionality coefficient is the surface area of the tank. Similarly, assuming a uniform distribution of the particles in operation, for centrifuge separators [22] defined the equivalent area factor Σ with SI units of m^2 as:

$$\Sigma = \frac{Q}{2v_g} \tag{4.12}$$

For a separator, $\Sigma = 1$ shows that its performance equals to the performance of a gravity tank with surface area of 1 m^2 at the same flow rate. A higher value of Σ is desired as it is an indication of the separator performance.

To develop an equivalent area relation for hydrocyclones, the flow rate is related to centrifugal acceleration (Eq. (4.5)) and the equivalent area factor Σ is obtained by combining Eqs.(4.12), (4.7) and (4.5) and replacing Q^2 with the pressure drop relation from Eq. (4.11) resulting in:

$$\Sigma = \frac{\pi L n D^{2n+1}[1-(D_o/D)^2]\Delta P}{\rho g (D-w)^{2n+1}[(D/D_o)^{2n}-1)]} \tag{4.13}$$

where w the width of the rectangular shape inlet section equals $r_2 - r_1$. Since the inlet section depth H does not appear in Eq. (4.13) for hydrocyclones with circular inlet pipes, by assuming $w = D_i$, the equivalent area is:

$$\Sigma = \beta \frac{L \Delta P}{\rho g} \tag{4.14}$$

where:

$$\beta = \frac{\pi n[1-(D_o/D)^2]}{(D/D_o)^{2n}-1} \left(\frac{1}{1-D_i/D}\right)^{2n+1} \tag{4.15}$$

This relationship can also be used for other inlet section types. The equivalent diameter to a circular pipe can be used in Eq. (4.15) if obtained from equating the inlet section area to the area of a circular pipe. Mathematically Eq. (4.15) is held if the following conditions hold: $D_o/D > 0$, $D_i/D < 1$, and $D_o/D \neq 1$. All of theses criteria are satisfied in practice for a typical hydrocyclone. The impact of the incoming flow and the overflow pipe (the portion of the overflow pipe inside the hydrocyclone called the vortex finder) wall causes turbulence in the flow. To avoid this turbulence, $(2D_i/D + D_o/D) \leq 1$ can be considered as a limit for inlet pipe and the vortex finder diameters.

Equation (4.15) indicates that for geometrically similar hydrocyclones, β depends on the value of n and the ratio of inlet (D_i) and overflow (D_o) diameters to hydrocyclone diameter (D). A hydrocyclone diameter could affect the value of β implicitly through the value of n, which could change the tangential velocity component [57]. However, it is believed that the value of n is independent of the hydrocyclone size in most cases [6] and for this reason β is considered a useful design parameter.

In developing the ESAM, the assumptions of Stokes' law for calculating radial velocity of particles are used and it is also assumed that the interaction between particles is negligible. This requires a low concentration of solid particles in the feed flow. The value of volume solid concentration for unhindered settling varies from 1% to 11% for spherical particles [6, 13]. For non-spherical particles this limit is approximately 4% [6]. At high solid concentration, particle-particle interactions reduce the settling velocity and hindered settling effects [30, 126] are significant.

The validity of Stokes' law assumption for hydrocyclones has been discussed in [62] by calculating the Re number of the settling particle and obtaining the particle sizes that satisfy $Re < 2$. Using the same method the Stokes' law is justified for the hydrocyclone and operating conditions in the current study. The obtained Re numbers are < 0.1 and show that the Stokes' law is a valid assumption in this research. Details of the calculations can be found in Appendix A-5.

4.3 Results and Discussion

4.3.1 Effect of design parameters

The experiments are performed according to the experimental procedure discussed in Chapter 3. The experimental results are used to validate the model and to investigate the effect of different variables on the model. The ESAM described in this study relates both operating and design parameters to the Σ, which in turn is a measure of hydrocyclone performance. Hydrocyclone total length L appears directly in the equivalent area factor relation and has a linear effect on Σ. The factor β in Eq. (4.15) is basically a function of design parameters; but it is indirectly related to the tangential velocity through the exponent n. However, according to [6], for every hydrocyclone the tangential velocity component changes only with the radial position as the value of n is independent of the operating conditions and does not change with the vertical position. Thus, β is considered a design parameter and evaluating the β factor can be useful in comparing different designs.

The different values for n reported in the literature are discussed in [6] where the method of measurement is described. This exponent for different designs is found to typically be between 0.7 and 0.9 [127]. An average value of 0.8 is suggested for hydrocyclones [80, 125] and this value is used for further investigation in the current study.

Values of β for different D_o/D and D_i/D is obtained from Eq. (4.15) and are plotted in Fig. 4.3. This figure shows that β increases with either increasing the ratio of the inlet diameter or the overflow diameter to the hydrocyclone diameter. The maximum value of β is obtained for large inlet and overflow outlet diameters. This

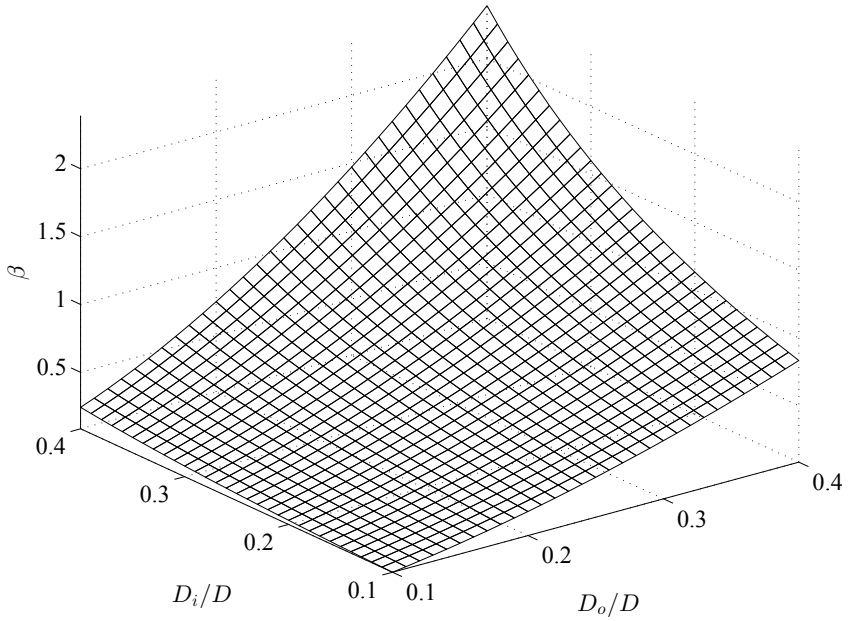

Figure 4.3: Value of β vs. inlet and overflow diameter ratios ($n = 0.8$)

is detailed in Fig. 4.4 and Fig. 4.5 for two different values of n. These figures show that β increases with either increasing the ratio of the inlet diameter or the overflow diameter to the hydrocyclone diameter. The maximum value of β is obtained for large inlet and overflow outlet diameter. Comparing the two figures shows that increasing the value of n decreases the β value. Also, β values according to Fig. 4.4 and Fig. 4.5 can change from about 0.05 for small diameters to about 5 for large inlet and overflow diameter. However, the condition $(2D_i/D+D_o/D) \leq 1$ restricts this range of diameters. This limit $(2D_i/D + D_o/D = 1)$ is shown by a dotted line on Fig. 4.4 and Fig. 4.5. The shaded areas above the dotted lines are where the inlet flow stream collides with the vortex finder wall and hence such diameters of the inlet and vortex finder should be avoided due to creating turbulence to the inlet flow stream. Thus, the values of β can not exceed 2 (for $n = 0.7$) and 1.9 (for $n = 0.9$) for the diameter ranges shown in the figures for hydrocyclones mentioned above. For a constant pressure drop, increasing the β results in a higher Σ and thus

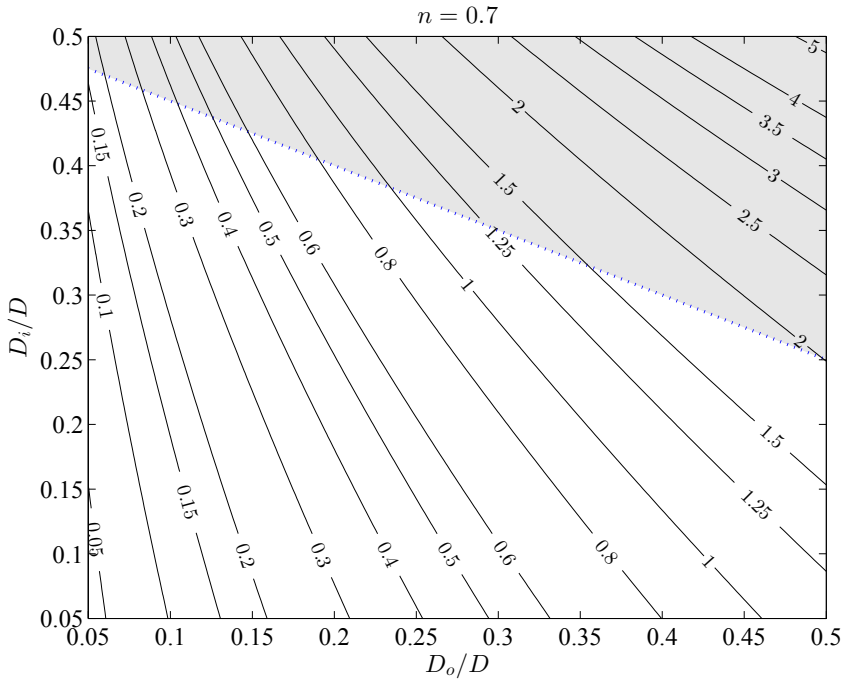

Figure 4.4: Contours of β for different values of D_i/D and D_o/D ($n = 0.7$); dotted line is where $2D_i/D + D_o/D = 1$; shaded area is where $2D_i/D + D_o/D > 1$

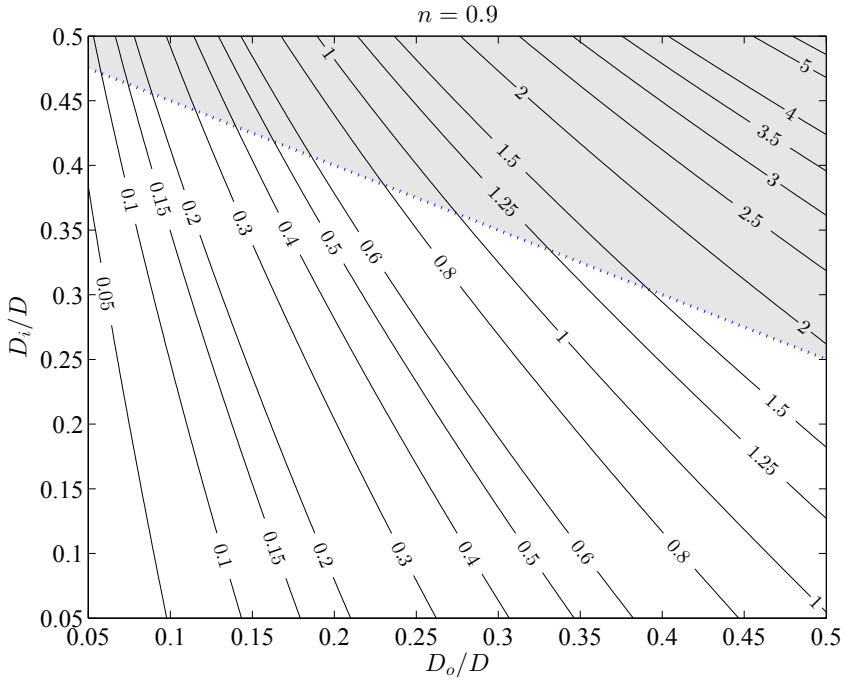

Figure 4.5: Contours of β for different values of D_i/D and D_o/D ($n = 0.9$); dotted line is where $2D_i/D + D_o/D = 1$; shaded area is where $2D_i/D + D_o/D > 1$

a smaller particle cut size according to Eq. (4.12). However, in most applications, changing the inlet and/or the outlet diameters changes the pressure drop, which affects the performance of the device. Increasing the equivalent settling area Σ of a hydrocyclone by increasing the overflow diameter is a better choice than increasing the inlet diameter because the equivalent area is more sensitive to the overflow diameter. This can be quantified by calculating the partial derivatives of β in terms of D_i/D or D_o/D as in Eq. (4.16) and Eq. (4.17).

$$\frac{\partial \beta}{\partial (D_i/D)} = \frac{\pi n(2n+1)[1-(D_o/D)^2]}{[(D/D_o)^{2n}-1]\,(1-D_i/D)^{2n+2}} \tag{4.16}$$

$$\frac{\partial \beta}{\partial (D_o/D)} = \frac{2\pi n\,(1-D_i/D)^{-2n-1}}{(D/D_o)^{2n}-1}\left[\frac{n\,[1-(D_o/D)^2]\,(D/D_o)^{2n+1}}{(D/D_o)^{2n}-1} - \frac{D_o}{D}\right] \tag{4.17}$$

The plots of the partial derivatives of β (sensitivity) in terms of D_i/D (D_o/D remains constant) and D_o/D (D_i/D remains constant) are shown in Fig. 4.6 for $n = 0.7$ and in Fig. 4.7 for $n = 0.9$ at three constant values of 0.1, 0.2 and 0.4 for D_i/D (or D_o/D). Changes in β as a result of changes in D_o/D (at a constant D_i/D) are greater than the changes in D_i/D changes (at a constant D_o/D). Since the appearance of the overflow diameter D_o in the β relation is due to the pressure drop, changing the pressure drop has more effect on β and the tangential velocity than changing the inlet diameter and keeping the pressure drop constant.

Comparing Fig. 4.6 and Fig. 4.7 shows that increasing the value of n results in increasing the slope of β with respect to D_i/D or D_o/D. These changes for overflow diameter are greater than the inlet diameter ratio and particularly for higher values of the overflow diameters.

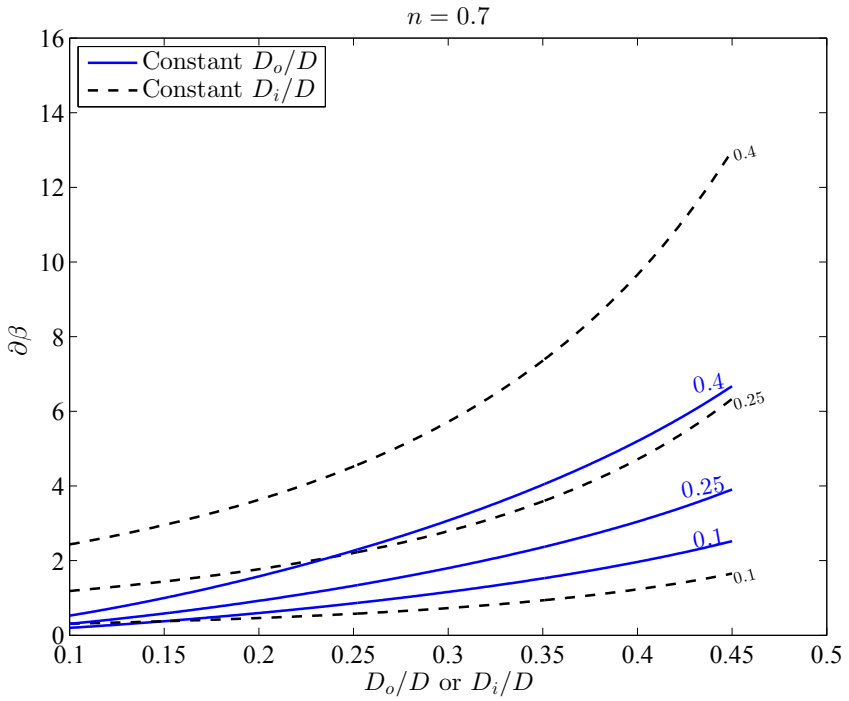

Figure 4.6: $\partial\beta/\partial(D_i/D)$ and $\partial\beta/\partial(D_o/D)$ for different values of D_i/D and D_o/D ($n = 0.7$)

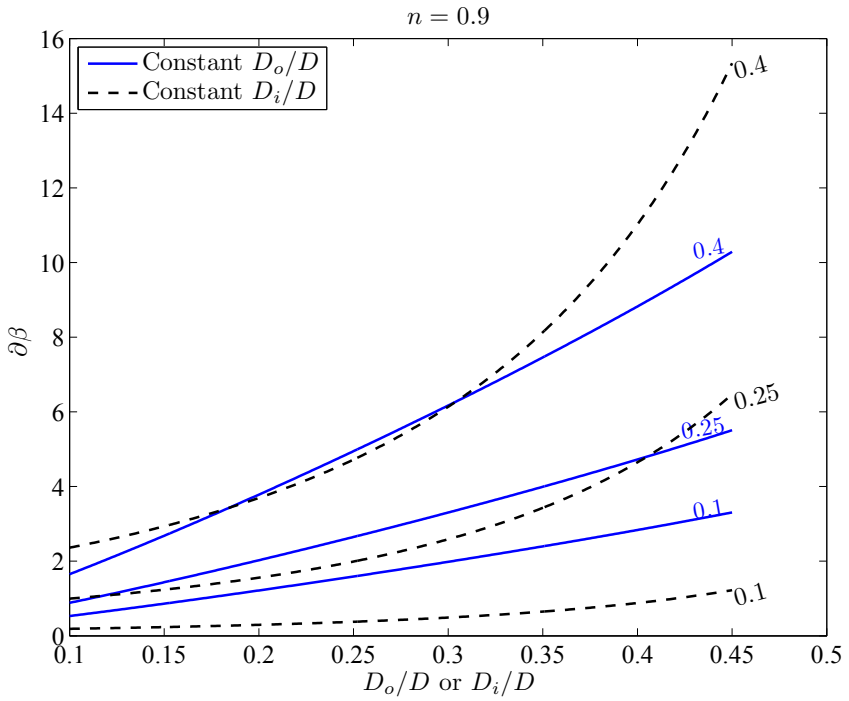

Figure 4.7: $\partial\beta/\partial(D_i/D)$ and $\partial\beta/\partial(D_o/D)$ for different values of D_i/D and D_o/D ($n = 0.9$)

4.3.2 Model validation

The experimental results are used to validate the ESAM. To do this, the Σ values are calculated from the ESAM (Σ_{model}) with the average chosen value of $n = 0.8$. These are plotted versus experimental values obtained from the experimental data (Σ_{exp}) for the current study. Values of Σ_{model} and Σ_{exp} are also calculated for other types of the hydrocyclones (Case 2, 3 and 4 in Table 3.3) assuming similar hydrocyclone diameter of 50 mm as in the hydrocyclone in the current study. The design parameters for these designs are also listed in Table 3.3.

To obtain the equivalent area factor from the experiments (Σ_{exp}) the underflow cut size at each test is determined by particle size analysis using the same method previously explained in Chapter 3 for the inlet flow particles. For the underflow cut size diameter Eq. (4.6) is used to calculate the settling velocity under gravitational acceleration. At each operating condition (constant flow rates and pressure drop) for a certain inlet flow rate, Σ_{exp} is calculated from Eq. (4.12). For the Rietema, Demco 4H and Bradley hydrocyclone designs, the values of Σ_{exp} are obtained from the experimental correlations in [5] by calculating the flow rate and cut size at similar pressure drops as in the current study. Pressure drop is calculated from the difference between the inlet and the underflow pressure.

The equivalent area factor from the ESAM (Σ_{model}) is calculated from Eq. (4.14) at each inlet flow rate for all designs. As pressure drop is required for obtaining Σ_{model} and to be able to compare the results of the experiment and the model, the same experimental pressure drop is used. The uncertainties in calculating Σ are explained in Appendix A-4.

The plots of Σ_{exp} and Σ_{model} ($n = 0.8$) resulted from the calculations for the

current study (and for Rietema, Demco 4H and Bradley hydrocyclones) are shown in Figs. 4.8 to Fig. 4.11. As can be seen from the figures, there is a discrepancy between the experimental data and the data predicted using the proposed $n = 0.8$. This is particularly noticeable for the Bradley hydrocyclone which using $n = 0.8$ leads to underestimated values of the equivalent area factor. To obtain the best match between the experiment and the ESAM results, the sum of squared errors (SSE) between the values of Σ_{model} and Σ_{exp} in each hydrocyclone is minimized by examining the exponent n). The resulted exponent after minimizing SSE is called the *optimized n* and is represented by n_p. The results of comparing the equivalent area factor between the ESAM and experiment using n_p are plotted in Fig. 4.12 to Fig. 4.15. Points on the 45° line indicate an exact match between ESAM and experiment. The lines of $\pm 15\%$ deviation from the best match are also plotted in the figure. The comparison in Fig. 4.8 and Fig. 4.12 shows a good agreement between the ESAM and experiment within 15%. The scattered experimental data are due to uncertainties in the experimental measurements for the operating variables and particle size measurement. The larger length of the hydrocyclone in the current study comparing the other types of hydrocyclones causes a noticeable difference between the scales of the equivalent area factors that can be seen in the figures.

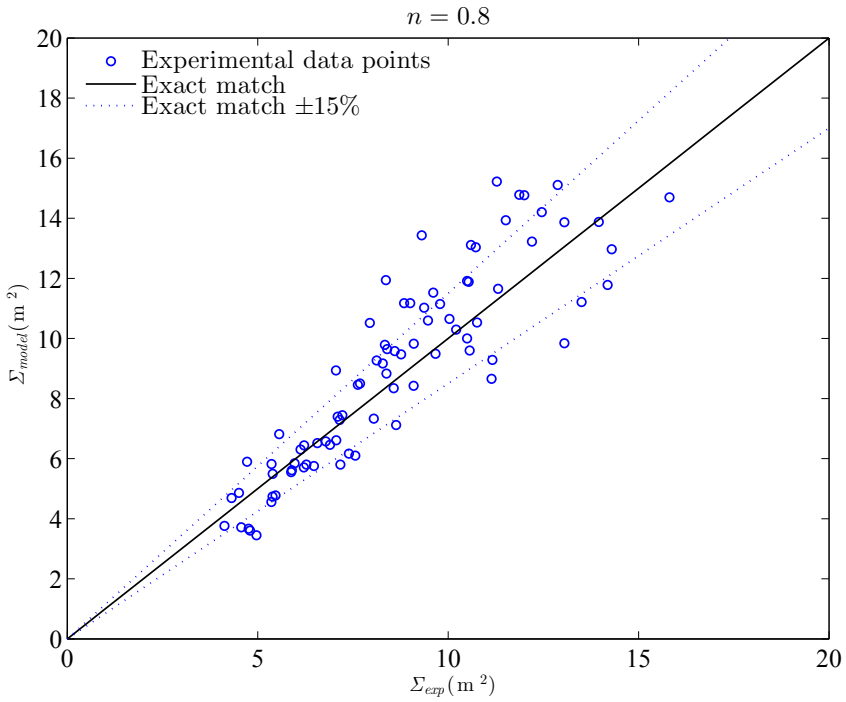

Figure 4.8: Comparison of experimental equivalent area factors and ESAM ($n = 0.8$) prediction for the current study.

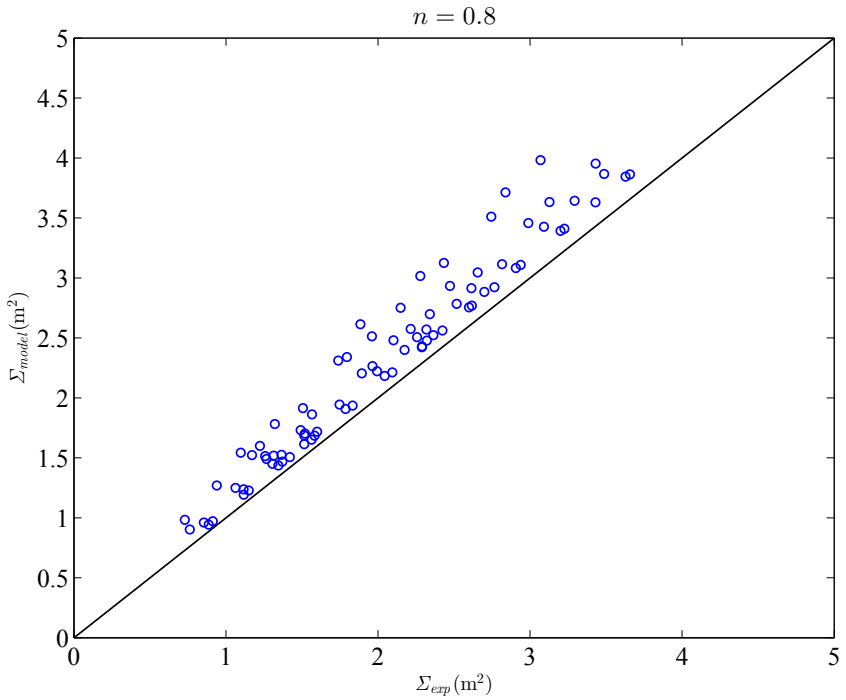

Figure 4.9: Experimental equivalent area factor vs. ESAM ($n = 0.8$) for similar pressure drops and inlet concentrations as in the current study for a Rietema hydrocyclone; experimental values are from the correlations in [5].

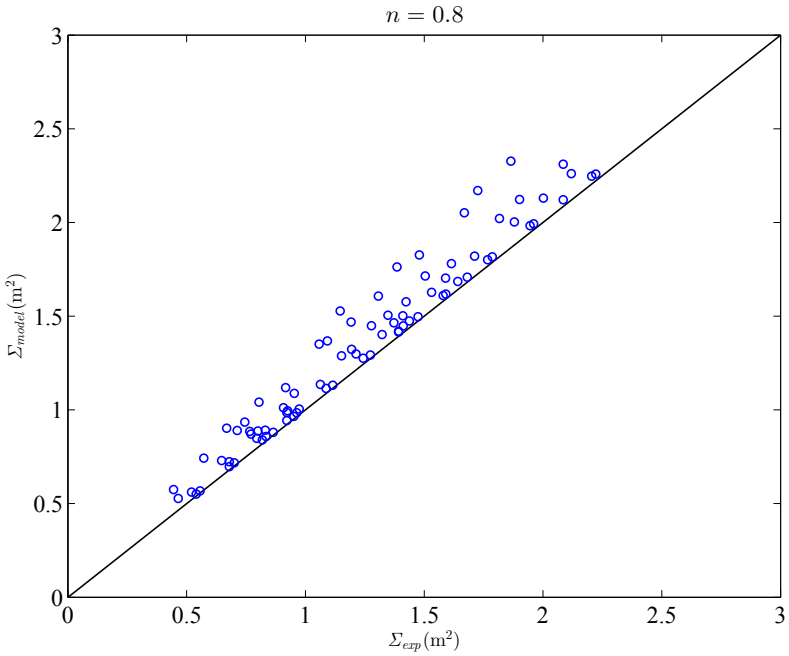

Figure 4.10: Experimental equivalent area factor vs. ESAM ($n = 0.8$) for similar pressure drops and inlet concentrations as in the current study for a Demco 4H hydrocyclone; experimental values are from the correlations in [5].

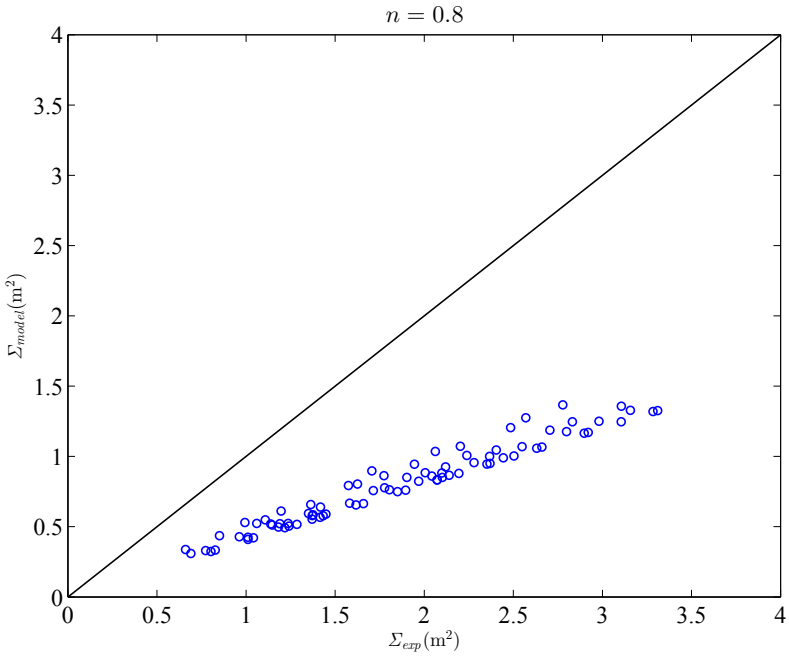

Figure 4.11: Experimental equivalent area factor vs. ESAM ($n = 0.8$) for similar pressure drops and inlet concentrations as in the current study for a Bradley hydrocyclone; experimental values are from the correlations in [5].

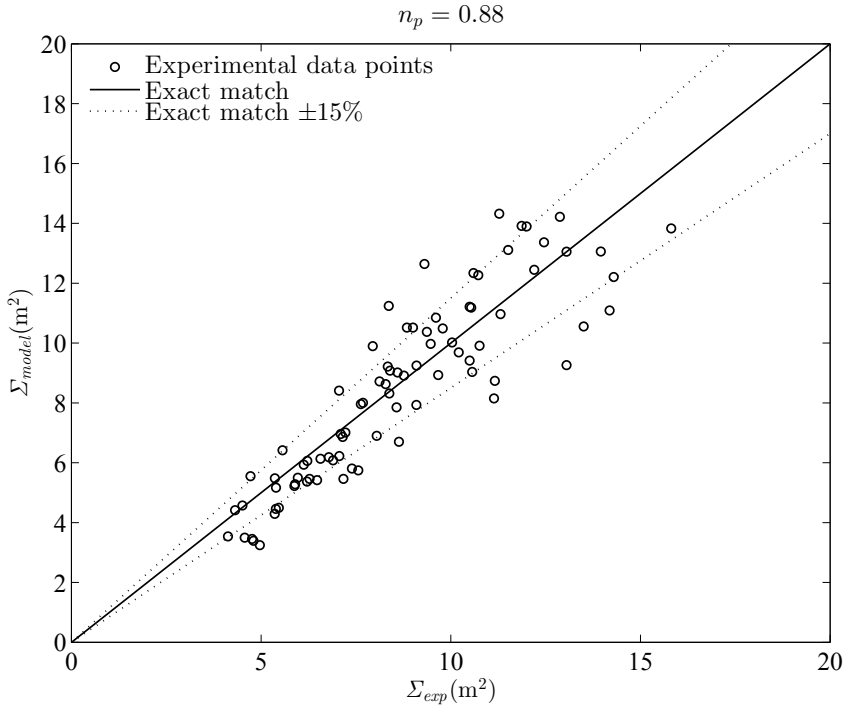

Figure 4.12: Comparison of experimental equivalent area factors and ESAM ($n_p = 0.88$) prediction for the current study.

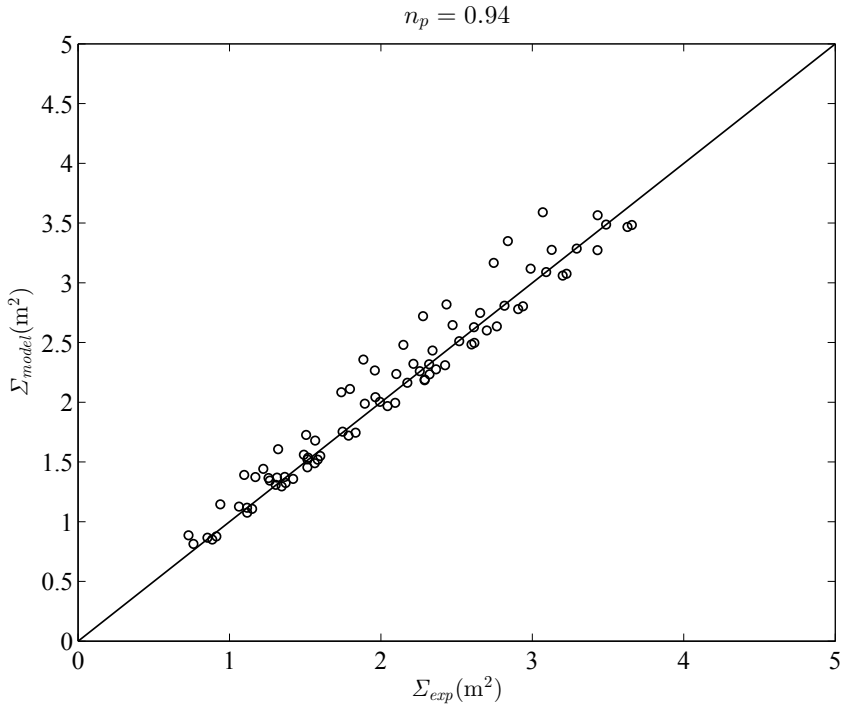

Figure 4.13: Experimental equivalent area factor vs. ESAM ($n_p = 0.94$) for similar pressure drops and inlet concentrations as in the current study for a Rietema hydrocyclone; experimental values are from the correlations in [5].

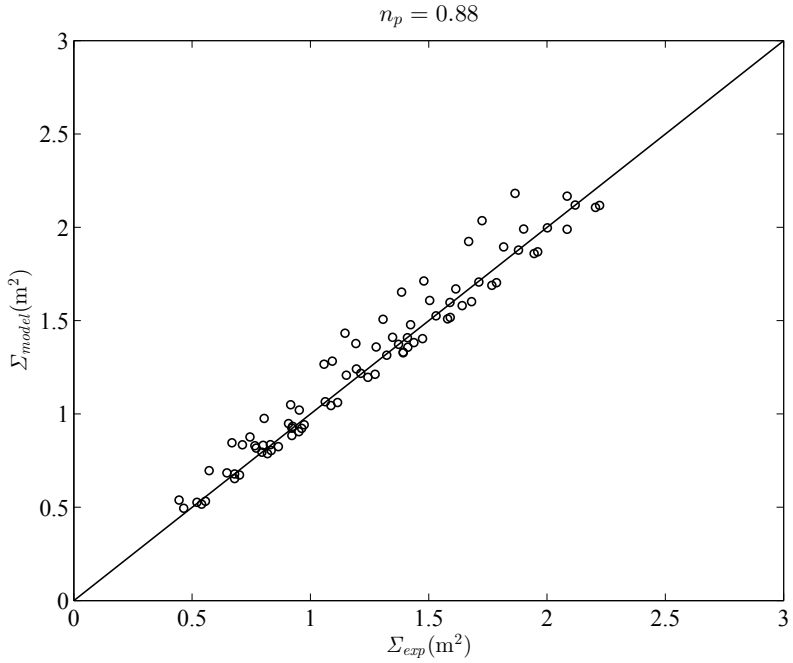

Figure 4.14: Experimental equivalent area factor vs. ESAM ($n_p = 0.88$) for similar pressure drops and inlet concentrations as in the current study for a Demco 4H hydrocyclone; experimental values are from the correlations in [5].

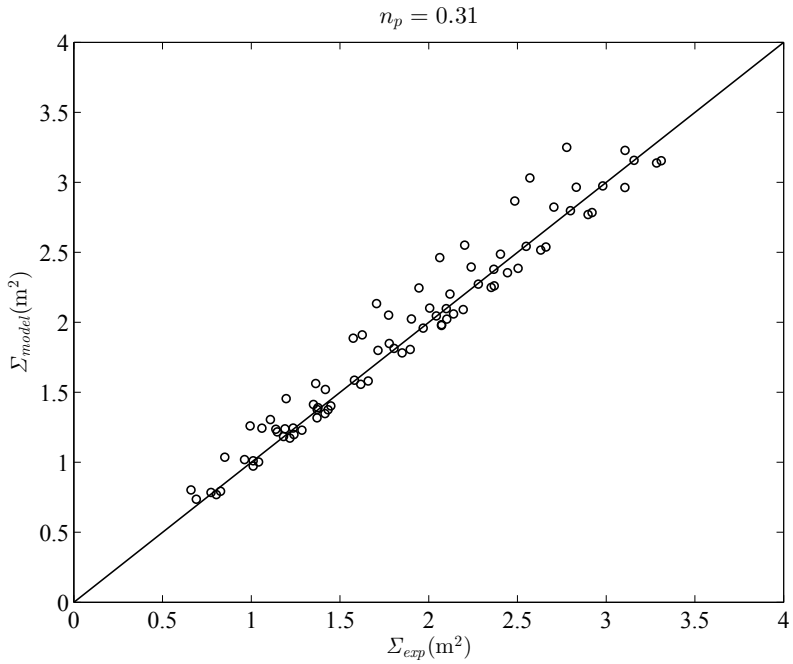

Figure 4.15: Experimental equivalent area factor vs. ESAM ($n_p = 0.31$) for similar pressure drops and inlet concentrations as in the current study for a Bradley hydrocyclone; experimental values are from the correlations in [5].

As can be seen from Fig. 4.8 and Fig. 4.12, the exponent n_p for the current study is 0.88, which is comparable with the value of 0.8 for n suggested in [125]. The obtained value of n_p is 0.94 for Rietema hydrocyclone, 0.88 for Demco 4H hydrocyclone and 0.31 for Bradley hydrocyclone shown in Fig. 4.13, Fig. 4.14 and Fig. 4.15, respectively. The values obtained from the ESAM as determined above, are close to the chosen value of $n = 0.8$ except for the Bradley hydrocyclone that there is a significant discrepancy between the two exponents.

To investigate the discrepancy between the ESAM prediction and experimental equivalent area factor observed for the Bradley hydrocyclone, the values of exponent n are compared with the literature. To do this, the experimentally obtained n for Bradley hydrocyclones are extracted from [6] and compared to the optimized values of n_p from the ESAM (optimized exponent for the best match between Σ_{model} and Σ_{exp}). The tests conditions and the results of the comparison are summarized in Table 4.1. The values in Table 4.1 indicate that the optimized exponents n_p from ESAM are in good agreement with the values of n measured experimentally with maximum deviation of 0.06. This denotes that the ESAM can be confidently used to approximate the n and hence Σ. Knowing this, the discrepancy in Σ values between the ESAM and experiment is attributed to the value of n used in the ESAM to predict the Σ in Bradley hydrocyclone. It shows that despite the generally accepted range for the exponent n (0.7-0.9 [127] or 0.5-0.9 [13]), for particular designs this may decrease to a small value such as 0.2. Therefore, the best value of n that fits the model for each design geometry should be obtained from the experimental results. To evaluate the effect of design parameters on the equivalent area factor, plots of Σ as a function of pressure drop (according to Eq. (4.15)) are

Table 4.1: Comparing the experimental value of the tangential velocity exponent n [6] and the optimized values using the ESAM (n_p); $D_i/D = 1/7.5$, $D_o/D = 1/5$; $D_u/D = 1/15$, $\theta = 9°$ (dimensions are defined in Fig. 2.3)

D (mm)	Pressure drop (kPa)	Inlet flow rate (m^3/hr)	n (experiment)	n_p (ESAM)
15	46.9	0.072	0.11	0.16
15	81.4	0.091	0.15	0.16
15	146.9	0.114	0.16	0.17
15	193.7	0.112	0.18	0.17
15	242.0	0.128	0.19	0.17
75	30.3	1.363	0.17	0.19
75	31.7	1.363	0.16	0.19
75	84.8	2.066	0.19	0.20
75	86.9	2.066	0.19	0.20
75	84.1	2.066	0.18	0.20
75	85.5	2.066	0.19	0.20
75	134.4	2.495	0.24	0.20
75	135.8	2.495	0.24	0.20
75	206.8	2.971	0.26	0.20

shown in Fig. 4.16 to Fig. 4.19 for the four types of hydrocyclones. Each plot compares the data of experimental Σ to the data with Σ from the ESAM with $n = 0.8$ and ESAM with optimized exponent n_p. This comparison has the advantage of including the effect of hydrocyclone total length L (see Fig. 2.3) which does not appear in β. From Fig. 4.16 to Fig. 4.18 it can be concluded that there is a good agreement between the ESAM and the experimental results. This shows that the proposed ESAM in Eq. (4.14) predicts well the effect of the design parameters on Σ. As discussed above, the discrepancy between the ESAM and the experimental points for the Bradley hydrocyclones in Fig. 4.19 is attributed to the specifications of this hydrocyclone that requires a smaller value of n to predict the tangential velocity profile. Therefore, the plot of the model with n_p shows an excellent match with the experimental data.

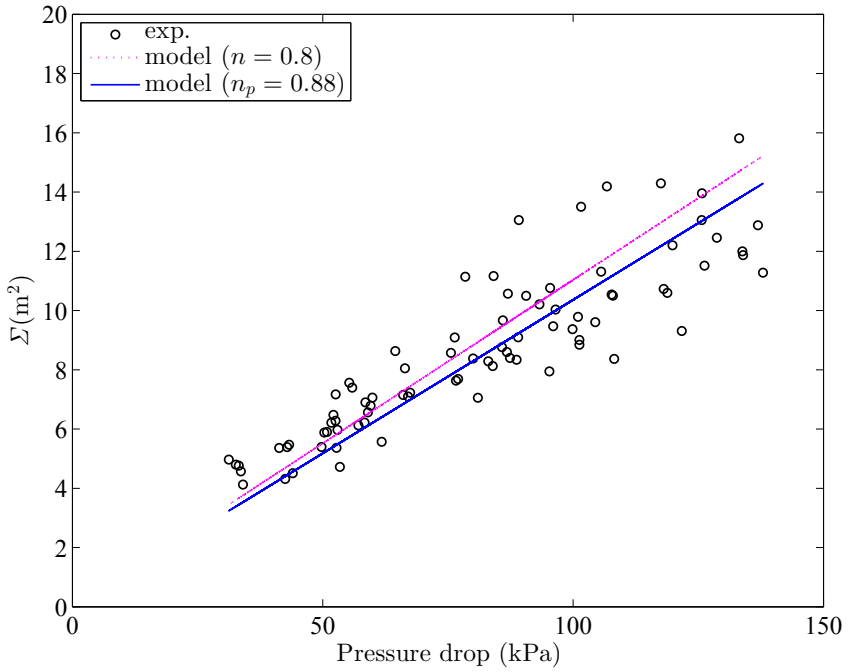

Figure 4.16: Current study; comparing the experimental equivalent area factor vs. pressure drops with the values predicted with ESAM ($n = 0.8$, $n_p = 0.88$) for similar pressure drops and inlet concentrations as in the current study.

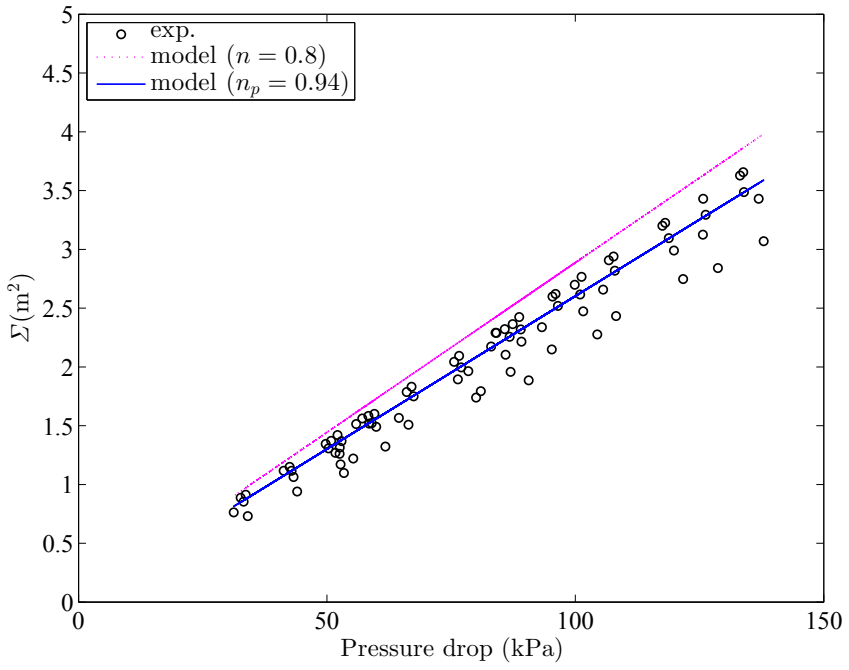

Figure 4.17: Rietema hydrocyclone; comparing the experimental equivalent area factor vs. pressure drops with the values predicted with ESAM ($n = 0.8$, $n_p = 0.94$) for similar pressure drops and inlet concentrations as in the current study; experimental values are based on correlations in [5].

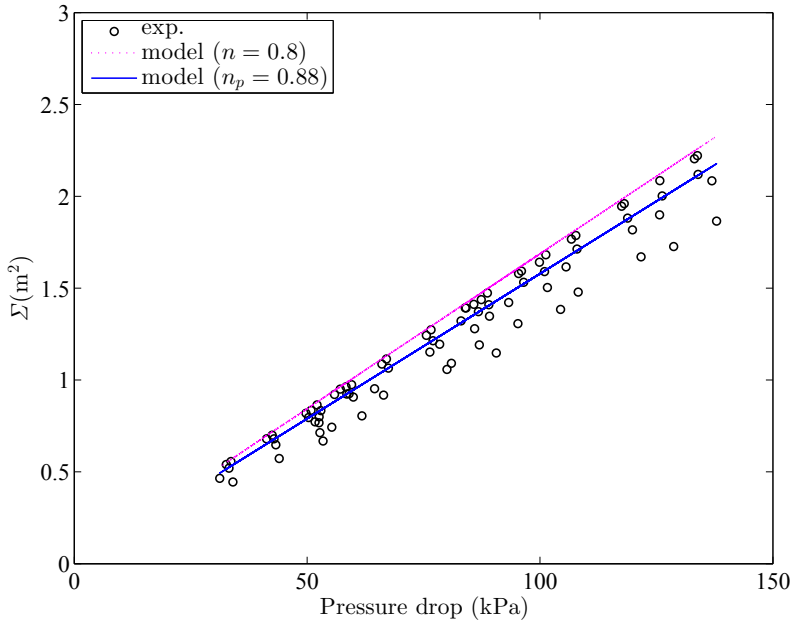

Figure 4.18: Demco 4H hydrocyclone; comparing the experimental equivalent area factor vs. pressure drops with the values predicted with ESAM ($n = 0.8$, $n_p = 0.88$) for similar pressure drops and inlet concentrations as in the current study; experimental values are based on correlations in [5].

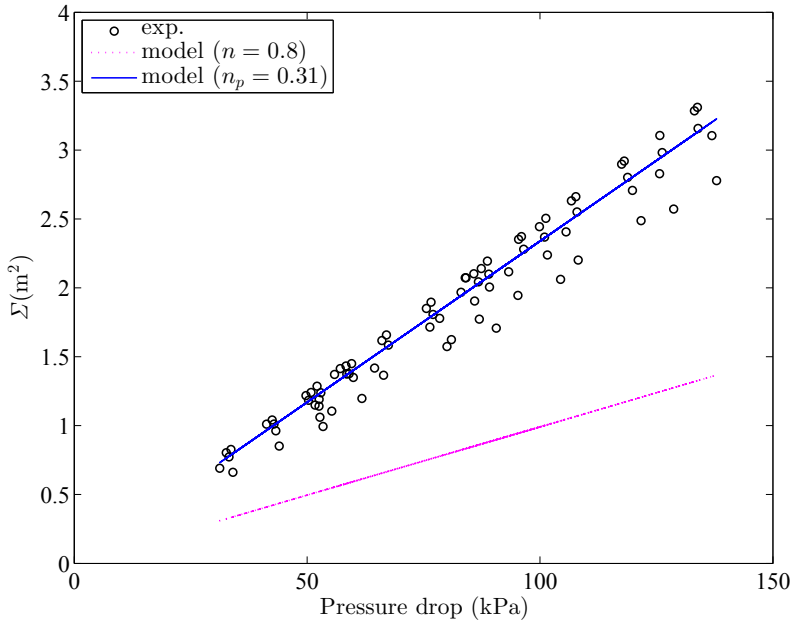

Figure 4.19: Bradley hydrocyclone; comparing the experimental equivalent area factor vs. pressure drops with the values predicted with ESAM ($n = 0.8$, $n_p = 0.31$) for similar pressure drops and inlet concentrations as in the current study; experimental values are based on correlations in [5].

4.3.3 Predicting the tangential velocity profile

Estimating the value of n for a hydrocyclone without needing velocity profile for tangential velocity component is an important aspect of the ESAM. Using the estimated value of n, the tangential velocity profile can also be predicted. Typically to determine the tangential velocity profile measuring of the velocity components is required [58, 128]. Velocimetery measurement in a hydrocyclone is difficult as a result of complicated flow geometry. In addition, some measurement techniques are invasive and some are difficult to perform in an industrial setting. Thus, an alternate method of determining the tangential velocity component (the most important velocity component affects the separation performance [58]) can be useful.

The following procedure is proposed as an alternative method of determining the tangential velocity profile in hydrocyclones on the basis of the ESAM:

1. Experimentally determine the flow rate, fluid properties (density and viscosity), particle density and the separation cut size (using a particle size analysis method).

2. From the information obtained in step 1, settling velocity is determined from Eq. (4.6).

3. The experimental equivalent area factor is calculated from Eq. (4.12).

4. Equating this value with Eq. (4.14) at a known pressure drop gives the value of n.

5. Then v_θ is calculated using Eq. (4.7) using n at the known flow rate and inlet section dimensions.

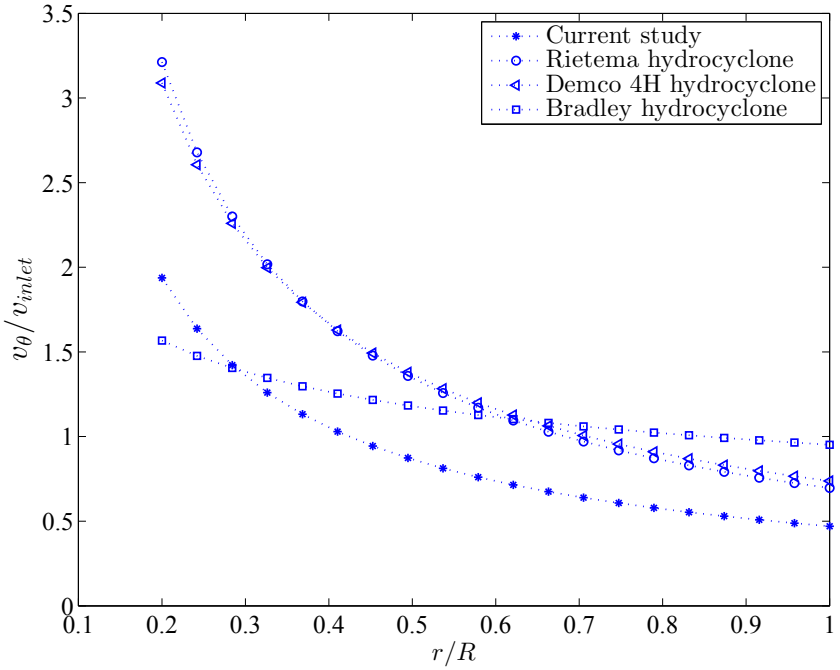

Figure 4.20: Normalized tangential velocity profiles using ESAM at separation zone vs. normalized radius for different hydrocyclones ($R = D/2$)

Following these steps the velocity profiles for the tangential velocity in four hydrocyclone cases are obtained. Fig. 4.20 shows the normalized tangential velocity (normalized with inlet velocity) at different normalized radii (the radial distance from the hydrocyclone centerline). Higher values of the v_θ/v_{inlet} is obtained for Rietema and Demco 4H hydrocyclones. This is interesting as the maximum equivalent area factor is observed in the hydrocyclone in the current study (compare Fig. 4.8 to Fig. 4.14) shows that the effects of the design parameters on the separation is also important. Considering Eq. (4.14), it is found that the total length of a hydrocyclone and the value of β that is dependent to design parameters are also important in determining the equivalent area factor. The longer length of the hydrocyclone in the current research is considered to cause higher equivalent area factor comparing other hydrocyclones.

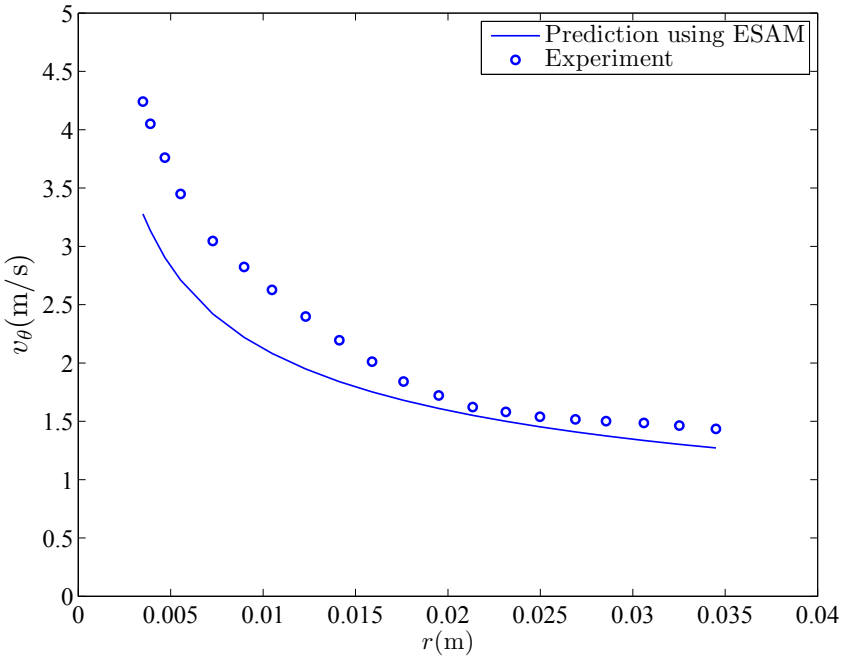

Figure 4.21: Comparison of predicted tangential velocity profiles vs. hydrocyclone radius (r) at separation zone and experimental data from [7] for test conditions as in Table 4.2; $R^2 = 0.71$

Experimental data from [7] are also used to examine the proposed method of tangential velocity profile prediction according to the above mentioned procedure. The hydrocyclone dimensions and test conditions are listed in Table 4.2. The value of exponent n_p is obtained by determining Σ_{model} and Σ_{exp}. Assuming that the liquid density equals 1000 kg/m^3 and using ESAM, Σ_{model} is determined. The experimental test in [7] had no solid particles and performed only for velocity measurements. Thus, Σ_{exp} for the test in [7] is calculated using the correlations developed in [5] assuming sand particles with $\Delta\rho = 1650$ kg/m^3, water as liquid with $\mu = 1$ mPa.s and low particle volume concentration as 0.05%. Equating these two equivalent area factors for the model and experiment results in $n_p = 0.41$. Using this optimized exponent and approximating the rectangular inlet pipe depth H from the equivalent area of the inlet circular pipe, v_θ is obtained using Eq. (4.7). This pre-

dicted tangential velocity is compared to the experimental data [7] in Fig. 4.21. The comparison shows a good agreement between the predicted values and the experimental data with more discrepancies for smaller radiuses. The predicted velocity profile is $v_\theta = 0.31/r^{0.41}$ and the profile resulted from the experimental data is $v_\theta = 0.25/r^{0.51}$ which show a difference of 0.1 between the exponents and 0.06 between the constants. This results in an average error of 14% between the predicted and the observed values shown in Fig. 4.21.

Employing this technique, information at a single data point can be used to estimate the velocity profile. Such an estimation is based on the assumptions used to develop the ESAM including Stokes' law, no hindered settling, spherical particles and for reverse flow hydrocyclones. However, having more experimental data points at different operating conditions results in a more accurate estimation of n by minimizing the sum of squared errors of prediction. Most of the measurements for the tangential velocity component are in pure water or lightly seeded water [7, 57, 58, 61] as the measurements are simpler to perform. However, these experiments do not replicate the real applications of the hydrocyclones in terms of the effects of particles on the tangential velocity component. Predicting the tangential velocity profile on the basis of the proposed method in this study does not required velocity measurement and is based on the experimental cut size.

Table 4.2: Hydrocyclone geometric parameters and experiment conditions from [7] for examining the tangential velocity profile (dimensions are defined in Fig. 2.3)

Parameter	Value
D (mm)	75
D_i (mm)	$0.28D$
D_o (mm)	$0.34D$
D_u (mm)	$0.16D$
L (mm)	$5D$
l (mm)	$0.4D$
ΔP (kPa)	25
Q (m^3/hr)	1.82

4.4 Conclusions

A mathematical model has been developed to predict the equivalent settling area factor in hydrocyclones (ESAM) and it has been validated using data from an experimental study. The experimental results are in good agreement with the ESAM prediction. ESAM can be used to predict the equivalent area factor for a variety of hydrocyclone designs. The equivalent area factor Σ can also be used to compare other centrifugal separators and a continuous settling tank to provide insight into the relative performance of different centrifugal separation techniques. The effects of hydrocyclone inlet and overflow diameters are studied. Σ in hydrocyclones is increased by increasing either the hydrocyclone inlet diameter or the overflow diameter, but it is more sensitive to the overflow diameter.

Since the model development basis is the centrifugal acceleration, the ESAM together with the experimental equivalent area obtained from performance experiments can be used to predict the tangential velocity profile in the hydrocyclone. This prediction is validated by comparison of the tangential velocity profile of a given hydrocyclone. This method has the benefit of predicting the tangential velocity profile without requiring complex and expensive instruments for velocimetry measurement.

The average value of 0.8 is suggested in the literature for the exponent n in the tangential velocity profile function for hydrocyclones. It is shown that the value of this exponent is significantly geometry dependent. For three of the hydrocyclone designs studied in this research, the exponent values are close to the average, while for Bradley hydrocyclone n is found to be 0.31. The proper exponent for each

hydrocyclone design can be determined from the ESAM by comparing with experimental data and the ESAM can now be used as a design tool for hydrocyclones.

Chapter 5

Effect of inlet concentration on equivalent area factor

5.1 Introduction

The equivalent settling area model (ESAM) in Chapter 4 does not consider the effect of concentration of solid particles in the feed stream. The developed ESAM presented in Eq. (4.14) and Eq. 4.15 is based on residence time theory [13] that does not take the concentration and hence hindering effect into account. To generalize the relation for predicting the separation performance at high concentration when hindered settling occurs, the ESAM should be modified. This chapter aims in modifying the ESAM for this effect. This is performed by applying different forms of concentration functions in the ESAM. Comparing the experimental data, the best predicting function is obtained through regression analysis.

To avoid confusion with ESAM, the modified equivalent settling area model (modified ESAM) for the effect of concentration is shown with Σ_c and is used to evaluate the effect of operating and performance parameters in hydrocyclones. A performance guideline chart is also developed for hydrocyclones using Σ_c.

5.2 Methodology

5.2.1 Concentration functions

High solid concentration increases the particle-particle interactions and hence reduces the particle settling velocity which is known as hindered settling velocity [26]. This velocity is usually correlated with gravity settling velocity obtained from Stokes' law [25] by multiplying in to a function of solid volume concentration such that [34]:

$$v_h = v_g f(c) \tag{5.1}$$

where v_h is the hindered settling velocity and c is the volume fraction of the particles in the mixture. Some types of function $f(c)$ that have been used in hydrocyclone studies in the literature are listed in Table 5.1. The functions have been used either to modify the radial terminal velocity of the particles in the hydrocyclone or to predict the separation cut size in the device which in turn is related to the settling velocity. This is discussed in 1.3.3 under "feed concentration" section. The references from reviewing the functions are given in column three of Table 5.1.

These functions are evaluated in this study to modify the ESAM for the effect of concentration. Each function is combined with the ESAM and the resulted relation (modified model) is used to obtain the data that predicts the equivalent settling area factor in a hydrocyclone for different concentrations. This predicted data is then compared to the experimental data to examine the capability of the modified model (and the concentration function) in predicting the equivalent area factor under the influence of solid concentration. The theoretical equivalent settling area

Table 5.1: Functions that are used in the literature for the effect of solid concentration on the hydrocyclone performance

Case	Function	Reference	Descriptions
$f_1(c)$	$(1-c)^{\alpha}$	[32]	$\alpha = 4.65$
$f_2(c)$	$c/(1-c)^{\alpha}$	[33]	$\alpha = 3$
$f_3(c)$	$10^{\alpha c}/(1-c)^{\beta}$	[66]	$\alpha = 10.82$, $\beta = 2$
$f_4(c)$	$\exp(\alpha c)$	[5]	$\alpha = 6.0$
$f_5(c)$	$(1-c)(1-c/\beta)^{\alpha}$	[70]	$\alpha = 1.5$, $\beta = 0.6$
$f_6(c)$	$c^{\alpha}/(1-c)^{\beta}$	[88]	$\alpha = 0.46$, $\beta = 4.5$

model ESAM is modified using a concentration function $f(c)$ such that:

$$\Sigma_c = \text{ESAM} f(c) \tag{5.2}$$

A regression code is developed to fit the experimental data. To obtain the best result for each regression analysis the function coefficient(s) (α or β) listed in Table 5.1 is allowed to be optimized. The results are then compared with each other and the function that provides the best match for the model is selected. The experimental data for separation from low to high solids concentration (up to 10%v/v) is used to determine the coefficient α or β.

5.2.2 Empirical data

Since the experiments in the current study are limited to low solid concentrations, the required data at higher concentrations to evaluate the concentration functions is obtained from empirical correlations available in the literature [5]. The correlations are for hydrocyclones with geometric proportions listed in Table 5.2. These geometric properties covers the most well-known hydrocyclone designs including Bradley [80], Rietema [106] and Demco 4H [129] hydrocyclones. The correlations used in this research are according to Eq. (5.3) to Eq. (5.8) [5].

$$R_w = 1.18\left(\frac{D}{D_o}\right)^{5.97}\left(\frac{D_u}{D}\right)^{3.10} Eu^{-0.54} \tag{5.3}$$

Table 5.2: Range of geometrical parameters [5]

Parameter	Range
D_i/D	0.14-0.28
D_o/D	0.20-0.34
D_u/D	0.04-0.28
L/D	3.30-6.93
l/D	0.33-0.55
θ	9°-20°

$$Stk_{50}Eu = 0.12\left(\frac{D}{D_o}\right)^{0.95}\left(\frac{D}{L-l}\right)^{1.33}\left[\ln(\frac{1}{R_w})\right]^{0.79}\exp(12.0c) \tag{5.4}$$

$$Eu = 43.5D^{0.57}\left(\frac{D}{D_i}\right)^{2.61}\left(\frac{D}{D_o^2+D_u^2}\right)^{0.42}\left(\frac{D}{L-l}\right)^{0.98}Re^{0.12}\exp(-0.51c) \tag{5.5}$$

$$\Delta P = \frac{\rho v^2 Eu}{2} = 36.3D^{-3.55}Q^{2.12}\left(\frac{D}{D_i}\right)^{2.61}\left(\frac{D}{D_o^2+D_u^2}\right)^{0.42}\left(\frac{D}{L-l}\right)^{0.98}\rho^{1.12}\mu^{-0.12}\exp(-0.51c) \tag{5.6}$$

$$Q = 1.84D^{-0.217}D_i^{1.231}(D_o^2+D_u^2)^{0.198}(L-l)^{0.462}\mu^{0.0566}\rho^{-0.528}\Delta P^{0.472}\exp(0.241c) \tag{5.7}$$

$$d = \left[\frac{18\mu D Stk_{50}}{(\rho_s-\rho)v}\right]^{0.5} = \frac{1.173D^{0.64}}{D_o^{0.475}(L-l)^{0.665}}\left[\frac{\mu\rho Q}{(\rho_s-\rho)\Delta P}\right]^{0.5}\left[\ln(\frac{1}{R_w})\right]^{0.395}\exp(6.0c) \tag{5.8}$$

Assuming a certain hydrocyclone diameter, the hydrocyclone dimensions are obtained from the aspect ratios from Table 5.2. For different well-known designs, the separation cut size and flow rate are calculated from Eq. (5.8) and Eq. (5.7) for

Table 5.3: Values of the variables set for obtaining experimental data

variable	value	Units
Liquid density, ρ	998	kg/m^3
Liquid viscosity, μ	0.001	Pa.s
Solid density, ρ_s	2500	kg/m^3
Pressure drop, ΔP	30-140	kPa
Inlet concentration, c	0.0125-0.10	v/v

the flow properties presented in Table 5.3. Knowing these values, the experimental equivalent area factor is then obtained for different inlet concentrations and pressure drops. Details of calculation method can be found in Chapter 2. This experimental data is used as the response value in the regression analysis.

5.3 Results and Discussion

5.3.1 Effect of concentration on ESAM

The effect of increasing the inlet concentration on the equivalent area is presented for a Bradley and a Rietema hydrocyclone. The experimental data is compared with the data from the ESAM for different solid volume concentrations vary from 1.25% to 10% shown in Fig. 5.1 and Fig. 5.2. Increasing the amount of solids in the inlet flow decreases the equivalent area factor, the effect that is not covered by the ESAM. It is seen from Fig. 5.1 and Fig. 5.2 that the data is deviated from the line of the best match by increasing the concentration such that the ESAM overpredicts the equivalent area factor under the effect of concentration. The same trend is observed for a Rietema hydrocyclone as shown in Fig. 5.2.

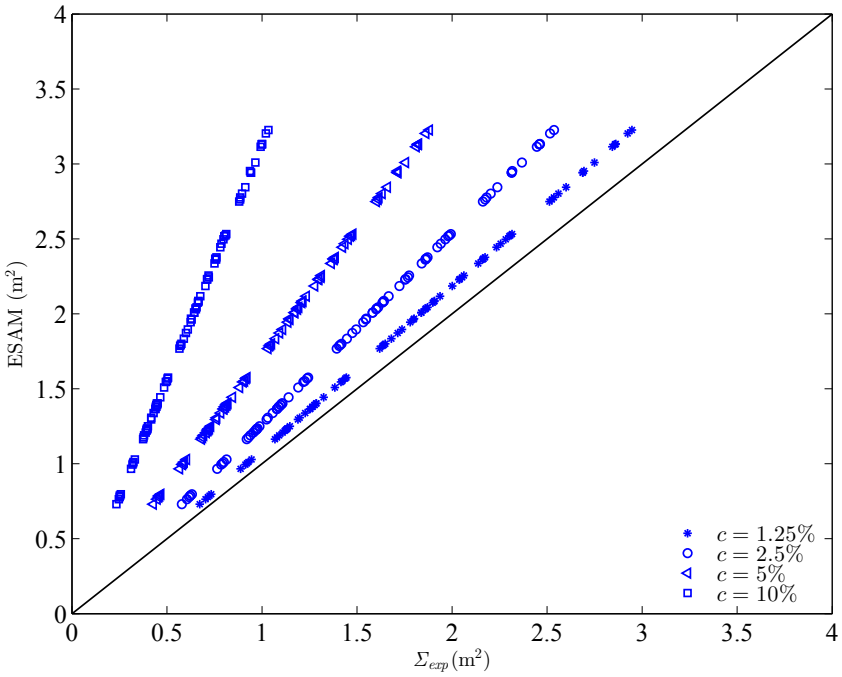

Figure 5.1: Comparison of the theoretical and experimental equivalent area factor at different solid volume concentration for a Bradley hydrocyclone

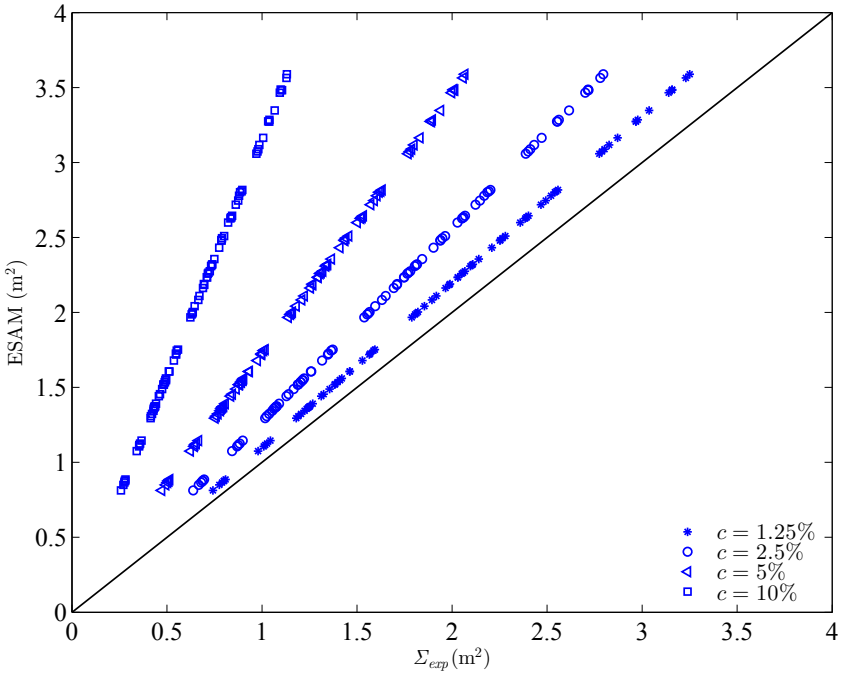

Figure 5.2: Comparison of the theoretical and experimental equivalent area factor at different solid volume concentration for a Rietema hydrocyclone

5.3.2 Modifying ESAM

Nonlinear regression along with Eq. (5.2) and functions listed in Table 5.1 is used to adjust the ESAM to match the experimental data. The value of n_p obtained in 4.3.2 for each type of hydrocyclone is used to calculate the equivalent area from the model. Therefore, the regression analysis is to obtain the coefficient(s) in the concentration functions. The regression results for any type of hydrocyclone within the range given in Table 5.2 and for hydrocyclone diameter ranges from 1 cm to 20 cm is tabulated in Table 5.4. To test if the coefficient (α or β) of the function is statistically significant in the model, the t-statistic [119] is used which tests the hypothesis that the true value of the coefficient is non-zero [119]. The probability of being no difference between the groups using the concentration function $f(c)$ and observed experimental data is measured by the p-value [119]. The standard errors

Table 5.4: Regression results for any hydrocyclone design

Variable	$f_1(c)$	$f_2(c)$	$f_3(c)$	$f_4(c)$	$f_5(c)$	$f_6(c)$
α	10.86	-0.25	-5.85	-11.36	5.73	-0.004
β	-	-	2 (fixed)	-	0.6 (fixed)	-11.10
SE	0.0059	0.3955	0.0036	0.0077	0.0040	α: 0.0001; β: 0.0058
t-statistics	1837	-1	-1621	-1467	1449	α: -68; β: -1930
p-value	0	0	0	0	0	α: 0; β: 0
R^2	0.999	-0.6720	0.999	0.999	0.999	0.999
RMS error	0.0601	3.300	0.0826	0.0768	0.0682	0.0444
AIC	-15046	28212	-11608	-12399	-13681	-18318

of the estimates (SE) (which is a measure of the accuracy of predictions), root mean squared (RMS) error (measures difference between predicted values by the model and the experimental values) and the coefficient of determination R^2 (that is the measure of how the values predicted by the model are close to the experimental data) are also presented in the Table 5.4 to evaluate the excellency of the fit to the data through the estimated coefficient(s) and the regression model.

The regression statistics show that most of the models provide a good estimation of the concentration function. The only function that cannot well predict the experimental data is $f_2(c)$, as the determination coefficient R^2 is about one in all models except for $f_2(c)$. Thus, the function $f_2(c)$ is removed from the study. All other models (functions) are statistically significant and RMS errors are small. This does not allow to reject or accept one model against the other models or to decide about the best function that can be used in Eq. (5.2) to predict the effect of concentration on the equivalent area factor. However, using the Akaike information criterion [130], it is possible to determine which model is more likely to be true model in regenerating the experimental data. Akaike information criterion (AIC)

is defined as [130]:

$$AIC = N \ln(\frac{RSS}{N}) + 2K \tag{5.9}$$

where N is the number of observations, K is the number of model parameters (predictors and response) involved in the regression, and RSS is residual sum of squares (sum of the square of the vertical distances of the data points from the fitted curve). The probability that one candidate model is better than another candidate model is obtained from the AIC values of every two candidate models. The Akaike information criterion AIC is an indication of how much more or less likely a model is true [131]. A model with lower AIC value is the model more likely to be correct and such a model has a higher probability of being the true model in comparison. Details about the calculations of these statistical parameters can be found in the related statistics references such as [132].

The AICs of the models in this study, are tabulated in Table 5.4 for the candidate models listed in Table 5.1. The probabilities of one model being the more likely model between every two models are tabulated in Table 5.5. Each score in this table indicates the probability of its function in percent from the above row against its relevant function in the left column. According to the Table 5.4, the AIC score in the model that includes $f_6(c)$ is the lowest among the other candidate models. Considering the function with the lowest AIC in Table 5.4 and comparing the probabilities from Table 5.5, the order of the functions from the most likely function to the least likely function is as $f_6(c) > f_1(c) > f_5(c) > f_4(c) > f_3(c)$. Therefore, $f_6(c)$ is expected more likely to be the true function in the model. However, it is observed from Table 5.4 that the coefficient α for this function is negative which means this model gives no value at zero concentration. This is not desired as it

Table 5.5: Probabilities in AIC test. Values are in percent

	$f_1(c)$	$f_3(c)$	$f_4(c)$	$f_5(c)$	$f_6(c)$
$f_1(c)$	50	0	0	0	100
$f_3(c)$	100	50	100	100	100
$f_4(c)$	100	0	50	100	100
$f_5(c)$	100	0	0	50	100
$f_6(c)$	0	0	0	0	50

creates a singularity point in the model which prevents generalization of the model to cover all possible concentration (including zero). Therefore, $f_6(c)$ cannot satisfy the requirements of the study and it is rejected for modification of ESAM. Thus, the function $f_1(c)$ that has the more probability after $f_6(c)$ and its domain covers all possible concentrations is selected to develop a modified model for predicting the equivalent area factor. This statistical investigation provides a strong evidence over choosing the function $f_1(c)$ for modifying ESAM in the current study. Considering coefficient α from Table 5.4, and replacing it for $f_1(c)$, the selected function to be used in the study is in the form:

$$f(c) = (1-c)^{10.86} \tag{5.10}$$

The modified equivalent area factor including the effect of concentration is then obtained using this function and combining Eq. (4.14), Eq. (4.15), Eq. (5.2) and Eq. (5.10) as:

$$\Sigma_c = \frac{\pi n[1-(D_o/D)^2]}{(D/D_o)^{2n}-1}\left(\frac{1}{1-D_i/D}\right)^{2n+1}\frac{L\Delta P}{\rho g}(1-c)^{10.86} \tag{5.11}$$

The accuracy of the proposed model for predicting the equivalent area factor obtained from Eq. (5.11) tested for a range of volume concentrations from 1.25% to 10% for different hydrocyclone types is shown in Fig. 5.3. The results sit within the lines of $\pm 5\%$ deviation from the best match. The modified equivalent settling area

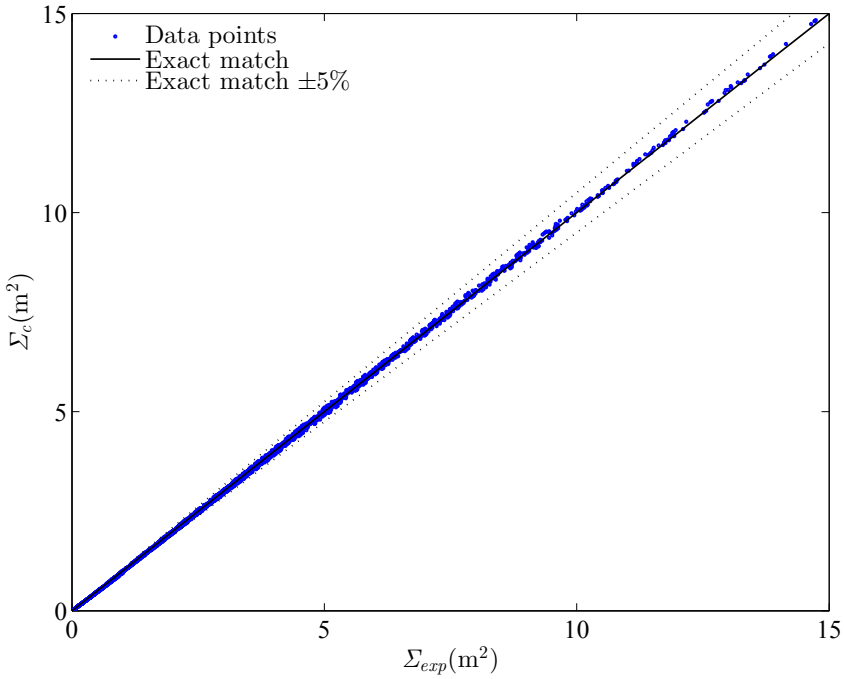

Figure 5.3: Accuracy of the proposed model in predicting the equivalent area factor for any hydrocyclone design.

in Eq. (5.11) is valid for the range of hydrocyclone design stated in Table 5.2. This relation can be used to study the hydrocyclone performance for variety of operating conditions.

5.3.3 Application of Σ_c

The effect of the inlet concentration on Σ_c according to Eq. (5.11) is shown in Fig. 5.4. The amount of Σ_c is shown in Fig. 5.4 for some selected ESAM values that are the values of Σ_c at zero concentration. Increasing the solid amount in the feed flow decreases the performance of the hydrocyclone. It also shows that for certain solid amounts in the feed flow the equivalent area factor of the hydrocyclones drops to less than 1 m^2. This shows that the hydrocyclone performance may reduce to performance of a gravity settling tank that has unit area. This may not be desired for a hydrocyclone in operation considering the cost of manufacturing, installation

and operating comparing a gravity settling tank. To avoid such condition when a single hydrocyclone is in use, there is a maximum solid concentration that should be reached. This maximum value can be determined from Eq. (5.11) by equating the relation to 1 and solving it for c. This concentration is calculated and depicted in Fig. 5.5, for different Σ values range from 1 to 50 m^2. As an example from this figure, point A (shown on the figure) is explained. A hydrocyclone that has equivalent area equal to 10 m^2 at very low (zero) concentration should be operated with less than 19.3%v/v feed solid concentration to perform more efficient than a gravity settling tank of a unit area that performs at ideal conditions (Stokes settling).

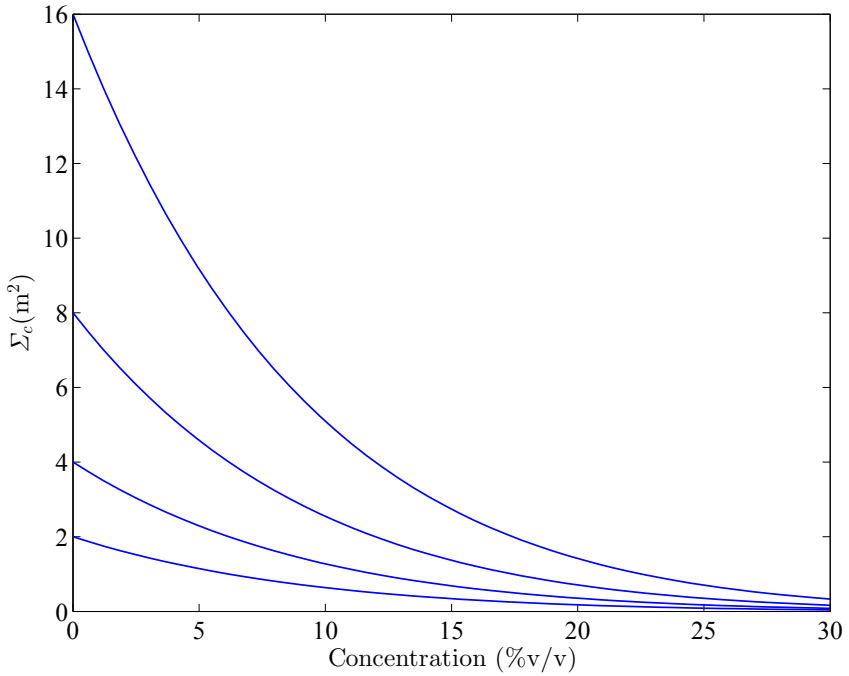

Figure 5.4: Effect of concentration on equivalent area factor at different ESAM values (the ESAM value of each line is the Σ_c value at zero concentration.)

Contours of Σ_c are plotted for a 5 cm hydrocyclone of type Bradley and Rietema in Fig. 5.6 and Fig. 5.7. It is seen from the figures that at the same concentration

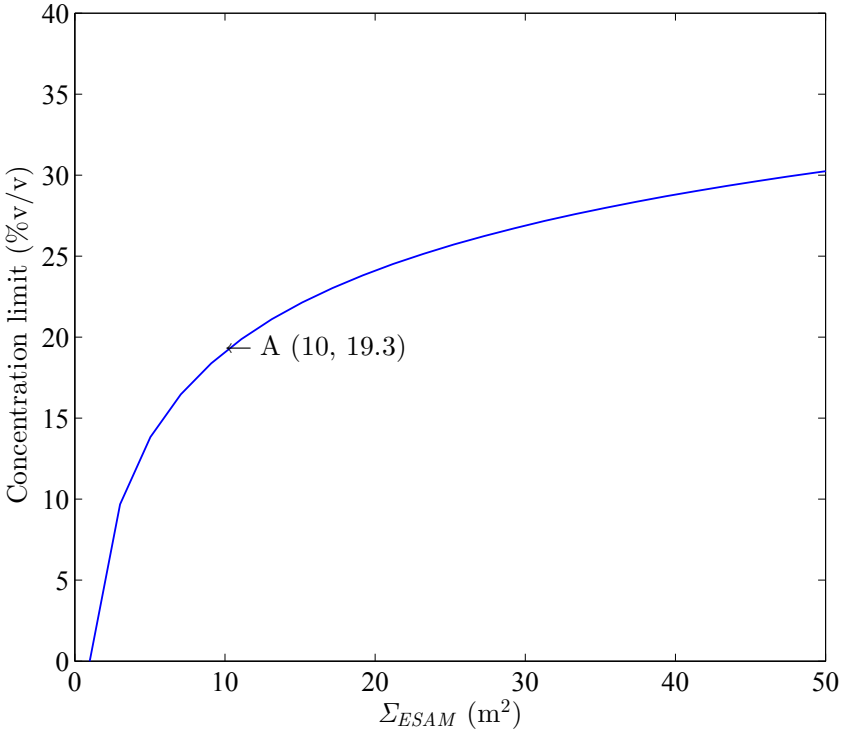

Figure 5.5: Maximum concentration in hydrocyclone to obtain $\Sigma_c = 1$

and pressure drop, a Rietema hydrocyclone has a higher equivalent area factor than a Bradley type. To achieve the same performance in a hydrocyclone when the concentration increases, the pressure drop should be increased. The interaction of the variables in calculating Σ_c for a Bradley and Rietema hydrocyclones are plotted in Fig. 5.8 and Fig. 5.9. This is limited to some hydrocyclone diameters and inlet concentrations for a range of pressure drop from 50 kPa to 300 kPa. Increasing the hydrocyclone diameter, increases Σ_c. As it can be seen from Fig.5.8 and Fig. 5.9, a Bradley hydrocyclone has about one fourth of the performance of a Rietema hydrocyclone for the same operating conditions. This is in accordance with the study of Bradley and Rietema hydrocyclones in [65].

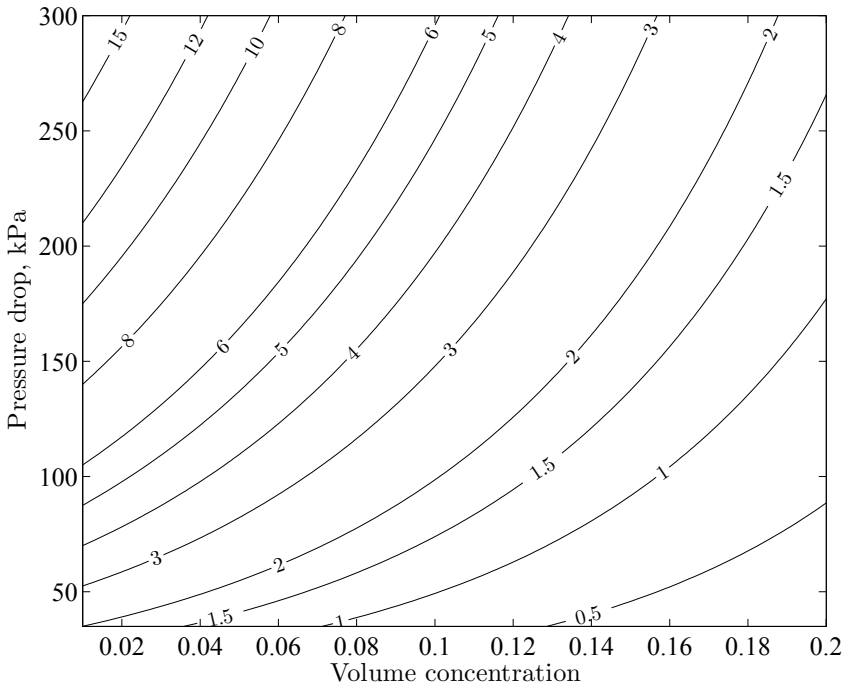

Figure 5.6: Contours of Σ_c for Bradley hydrocyclone with 5 cm diameter

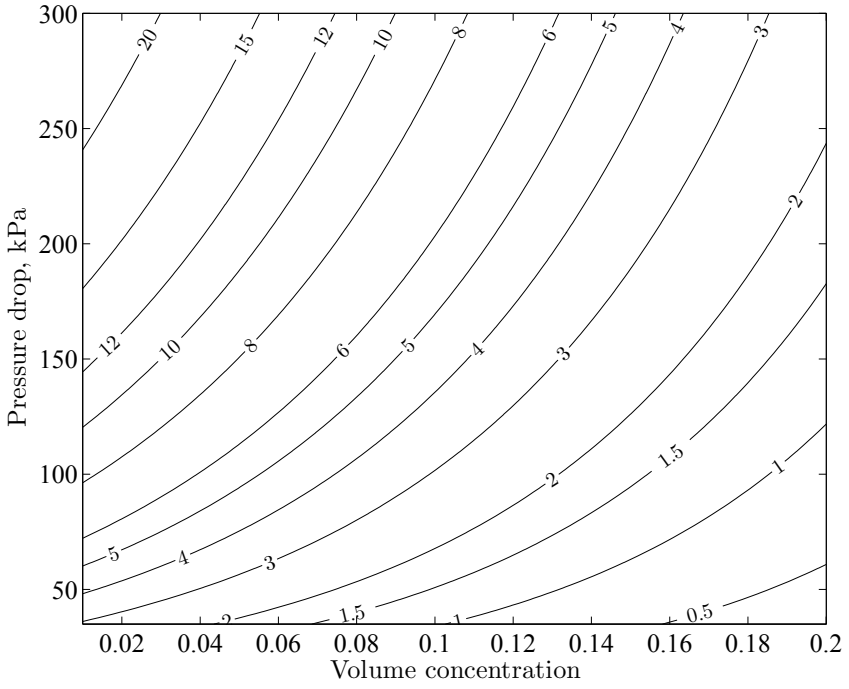

Figure 5.7: Contours of Σ_c for Rietema hydrocyclone with 5 cm diameter

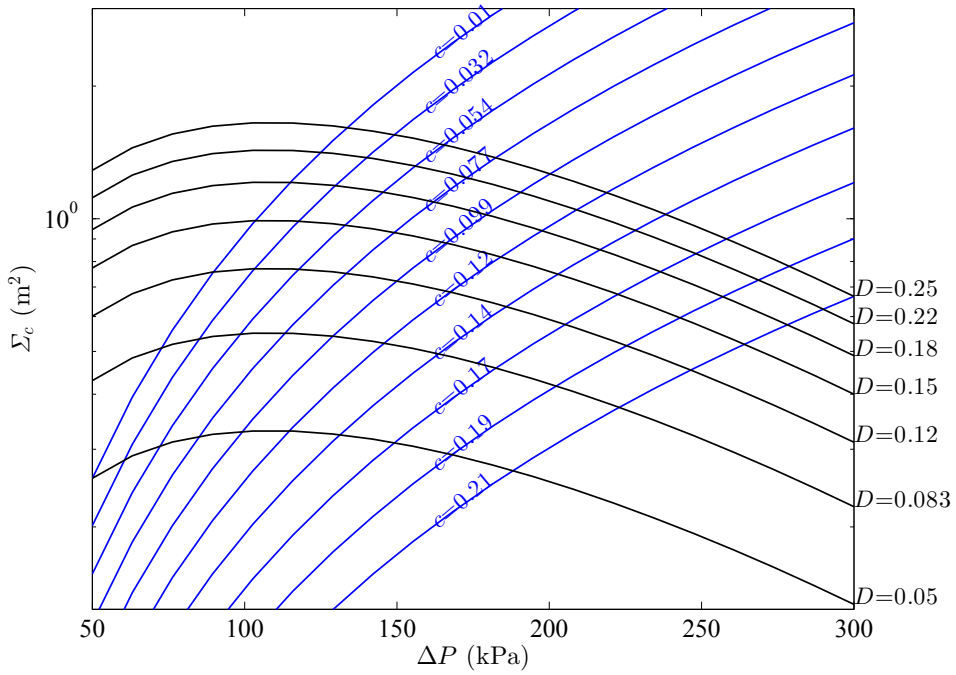

Figure 5.8: Effect of pressure drop, inlet concentration (fraction) and hydrocyclone diameter on Σ_c in Bradley hydrocyclones

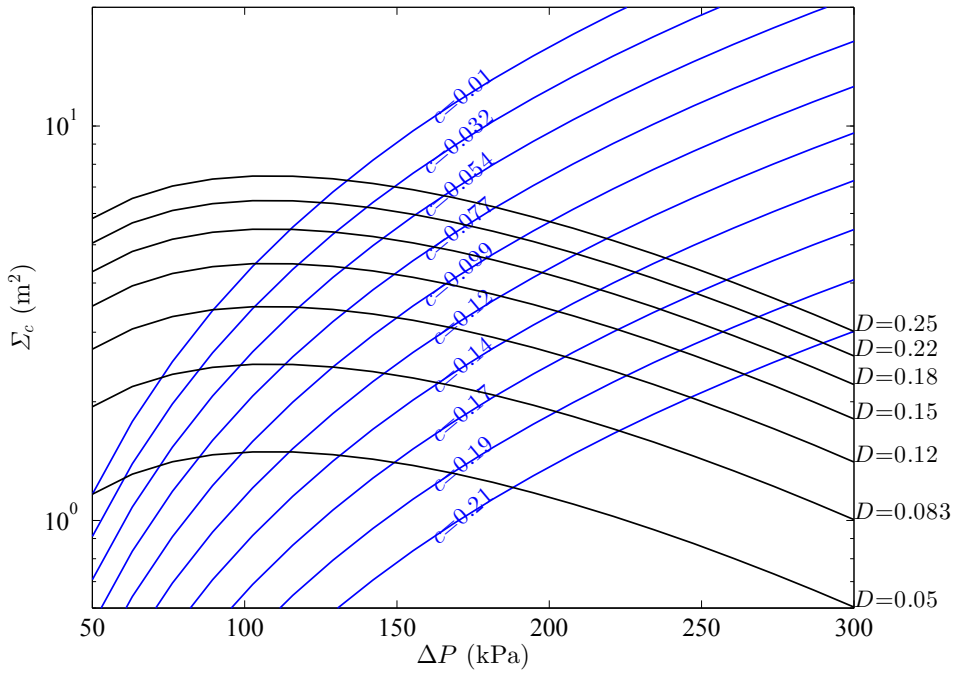

Figure 5.9: Effect of pressure drop, inlet concentration (fraction) and hydrocyclone diameter on Σ_c in Rietema hydrocyclones

5.3.4 Developing guidelines for hydrocyclones

Performance charts

It has been shown in Chapter 2 that there is a need for developing a performance chart based on the principle concepts of the separation theories in hydrocyclones. The modified equivalent area factor developed in this chapter provides a tool to satisfy this need. Knowing that flow rate and particle size are typically the main parameters to select or design a hydrocyclone, a performance chart is developed to predict the hydrocyclone performance based on these parameters. This can be done using the developed model for the equivalent area factor as it is coupled with hydrocyclone flow rate and particle size according to Eq. (1.4) and Eq. (1.8). To do this, for hydrocyclone diameters range from 1 cm to 50 cm, pressure drop range from 35 kPa to 600 kPa and inlet concentration range from 0.1%v/v to 20%v/v, flow rate and Σ_c are calculated from Eq. (5.7) and Eq. (5.11). Knowing the flow rate and the equivalent area factor, settling velocity is obtained from Eq. (1.8). This procedure is performed for a hydrocyclone with design parameters according to the range given in Table 5.2. The liquid and solid phase properties in the calculations are listed in Table 5.3. The performance lines for Bradley and Rietema type hydrocyclones are shown in Fig. 5.10 to 5.13 for three nominal pressure drops and at two different solid volume concentrations $c = 1\%$v/v and $c = 20\%$v/v, respectively. These are shown as plots of flow rate versus two times settling velocity ($2v_g$). Comparing Fig. 5.10 and Fig. 5.11 for Bradley hydrocyclones and Fig. 5.12 and Fig. 5.13 for Rietema hydrocyclones it can be seen that at a constant flow rate, the gravitational settling velocity (x axis) increases significantly by increasing the concentration. Thus, the equivalent area factor that is the ratio of flow rate Q to $2v_g$

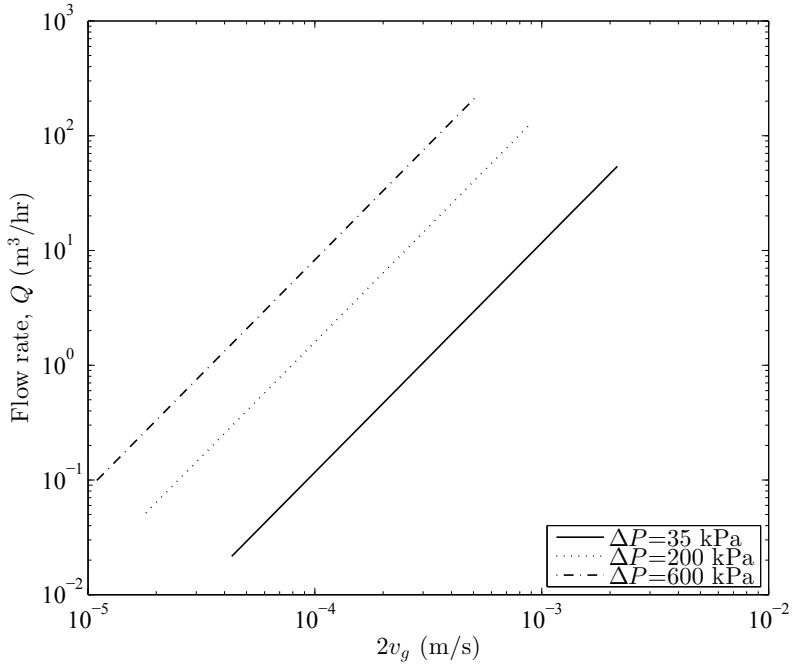

Figure 5.10: Hydrocyclone performance in Bradley hydrocyclones obtained from equivalent area factor; $c = 1\%$v/v

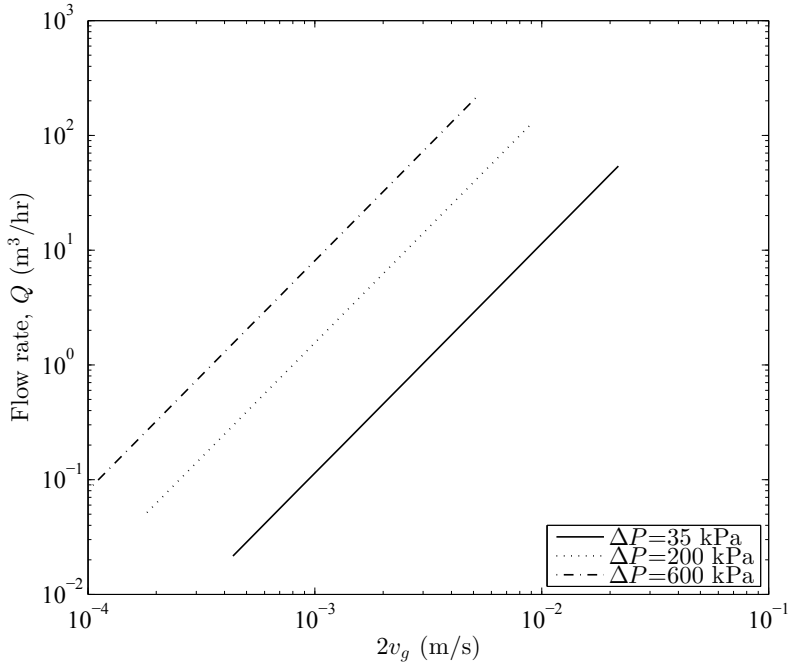

Figure 5.11: Hydrocyclone performance in Bradley hydrocyclones obtained from equivalent area factor; $c = 20\%$v/v

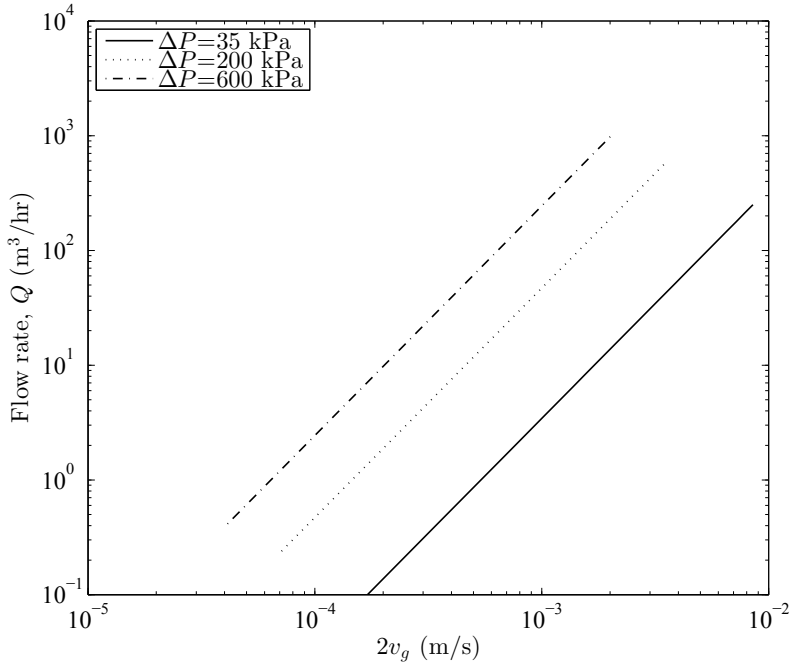

Figure 5.12: Hydrocyclone performance in Rietema hydrocyclones obtained from equivalent area factor; $c = 1\%$v/v

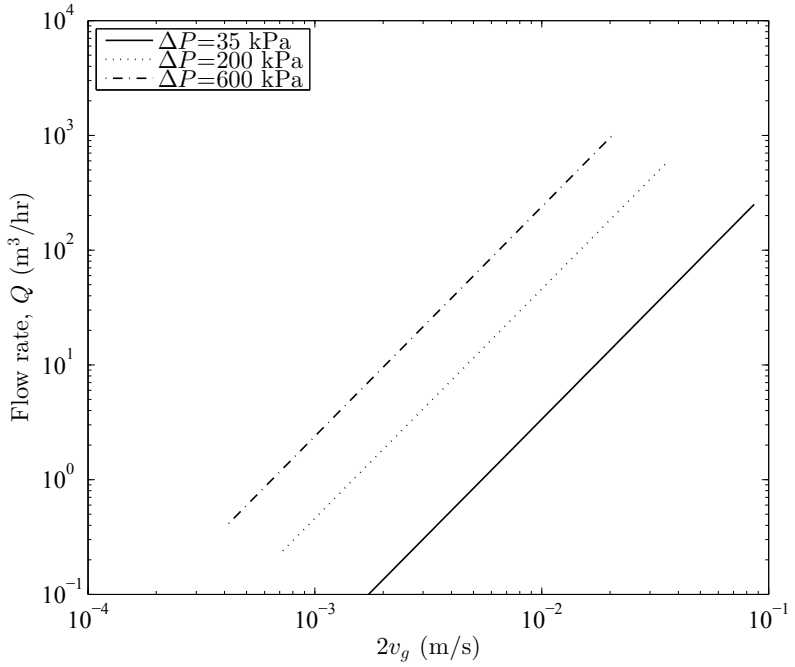

Figure 5.13: Hydrocyclone performance in Rietema hydrocyclones obtained from equivalent area factor; $c = 20\%$v/v

(according to Eq. (1.8)) decreases with increasing concentration. This can reduce to about 10 times for a high concentration inlet flow even at a high pressure drop equal to 600 kPa.

Comparing the performance of Bradley and Rietema hydrocyclones i.e. Fig. 5.10 with Fig. 5.12 and Fig. 5.11 with Fig. 5.13, a Rietema hydrocyclone can handle more flow rate than a Bradley hydrocyclone at a similar pressure drop and inlet concentration.

To develop a guideline chart for hydrocyclones, performance curves are generated for hydrocyclones for the aspect ratio range given in Table 5.2 at different concentration and pressure drops for different hydrocyclone types. The curves are bounded to obtain a performance guideline chart that covers the whole range of applications for hydrocyclones of different types and sizes. The obtained chart is shown in Fig. 5.14. Experimental data from literature [1–3] and data from a hydrocyclone manufacturer (FLSmidth Krebs Hydrocyclone [4]) are used to validate the developed chart. Also, more data points are generated using sets of empirical models presented in Eq. (5.3) to Eq. (5.8) for Bradley and Rietema types hydrocyclones. The results are shown in Fig. 5.14. Comparing these sets of data with the chart shows that the chart well predicts the hydrocyclone performance as the data are within the developed region. This chart is also compared with LPC [10] and the results show that the LPC can be replaced with the current chart. This chart is developed based on a model that includes the physics of the separation in hydrocyclones. More discussion on this can be found in Chapter 2 where the initial attempts to develop a performance chart based on empirical and semi-empirical correlations have been detailed. This performance chart however, has been developed from the

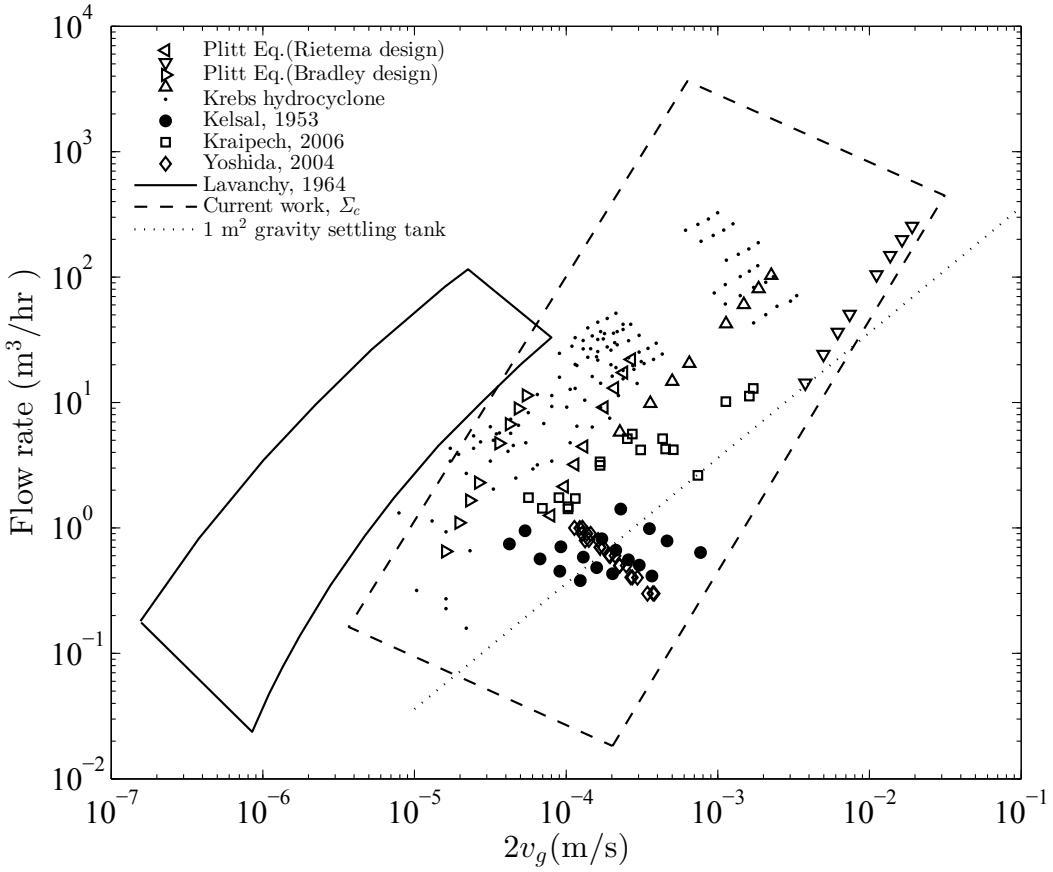

Figure 5.14: Hydrocyclone performance chart compared to data from the literature and LPC

basic principles. The performance chart can be used to compare the hydrocyclone performance with other centrifugal separators and the gravity settling tank. The performance of hydrocyclones is also compared with the performance of a continuous gravity settling tank with unit area in Fig. 5.14. It is seen that a single hydrocyclone may have lower performance than a gravity settling tank depending on operating conditions.

Using the developed performance chart for the hydrocyclones, the LPC can be updated. This update performance chart is shown in Fig. 5.15. This chart confirms the previous proposed chart in Chapter 2 (Fig. 2.8).

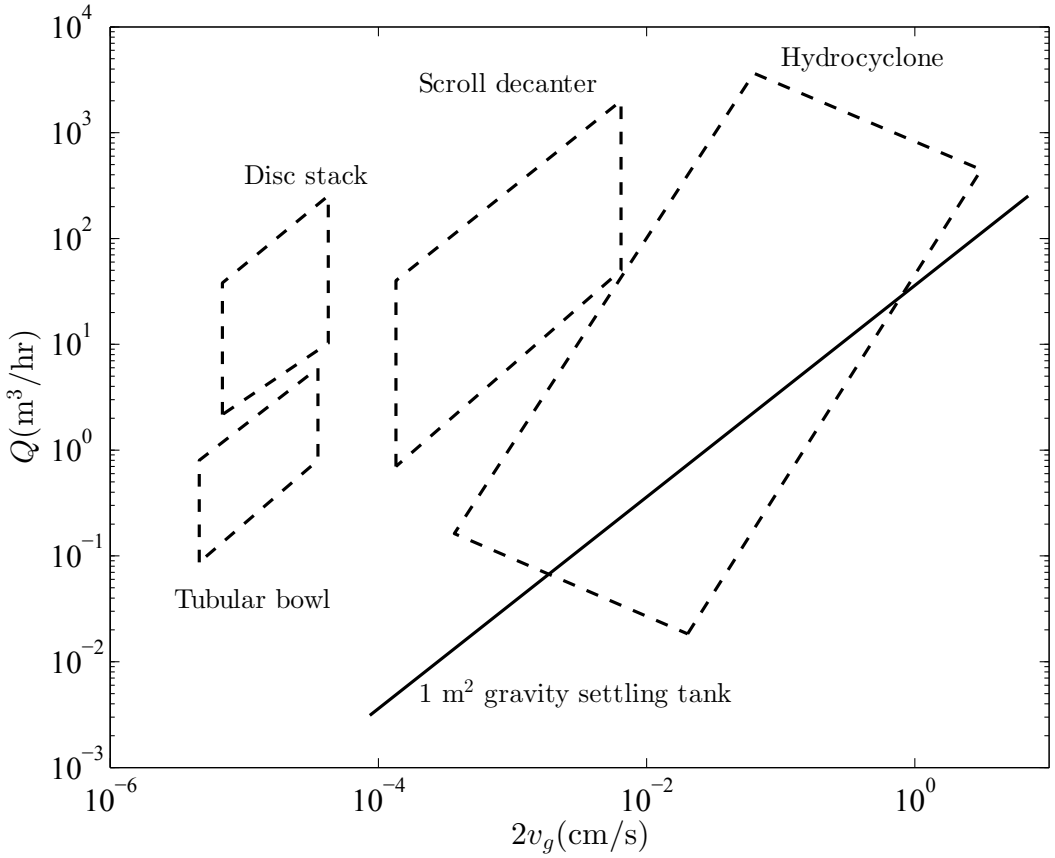

Figure 5.15: Performance of sedimenting centrifugal separator devices compared with 1 m^2 gravity settling tank

Separation cut size in hydrocyclones

The effect of the pressure drop and the hydrocyclone diameter on the separation cut size is shown in Fig. 5.16 to Fig. 5.19 for Bradley and Rietema hydrocyclones for concentrations $c = 1\%$v/v and $c = 20\%$v/v, respectively. As can be seen, increasing the hydrocyclone diameter or decreasing the pressure drop while the other variable is constant, results in increasing the cut size. To achieve a same cut size at a constant concentration while the hydrocyclone diameter increases, the pressure drop should be increased. However, making a high pressure drop may not be always possible due to practical limits or energy/cost concerns and hence a package of multiple hydrocyclones of small size can be an option.

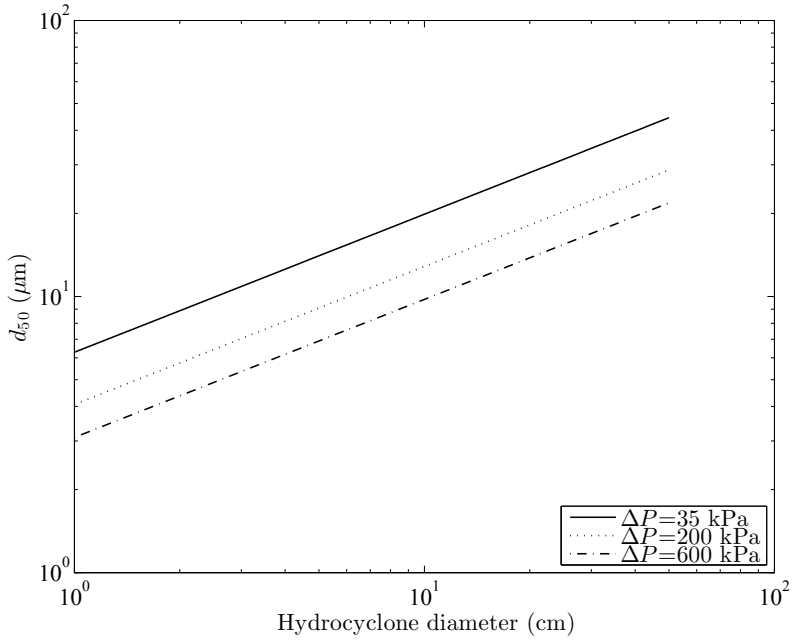

Figure 5.16: Separation cut size in Bradley hydrocyclones; $c = 1\%$v/v

Comparing the cut size of a Bradley and a Rietema hydrocyclone of the same size in Fig. 5.16 to Fig. 5.19, it is observed that a Bradley hydrocyclone has a smaller cut size than a Rietema hydrocyclone for a similar pressure drop and hy-

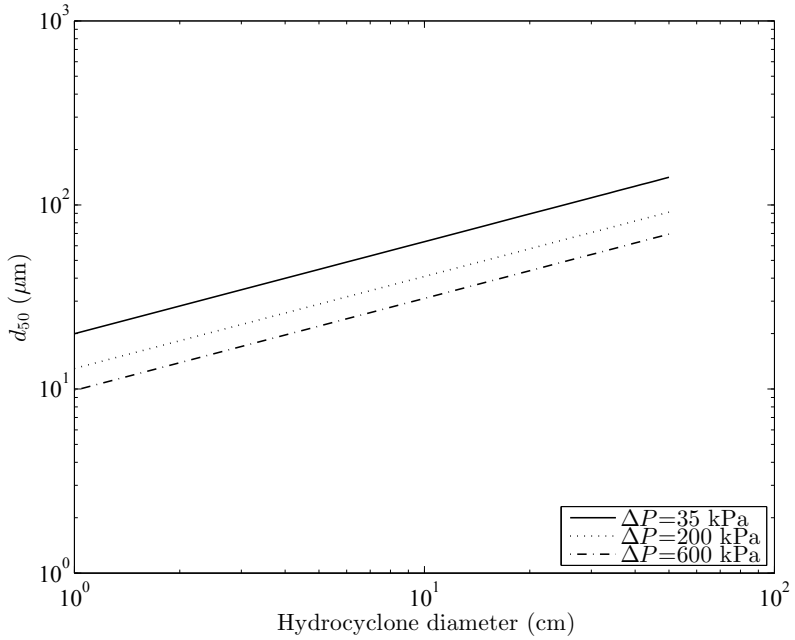

Figure 5.17: Separation cut size in Bradley hydrocyclones; $c = 20\%$v/v

drocyclone diameter. This matches the trends observed in [65] that compares the Bradley and Rietema hydrocyclones based on empirical correlations. It is also observed that increasing hydrocyclone diameter results in reducing the cut size for both the Bradley and Rietema hydrocyclones. It can be also concluded from comparing Fig. 5.16 and Fig. 5.17 or Fig. 5.18 and Fig. 5.19 that increasing the inlet concentration results in larger cut size in a Bradley or a Rietema hydrocyclone. This is due to the effect of hindered settling in hydrocyclones [13] at higher concentrations that reduces the settling velocity of particles.

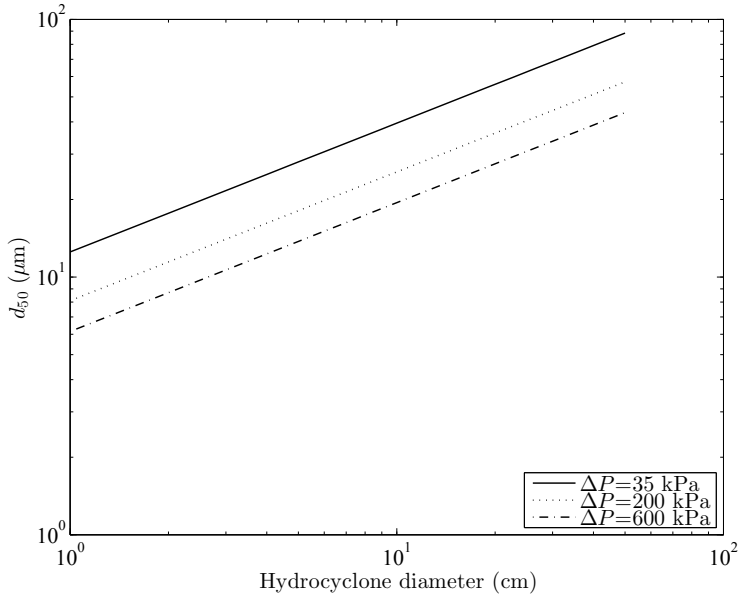

Figure 5.18: Separation cut size in Rietema hydrocyclones; $c = 1\%$v/v

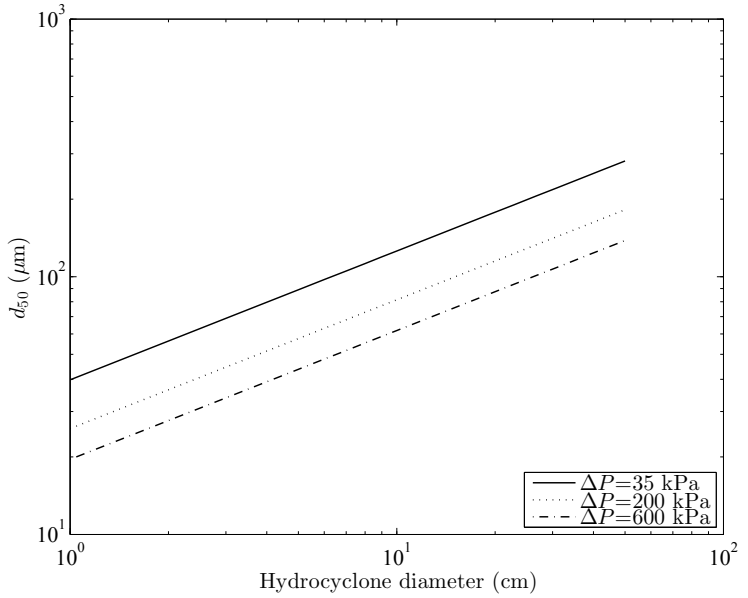

Figure 5.19: Separation cut size in Rietema hydrocyclones; $c = 20\%$v/v

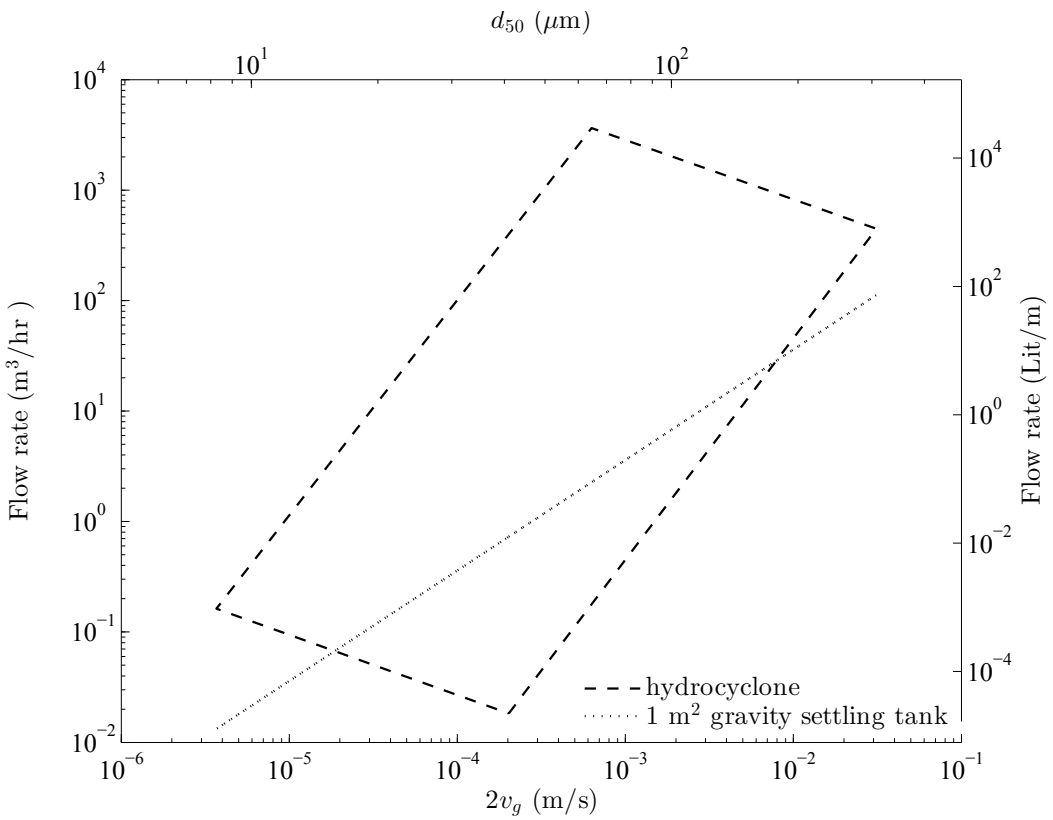

Figure 5.20: Hydrocyclone performance chart compared to gravity settling tank, top horizontal axis: separation cut size for density difference = 1500 kg/m^3

The separation cut size is also calculated for the hydrocyclone performance chart of Fig. 5.14. The resulted chart is shown in Fig. 5.20 and the separation cut size values are the second horizontal axis of the chart on the top. The cut size on this axis is obtained from the settling velocity relation Eq. (1.8) for density difference between solid and liquid equal to 1500 kg/m^3. According to the figure, the hydrocyclones can be used to separate particles from about 5 μm to about 300 μm that is well matched with the range presented in [12].

5.3.5 *G-factor*

An important factor to compare the performance of centrifugal separators is *G-factor*. This factor provides an understanding about the amount of force that is applied on a particle under a centrifugal acceleration field comparing the gravity acceleration. The ratio of centrifugal acceleration to gravity acceleration is known as *G-factor* [123, 133] (*G-level* or relative centrifugal force) that is:

$$\textit{G-factor} = \frac{r\omega^2}{g} \tag{5.12}$$

where r is the rotation radius, ω is angular velocity of rotation and g is gravity acceleration. This can be rewritten using the tangential velocity component v_θ such that:

$$\textit{G-factor} = \frac{v_\theta^2}{rg} \tag{5.13}$$

This is some times confused in the literature with g-force [12, 134] that is *G-factor* multiplied by the acceleration due to the gravity. For a range of hydrocyclone diameters from 1 cm to 50 cm this factor is calculated for Bradley and Rietema hydrocyclones. *G-factor* for different pressure drops in hydrocyclones are shown in Fig. 5.21 and Fig. 5.22. *G-factor* decreases with increasing the hydrocyclone diameter and increases with increasing the pressure drop. As pressure drop is coupled with flow rate, this is due to increasing the flow rate which in turn increases the tangential velocity. It has also been shown in Eq. (4.10) that increasing the pressure drop in hydrocyclones increases the centrifugal acceleration.

Comparing two types of hydrocyclones, a Bradley hydrocyclone provides higher *G-factor* (or centrifugal acceleration) for a given hydrocyclone size and pressure drop comparing a Rietema hydrocyclone. This affects the separation cut size, as the

Table 5.6: Capacity and *G-factor* values for different centrifugal separators

Centrifugal separator	*G-factor*	Throughput (m^3/hr)	Reference
Disk stack	Up to 14,000	200 (max)	[16]
Scroll decanter	2,000 - 6,000	$<$100	[16]
Tubular bowl	14,000 - 65,000	4 (max)	[16]
Basket	Up to 1,600	6 - 10	[16]
Hydrocyclone	$\sim$ 5 - $\sim$ 45,000	Up to 7,000	Current study

settling velocity is proportional to *G-factor*, such that the lower cut size is obtain in higher *G-factor*s. This is seen comparing Fig. 5.16 and Fig. 5.18 or Fig. 5.17 and Fig. 5.19. The separation cut size is smaller in Bradley hydrocyclones than Rietema hydrocyclone for similar operating conditions and hydrocyclone diameters. Thus, the previous observations are confirmed with the expectations obtained based on *G-factor*.

G-factor in hydrocyclones can reach up to $\sim$ 45,000 in small hydrocyclones (about 1 cm diameter) and can drop to $\sim$ 5 for large hydrocyclones (about 50 cm diameter). The *G-factor* and capacity of hydrocyclones that obtained in the current study are compared with *G-factor* of other sedimenting centrifuge separators in Table 5.6. A hydrocyclone has relatively high *G-factor* and throughput comparing the other centrifuge separator devices. This together with other advantages of hydrocyclones discussed in Chapter 2, make these device a good choice for many separation applications. However, high *G-factor* is achievable with small hydrocyclones where the throughput is low.

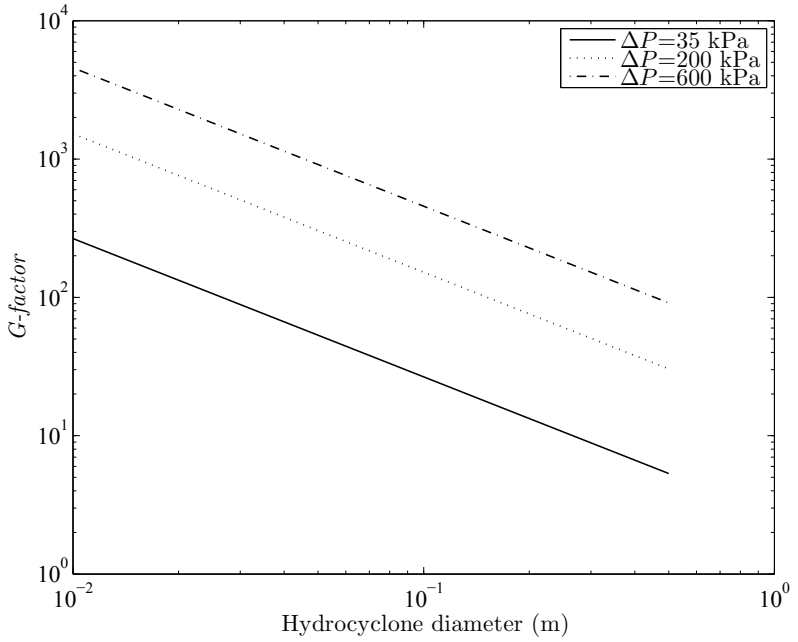

Figure 5.21: Changes in *G-factor* with hydrocyclone diameter in Bradley hydrocyclones

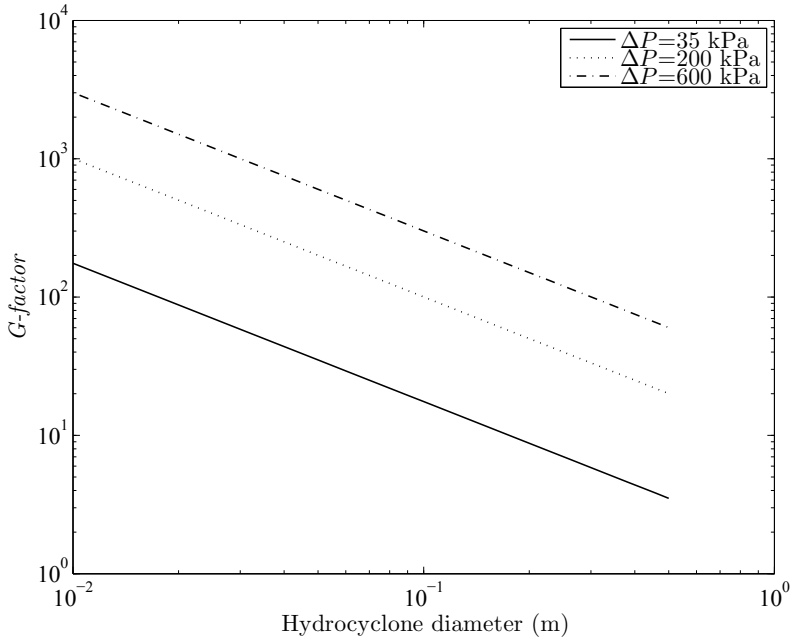

Figure 5.22: Changes in *G-factor* with hydrocyclone diameter in Rietema hydrocyclones

5.4 Conclusions

Effect of concentration on the separation performance of hydrocyclones is studied by developing a model for equivalent area factor. The equivalent settling area model (ESAM) is modified by combining it with a function of inlet flow solid concentration. This function is chosen among a number of candidate models from the literature. Different types of functions that are used in the literature for hydrocyclones are evaluated and modified in the current study to predict the equivalent area factor.

Comparing experimental data and predictions from the modified models and performing statistical analysis, the best predictive functions is determined and ESAM is modified. The modified ESAM (Σ_c) is used to develop a performance chart for hydrocyclones. This performance chart is based on the physics of the separation phenomenon in hydrocyclones and the principle theories. The chart is validated using experimental data and the data from a hydrocyclone manufacturer data sheet. The validated performance chart can be used to replace previous performance charts in the literature. The model is also used to study the behavior of hydrocyclones for cut size and centrifugal acceleration in terms of *G-factor*. It is shown that *G-factor* in hydrocyclones can reach to $\sim$ 45,000 in small hydrocyclones that is noticeably higher than other centrifugal separators.

For the two well-known Bradley and Rietema design hydrocyclones, a Bradley hydrocyclone can provide a smaller separation cut size than a Rietema hydrocyclone at the same operating conditions. However, a Rietema hydrocyclone can handle larger flow rates than a Bradley hydrocyclone for the same hydrocyclone

diameter.

Chapter 6

Underflow pumping in hydrocyclones

6.1 Introduction

Typically, the hydrocyclone underflow discharges through an apex to the open atmosphere at atmospheric pressure. Using a pump in the underflow, the underflow stream can be controlled for varying conditions. In addition, flow blockage in the apex is reduced as the pump draws the flow. A pump for the underflow equipped with a variable frequency drive (VFD) motor can be used in controlling the underflow rate of a hydrocyclone. Using water in the system it has been shown that changing the speed of the pump connected to the underflow pipe has a similar effect to changing the underflow discharge orifice diameter [122]. Since most of the studies in the literature investigate discharging the hydrocyclone outlet to the atmospheric pressure, the lack of information on the influence of using a pump in the hydrocyclone underflow is the motivation of this work.

In the following sections, flow rates, flow ratio, pressures at inlet and outlets and the underflow concentration operating conditions of the hydrocyclone are varied and separation performance and grade efficiency for several underflow pumping

rates are examined.

Pressure ratio $P^* = P_u/P_o$ is defined as the ratio of absolute underflow pressure (P_u) to the absolute overflow pressure (P_o) and is used in this study to evaluate the effect of underflow pumping on the hydrocyclone performance and operating parameters. Unlike a standard hydrocyclone the underflow pressure is significantly changed by changing the pump speed. The pressure ratio P^* is analyzed to develop a model.

6.2 Method of determining reduced grade efficiency

The particle separation efficiency of a hydrocyclone for a particular particle size is defined as the mass of separated solid particles of that size (in the underflow) to the mass of the particles of the same size in the feed stream. This efficiency is called grade efficiency [13] and is often plotted for the size distribution of the particles in the feed to the hydrocyclone. Grade efficiency $G(x)$, where x is the particle size (PS), can be obtained from the particle size distribution of the feed flow and either of the outlet streams (underflow or overflow).

The nature of flow splitting in the hydrocyclone results automatically in some efficiency. The inlet flow splits into two streams and each stream goes to either of the outlets (see Fig. 3.4). Since each part includes a mixture of solid and liquid particles, this leads to some efficiency regardless of the operating conditions. For this reason, the flow splitting separation efficiency is subtracted from the grade efficiency to remove the effect of flow splitting on grade efficiency such that [12]:

$$G'(x) = \frac{G(x) - R_f}{1 - R_f} \tag{6.1}$$

where $G'(x)$ is the resulting efficiency and is called reduced grade efficiency and

R_f is flow ratio. This $G'(x)$ is used to compare the separation efficiencies under different conditions or for different hydrocyclone devices. Similar to $G(x)$, reduced grade efficiency is usually reported as a function of particle size x and not a single number. The concepts of grade and reduced grade efficiency are schematically shown in Fig. 6.1. The reduced cut size is also obtained from the reduced grade efficiency curve as defined in Fig. 6.1.

A simple alternative method for determining $G'(x)$ assumes a log-normally distribution of particles in the inlet flow [135]. In this method $G'(x)$ is obtained by a single particle size distribution collected at the inlet and volume concentration measurement of the feed flow and the underflow at each test condition. This technique is evaluated in this study as it has been proposed as a simple method of determining $G'(x)$. The advantage of this method is that it is simple since a PSD measurement for each experiment is not required. However, the disadvantage is that it does not necessarily converge to a solution when there is a nonlinearity of the error function in the log-normal distribution. Therefore, the presented reduced grade efficiencies are obtained from the PSDs of the inlet and the underflow streams that are measured every time for each test in this study. Details of calculation of reduced graded efficiency using the PSD of the inlet and the underflow can be found in [12].

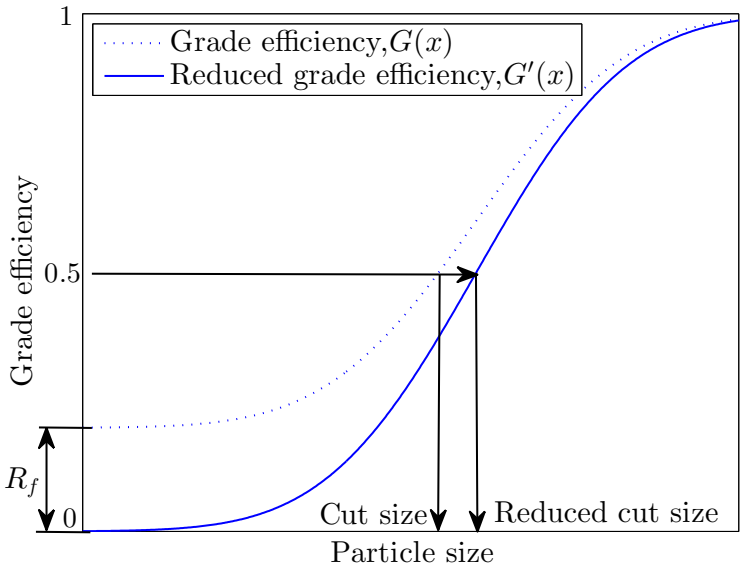

Figure 6.1: Schematics of grade efficiency and reduced grade efficiency curves and the effect of the flow ratio [12]

6.3 Experiment

The effect of the underflow pumping is examined using experiments performed according to Chapter 3. The flow properties are studied for different flow rates. The underflow flow rate is controlled by the underflow pump VFD. The results of the experiments related to the underflow pumping are discussed in this chapter.

6.4 Results and discussion

As a baseline, the experiments are initially performed with only water only in the system and the results have been published [122]. Next, experiments with varying concentrations of solid particles are performed.

6.4.1 Mixture viscosity

The effect of solid concentration on the viscosity of the mixture is investigated. This effect is expected to be negligible based on this expression for viscosity [136]:

$$\frac{\mu_m}{\mu_o} = 1 + 2.5c + 10.5c^2 + 0.00273\exp(16.6c) \tag{6.2}$$

where μ_m is the mixture of solid and liquid viscosity, μ_o is the viscosity at zero concentration and c is the volume concentration of solid particles in the mixture. The predicted results of viscosity from Eq. (6.2) are compared with experimentally measured viscosity in Table 6.1. It can be seen that, the viscosity does not change significantly by increasing the solid concentration from zero to 2% (the maximum concentration used in this research) and the mixture behaves as a Newtonian fluid for the experiments that have low concentration (maximum concentration in this study is 2%v/v).

Table 6.1: Measured and predicted viscosity of the mixture at different concentrations with standard deviation of measurements

Concentration, c (%v/v)	Predicted viscosity(Pa.s)	Measured viscosity (Pa.s)	Standard Dev.
0	0.00100	0.00102	1.31E-05
0.1	0.00101	0.00104	1.24E-05
0.5	0.00102	Not measured	–
1	0.00103	0.00107	2.40E-05
2	0.00106	Not measured	–
3	0.00109	0.00110	1.33E-05
5	0.00116	0.00119	4.06E-06

6.4.2 Grade efficiency

The influence of the underflow pumping on the grade efficiency at a constant feed pump speed (n_{FPS} = 1800 rpm) is shown in Fig. 6.2. Increasing n_{FPS} increases the flow ratio the y intercept of the curves and $G(x)$ for PS <2 μm). As a part of the liquid is mixed with the particles and leaves the hydrocyclone with the coarse section in the underflow (appears in the flow ratio parameter R_f that is the ratio of the underflow flow rate to the feed flow rate), the grade efficiency cannot explain the real efficiency without removing the effect of the flow splitting on the efficiency.

The reduced grade efficiency curves for the test conditions in Fig. 6.2 are plotted in Fig. 6.3 using Eq. (6.1). To obtain $G'(x)$, the flow ratio R_f for each efficiency curve is determined from the y intercept of the efficiency curve in Fig. 6.2. The cut sizes associated with this plot are the same. This particle size is called reduced cut size (d'_{50}) and is equal to 4.4 μm. The plots of $G'(x)$ show that using the pump in the underflow does not have significant effect on the reduced grade efficiency and it mainly changes the flow ratio. This is a noticeable result as it is expected that the underflow pumping simulates the changes in the underflow pipe diameter. Typically changing the underflow pipe diameter changes the separation cut size. Therefore,

further investigations with variety of particle size distributions are needed to justify the effect of underflow pumping on the cut size.

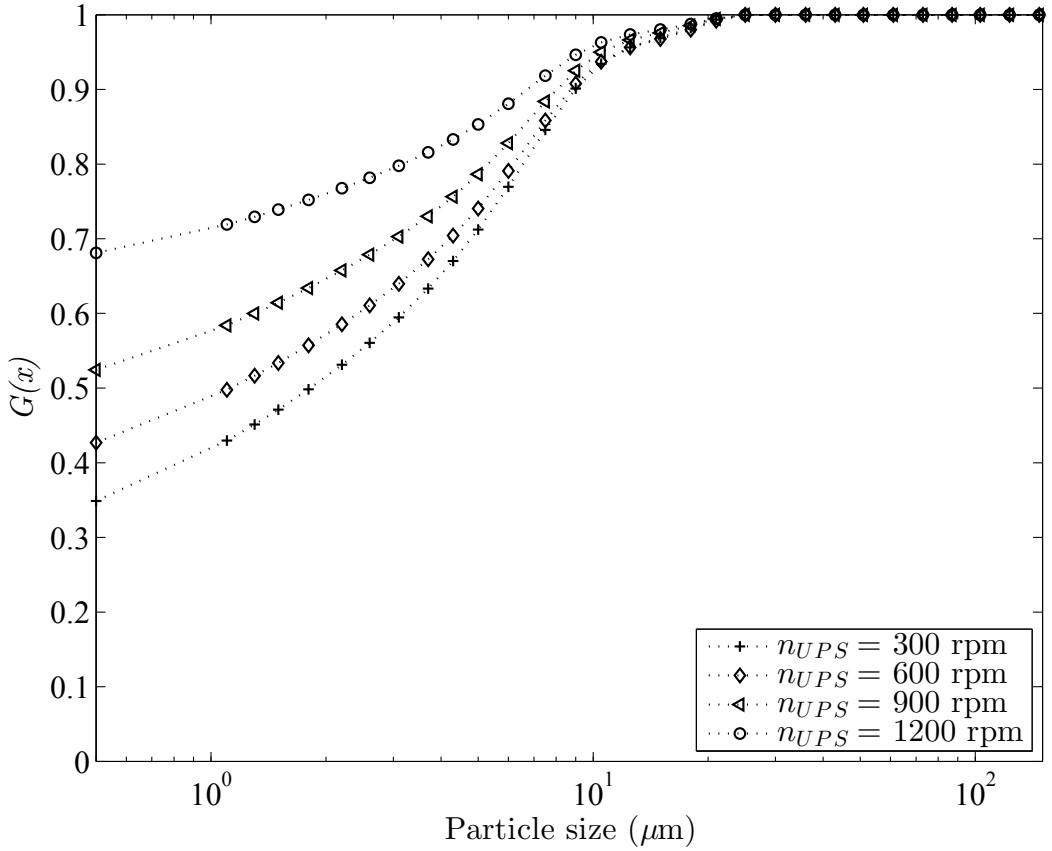

Figure 6.2: Effect of underflow pumping on the grade efficiency $G(x)$ of the hydrocyclone for different underflow pump speeds; $n_{FPS} = 1800$ rpm; $c = 0.5\%$

To evaluate the effect of the concentration on the reduced grade efficiency, the curves of $G'(x)$ at a constant feed pump speed ($n_{FPS} = 1800$ rpm), a constant underflow pump speed ($n_{UPS} = 1500$ rpm) for varying concentrations are plotted in Fig. 6.4. Increasing the concentration from 0.1%v/v to 2%v/v in the feed stream of the hydrocyclone leads to an increase in the separation reduced cut size from 4.88 μm to 5.94 μm as shown in Fig. 6.4. As there is only a small change in feed concentration, the curves are not significantly different, however, they match the trend that is observed by increasing the inlet concentration [26].

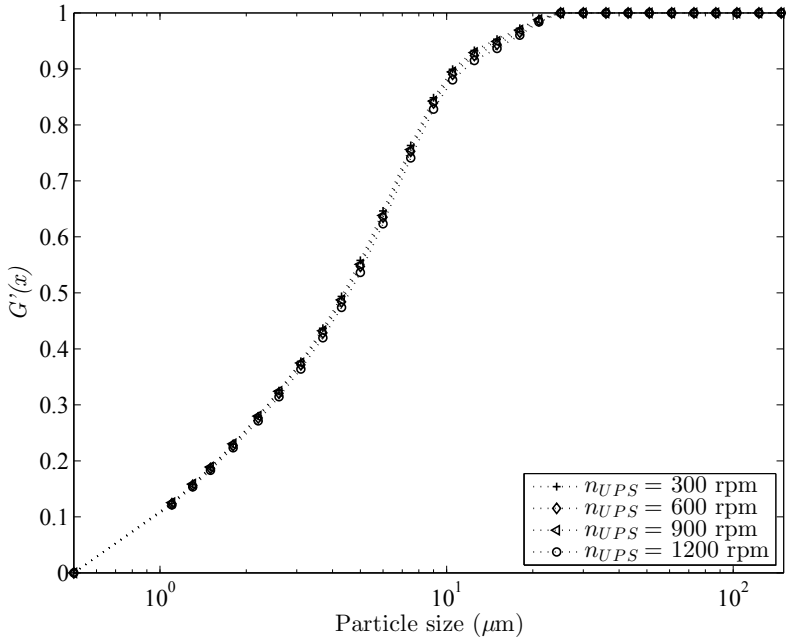

Figure 6.3: Effect of underflow pumping on the reduced grade efficiency $G'(x)$ of the hydrocyclone for different underflow pump speeds; $n_{FPS} = 1800$ rpm; $c = 0.5\%$

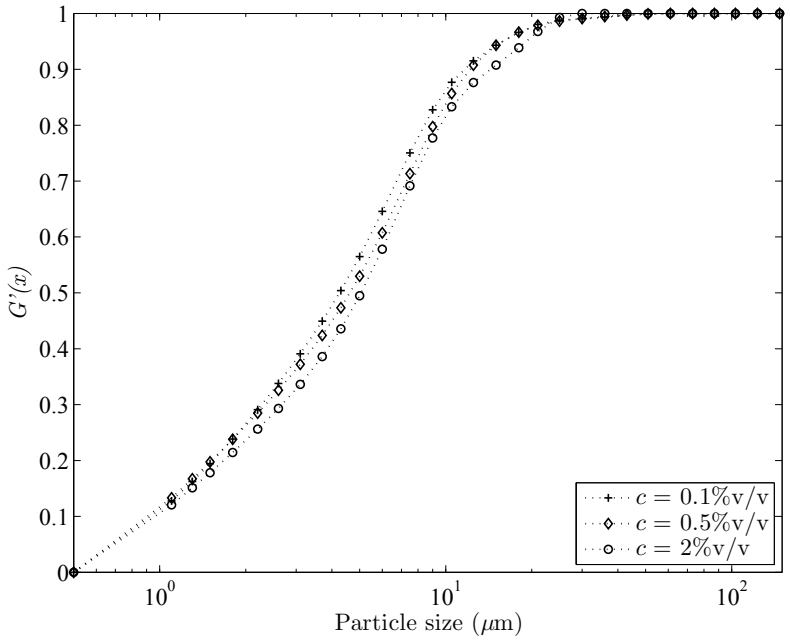

Figure 6.4: Effect of concentration on the reduced grade efficiency of hydrocyclone; $n_{FPS} = 1800$ rpm, $n_{UPS} = 1500$ rpm

6.4.3 The underflow pumping effect on hydrocyclone operation

The effect of using the underflow pump on flow rate, flow ratio and pressures are investigated as a function of pressure ratio ($P^* = P_u/P_o$). This is a non-dimensional variable that represents the underflow pressure changes. The rationale for this is discussed next.

Inlet flow rate

The effect of the changes in the inlet (feed) flow rate Q with respect to P^* is plotted in Fig. 6.5 for three feed pump speeds. It shows that the inlet flow rate decreases slightly with increasing the pressure ratio. A decrease in Q occurs with a decrease in the underflow to the overflow pipe diameter (D_u/D_o) ratio [13] as shown in Fig. 6.6. This leads to the idea that P^* can be used to control the hydrocyclone performance in an analogous way to changing the underflow pipe size. The effect of P^* and D_u/D_o is opposed as increasing P^* has a similar effect on the inlet and the underflow flow rates as of reducing the underflow/overflow pipe diameter ratio.

Inlet and outlet pressures

Changes in the inlet pressure (P_i), overflow pressure (P_o), overflow pressure drop ($\Delta P = P_i - P_o$) and underflow pressure (P_u) as a result of increasing the pressure ratio (P^*) are shown in Fig. 6.7 to Fig. 6.11 (all pressures are absolute). Increasing the pressure ratio does not have a significant effect on the inlet pressure or the pressure drop as seen in Fig. 6.7 and Fig. 6.10, respectively. The overflow pressure shown in Fig. 6.8 increases with the pressure ratio although the amount is less than 1 kPa at each n_{FPS}. However, this increase is not significant comparing the order of magnitude of the other pressures in the experiment. This is shown in

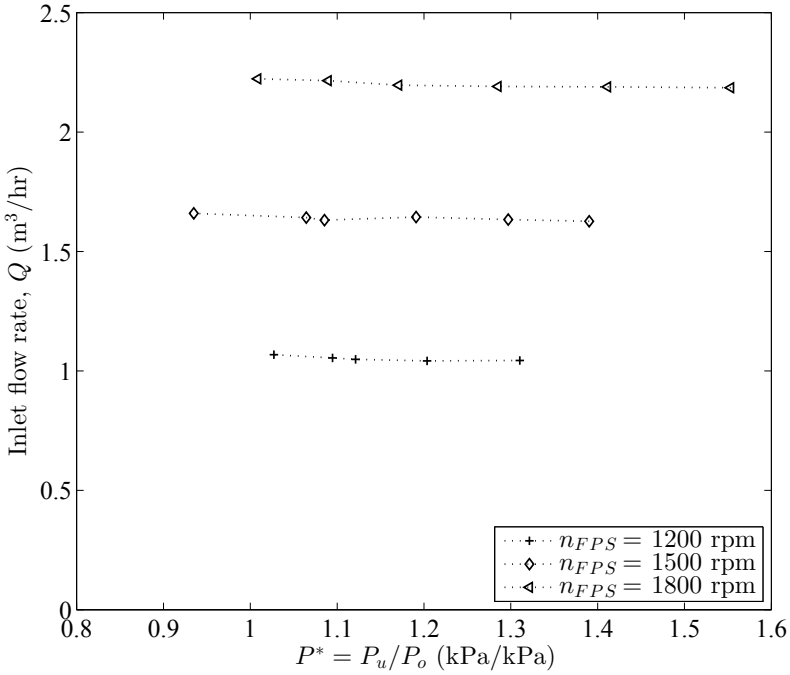

Figure 6.5: Inlet flow rate: effect of changes in the pressure ratio at 3 feed pump speeds (n_{FPS}); $c = 0.5\%$v/v.

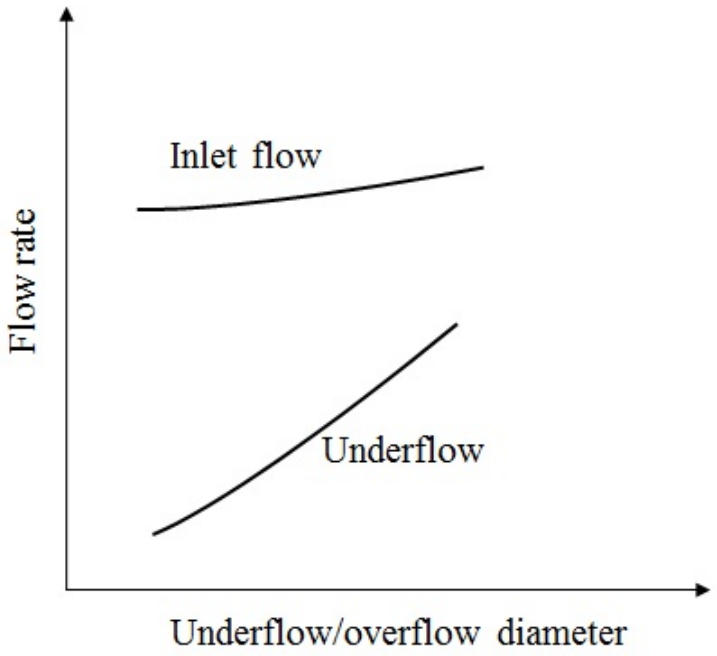

Figure 6.6: Effect of changes in the underflow/overflow diameter ratio on flow rates of inlet and underflow [13].

Fig. 6.9 for a different scale. Since, the inlet pressure is not significantly affected by underflow pumping, this shows that the upstream pressure is almost independent of the downstream pressure changes. This is similar to changes in the underflow pipe diameter or underflow flow rate by using a valve and shows that underflow pumping can be used to achieve a similar effect. The overflow pressure can also be considered as a constant pressure relative to the inlet and underflow pressures. This means $P^* = P_u/P_o$ is only affected linearly by underflow pressure P_u. Therefore, P^* can be used as a normalized variable that represents the behavior of the underflow pressure.

The linearity of P^* in underflow pressure is seen in Fig. 6.11. This is to show that the pressure ratio represents the underflow pressure in terms of a dimensionless variable. Increasing the pressure ratio results in increasing the underflow pressure that is an indication of less suction in the underflow pipe. Comparing the pressure changes from Fig. 6.7 to Fig. 6.11, the pressure ratio P^* has the strongest (almost linear) effect on the underflow pressure. This indicates that the underflow pressure drop ($\Delta P_u = P_i - P_u$) is the most effective pressure drop in this experimental setup for predicting the hydrocyclone behavior. The effects of changes in the variables with respect to the changes in the underflow pressure drop are also shown in Fig. 6.12 to Fig. 6.16. This pressure drop can also be normalized for further investigations, however, the pressure ratio is discussed here as it represents the underflow pressure changes as a result of the underflow pumping regardless of the pressure changes at the inlet.

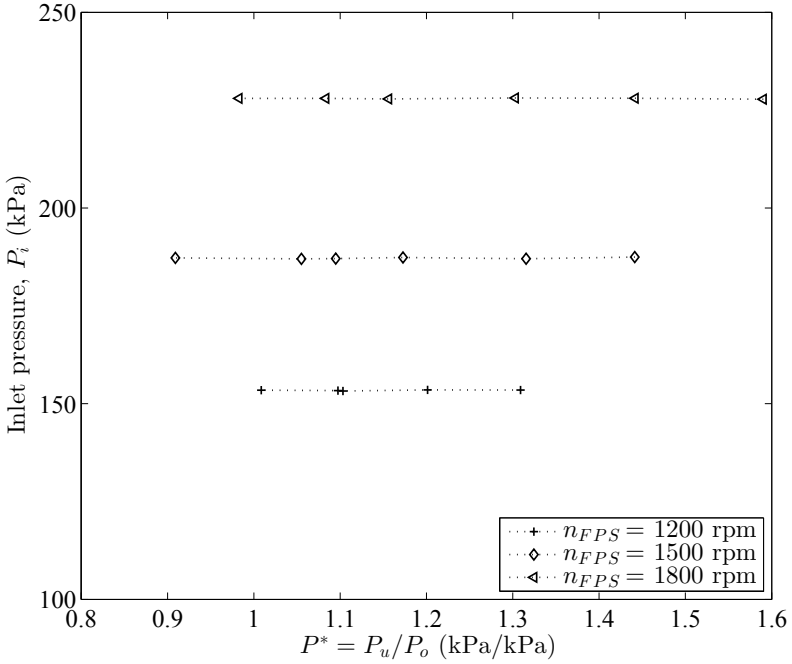

Figure 6.7: Inlet pressure: effect of changes in the pressure ratio at three feed pump speeds (n_{FPS}); $c = 2\%$v/v.

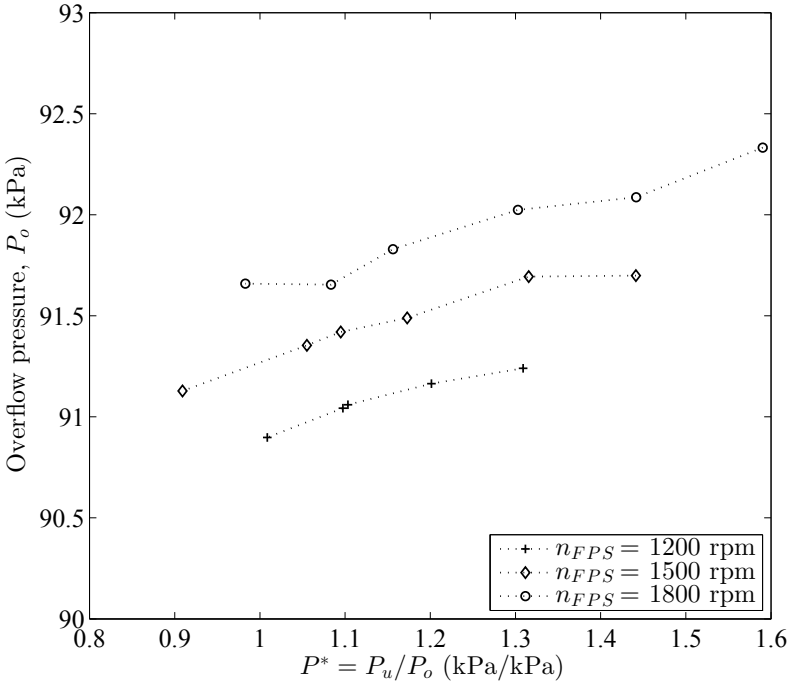

Figure 6.8: Overflow pressure: effect of changes in the pressure ratio at three feed pump speeds (n_{FPS}); $c = 2\%$v/v.

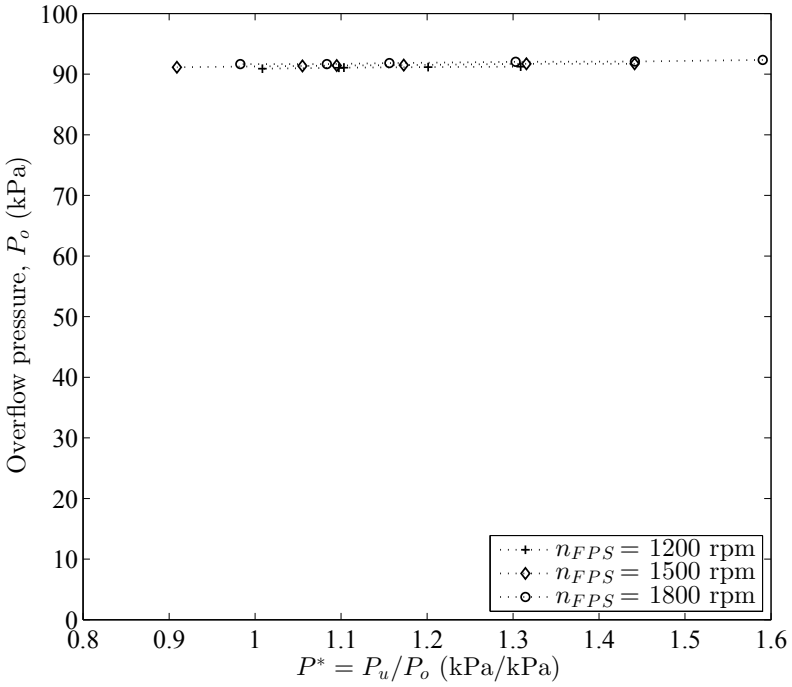

Figure 6.9: Overflow pressure: effect of changes in the pressure ratio at three feed pump speeds (n_{FPS}); $c = 2\%$v/v.

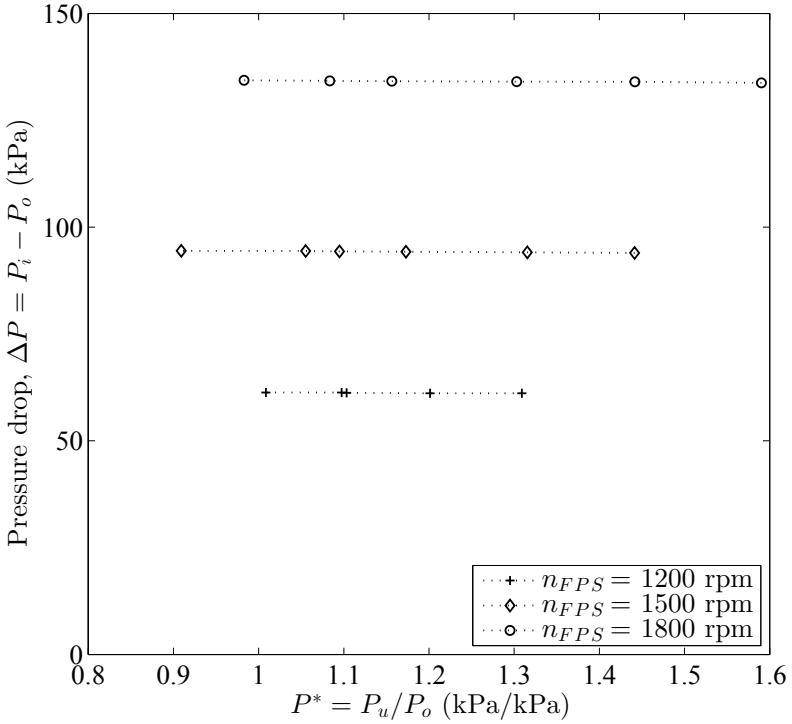

Figure 6.10: Pressure drop: effect of changes in the pressure ratio at three feed pump speeds (n_{FPS}); $c = 2\%$v/v.

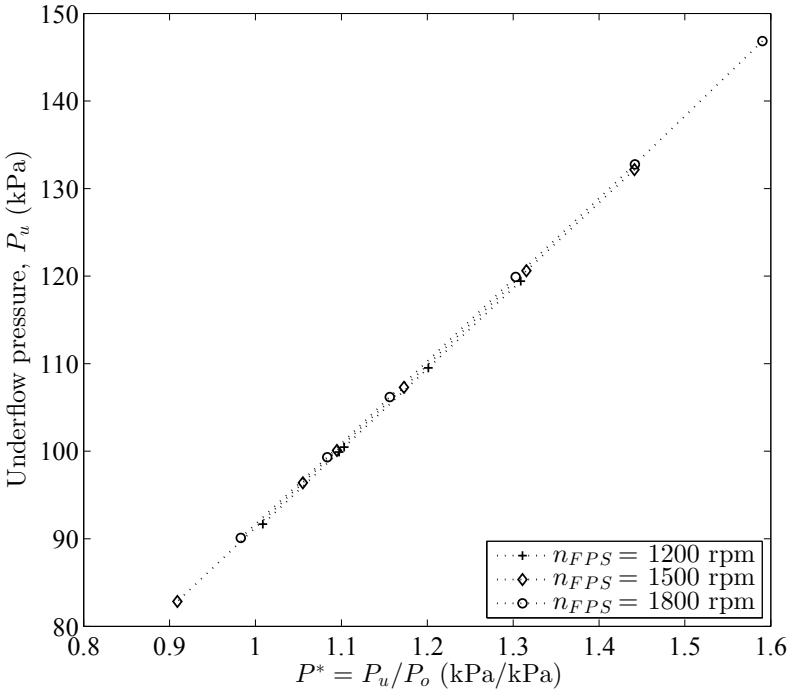

Figure 6.11: Underflow pressure: effect of changes in the pressure ratio at three feed pump speeds (n_{FPS}); $c = 2\%$v/v.

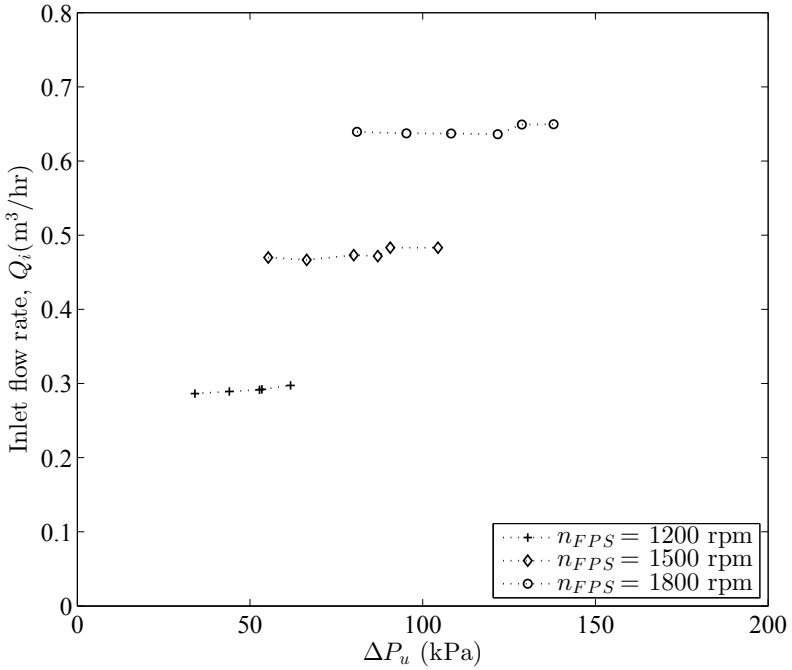

Figure 6.12: Inlet flow rate: effect of changes in the underflow pressure drop at three feed pump speeds (n_{FPS}); $c = 2\%$v/v.

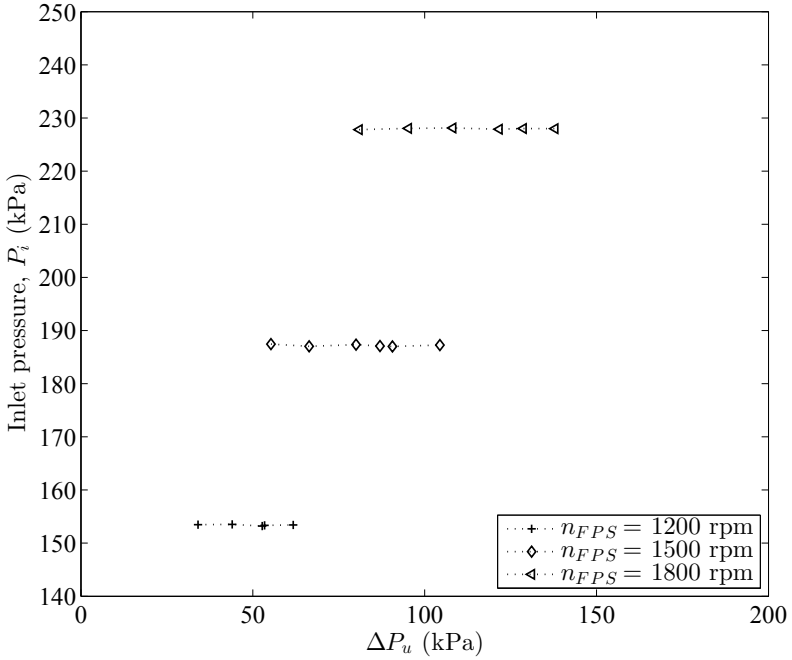

Figure 6.13: Inlet pressure: effect of changes in the underflow pressure drop at three feed pump speeds (n_{FPS}); $c = 2\%$v/v.

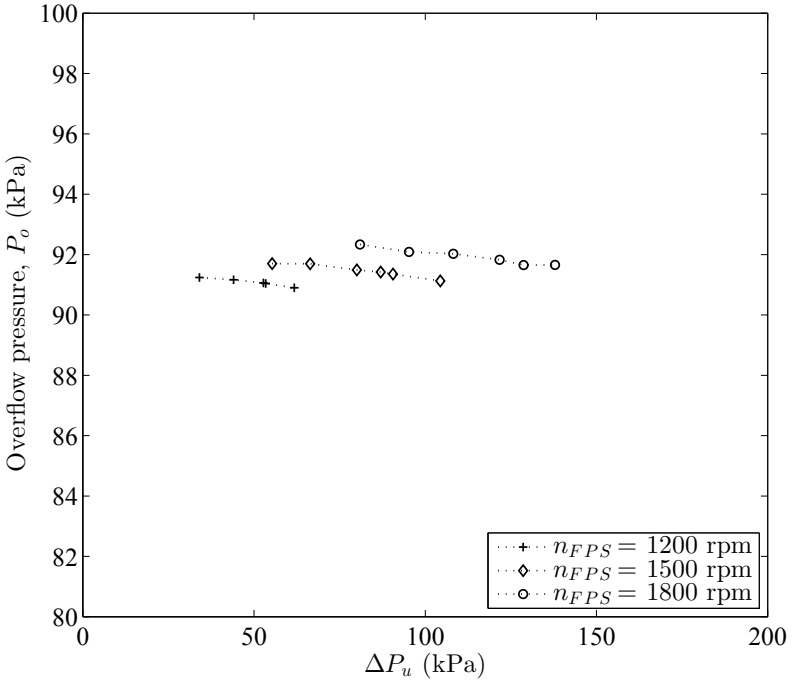

Figure 6.14: Overflow pressure: effect of changes in the underflow pressure drop at three feed pump speeds (n_{FPS}); $c = 2\%$v/v.

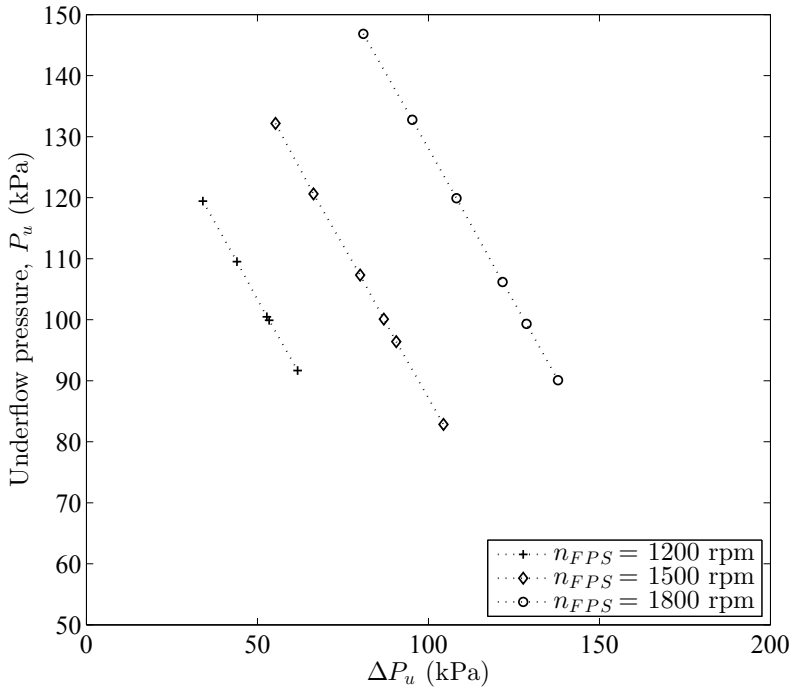

Figure 6.15: Underflow pressure: effect of changes in the underflow pressure drop at three feed pump speeds (n_{FPS}); $c = 2\%$v/v.

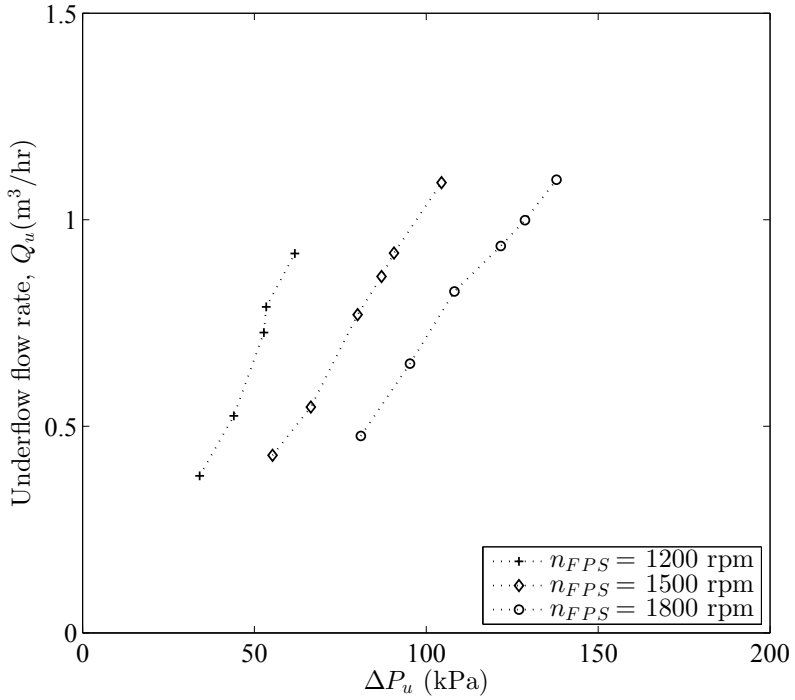

Figure 6.16: Underflow flow rate: effect of changes in the underflow pressure drop at three feed pump speeds (n_{FPS}); $c = 2\%$v/v.

Underflow concentration

The pressure ratio influence on the underflow discharge concentration c_u is shown in Fig. 6.17 for three different feed concentrations. As the underflow pump speed decreases (higher P^* and less suction in the underflow) it is expected that less water is pulled toward the underflow and the underflow concentration increases with increasing the pressure ratio as it can be seen in Fig. 6.17. Increasing the feed concentration, obviously increases the underflow concentration. To evaluate the interaction of feed concentration and the underflow pumping effect, c_u is normalized with the feed concentration c and the results are plotted in Fig. 6.18. The curves in Fig. 6.18 show an increase for the normalized concentration $\bar{c}_u = c_u/c$ when the feed concentration increases from 0.1%v/v to 2%v/v as the pressure ratio increases. There is no distinguishable discrepancy between the curves of 0.5%v/v and 2%v/v feed concentration for pressure ratios less than 1.3 as the plot of 2%v/v concentration is located within the error bars of the plot of 0.5%v/v concentration. However, an increase in the $\bar{c}_u = c_u/c$ is observed after point $P^* = 1.3$ for higher pressure ratios.

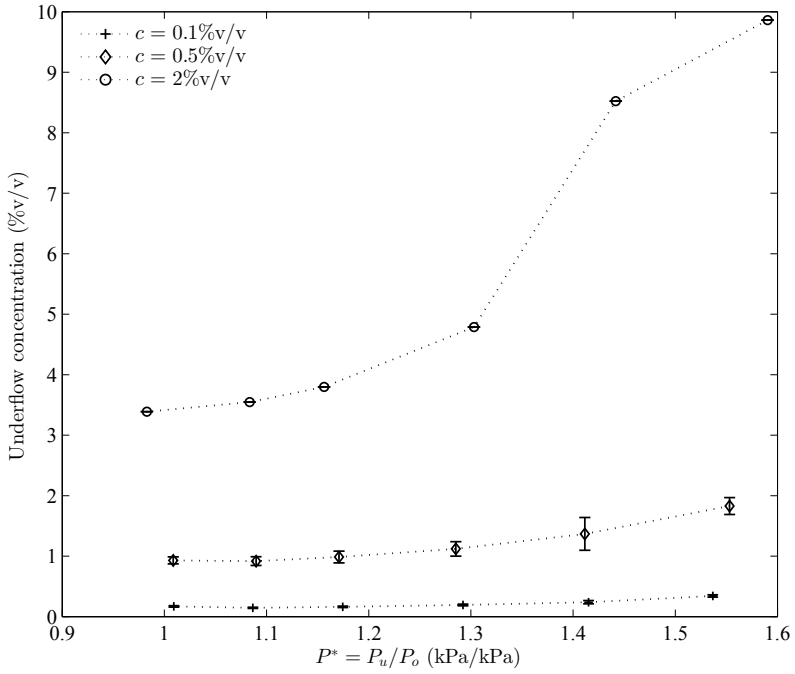

Figure 6.17: Effect of changes in the pressure ratio on the underflow solid volume concentration at different feed concentration; $n_{FPS} = 1800$ rpm

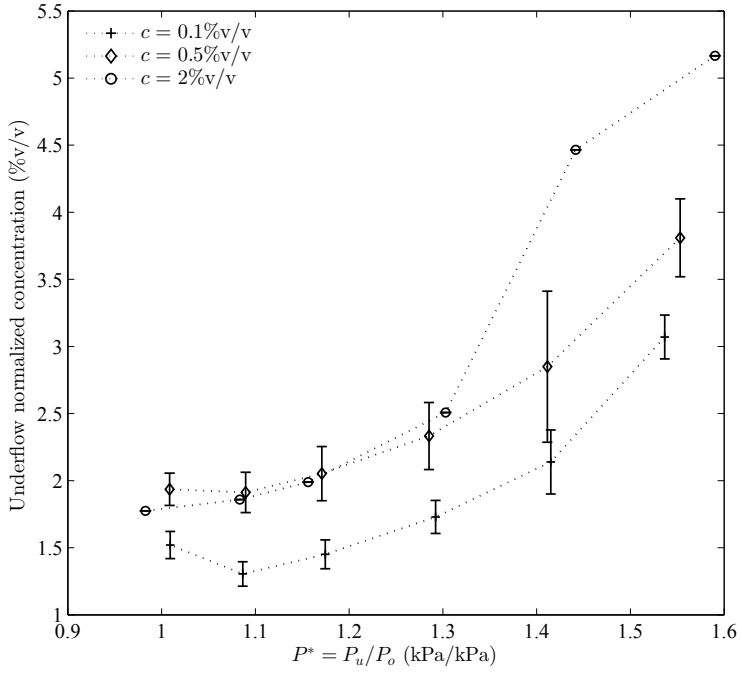

Figure 6.18: Effect of changes in the pressure ratio on the normalized underflow solid volume concentration $\bar{c}$ at different feed concentration; $n_{FPS} = 1800$ rpm

Flow ratio R_f

The flow ratio is an important parameter in controlling a hydrocyclone as it is a direct function of the inlet flow or the underflow flow rate. To understand the behavior of the flow ratio with respect to the underflow pumping, the effect of the pressure ratio P^* on the flow ratio is shown in Fig. 6.19. As a result of less suction, R_f decreases with increasing the pressure ratio. Increasing the concentration decreases R_f which results in less flow in the underflow (at a fixed inlet flow rate) at higher concentrations. This is attributed to the accumulation of the solids in the underflow discharge zone which reduces the discharge area and results in a higher flow rate through the overflow pipe. The reduction in the inlet flow rate with increasing P^* that is observed in Fig. 6.5 is also a factor but not as significant as the changes in the underflow flow rate.

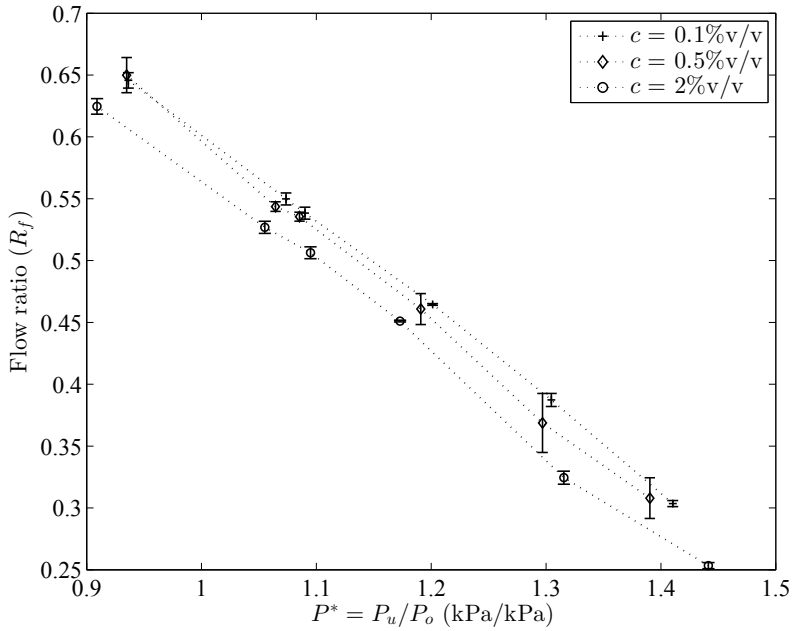

Figure 6.19: Effect of changes in the pressure ratio on the flow ratio at different feed concentration; $n_{FPS} = 1500$ rpm

6.4.4 Model development for predicting pressure ratio

The development of a correlation for predicting the effect of the underflow pumping and comparing it to changing underflow/overflow diameter is a major objective of this study. The main performance factors are: pressures and flow rates at the hydrocyclone entrance and outlets, inlet concentration and the inlet particle cut size. Both linear and nonlinear regression approaches are applied to find the model that can explain the pressure ratio and hence underflow pressure changes for 54 experimental points. The fixed parameters in the experiment such as liquid and solid densities or the density difference and diameters are not involved in the model developmental.

The underflow pumping effect is evaluated using the pressure ratio P^*. Linear and nonlinear models with predictor variables including pressure drop, inlet cut size, inlet concentration, inlet flow rate and flow ratio are tested for predicting the pressure ratio. From the statistical analysis, it is found that the inlet particle cut size and concentration are not significant. The remained parameters involved in the model development are normalized inlet flow rate ($Q_n = Q/Q_{avg}$) where Q_{avg} is the mean value for all recorded flow rates, flow ratio (R_f), normalized pressure drop ($\Delta P/P_i$) and inlet solid volume concentration (c). Linear and nonlinear regressions are detailed next.

Linear regression approach

For the linear regression, polynomials of different orders up to the order of four of the function variables are tested. According to the hypothesis tests for significance level of the coefficients, a polynomial function of the order of one is found to be more significant. The linear model is then in the form:

$$P^* = \alpha_0 + \alpha_1 Q_n + \alpha_2 R_f + \alpha_3 \Delta P/P_i + \alpha_4 c \tag{6.3}$$

Table 6.2: Estimated coefficients and statistics parameters for pressure ratio (P^*) in linear regression

Coefficient	Estimate	SE	t-Statistics	p-value
α_0	2.858	0.5189	5.507	1.32E-06
α_1	0.649	0.5180	1.253	0.2159
α_2	-1.097	0.0948	-11.56	1.29E-15
α_3	-3.502	2.0027	-1.748	0.0866
α_4	-0.018	0.0163	-1.120	0.2680
RMS Error	0.0852		R^2	0.76
Model p-value	1.27E-14		Adjusted R^2	0.74

The statistical information for estimated coefficient for the linear correlation function in Eq. (6.3) is presented in Table 6.2. This is including standard error of the coefficients (SE) that measures how precisely the model estimates the coefficient, root mean squared (RMS) errors that is a measure of the spread of the estimated response values around their average, t-statistics and p-value (an indication of significance of estimated coefficient or model under investigation for regression analysis), R^2 (an indication of the goodness of a fit) and adjusted R^2 (adjusted R^2 for the number of parameters involved in the regression). The t-statistics and p-values of each coefficient in Table 6.2 show that all the coefficients except concentration are

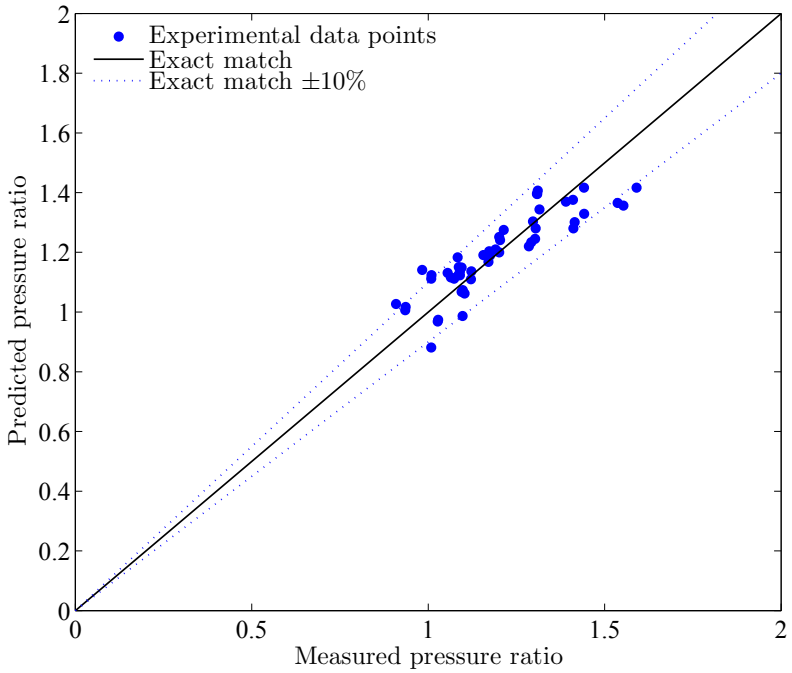

Figure 6.20: Linear regression: a comparison of measured and predicted values of pressure ratio P^*

significant [132]. Typically coefficients with p-values smaller than 0.05 are considered to be significant [137]. As can be seen from Table 6.2 this value for the flow rate and the inlet concentration coefficient (α_1 and α_4) are much greater than 0.05. However, since removing these variables does not improve the regression, to show the effect of the feed concentration it is decided to keep these coefficients in the model. The model p-value equals 1.27E-14 shows the significance of the model in predicting P^*. The R^2 and adjusted R^2 shows overall fit for the data that predicts 76% variability of the predictors in the model. The predicted values of the P^* from the model presented in Eq. (6.3) are compared with the experimental values in Fig. 6.20. It is observed that the developed linear model predicts the pressure ratio within the $\pm$10% deviation from the exact line.

Nonlinear regression approach

Similar to the linear regression, Q_n, R_f, $\Delta P/P_i$ and c are found to be the main parameters involved in predicting P^*. Using trial and error with some nonlinear functions a useful predicting function is found to be:

$$P^* = Q_n^{\beta_1} R_f^{\beta_2} (\Delta P/P_i)^{\beta_3} \exp(\beta_4 c) \tag{6.4}$$

This model predicts the variations in the P^* with R^2 equals 90.1%. The statistics related to the nonlinear regression are listed in Table 6.3. All coefficients of the nonlinear model in Eq. 6.4 are found to be significant as the p-values are smaller than (or close to) 0.05. Unlike the linear regression modeling, solid concentration is observed to have more significant role in predicting the pressure ratio in nonlinear modeling. The outcome of the model against the experimental values are plotted in Fig. 6.21. This figure also shows that the developed nonlinear model predicts the pressure ratio within $\pm 10\%$ deviation from the experimental results.

Table 6.3: Estimated coefficients and statistics parameters for pressure ratio (P^*) in nonlinear regression

Coefficient	Estimate	SE	t-Statistics	p-value
β_1	-0.3249	0.0360	-9.004	4.8487E-12
β_2	-0.4508	0.0215	-20.906	2.2768E-26
β_3	0.2569	0.0294	8.7237	1.2906E-11
β_4	-0.0144	0.0080	-1.7987	0.0781
RMS Error	0.0541		R^2	0.901
Model p-value	2.42E-67		Adjusted R^2	0.895

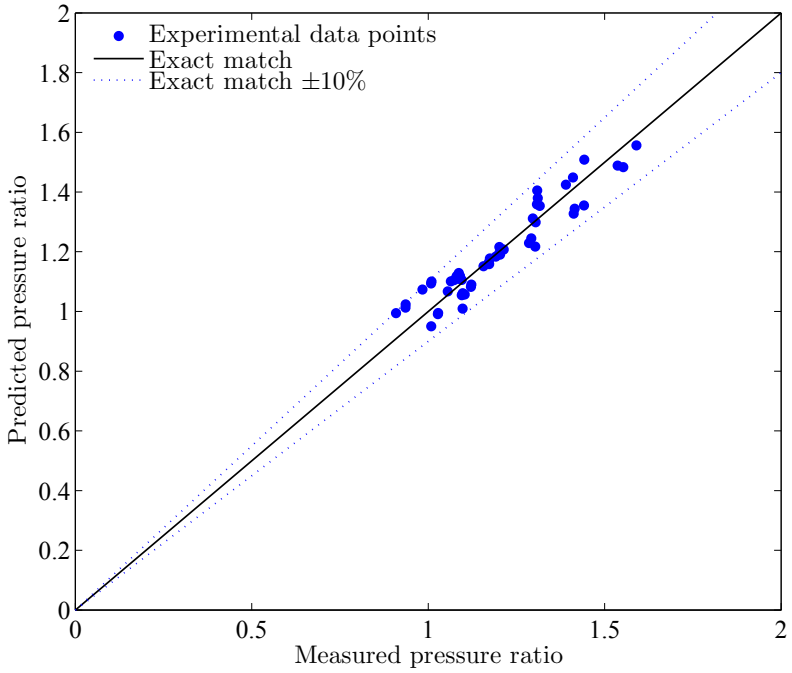

Figure 6.21: Nonlinear regression: a comparison of measured and predicted values of pressure drop ratio P^*

Model selection

Investigating the statistics of the both linear and nonlinear models presented in Eq. 6.3, Eq. 6.4, Table 6.2 and Table 6.3, it is clear that the nonlinear model provides a better prediction of the data. This investigation provides a strong evidence over choosing the nonlinear model for predicting the P^* in the current study. Therefore, the correlation which predicts the pressure ratio for the hydrocyclone design of the current study and for solid volume concentration lower than 2%v/v is:

$$P^* = Q_n^{-0.325} R_f^{-0.451} (\Delta P/P_i)^{0.0257} \exp(-0.014c) \tag{6.5}$$

This correlation is dimensionless.

The obtained correlation can be used for further study on hydrocyclone control. Since, no similar setup is seen in the literature (with a pump in the underflow) a separate test with the experimental setup is performed with a different concentration ($c = 1\%$) and the data is used to validate the model. The results of this cross validation are shown in Fig. 6.22. The nonlinear model predicts the pressure ratio within $\pm 10\%$ from the experimentally observed values for this new test.

The coefficients of Eq. 6.5 indicate that the inlet flow rate and the flow ratio have a stronger effect on pressure ratio than pressure drop and feed concentration. The effect of changes in the pressure ratio with flow ratio at a constant Q_n equal to one is shown in Fig. 6.23. It can be seen that as pressure ratio decreases the flow ratio increases showing increase in the underflow flow rate.

The slopes of changes in P^* with respect to changes in each model variable are plotted versus flow ratio R_f in Fig. 6.24 to Fig. 6.27 for three nominal Q_n. The changes in P^* with respect to R_f are one order of magnitude greater than changes with respect to Q_n and $\Delta P/P_i$ and two orders of magnitude with respect to c. This

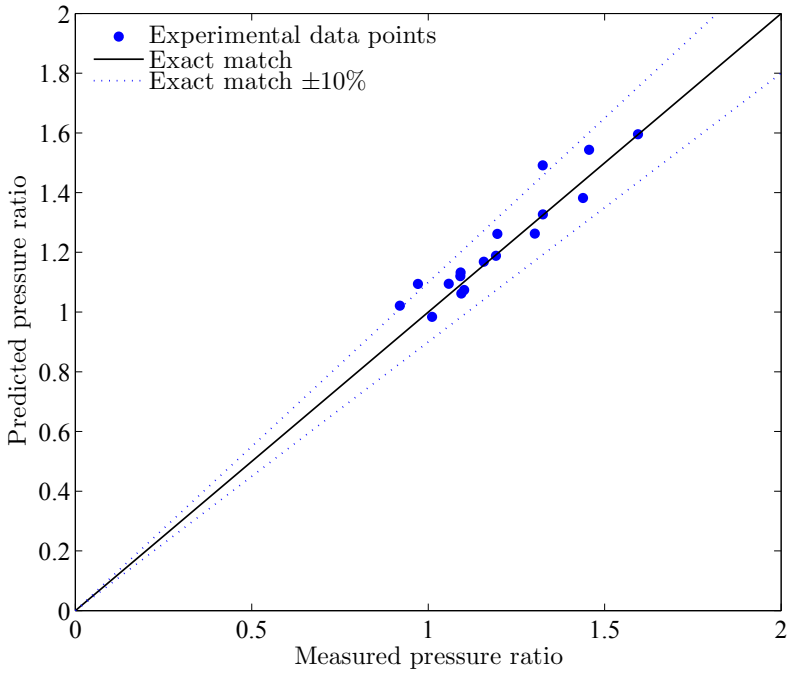

Figure 6.22: Cross validation for pressure ratio using nonlinear developed model; $c = 1\%$v/v

shows that the pressure ratio P^* is most sensitive to flow ratio and the inlet solid volume concentration has the least influence on P^*. Therefore, the flow ratio is the most effective way to manipulate the pressure ratio for controlling the hydrocyclone performance.

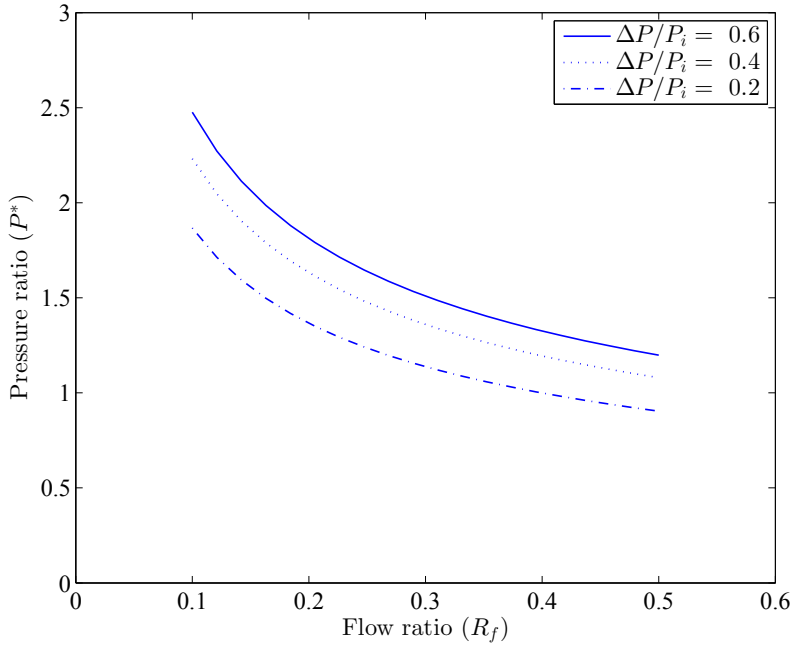

Figure 6.23: Effect of changes in flow ratio on pressure ratio; $Q_n = 1$; $c = 1\%$v/v

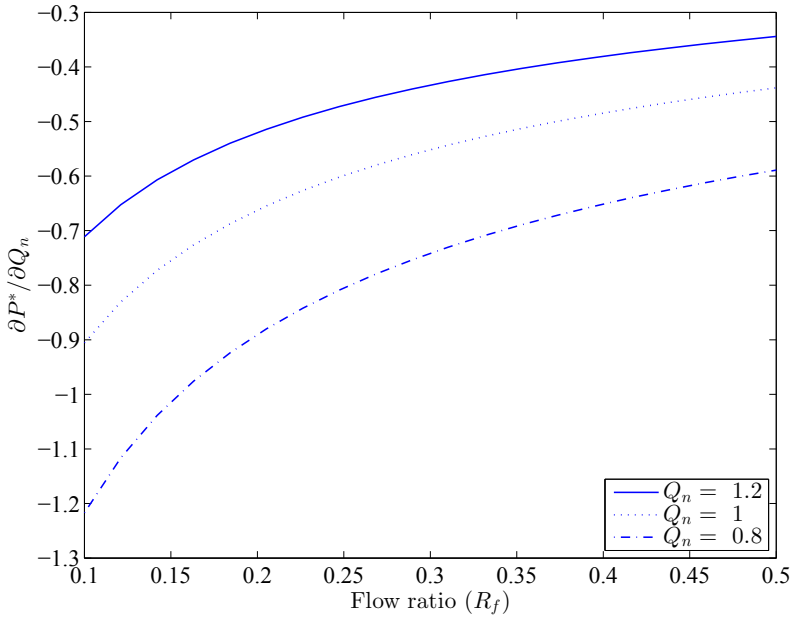

Figure 6.24: Pressure ratio sensitivity to normalized flow rate; $\Delta P/P_i = 0.95$; $c = 1\%$v/v

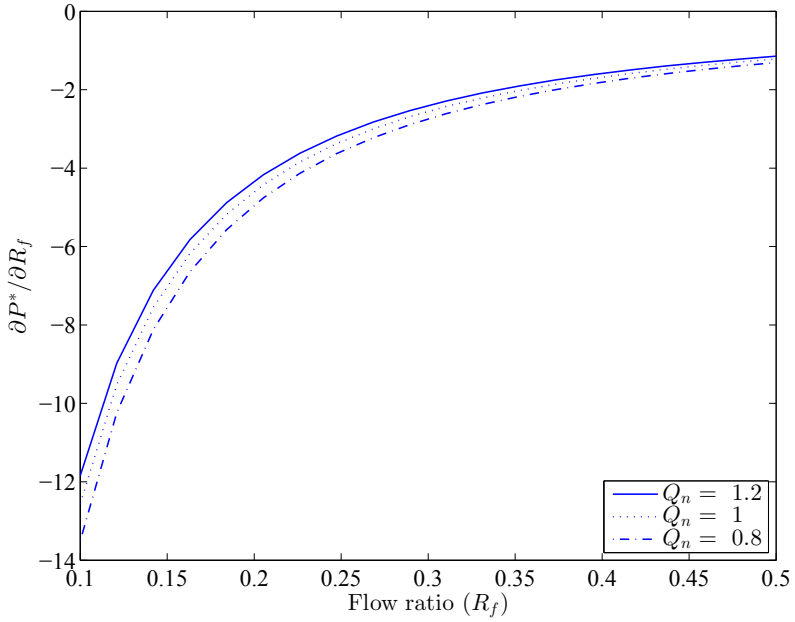

Figure 6.25: Pressure ratio sensitivity to flow ratio; $\Delta P/P_i = 0.95$; $c = 1\%$v/v

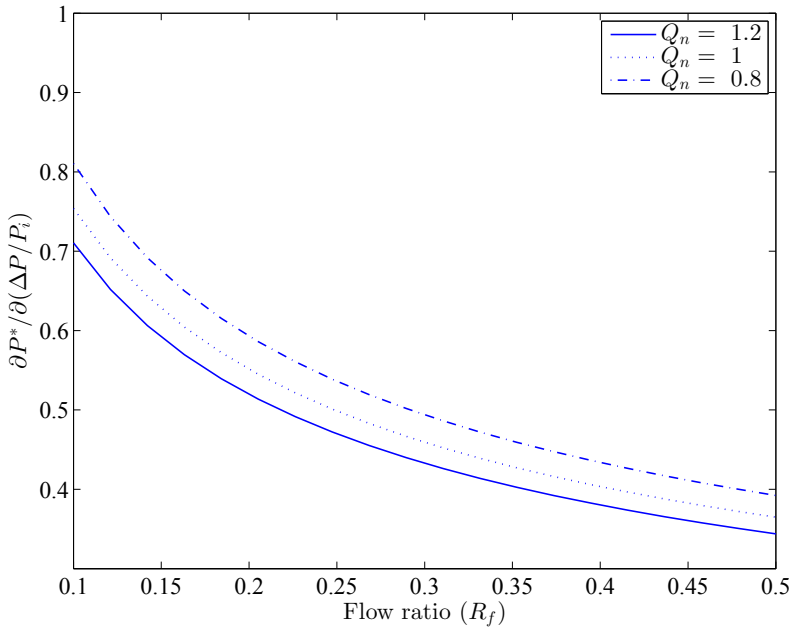

Figure 6.26: Pressure ratio sensitivity to pressure drop/inlet pressure ratio; $\Delta P/P_i = 0.95$; $c = 1\%$v/v

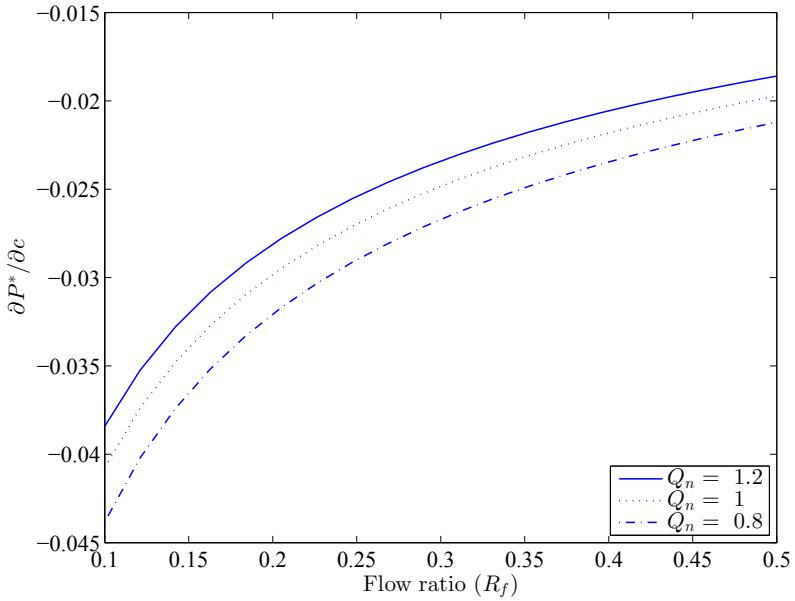

Figure 6.27: Pressure ratio sensitivity to inlet volume concentration; $\Delta P/P_i = 0.95$; $c = 1\%$v/v

6.5 Conclusions

The effect of pumping the underflow of a hydrocyclone is studied experimentally by using the soda lime particles in the water. Three different solid concentrations (maximum 2%v/v) and different flow rates by changing the feed pump speeds are examined. Using a pump in the underflow of a hydrocyclone separator can help adjusting the device to accommodate fluctuations in the inlet flow. This is similar to using a valve in the underflow or changing the apex size and is used to control the hydrocyclone performance.

The results of the study show that increasing the feed volume solid concentration from 0.1% to 2% increases the separation reduced cut size from 4.88 μm to 5.94 μm. The ratio of the underflow to overflow absolute pressures is defined as pressure ratio P^* and is used to study the underflow pumping effect on the performance. The changes in the inlet flow rate with the pressure ratio shows that the inlet flow rate increases slightly with decreasing the pressure ratio. This trend is similar to increasing the underflow pipe diameter which is another method of adjusting the hydrocyclone performance according to the feed flow conditions. The changes in the inlet and outlet pressures, pressure drops and the flow ratio are also studied but no significant changes are observed with the underflow pumping.

The data of the 54 experimental tests is used to develop a correlation to predict the pressure ratio. The linear and nonlinear regression are examined and the nonlinear model provides a better fit with predicting the hydrocyclone behavior. A nonlinear model, for predicting the pressure ratio, is defined in Eq. 6.5. It is observed that the most and the least sensitive influencing variables on the pressure

ratio are flow ratio and inlet concentration, respectively. This model can be used for further studies on controlling the hydrocyclone separation performance.

Chapter 7

Conclusions and future work

7.1 Conclusions

This study is aimed to model the performance of hydrocyclones in terms of an equivalent settling area factor. This factor is used for centrifugal separators in order to compare the performance of the device and for scaling up a centrifuge separator. Investigating the literature, it is found that there is a lack of such a model for hydrocyclones. Developing the equivalent area factor for hydrocyclones allows comparing the performance of the device with other centrifuges. It also provides a tool to develop guideline charts that are useful in centrifugal separator selection and design.

Using the empirical equations of Plitt [71] and the Rietema relation [63] for separation cut size in hydrocyclones, performance of hydrocyclones are evaluated in terms of equivalent area factor. Comparing the obtained data with literature it is observed that the guideline performance chart of Lavanchy [10], does not predict the hydrocyclone performance well. This is discussed in detail in Chapter 2. Thus, a theoretical model based in the first principles is needed for more investigation.

To compare the energy consumption in different centrifugal separators includ-

ing hydrocyclones, a model is developed in this research. Considering a single particle suspended in a centrifugal field and the relevant forces, the specific energy consumption for sedimenting the particle is calculated. Comparison of the specific energy consumption of the centrifuges and the hydrocyclone, it is observed that a hydrocyclone consumes less energy to separate a particle than the other types of centrifugal separators.

A theoretical equivalent settling area model (ESAM) is developed. This model replaces the simplifications of the residence time theory with estimating an average vertical velocity component from the flow rate in the cylindrical portion of the hydrocyclone and also bringing the tangential velocity component into account. The model predicts the equivalent area in terms of design parameters and the operating variables. Following the model development, ESAM is validated performing the experiments.

Experimental setup including a test rig with a 5 cm hydrocyclone is used to measure the separation performance of the hydrocyclone. The information from the experiments is used to validate the ESAM. The experiments are performed at different inlet concentrations and for different operating conditions. At all experimental points a sample from the inlet and outlet flows is collected to determine the particle size distribution and separation cut size. This set up uses a pump attached to underflow that facilitates manipulating the underflow.

The experimental results are in good agreement with the ESAM prediction. ESAM can be used to predict the equivalent area factor for a variety of hydrocyclone designs. The equivalent area factor Σ can also be used to compare other centrifugal separators and a continuous settling tank to provide insight into the rel-

ative performance of different centrifugal separation techniques. Using the ESAM, the effects of hydrocyclone design parameters such as inlet and overflow diameters are studied. It is observed that Σ in hydrocyclones is increased by increasing either the hydrocyclone inlet diameter or the overflow diameter, but it is more sensitive to the overflow diameter.

Since the model development basis is the centrifugal acceleration which is in turn related to the tangential velocity, the ESAM together with the experimental equivalent area obtained from performance experiments can be used to predict the tangential velocity profile in the hydrocyclone. This prediction is validated by comparison of the tangential velocity profile of a given hydrocyclone. This method has the benefit of predicting the tangential velocity profile without requiring complex and expensive instruments for velocimetry measurement.

The average value of 0.8 is suggested in the literature for the exponent n in Eq. (2.12) in the tangential velocity profile function for hydrocyclones. It is shown that the value of this exponent is significantly geometry dependent. For three of the hydrocyclone designs studied in this research, the exponent values are close to the average, while for Bradley hydrocyclone n is found to be 0.31. The proper exponent for each hydrocyclone design can be determined from the ESAM by comparing with experimental data and the ESAM can be used as a design tool for hydrocyclones for applications limited to low feed solid concentration.

To include the effect of solid concentration in the model, ESAM is modified by multiplying it in a concentration function. Several forms of solid volume concentration functions are examined and performing detail statistical analyses and using experimental data the best function is selected. The modified ESAM (Σ_c) can pre-

dict the equivalent area factor for concentration variation according to Eq. (5.11). The limits in operating hydrocyclones to achieve a minimum equivalent area is discussed based on this model. It is shown that the maximum concentration that drops the hydrocyclone equivalent area to 1 m^2 can be obtained from Σ_c as shown in Fig. 5.5. This modified model is is used to develop a guideline charts for hydrocyclones by calculating the hydrocyclone performance for different sizes and operating conditions. The developed performance chart is evaluated with data from literature and a manufacture data. It is observed from Fig. 5.14 that the developed chart well covers the data points and can be used for device selection among the centrifugal separator or for hydrocyclone designs. A design flow chart is provided in this study shown in Fig. 2.11.

Finally, the underflow pumping effect on the operating variables and performance of the hydrocyclone is investigated. This is a new experimental setup for hydrocyclones as the common setups discharge the underflow to atmospheric pressure. The pump allows changing the underflow rate by controlling the underflow pump speed. This study shows that the pump can simulate the function of valves used in the underflow pipe. The effect of underflow pumping on operating parameters is discussed and a correlation is developed to predict the ratio of the underflow pressure to overflow pressure P^*. This parameter is found to be significantly affected by the flow ratio and pressure drop in hydrocyclones.

7.2 Future work

Further studies that can be done as a continuation of the current study are listed below:

- The hydrocyclone equivalent area factor can be tested for smaller and larger hydrocyclones to investigate the effect of design parameters particularly hydrocyclone diameter and underflow pipe size.

- An optimization study can be conducted based on the model developed in the study for hydrocyclones. This can optimized the hydrocyclone size and reduce the pressure drop and hence energy consumption in hydrocyclone. Considering the performance of Bradley and Rietema hydrocyclones discussed in the study, and intermediate design can be investigated.

- The energy consumption models developed in this research are based on forces applying on a single particle in the centrifugal separators. This model can be generalized for the effect of particles concentration in centrifuge and hydrocyclone separators.

- Determining velocity profile at higher concentrations provides more information about the effect of solid concentration and hindered settling on hydrocyclone performance in terms of equivalent area factor. In particular, investigating the tangential velocity profile under such conditions can help better understanding about the use of the developed model to predict this velocity profile. Most of the current researches in the literature for studying the velocity profiles are under low feed concentration.

- The effect of underflow pumping can be tested under different test conditions including the type of mixture, hydrocyclone design and size and operating conditions. This information is required to generalize the developed correlations for hydrocyclones.

- Effect of overflow pumping can be investigated in a similar way that performed for underflow in this research. This can be combined with the underflow pumping for controlling hydrocyclones performance or may found some potential applications where there is a limit for discharging the outlet flow into atmosphere.

- Controlling the hydrocyclone performance using the pump in the underflow can be an important research particularly for the applications that the underflow clogging or the underflow control valve to response the feed flow fluctuation is an issue. The correlations developed in the current study provide great tools for developing a control procedure.

7.3 List of contributions

The following is a list of contributions from this thesis in the form of conference and journal publications.

7.3.1 Journal papers

- R. Sabbagh, M. G. Lipsett, C. R. Koch, D. S. Nobes, Hydrocyclone Performance and Energy Consumption Prediction: A Comparison with Other Centrifugal Separators, Separation Science and Technology 50 (6) (2015) pp. 788-801. doi:10.1080/01496395.2014.978463.

- R. Sabbagh, M. G. Lipsett, C. R. Koch, D. S. Nobes, Predicting Equivalent Settling Area Factor in Hydrocyclones; A Method for Determining Tangential Velocity Profile, Submitted to Separation and Purification Technology Journal, SEPPUR-D-15-01191.

- R. Sabbagh, M. G. Lipsett, C. R. Koch, D. S. Nobes, Experimental study of using underflow pump for hydrocyclones and developing a correlation, In preparation for publication.

- R. Sabbagh, M. G. Lipsett, C. R. Koch, D. S. Nobes, Effect of inlet concentration on the hydrocyclone equivalent settling area factor, In preparation for publication.

7.3.2 Conference papers

- R. Sabbagh, M. G. Lipsett, C. R. Koch, D. S. Nobes, Theoretical and experimental study of hydrocyclone performance and equivalent settling area, ASME 2014 International Congress and Exposition IMECE2014, ASME, Montreal, Que-

bec, Canada, 2014. doi:10.1115/IMECE2014-37482.

- R. Sabbagh, M. G. Lipsett, C. R. Koch, and D. S. Nobes, A mathematical model of equivalent settling area for predicting hydrocyclone separation performance, European Conference on Fluid Particle Separation-FP S2014, pp. 61-62, Lyon, France, 2014.

References

[1] W. Kraipech, W. Chen, T. Dyakowski, and A. Nowakowski. The performance of the empirical models on industrial hydrocyclone design. *International Journal of Mineral Processing*, 80(2-4):100–115, 2006.

[2] D. F. Kelsall. A further study of the hydraulic cyclone. *Chemical Engineering Science*, 2:254–272, 1953.

[3] H. Yoshida, T. Takashina, K. Fukui, and T.i Iwanaga. Effect of inlet shape and slurry temperature on the classification performance of hydro-cyclones. *Powder Technology*, 140(1-2):1–9, 2004.

[4] B. Palma. FLSmidth Krebs Inc., personal communication, May 2013.

[5] M.A.Z. Coelho and R.A. Medronho. A model for performance prediction of hydrocyclones. *Chemical Engineering Journal*, 84(1):7–14, 2001.

[6] D. Bradley. *The hydrocyclone*. Pergamon Press Ltd., Oxford, London, 1965.

[7] B. Dabir and C. A. Petty. Measurements of Mean Velocity Profiles in a Hydrocyclone Using Laser Doppler Anemometry. *Chemical Engineering Communications*, 48:377–388, 1986.

[8] F. M. Tiller, W. Li, and W. Chen. Solid-liquid separation. In *Albrights Chem-*

ical Engineering Handbook, chapter 22, pages 1597–1666. CRC Press, Boca Raton, FL USA, 2009.

[9] G. Towler and R. Sinnott. *Chemical Eengineering Design*. Butterworth-Heinemann, London UK, 2008.

[10] A. C. Lavanchy, F. W. Keith, and J. W. Beams. Centrifugal separation. *Kirk-Othmer Encyclopedia of Chemical Technology*, 4:710–758, 1964.

[11] H. Axelsson and B. Madsen. Centrifuges, sedimenting, 2012.

[12] L. Svarovsky. *Solid/liquid separation*, volume 34. Butterworth-Heinemann, 4th ed. edition, January 2000.

[13] L. Svarovsky. *Hydrocyclones*. Holt Rinehart and Winston, 1984.

[14] E. S. Tarleton and R. J. Wakeman. Data acquisition, analysis and scale-up. In *Solid / Liquid Separation : Equipment Selection and Process Design*, pages 152–200. Elsevier Science, 2007.

[15] R. Sabbagh, M. G. Lipsett, C. R. Koch, and D. S. Nobes. Hydrocyclone Performance and Energy Consumption Prediction: A Comparison with Other Centrifugal Separators. *Separation Science and Technology*, 50(6):788–801, 2015.

[16] E. S. Tarleton and R. J. Wakeman. Solid/liquid separation equipment. In *Solid/Liquid Separation: Equipment Selection and Process Design*, volume 28, pages 1–77. Elsevier Science, August 2007.

[17] H. Anlauf. Recent developments in centrifuge technology. *Separation and Purification Technology*, 58(2):242–246, December 2007.

[18] U. Schaflinger. Review article Centrifugal separation of a mixture. *Fluid Dynamics Research*, 6:213–249, 1990.

[19] C. M. Ambler. The fundamentals of separation, including Sharples Sigma Value for predicting equipment performance. *Industrial & Engineering Chemistry*, 53(6):429–429, June 1961.

[20] Z. Berk. Centrifugation. In *Food Process Engineering and Technology*, pages 217–232. Elsevier Inc., 2009.

[21] C. M. Ambler. The Evaluation of Centrifuge Performance. *Chemical Engineering Progress*, 48(3):150–158, 1952.

[22] C. M. Ambler. The theory of scaling up laboratory data for the sedimentation type centrifuge. *Journal of biochemical and microbilogical technology and engineering*, 1(2):185–205, 1959.

[23] F. W. Keith. Centrifugal concentration and coalescence equipment. *Chemical Engineering Progress*, 59(4):35–42, 1963.

[24] C. Bernhardt. *Particle size analysis; Classification and sedimentation methods*. Springer Science+Business Media Dordrecht, 1994.

[25] R. L. Panton. *Incompressible Flow*. John Wiley & Sons, Inc. All, fourth edition, 2013.

[26] T. Braun and M. Bohnet. Influence of feed solids concentration on the performance of hydrocyclones. *Chem. Eng. Technol.*, 13:15–20, 1990.

[27] J.R Richardson, J.F.; Harker, J.H.; Backhurst. Centrifugal Separations. In *Coulson and Richardson's Chemical Engineering*, volume 99, pages 377–378. March 2002.

[28] R. G. Holdich. Centrifugal separation. In *Fundamentals of Particle Technology*, page 173. Midland Information Technology and Publishing, Loughborough, UK, 2002.

[29] E. Ortega-Rivas. Hydrocyclones. In *Ullmann's Encyclopedia of Industrial Chemistry*, volume 18, pages 207–233. Wiley-VCH Verlag GmbH & Co. KGaA, Weinheim, 2012.

[30] A. Zeidan, S. Rohani, A. Bassi, and P. Whiting. Review and comparison of solids settling velocity models. *Reviews in Chemical Engineering*, 19(5):473–530, 2003.

[31] D. K. Basson, S. Berres, and R. Bürger. *Applied Mathematical Modelling*.

[32] J. F. Richardson and W. N. Zaki. Sedimentation and fluidisation: Part I. *Transactions of the Institution of Chemical Engineers*, 32:S82–S100, 1954.

[33] H. H. Steinour. Rate of sedimentation. *Industrial & Engineering Chemistry*, 36(9):840–847, 1944.

[34] J. H. Masliyah. Hindered settling in a multi-species particle system. *Chemical Engineering Science*, 34:1166–1168, 1979.

[35] H. A. Nasr-el din, J. Masliya, and K. Nandakumar. Continuous separation of suspensions containing light and heavy particle species. *The Canadian Journal of Chemical Engineering*, 77(October):1003–1012, 1999.

[36] T. E. Baldock, M. R. Tomkins, P. Nielsen, and M. G. Hughes. *Coastal Engineering*.

[37] J.F. Richardson, J.H. Harker, and J.R. Backhurst. Particle Technology and Separation Processes. In *Coulson and Richardsons Chemical Engineering*, volume 2. Butterworth-Heinemann, Elsevier Science, Oxford UK, 5th edition, 2002.

[38] A. Records and K. Sutherland. *Decanter centrifuge handbook*. Elsevier Science Ltd., Oxford UK, 2001.

[39] W.W.F. Leung. Disk Centrifuge. In *Centrifugal separations in biotechnology*, pages 59–94. Elsevier: Amsterdam, 2007.

[40] L. K. Wang, S. Chang, Y. Hung, H. S. Muralidhara, and S. P. Chauhan. Centrifugation clarification and thickening. In *Biosolids treatment processes*, volume 6, pages pp 101–134. Humana Press Inc., NJ, 2007.

[41] A. G. Letki. Preparative centrifugation. In *Encyclopedia of Separation Science*, volume 93, pages 200–4. Academic Press, 2000.

[42] W.W.F. Leung. Selection and Sizing of Centrifuges. In *Centrifugal separations in biotechnology*, pages 165–188. Elsevier: Amsterdam, 2007.

[43] T. D. Loggio and A. Letki. New directions in centrifuging. *Chemical Engineeing -New York*, 101(1):70–76, 1994.

[44] J. C. Smith. Selection of Centrifuges for Chemical Processing. *Industrial & Engineering Chemistry*, 39(4):474–479, 1947.

[45] W Wieking. Centrifuges. In *Encyclopedia of Dairy Sciences*, pages 244–251. Academic Press, London UK, 2002.

[46] A. Letki and N. Corner-Walker. Centrifugal separation. *Kirk-Othmer Encyclopedia of Chemical Technology*, 5:505–551, 2004.

[47] R. Perry and D. Green. Centrifuges. In *Perrys Chemical Engineers Handbook*. McGraw-Hill, New York, 8 edition, 2008.

[48] J. C. Smith. Centrifugal separators. *Chemical Engineeing -New York*, 67:148, 1960.

[49] J. C. Smith. Cost and performance of centrifugals. *Chemical Engineeing -New York*, 59:140–147, 1952.

[50] V. M. Matta and R. A. Medronho. A new method for yeast recovery in batch ethanol fermentations: filter aid filtration followed by separation of yeast from filter aid using hydrocyclones. *Bioseparation*, 9(1):43–53, January 2000.

[51] D. Voisard, F. Meuwly, P. A. Ruffieux, G. Baer, and A. Kadouri. Potential of cell retention techniques for large-scale high-density perfusion culture of suspended mammalian cells. *Biotechnology and bioengineering*, 82(7):751–65, June 2003.

[52] E. A. Elsayed, R. A. Medronho, R. Wagner, and W.-D. Deckwer. Use of Hydrocyclones for Mammalian Cell Retention: Separation Efficiency and

Cell Viability (Part 1). *Engineering in Life Sciences*, 6(4):347–354, August 2006.

[53] D. A. Baranov, A. I. Pronin, V. A. Dikov, A. A. Ivanov, N. A. Kolesova, I. A. Balakhnin, and M. G. Lagutkin. Hydrocyclones for the chemical industry and cleaning devices for circulating and waste water. *Chemical and Petroleum Engineering*, 43(7-8):385–388, July 2007.

[54] M. Habibian, M. Pazouki, H. Ghanaie, and K. Abbaspour-Sani. Application of hydrocyclone for removal of yeasts from alcohol fermentations broth. *Chemical Engineering Journal*, 138(1-3):30–34, May 2008.

[55] I. C. Bicalho, J. L. Mognon, J. Shimoyama, C. H. Ataíde, and C. R. Duarte. Separation of yeast from alcoholic fermentation in small hydrocyclones. *Separation and Purification Technology*, 87:62–70, March 2012.

[56] W. M.G.T. Van den Broek, R. Plat, and M. J. van der Zande. Comparison of plate separator, centrifuge and hydrocyclone. In *SPE International Oil and Gas Conference and Exhibition in China*, number SPE-48870-MS, Beijing, China. Society of Petroleum Engineers.

[57] Q. Zhao and G. Xia. A theoretical model for calculating pressure drop in the cone area of light dispersion hydrocyclones. *Chemical Engineering Journal*, 117(3):231–238, 2006.

[58] J. Bergstrom and H. Vomhoff. Experimental hydrocyclone flow field studies. *Separation and Purification Technology*, 53(1):8–20, 2007.

[59] M. S. Brennan, M. Fry, M. Narasimha, and P. N. Holtham. Water velocity measurements inside a hydrocyclone using an Aeroprobe & Comparison with CFD predictions Department of Chemical Engineering. Number December, pages 1131–1136, 2007.

[60] L. P. M. Marins, D. G. Duarte, J. B. R. Loureiro, C. A. C. Moraes, and A. P. S. Freire. LDA and PIV characterization of the flow in a hydrocyclone without an air-core. *Journal of Petroleum Science and Engineering*, 70(3-4):168–176, 2009.

[61] Y. Liu, Q. Yang, P. Qian, and H. Wang. Experimental study of circulation flow in a light dispersion hydrocyclone. *Separation and Purification Technology*, 137:66–73, 2014.

[62] D. Bradley. A theoretical study of the hydraulic cyclone. *Industrial Chemistry*, 34:473–80, 1958.

[63] K. Rietema. Performance and design of hydrocyclonesIII. *Chemical Engineering Science*, 15(3-4):310–319, 1961.

[64] C. C. Hwang, H. Q. Shen, G. Zhu, and M. M. Khonsari. On the Main Flow Pattern in Hydrocyclones. *Journal of Fluids Engineering*, 115(March):21–25, 1993.

[65] L.R. Castilho and R.A. Medronho. A simple procedure for design and performance prediction of Bradley and Rietema hydrocyclones. *Minerals Engineering*, 13(2):183–191, 2000.

[66] K. Nageswararao, D.M. Wiseman, and T.J. Napier-Munn. Two empirical hydrocyclone models revisited. *Minerals Engineering*, 17(5):671–687, 2004.

[67] Th. Neesse and J. Dueck. Dynamic modelling of the hydrocyclone. *Minerals Engineering*, 20(4):380–386, April 2007.

[68] E. Donskoi, S. Suthers, J. Campbell, and T. Raynlyn. Modelling and optimization of hydrocyclone for iron ore fines beneficiation using optical image analysis and iron ore texture classification. *International Journal of Mineral Processing*, 87(3-4):106–119, July 2008.

[69] S. Amini, D. Mowla, M. Golkar, and Feridun Esmaeilzadeh. Mathematical modelling of a hydrocyclone for the down-hole oil-water separation (DOWS). *Chemical Engineering Research and Design*, 90(12):2186–2195, 2012.

[70] J. Dueck, M. Farghaly, and T. Neesse. The theoretical partition curve of the hydrocyclone. *Minerals Engineering*, 62:25–30, 2014.

[71] L.R. Plitt. A mathematical model of the hydrocyclone classier. *CIM Bulletin*, 69(776):114–123, 1976.

[72] J. Severino, L. Gomez, S. Wang, R. Mohan, and O. Shoham. Mechanistic Modeling of Solids Separation in Solid/Liquid Hydrocyclones. In *Proceedings of SPE Annual Technical Conference and Exhibition*, pages 4–9. Society of Petroleum Engineers, October 2009.

[73] M. Narasimha, M. Brennan, and P. N. Holtham. A review of CFD modelling

for performance predictions of hydrocyclone. *Engineering Applications of Computational Fluid Mechanics*, 1(2):109–125, 2007.

[74] Q. Yang, H. Wang, Y. Liu, and Z. Li. Solid/liquid separation performance of hydrocyclones with different cone combinations. *Separation and Purification Technology*, 74(3):271–279, 2010.

[75] M. Ghadirian, R. E. Hayes, J. Mmbaga, A. Afacan, and Z. Xu. On the simulation of hydrocyclones using CFD. *Canadian Journal of Chemical Engineering*, 91(May):950–958, 2013.

[76] N. Chakraborti and J. D. Miller. Fluid Flow in Hydrocyclones : A Critical Review. *Mineral Processing and Extractive Metallurgy Review*, 11:211–244, 1992.

[77] M. Narasimha, M. S. Brennan, and .P N. Holtham. A Review of Flow Modeling for Dense Medium Cyclones. *Coal Preparation*, 26(2):55–89, 2006.

[78] F. Concha. Flow Pattern in Hydrocyclones. *Kona-Powder and Particle*, 25(25):97–132, 2007.

[79] R. Sabbagh, M. G. Lipsett, C. R. Koch, and D. S. Nobes. A mathematical model of equivalent settling area for predicting hydrocyclone separation performance. In *European Conference on Fluid Particle Separation-FPS 2014*, pages 61–62, Lyon, France, 2014. Société Française des Séparations Fluides-Particles.

[80] D. Bradley and D. J. Pulling. Flow patterns in the hydraulic cyclone and

their interpretation. *Transactions of the Institution of Chemical Engineers*, 37, 1959.

[81] M. W. Mikhail, A. I. A. Salama, and R. Burns. Fine particles removal from oil sand tailings by hydrocyclone. *CIM Bulletin*, 90(1015):86–90, 1997.

[82] J.G. Severino. *Mechanistic Modeling of Solid-Liquid Separation in Small Diameter Hydrocyclones*. PhD thesis, The University of Tulsa, 2007.

[83] Th. Neesse, M. Schneider, J. Dueck, V. Golyk, S. Buntenbach, and H. Tiefel. Hydrocyclone operation at the transition point rope/spray discharge. *Minerals Engineering*, 17(5):733–737, 2004.

[84] W. Kraipech, W. Chen, F.J. Parma, and T. Dyakowski. Modelling the fish-hook effect of the flow within hydrocyclones. *International Journal of Mineral Processing*, 66(1-4):49–65, September 2002.

[85] L. Svarovsky and G. Svarovsky. *Hydrocyclones, volume II*. George Svarovsky, 2013.

[86] G. J. C. Childs, W. M. Finch, and N. G. Smith. The effect of high concentration on the performance of a hydrocyclone with fine particle feeds. In *Hydrocyclones 96*, pages 255–262. Wiley, London UK, 1996.

[87] H. Schubert. Which demands should and can meet a separation model for hydrocyclone classification? *International Journal of Mineral Processing*, 96(1-4):14–26, September 2010.

[88] J. Dueck and Minkov L. L. Non-stokesian sedimentation as applied to the

analysis of the interaction of particles in a suspension. *Journal of Engineering Physics*, 85(1):19–28, 2012.

[89] J. Dueck, Th. Neesse, and L. Minkov. On the partition function of a hydrocyclone considering the collective sedimentation in a polydisperse suspension. *International Journal of Transport Phenomena*, 13(4):257–266, 2014.

[90] R. K. Tue Nenu, H. Yoshida, K. Fukui, and T. Yamamoto. Separation performance of sub-micron silica particles by electrical hydrocyclone. *Powder Technology*, 196(2):147–155, December 2009.

[91] W. Yuling, Z. Yuemin, and Y. Jianguo. Density distribution in a heavy-medium cyclone. *Mining Science and Technology (China)*, 21(2):175–179, March 2011.

[92] T. Neesse, H. Tiefel, and P. Kaniut. Volume split control of a hydrocyclone group. *Minerals Engineering*, 20(4):355–360, April 2007.

[93] T. Dyakowski, L. F. C. Jeanmeure, and A. J. Jaworski. Applications of electrical tomography for gas-solids and liquid-solids flows - A review. *Powder Technology*, 112(3):174–192, 2000.

[94] V. Krishna, R. Sripriya, V. Kumar, S. Chakraborty, and B.C. Meikap. Identification and prediction of air core diameter in a hydrocyclone by a novel online sensor based on digital signal processing technique. *Chemical Engineering and Processing: Process Intensification*, 49(2):165–176, February 2010.

[95] L. Chu, W. Chen, and X. Lee. Enhancement of hydrocyclone performance by controlling the inside turbulence structure. *Chemical Engineering Science*, 57(1):207–212, January 2002.

[96] H.I. Schlaberg, F.J.W. Podd, and B.S. Hoyle. Ultrasound process tomography system for hydrocyclones. *Ultrasonics*, 38(1-8):813–6, March 2000.

[97] R. Hou, A. Hunt, and R.A. Williams. Acoustic monitoring of hydrocyclones. *Powder Technology*, 124(3):176–187, April 2002.

[98] J. V. V. Magrieta Jeanette, A. Chris, A. Lidia, B. Chandon, and D. J. Corné. On-line monitoring of dynamic hydrocyclone behaviour. In *Automation in Mining, Mineral and Metal Processing, 13th IFAC Symposium on Automation in Mining, Mineral and Metal Processing*, pages 87–91, University of Stellenbosch, South Africa, 2010. University of Stellenbosch, South Africa.

[99] Z. Liu, Y. Zheng, L. Jia, and Q. Zhang. An experimental method of examining three-dimensional swirling flows in gas cyclones by 2D-PIV. *Chemical Engineering Journal*, 133:247–256, 2007.

[100] M. Schneider and Th. Neess e. Overflow-control system for a hydrocyclone battery. *International Journal of Mineral Processing*, 74:S339–S343, December 2004.

[101] I. C. Bicalho, J. L. Mognon, J. Shimoyama, C. H. Ataíde, and C. R. Duarte. Effects of operating variables on the yeast separation process in a hydrocyclone. *Separation Science and Technology*, 48(6):915–922, 2013.

[102] J. Dueck, E. Pikushchak, L. Minkov, M. Farghaly, and Th. Neesse. Mechanism of hydrocyclone separation with water injection. *Minerals Engineering*, 23(4):289–294, 2010.

[103] K. Udaya Bhaskar, B. Govindarajan, J. P. Barnwal, K. K. Rao, and T. C. Rao. Modelling studies on a 100 mm water-injection cyclone. *Physical Separation in Science and Engineering*, 13(3-4):89–99, 2004.

[104] A. A. Ahmed, G. A. Ibraheim, and M. A. Doheim. The influence of apex diameter on the pattern of solid / liquid ratio distribution within a hydrocyclone. pages 395–402, 1985.

[105] K. Saengchan, A. Nopharatana, and W. Songkasiri. Enhancement of tapioca starch separation with a hydrocyclone: effects of apex diameter, feed concentration, and pressure drop on tapioca starch separation with a hydrocyclone. *Chemical Engineering and Processing: Process Intensification*, 48(1):195–202, 2009.

[106] K. Rietema. Performance and design of hydrocyclonesIV. *Chemical Engineering Science*, 15(3-4):320–325, 1961.

[107] W. Chen. Evaluation of hydrocyclone models for practical applications. *Chemical Engineering Journal*, 80(1-3):295–303, 2000.

[108] L Rovinsky. Application of separation theory to hydrocyclone design. *Journal of Food Engineering*, 26(2):131–146, 1995.

[109] W. Don and R. H. Perry. Centrifuges. In *Perry's Chemical Engineers' Handbook*. McGraw-Hill New York, 6th edition, 1984.

[110] W. Leung. *Industrial Centrifugation Technology*. McGraw-Hill, 1998.

[111] Optimass 7000 technical datasheet (TD OPTIMASS 7000 R08 en), Krohne Messtechnik GmbH & Co. KG, Duisburg, 2009.

[112] Proline Promass 80I, 83I technical information (TI075D/06/en/05.10), Endress+Hauser, Reinach, 2010.

[113] Standard Practice for Static Calibration of Electronic Transducer-Based Pressure Measurement Systems for Geotechnical Purposes. In *ASTM Standard D5720 -95*. ASTM International, West Conshohocken, PA, 2002.

[114] MFC 300 Signal converter for mass flowmeters Description of Modbus interface, Electronic Revision: ER 3.3.xx (SW.REV. 3.3x), Modbus version 1.0.x, 4000744801 - AD Modbus MFC 300 R01 en , Krohne Messtechnik GmbH & Co. KG, Duisburg, 2009.

[115] Optimass Concentration Handbook, MFC 300 mass flow converter, 7.02285.22.00, Krohne Messtechnik GmbH & Co. KG, Duisburg. pages 1–28, 2007.

[116] Serial Communication Expansion Boards MN1310, Catalog No. EXB001A01, Installation and Operating Manual, Baldor, 2003.

[117] Series 15H Inverter Control, MN715, Installation and Operating Manual, Baldor Morors and Drives, 2002.

[118] A. C. Hoffmann and L. E. Stein. *Gas Cyclones and Swirl Tubes*. Springer, Berlin, 2nd edition, 2008.

[119] T. T. Soong. *Fundamentals of probability and statistics for engineers*. John Wiley & Sons Ltd, West Sussex, England, 2004.

[120] W. Witt, T. Stübinger, and J. List. Laser diffraction for particle size analysis at absolute precision. In *World Congress on Particle Technology, WCPT6 2010*, pages 1–4, Nürnberg, Germany, 2010.

[121] A. J. Wheeler and A. R. Ganji. *Introduction to Engineering Experimentation*. Prentice Hall, Englewood Cliffs, N.J, 3rd edition, 2010.

[122] R. Sabbagh, M. G. Lipsett, C. R. Koch, and D. S. Nobes. Theoretical and Experimental Study of Hydrocyclone Performance and Equivalent Settling Area . In *Proceedings of the ASME 2014 International Congress & Exposition IMECE2014, Montreal, Canada*, Montreal, Canada, 2014. ASME.

[123] A. Rushton, A. S. Ward, and R. G. Holdich. Centrifugal Separation. In *Solid-Liquid Filtration and Separation Technology*. Wiley-VCH, 1st edition, 1996.

[124] M. J. Fisher and R. D. Flack. Velocity distributions in a hydrocyclone separator. *Experiments in Fluids*, 32:302–312, 2002.

[125] T. Neesse and J. Dueck. Air core formation in the hydrocyclone. *Minerals Engineering*, 20:349–354, 2007.

[126] J. F. Richardson and W. N. Zaki. Sedimentation and fluidisation: Part i. *Chemical Engineering Research and Design*, 75(3):S82–S100, 1997.

[127] C. T. Crowe. *MutiphaseFlow Handbook*. CRC Press, Boca Raton, USA, 2006.

[128] K. D. Jensen. Flow Measurements Techniques. *Journal of Braz. Soc. of Mech. Sci. & Eng.*, XXVI(4):400–419, 2004.

[129] M.A.Z. Coelho and R.A. Medronho. An evaluation of the Plitt and Lynch and Rao models for the hydrocyclones. In L. Svarovsky and M.T. Thew, editors, *Hydrocyclones*, volume 12 of *Fluid Mechanics and Its Applications*, pages 63–72. Springer Netherlands, 1992.

[130] J. O. Rawlings, S. G. Pantula, and D. Dickey. *Applied Regression Analysis : A Research Tool*. Springer, New York, 2nd edition, 1998.

[131] H. Motulsky and A. Christopoulos. *Fitting models to biological data using linear and nonlinear regression. A practical guide to curve fitting*. Oxford University Press, 2003.

[132] S. Chatterjee and J. S. Simonoff. *Handbook of Regression Analysis*. John Wiley & Sons, Inc., Hoboken, New Jersey, 2013.

[133] J. R. Couper, W. R. Penney, J. R. Fair, and S. M. Walas. Solid-Liquid Separation. In *Chemical Process Equipment Selection and Design Revised Second Edition*, pages 325–355. 2010.

[134] A. Davailles, E. Climent, and F. Bourgeois. Fundamental understanding of swirling flow pattern in hydrocyclones. *Separation and Purification Technology*, 92:152–160, 2012.

[135] L. Svarovsky and M. T. Thew. A new method of testing hydrocyclone grade efficiency. In *Hydrocyclones: Analysis and Applications*, page 413. Springer Science & Business Media, Letchworth, England, 1992.

[136] D. G. Thomas. Transport characteristics of suspension: VIII. A note on the viscosity of Newtonian suspensions of uniform spherical particles. *Journal of Colloid Science*, 20(3):267–277, 1965.

[137] A. Gelman and J. Hill. *Data analysis using regression and multi-level/hierarchical models*. Cambridge University Press, Cambridge, UK, 2007.

Appendix

A-1 Phase based separation techniques

Table A-1 shows phase based separation techniques [37]. Among these, solid liquid separation techniques are listed in detail in the next section.

Table A-1: Phase based separation techniques

		MAJOR COMPONENT		
		Solid	Liquid	Gas/Vapor
MAJOR COMPONENT	Solid	Sorting, Screening, Hydrocyclones, Classifiers, Jigs, Tables, Centrifuges, Dense media, Flotation, Magnetic, Electrostatic	Pressing, Drying	Crushing, Heating
	Liquid	Thickeners, Clarifiers, Hydrocyclones, Filtration, Centrifuges, Crystallizers, Evaporators	Decanters, Coalescers, Solvent extraction, Distillation, Adsorption, Ion exchange	Stripping
	Gas/Vapor	Gravity settlers, Impingement settlers, Cyclones, Filters, Wet scrubbers, Electrostatic precipitators	Separating vessels, Demisting pads, Cyclones, Wet scrubbers, Electrostatic precipitators	Adsorption, Absorption

Appendix

A-2 Solid liquid separation techniques and range of application

A list of different solid liquid separation methods is summarized based on the information from [14] in Table A-2. This list gives the range of particle size and solid concentration for each equipment. A flow chart that shows the classification of the solid liquid separation equipment is also plotted in Fig. A-1.

Table A-2: Solid liquid separation technique and range of application

Gravity thickeners and clarifiers			
	• Circular basin thickener		0.1–500 µm and <20% w/w
	• High capacity thickeners		
		➢ *Circular*	0.1–300 µm and <15% w/w
		➢ *Deep cone*	0.1–300 µm and <15% w/w
		➢ *Lamella*	1–150 µm and <15% w/w
	• Clarifiers		1–50 µm and <15% w/w
Hydrocyclones			
	• Conical reverse flow		5–200 µm and 2–40% w/w
	• Circulating bed		2–500 µm and 2–25% w/w
Centrifuges			
	• Sedimenting centrifuges		
		➢ *Tubular bowl*	0.1–100 µm and <5% w/w
		➢ *Basket*	0.1–100 µm and <5% w/w
		➢ *Disc stack*	0.1–100 µm and 0.05–2% w/w
		➢ *Scroll decanter*	1–5000 µm and 4–40% w/w
	• Filtering centrifuges		
		➢ *Basket*	10–1000 µm (pendulum), 2–1000 µm (peeler) and 4–30% w/w
		➢ *Cone screen*	80–10000 µm (slip discharge), 100–10000 µm (vibratory, oscillatory or tumbling), 60–5000 µm (worm screen) and 10–40% w/w
		➢ *Pusher*	40–7000 µm and 10–40% w/w
		➢ *Baffle*	100–7000 µm and 10–40% w/w
		➢ *Inverting bag centrifuge*	2–1000 µm and 5–30% w/w
Filters			
	• Vacuum filters		
		➢ *Single leaf*	1–500 µm and 1–10% w/w (Nutsche); 20–80,000 µm and 5–30+% w/w (tipping pan)
		➢ *Multi-element leaf*	1–100 µm and 5–30+% w/w
		➢ *Horizontal belt*	20–80000 µm and 5–30+% w/w
		➢ *Horizontal rotary*	20–80000 µm and 10–30+% w/w (table), 5–30+% w/w (tilting pan)
		➢ *Rotary drum*	1–200 µm (bottom fed, knife or belt discharge), 1–50 µm (bottom fed, roller discharge), 1–70 µm (bottom fed, string discharge), 1–600 µm (top fed), 10–600 µm (internal fed drum)
		➢ *Rotary disc*	1–700 µm and 5–20% w/w
	• Pressure filters and presses		
		➢ *Single leaf*	1–200 µm and <1–20+% w/w
		➢ *Multi-element leaf or candle*	1–100 µm and <1–20+% w/w (horizontal element), 0.5–100 µm and <1–20% w/w (vertical element), 0.5–100 µm and <1–20% w/w (tubular candle element)
		➢ *Filter presses*	1–100 µm and <1–30+% w/w
		➢ *Sheet filter*	0.1–80 µm and <<1–5% w/w
		➢ Variable-volume	

		filters and presses	
		○ *Horizontal diaphragm filter press*	1–200 µm and 0.3–30+% w/w
		○ *Vertical diaphragm filter press*	1–200 µm and 0.2–30+% w/w
		○ *Tube press*	1–200 µm and 0.3–30+% w/w
		○ *Expression press*	1–200 µm and 10–80% w/w
		➢ Continuous pressure filters	
		○ *Belt press*	1–200 µm and 0.2–30+% w/w
		○ *Tower press*	1–300 µm and 0.1–25+% w/w
		○ *Rotary pressure drum*	1–100 µm and 5–30+% w/w
		○ *Rotary pressure disc*	1–100 µm and 5–30+% w/w
		➢ Cartridge filter	0.4–50 µm and <0.1% w/w
		➢ Bag filter	10–300 µm and 0.2–10% w/w
	• Precoat filters		
		➢ Precoat rotary drum	0.5–100 µm and <1% w/w
		➢ Precoat pressure	0.1–40 µm and <1% w/w
	• Depth filters		
		➢ Sand bed	0.2–60 µm (pressure fed), 0.2–50 µm (gravity fed) and <0.1% w/w
		➢ Fibre bed	0.1–40 µm and <1% w/w
Classifiers			
	• Hydraulic		50–2000 µm and 4–40% w/w
	• Mechanical		100–3000 µm and 4–40% w/w
	• Screen		45–100000 µm and 20–40% w/w
Membrane filters			
	• Dead-end		0.1–10 µm and <1% w/w
	• Low shear crossflow		
		➢ Ultrafilters	0.001–0.05 µm and <20% w/w
		➢ Microfilters	0.05–20 µm and <20% w/w
	• High shear crossflow		0.1–20 µm and <25% w/w
Force field assisted separations			
	• Magnetic field		<40–4000 µm and 5–20% w/w (LIMS or HIMS), <400 µm and <10% w/w (HGMS)
	• High voltage electric field		<20 µm and <10% w/w
	• Low voltage electric field		<10 µm
	• Ultrasonic field		<10 µm and <10% w/w
Other equipment			
	• Flotation		<300–2000 µm and 1–20% w/w
	• Strainer		5–200 µm and <0.1% w/w
	• Gravity Nutsche filters		100–10000 µm and 1–10% w/w
	• Gravity belt filter		100–10000 µm and <3% w/w

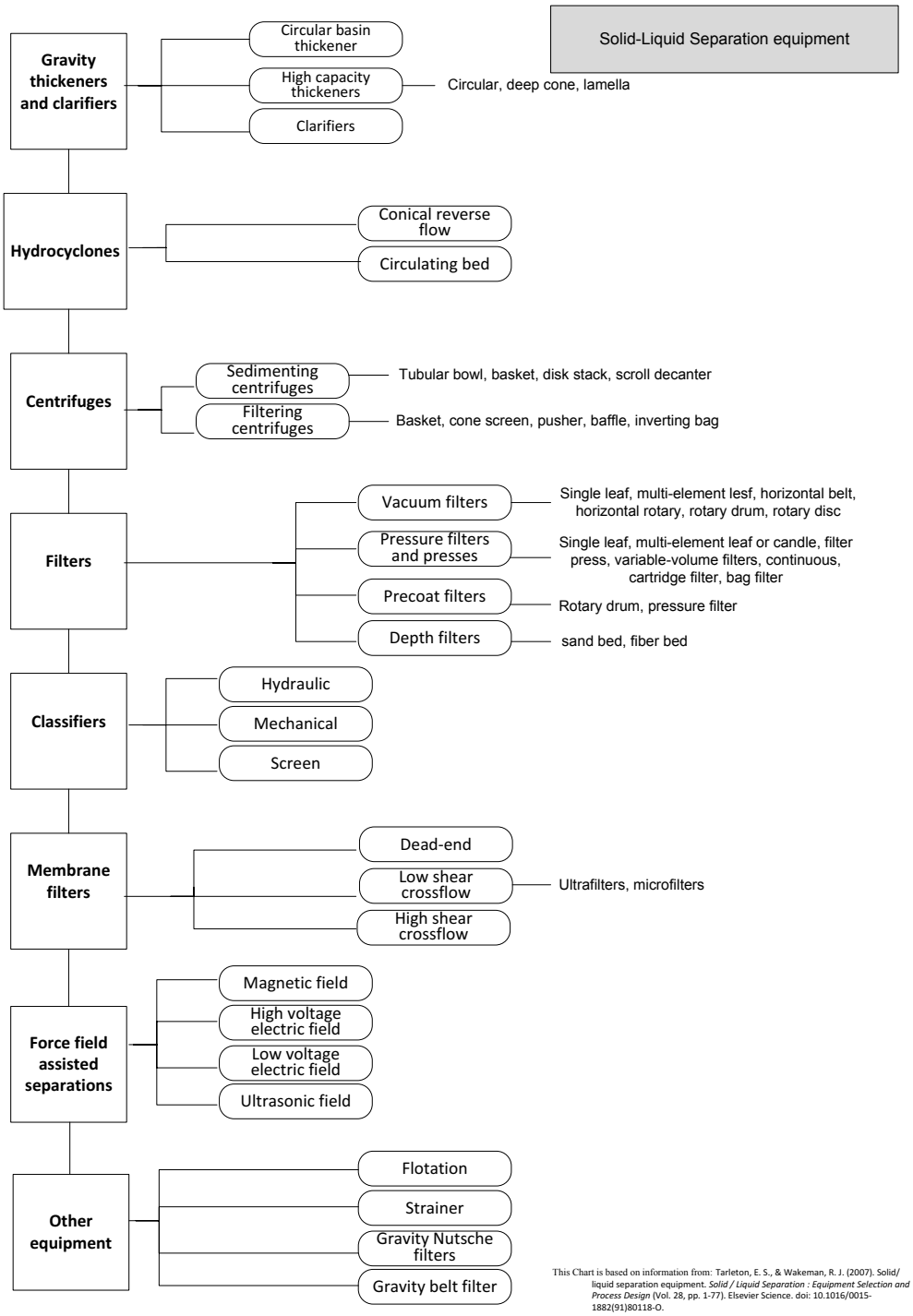

Figure A-1: Classification of solid liquid separation techniques. The information extracted from [14]

Appendix

A-3 Particle size terminology

Separation equipment usually classified according to particle size or the scientific principle that is used for separation. Since there is no exact definition for categorizing particle under ultra, nano, micro etc. different manufacturers and authors use different terms. A simple terminology [8] that may help in understanding the particle size is listed in Table A-3. An example of particles and solid-liquid separation technique is also presented in the table.

Table A-3: A simplified particle size terminology [8]

size (μm)	Terminology	Example	Solid/Liquid Separation Method
0-0.001	Ionic	Aqueous salts	Nanofiltration, reverse osmosis, chromatography
0.001-0.1	Macro-molecular	Virus, colloids	Ultrafiltraton
0.1-10	Fine particle	Pigments, clay, bacterias	Microfiltration, cake filtration, deep-bed filtration, centrifugation
10-100	Medium size	Bacteria, yeast, fibers, fine sand	Cake filtration, gravity sedimentation, floatation, cycloning
100-1000	Large	Coarse sand	Screens, shakers

Appendix

A-4 Equivalent area factor uncertainty

Uncertainty of Σ

The uncertainty for calculating the equivalent area factor in the experiments are also obtained. This is calculated using the developed equation for Σ, Eq. (4.14) such that:

$$\Sigma = \beta \frac{\Delta P L}{\rho g} \tag{A-1}$$

$$\delta_{\Sigma}^{2} = \left(\delta_{\beta}\frac{\partial \Sigma}{\partial \beta}\right)^{2} + \left(\delta_{L}\frac{\partial \Sigma}{\partial L}\right)^{2} + \left(\delta_{\rho}\frac{\partial \Sigma}{\partial \rho}\right)^{2} + \left(\delta_{g}\frac{\partial \Sigma}{\partial g}\right)^{2} + \left(\delta_{(\Delta P)}\frac{\partial \Sigma}{\partial (\Delta P)}\right)^{2} \tag{A-2}$$

where δ denotes the uncertainty of the variable. Since the value of β is obtained constant equal to 1.14 considering the value of $n = 0.88$ obtained for the hydrocyclone in the current study and knowing that hydrocyclone length L and g are constant, Eq. (A-2) is simplified to:

$$\delta_{\Sigma}^{2} = \left(\delta_{\rho}\frac{\partial \Sigma}{\partial \rho}\right)^{2} + \left(\delta_{(\Delta P)}\frac{\partial \Sigma}{\partial (\Delta P)}\right)^{2} \tag{A-3}$$

Replacing the differentiations gives:

$$\delta_{\Sigma}^{2} = \left(\delta_{\rho}(\frac{-\Delta P \beta L}{g\rho^{2}})\right)^{2} + \left(\delta_{(\Delta P)}\frac{L\beta}{\rho g}\right)^{2} \tag{A-4}$$

Replacing the values in Eq. (A-4) the uncertainties for Σ is obtained. In this calculation uncertainty of the liquid density ρ assumed to take the maximum value of 0.55 kg/m^3 for 2°C change in temperature during the experiment. The results of the uncertainty calculation for Σ are shown in Fig. A-2 for different underflow

pump speeds. It can be seen that the Σ uncertainty can reach to a maximum value of 0.21 m^2 while the minimum uncertainty is 0.05 m^2.

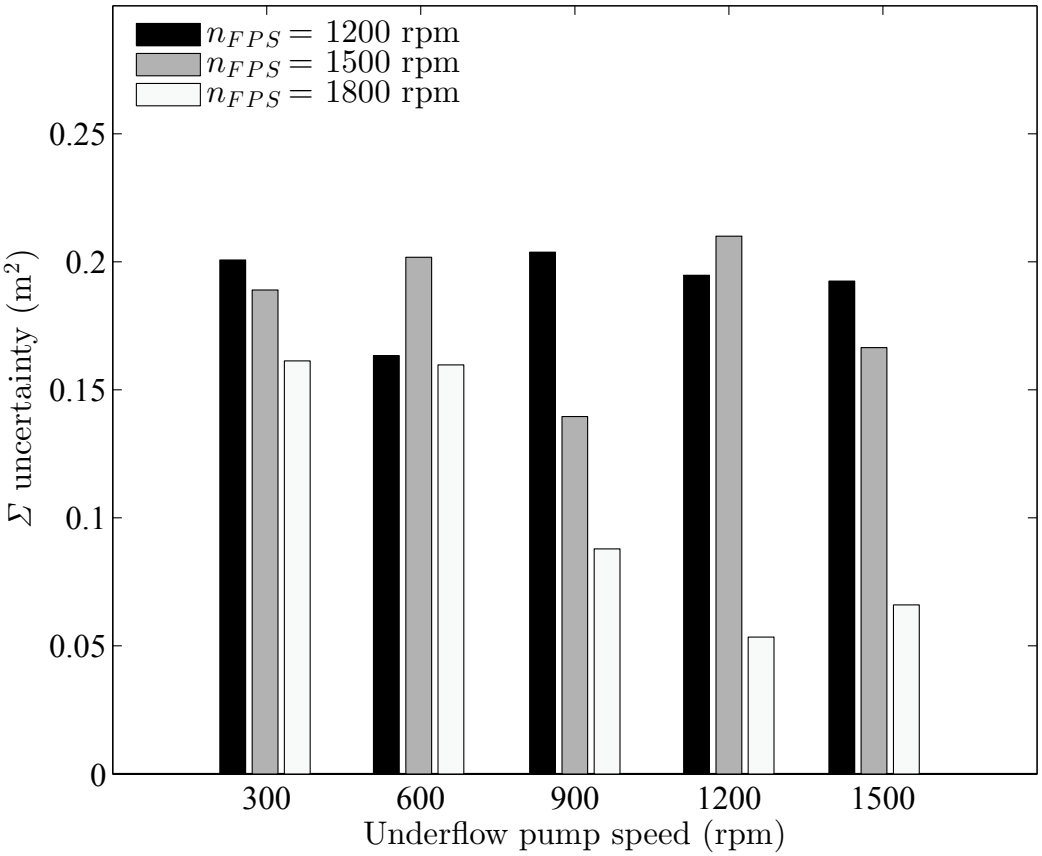

Figure A-2: Uncertainty in calculating equivalent area factor Σ; $c = 0.1\%$v/v.

Uncertainty of Σ_c

Uncertainty of the modified equivalent area factor Σ_c that is a function of inlet volume concentration c is obtained using Eq. (5.11) such that:

$$\Sigma_c = \beta \frac{\Delta P L}{\rho g}(1-c)^{10.86} \qquad \text{(A-5)}$$

$$\delta_{\Sigma_c}^2 = \left(\delta_\beta \frac{\partial \Sigma_c}{\partial \beta}\right)^2 + \left(\delta_L \frac{\partial \Sigma_c}{\partial L}\right)^2 + \left(\delta_\rho \frac{\partial \Sigma_c}{\partial \rho}\right)^2 + \left(\delta_g \frac{\partial \Sigma_c}{\partial g}\right)^2 + \left(\delta_{(\Delta P)} \frac{\partial \Sigma_c}{\partial (\Delta P)}\right)^2 + \left(\delta_c \frac{\partial \Sigma_c}{\partial c}\right)^2 \qquad \text{(A-6)}$$

where δ denotes the uncertainty of the variable. Performing a similar procedure as for uncertainty of Σ, Eq. (A-6) is simplified to:

$$\delta_{\Sigma_c}^2 = \left(\delta_\rho \frac{\partial \Sigma_c}{\partial \rho}\right)^2 + \left(\delta_{(\Delta P)} \frac{\partial \Sigma_c}{\partial (\Delta P)}\right)^2 + \left(\delta_c \frac{\partial \Sigma_c}{\partial c}\right)^2 \qquad \text{(A-7)}$$

After differentiating this gives:

$$\delta_{\Sigma_c}^2 = \left(\delta_\rho (\frac{-\Delta P \beta L}{g\rho^2})(1-c)^{10.86}\right)^2 + \left(\delta_{(\Delta P)} \frac{L\beta}{\rho g}(1-c)^{10.86}\right)^2 + \left(10.86 \frac{-\beta_L \Delta P}{\rho g} \delta_c (1-c)^{9.86}\right)^2 \qquad \text{(A-8)}$$

Replacing the values in Eq. (A-8) the uncertainties for Σ_c is obtained. The results of the uncertainty calculation for Σ_c are shown in Fig. A-3 for different underflow pump speeds. It can be seen that the Σ uncertainty can reach to a maximum value of 0.23 m^2 while the minimum uncertainty is 0.06 m^2.

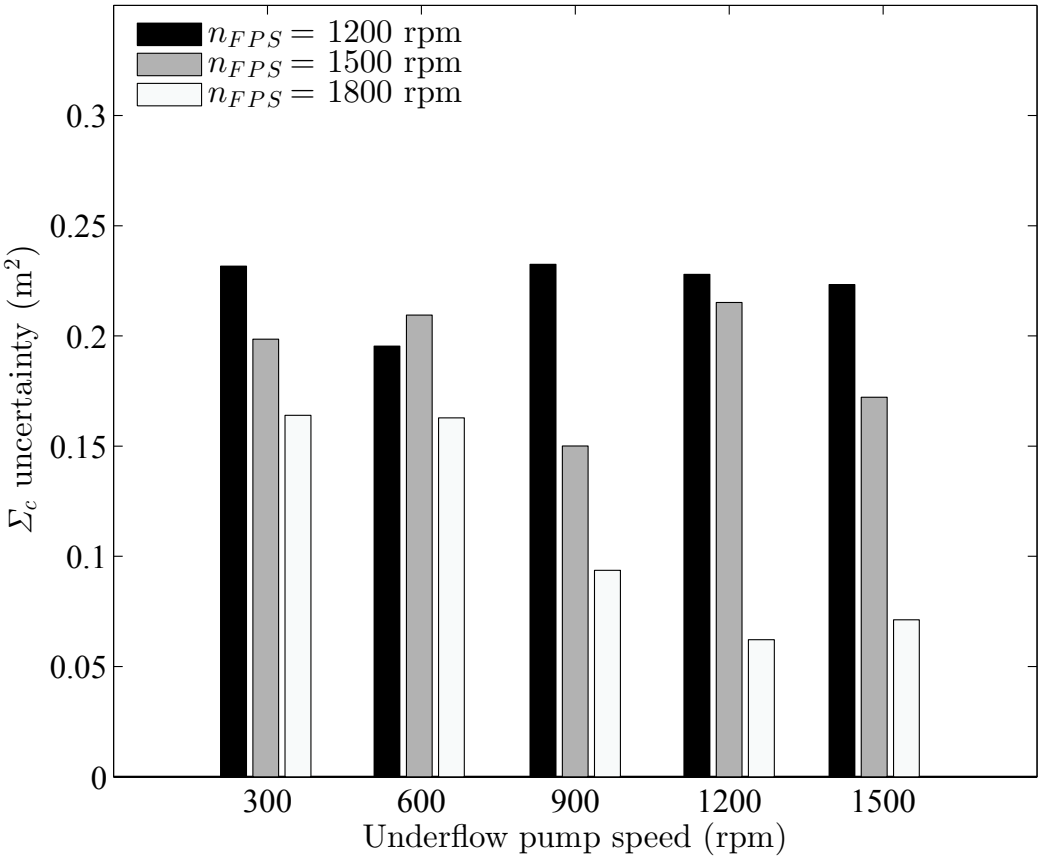

Figure A-3: Uncertainty in calculating modified equivalent area factor Σ_c; $c = 0.1\%$v/v.

Uncertainty of Σ_{exp}

Uncertainty of the experimentally measured equivalent area factor Σ_{exp} is obtained using Eq. (A-9) and Eq. (A-10) such that:

$$\Sigma_{exp} = \frac{Q}{2v_g} \tag{A-9}$$

$$\delta^2_{\Sigma_{exp}} = \left(\frac{\delta_Q}{2v_g}\right)^2 + \left(\delta_{v_g}\frac{Q}{2v_g^2}\right)^2 \tag{A-10}$$

where δ denotes the uncertainty of the variable. The uncertainty of the settling velocity δ_{v_g} is obtained such that:

$$\delta^2_{v_g} = \left(\delta_{\Delta\rho}\frac{d^2}{18\mu}\right)^2 + \left(2d\delta_d\frac{\Delta\rho}{18\mu}\right)^2 + \left(\delta_\mu\frac{\Delta\rho d^2}{18\mu^2}\right)^2 \tag{A-11}$$

Replacing the values in Eq. (A-11) and Eq. (A-10) the uncertainties for Σ_{exp} is obtained. The results of the uncertainty calculation for Σ_{exp} are shown in Fig. A-4 for different underflow pump speeds. It can be seen that the Σ_{exp} uncertainty can reach to a maximum value of 2.18 m^2 while the minimum uncertainty is 1.07 m^2.

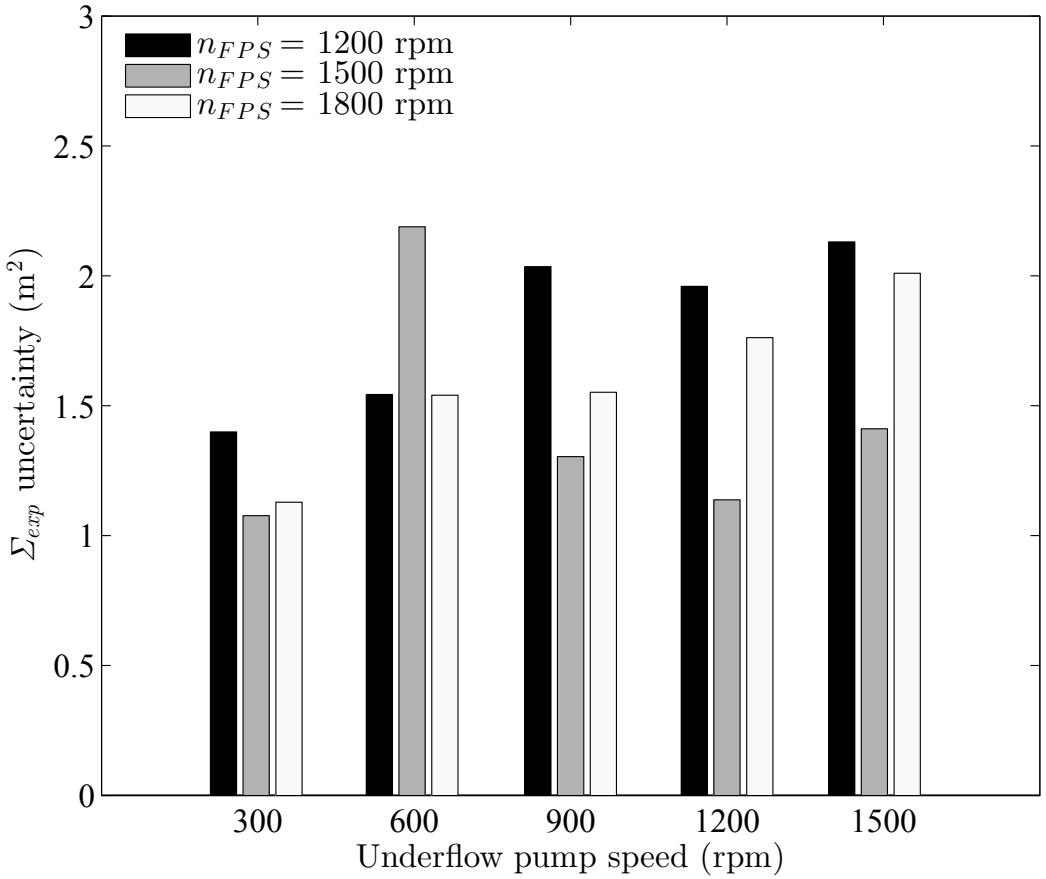

Figure A-4: Uncertainty in calculating modified equivalent area factor Σ_{exp}; $c = 0.1\%$v/v.

Appendix

A-5 Justification of Stokes' law

The validity of Stokes' law for the hydrocyclone in the current study is evaluated by calculating the particle Reynolds number Re_p [62] in the hydrocyclone at distance r from the center-line.

The centrifugal acceleration of a settling particle is v_θ^2/r and the settling velocity of the particle v_p with diameter d under this centrifugal acceleration is obtained such that:

$$v_p = \frac{\Delta\rho d^2}{18\mu}\frac{v_\theta^2}{r} \qquad \text{(A-12)}$$

where v_θ is obtained from Eq. (2.15). The particle settling velocity v_p is now used to calculate Re_p such that:

$$Re_p = \frac{\rho v_p d}{\mu} \qquad \text{(A-13)}$$

Combining Eq. (A-13) with Eq. (A-12) gives:

$$Re_p = \frac{\rho\Delta\rho d^3}{18\mu^2}\frac{v_\theta^2}{r} \qquad \text{(A-14)}$$

For average inlet flow rate $Q = 1.8$ m^3/hr from the experiments and the tangential velocity exponent $n = 0.88$ (as obtained for the hydrocyclone in the current study in Chapter 4), the tangential velocity profile is obtained. The result is shown in Fig. A-5. For solid-liquid density difference $\Delta\rho = 1500$ kg/m^3 (between soda lime glass beads particles and water), liquid viscosity $\mu = 1$ mPa.s, particle size $d = 10$ μm and liquid density $\rho = 1000$ kg/m^3 the values of Re_p are obtained from Eq. (A-14) and plotted in Fig. A-6. As it can be seen from this figure, at any radial location in the hydrocyclone $Re_p < 1$ and hence the Stokes' law is a valid assumption.

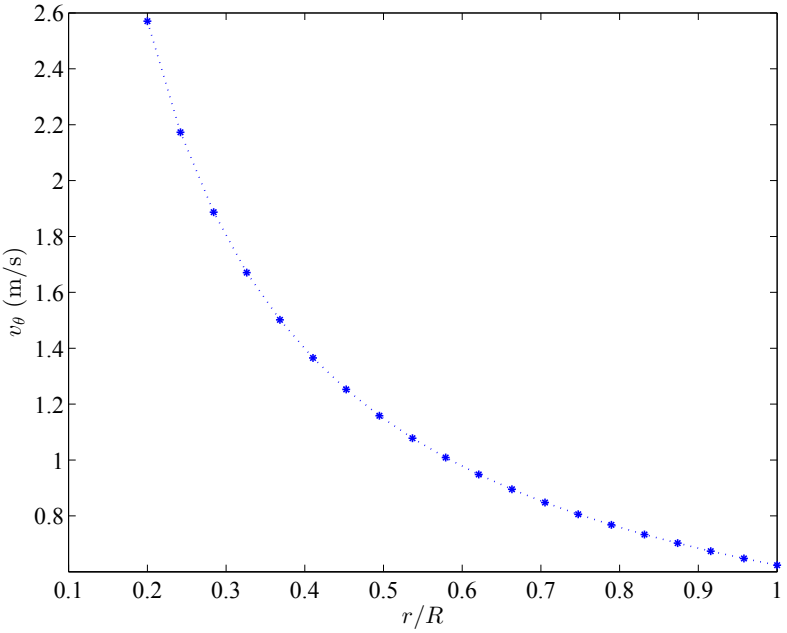

Figure A-5: Tangential velocity profile for the hydrocyclone in the current study; $R = D/2$ where D is hydrocyclone diameter

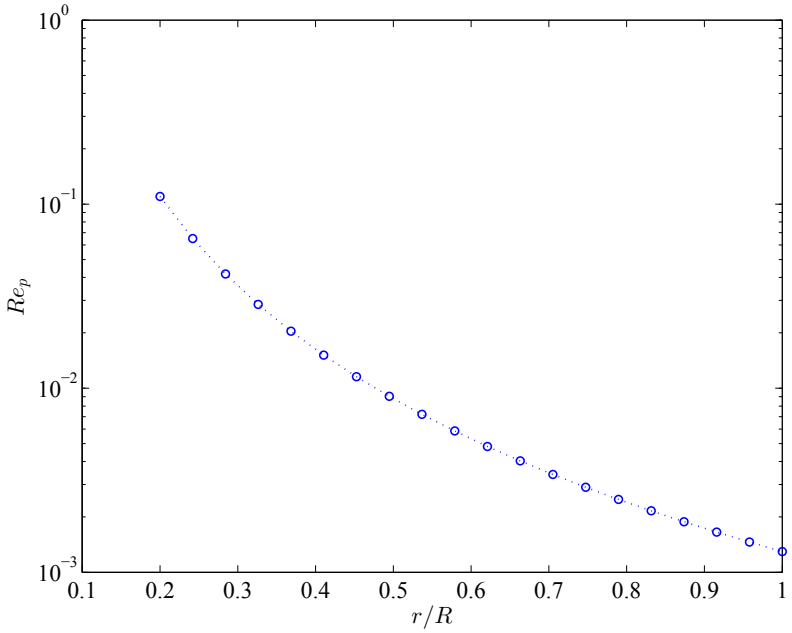

Figure A-6: Particle Reynolds number for the hydrocyclone in the current study; $R = D/2$ where D is hydrocyclone diameter